UNIVERSITÉ DU QUÉBEC

DOCTORAT PRÉSENTÉ À
L'UNIVERSITÉ DU QUÉBEC À TROIS-RIVIÈRES
COMME EXIGENCE PARTIELLE
DU DOCTORAT EN INGÉNIERIE
OFFERT EN EXTENSION
EN VERTU D'UN PROTOCOLE D'ENTENTE
AVEC L'UNIVERSITÉ DU QUÉBEC À CHICOUTIMI

PAR
Ehsan Ameri

ROBUST DESIGN AND MANUFACTURING OF UNIDIRECTIONAL HYBRID FLAX-PAPER ECO-COMPOSITES

MAI 2016

UNIVERSITÉ DU QUÉBEC

DOCTORAT EN INGÉNIERIE (PH. D.)

Programme offert par l'Université du Québec à Chicoutimi (UQAC)

en extension avec

l'Université du Québec à Trois-Rivières (UQTR)

Cette thèse a été dirigée par : Ehsan Ameri

Gilbert Lebrun, directeur de recherche, PhD	Université du Québec à Trois-Rivières
Luc Laperrière, codirecteur de recherche, PhD	Université du Québec à Trois-Rivières

Jury d'évaluation de la thèse :

Gilbert Lebrun, PhD	Université du Québec à Trois-Rivières
Luc Laperrière, PhD	Université du Québec à Trois-Rivières
Georges Abdul-Nour, PhD	Université du Québec à Trois-Rivières
Bruno Chabot, PhD	Université du Québec à Trois-Rivières
Larry Lessard, PhD	McGill University

Thèse soutenue le 25 04 2016

Résumé

Problématique

De nos jours, les fibres naturelles (lin, chanvre, jute, etc.) deviennent de plus en plus populaires pour remplacer la fibre de verre dans les matériaux composites. Ceci est non seulement dû à leur module d'élasticité spécifique (rigidité divisée par la densité) plus élevé que celui des fibres de verre mais aussi à leurs avantages environnementaux et leur durabilité. En effet les fibres naturelles sont obtenues à partir de ressources renouvelables et leur production est moins énergivore et moins coûteuse que celle des fibres synthétiques comme la fibre de verre. De plus, elles sont biodégradables et donc non polluantes lors de leur recyclage. Ces caractéristiques en font une alternative écologique et durable.

Le Canada est le premier producteur mondial de lin, principalement pour le grain. La fibre est peu exploitée et elle est rejetée car coupée de façon aléatoire et laissée dans les champs lors de la récolte du grain. Il y a donc possibilité de récupérer la fibre dans des produits de matériaux composites à valeur ajoutée. Ces nouveaux matériaux sont moins dépendants des ressources pétrolières, tout en étant plus respectueux de l'environnement.

Les fibres de lin sont caractérisées par une rigidité spécifique supérieure à celle des fibres de verre et donc elles peuvent être considérées comme un remplacement potentiel de la fibre de verre dans les pièces composites. Les matériaux composites à base de fibres naturelles courtes sont déjà mis en œuvre dans l'industrie pour produire des pièces non structurelles. Afin de développer des éco-composites capable d'être utilisés dans les structures, il faut développer des renforts à fibres longues et continues. La plupart des renforts à fibres longues

sont bidirectionnels (fibres tissées) et sont fabriqués par les technologies de l'industrie du textile. Ce type de renfort est moins performant que les composites unidirectionnels (fibres alignées) car les chevauchements des fils dans les tissés représentent un point faible à partir duquel la rupture du matériau peut s'initier.

Objectif

Les travaux de cette thèse visent à développer et caractériser un renfort unidirectionnel (UD) lin/papier contenant une couche UD de fils de lin alignés dont la cohésion est assurée par une couche de papier de fibres courtes de Kraft (fibres de bois). Les performances de ce nouveau renfort comprennent sa perméabilité à l'écoulement de résine liquide, le comportement en traction du composite qui en résulte une fois imprégné, ainsi que sa résistance au cisaillement (cohésion à sec entre les fibres de lin et de papier).

La résistance au cisaillement du renfort est un indice de qualité assurant que les fils restent autant que possible intacts (alignés) lors de la manipulation du renfort et autant que possible pendant l'injection de la résine. La perméabilité et la performance à la traction du composite (particulièrement sa rigidité spécifique) constituent pour leur part les bases permettant d'évaluer si des pièces composites fabriquées à partir de ce renfort peuvent concurrencer les composites à fibres de verre.

Les paramètres étudiés du renfort comprennent la densité surfacique (ou grammage) des couches de lin et de papier, la pression de formation de renfort, ainsi que sa température de séchage. De plus les effets des différents taux de fibres et des différentes configurations (architectures) du renfort sont aussi étudiés. La possibilité de produire le renfort hybride UD

lin/papier à grande échelle (machine d'Innofibre du Cégep de Trois-Rivières) est finalement évaluée.

Selon la définition théorique de la conception robuste, un produit ou un procédé est robuste s'il est peu sensible aux effets des sources de variabilité rencontrées dans son cycle de vie, même si les sources elles-mêmes n'ont pas été éliminées. Considérant que les propriétés des fibres naturelles ont une variabilité inhérente, un objectif important de cette thèse consiste à étudier l'influence des différents paramètres sur la variation des propriétés pour ainsi appliquer une méthode de conception paramétrique robuste du nouveau renfort.

À plus long terme le projet consiste à fabriquer des pièces composites de géométries et dimensions arbitraires en utilisant le renfort hybride UD lin/papier. Ce projet, lancé au laboratoire de mécanique et éco-matériaux (LMEM) en 2010, se compose de quatre phases : choix des constituants, conception de renforts, étude du comportement de composites plans, et finalement moulage et conception de pièces composites plus complexes. Toutes ces phases ne peuvent bien sûr être adressées dans un seul projet de thèse. Pour cette raison, dans cette thèse seule les phases de conception (paramétrique robuste) du renfort et d'analyse de son comportement sur des échantillons planaires sont adressées.

Matériel et méthodes

Les bobines de fils de lin sont fournies par Safilin (France) est sont faites à 100 % de lin européen. Des densités linéaires (Tex) de 200 g/km et 400 g/km sont utilisées dans cette étude. La pâte à papier Kraft d'une consistance de 10 % est fournie par Innofibre. Pour mouler les plaques composites, une résine Adtech Marine 820 epoxy mélangée avec 18 % en

poids de durcisseur Marine 824 est utilisée. Le fluide utilisé pour les essais de perméabilité est l'huile moteur SAE 20W-50.

Pour fabriquer les échantillons de renfort en laboratoire, quatre étapes principales sont requises. Premièrement, l'alignement des fils de lin permet de développer la couche unidirectionnelle. La couche de papier Kraft est ensuite fabriquée en milieu humide sur une formette dynamique. La couche de fils de lin et la feuille humide sont ensuite assemblées par pressage entre rouleaux. Le renfort hybride résultant est finalement séché sur rouleau chauffant. Lors des deux dernières étapes, des liaisons mécaniques et chimiques sont développées entre les fibres de lin UD et de papier.

Pour fabriquer le renfort hybride lin/papier sur la machine à papier d'Innofibre, les fils de lin sont alimentés sur la table de formation de la machine. Ceci est réalisé en utilisant un support d'alimentation spécialement conçu à cet effet. Jusqu'à 16 bobines peuvent y être installées. Afin d'ajuster l'espace entre les fils de lin, différents peignes calibrés sont utilisés. Trois types de peignes ont été utilisés dans cette étude pour permettre des espacements différents entre les fils. Le premier peigne permet d'alimenter dix fils au total avec un pouce d'espace entre chacun. Les deux autres peignes permettent d'alimenter seize fils par pouce. Les renforts produits avec les deux derniers peignes peuvent être utilisés dans les matériaux composites unidirectionnels, alors que ceux obtenus avec le premier peigne pourraient être potentiellement utilisés dans des applications d'emballage renforcé.

La résistance au cisaillement entre les fibres de lin et de papier (appelée 'Internal Bond Strength' ou IBS dans cette thèse) est estimée avec une méthode initialement développée

pour les papiers. La méthode originale a été modifiée pour s'adapter au renfort de cette étude. Des échantillons de 25 mm × 150 mm (1 po. × 6 po.) sont préparés. À chaque bout, soit la couche de papier, soit les fils de lin, sont décollés de telle manière qu'au milieu de l'échantillon il ne reste qu'une zone de 25 mm × 25 mm (1 po.^{2}) où les deux couches co-existent. Ensuite, les échantillons sont soumis à une force de traction engendrant une force de cisaillement (convertie en valeur IBS) dans la zone jointée.

Le moule de perméabilité développé dans cette étude se compose d'une plaque supérieure en verre trempé de 19 mm d'épaisseur. La plaque inférieure est faite d'acier inoxydable d'une épaisseur d'un pouce. La plaque de verre trempé permet la visualisation et le suivi du front d'écoulement. Le verre est trempé pour assurer une déflexion négligeable sous l'effet de la pression d'injection. Des cales de précision Starrett ont été utilisées pour ajuster la hauteur de la cavité. Cet ajustement est nécessaire au contrôle du taux de fibres. Au milieu de chaque échantillon de renfort, un trou de diamètre de 12 mm est percé pour créer un point d'injection et améliorer la précision des résultats de perméabilité. L'huile moteur est finalement injectée sous un vide constant de 100 kPa fourni par une pompe à vide connectée aux quatre coins du moule.

La mesure de perméabilité se décline en diverses catégories : perméabilité saturée ou insaturée, perméabilité à pression d'injection constante ou à débit d'injection constant, perméabilité unidirectionnelle (1D) ou radiale (2D). Dans cette étude, la perméabilité insaturée est mesurée en utilisant l'injection radiale à pression d'injection constante. La mesure est basée sur les rayons majeur et mineur instantanés du front d'écoulement elliptique. Les données

temporelles sont ensuite traitées selon une méthode développée dans la littérature pour l'écoulement radial d'un fluide dans un milieu poreux orthotrope, afin de calculer la perméabilité K_1 dans le sens des fils de lin et la perméabilité K_2 dans le sens perpendiculaire aux fils de lin.

Pour mesurer les rayons majeur et mineur du front d'écoulement, un code de Matlab® a été développé (appelé 'code A' dans cette thèse). Ce code interpole une ellipse théorique sur le front d'écoulement et calcule la longueur instantanée des rayons majeur et mineur en unité de pixel. La connaissance des dimensions de l'ellipse (en utilisant deux règles perpendiculaires dans les images captées) permet de convertir les unités de pixels en dimensions physiques. Un autre code de Matlab® (appelé 'code B' dans cette thèse) est aussi utilisé pour calculer les valeurs de K_1 et K_2 à partir des rayons majeur et mineur et leurs temps d'injection correspondants. La validité des deux codes A et B a été vérifiée par comparaison avec des mesures directes.

Le moulage par transfert de résine ('Resin Transfert Molding' ou RTM) est utilisé pour fabriquer les plaques de composite à partir du renfort hybride UD lin/papier. Les parties inférieure et supérieure du moule sont dans ce cas toutes deux faites d'acier inoxydable (déflexion négligeable pendant l'injection de résine). Comme pour le moule de perméabilité, des cales de précision sont utilisées pour ajuster la hauteur de la cavité et ensuite le taux de fibres. Pour tous les composites fabriqués dans cette étude, huit couches de renfort sont empilées. Le montage de RTM permet une pression d'injection de 4 bars et dans ce cas, l'imprégnation du renfort se fait de façon unidirectionnelle.

Des renforts à un taux volumique de fibres de 35 % sont d'abord imprégnés. À la fin de l'injection, la plaque supérieure du moule est déplacée vers le bas en serrant les vis, pour atteindre le taux de fibres désiré. L'excès de résine est ainsi évacué du moule. Cette technique permet de bien imprégner le renfort (faible taux de vide ou porosité) malgré la faible perméabilité de la couche papier. Après le moulage les plaques composites sont maintenues à 80°C pendant 4 heures pour assurer une polymérisation complète.

Pour l'essai de traction réalisé selon la norme ASTM D3039, des échantillons de dimension 250 mm × 15 mm sont coupés à partir des plaques moulées. Au moins cinq échantillons sont testés pour chaque type de composite (4 répétitions). Les composites à fibres naturelles montrent un point d'inflexion ('knee point') durant l'essai de traction et donc leur courbe de traction est bilinéaire. Le module avant le point d'inflexion (E_1) est estimé dans l'intervalle de déformation de 0.025-0.1 %, et un autre module après le point d'inflexion (E_2) est estimé dans l'intervalle de déformation de 0.3-0.4 %.

Les causes principales de variabilité (écart-type) dans les résultats de cette étude incluent les procédés de fabrication (comprenant tant la fabrication du renfort sec que du composite), les méthodes de mesure (IBS, perméabilité, propriétés en traction), le facteur humain (erreurs de manipulation et d'expérimentation), ainsi que la variabilité du matériau naturel. Cette dernière inclut la variabilité inhérente des propriétés des fibres naturelles ainsi que la variabilité associée aux valeurs (niveaux) des paramètres matériau utilisés dans les plans d'expérience. Les incertitudes liées aux procédés de fabrication sont ici limitées par le développement d'un processus de fabrication de haute qualité. Il en va de même pour les incertitudes liées aux

mesures (caractérisation du matériau). La méthode de conception paramétrique robuste utilisée dans cette thèse adresse donc la variabilité associée aux valeurs (niveaux) des paramètres du matériau.

Un algorithme tiré de la littérature est utilisé pour réaliser la conception paramétrique robuste. Selon cet algorithme, deux prérequis devraient être vérifiés pour les paramètres matériau afin de permettre l'optimisation robuste. Premièrement, il devrait y avoir au moins un paramètre qui affecte la moyenne et un paramètre qui affecte l'écart-type des résultants. Deuxièmement, la relation entre ces paramètres devrait mener à un résultat quadratique.

Un plan d'expérience avec quatre paramètres du renfort, chacun à deux niveaux (nommé '1er Design Of Experiment' ou 1er DOE), est considéré pour évaluer le premier prérequis. Les paramètres dans ce plan d'expérience incluent la densité surfacique de la feuille de papier (paramètre A), la densité surfacique de la couche de lin (paramètre B), la pression de formage (paramètre C) et la température de séchage (paramètre D). Les échantillons de renfort sont fabriqués selon ce 1er DOE, à partir duquel les propriétés d'IBS, les perméabilités K_1 et K_2 ainsi que les performances en traction sont tirées.

Résultats

IBS

Des composants à base de cire sur la surface des fils de lin ont été prélevés en utilisant un extracteur Soxhlet. L'analyse des composants par spectroscopie infrarouge à transformée de Fourier (FTIR) montre qu'ils contiennent un grand nombre de groupements chimiques de type CH_3. Ces groupements chimiques sont capables de créer des liaisons de Van der Waals

entre eux ainsi qu'avec des groupements hydroxyle libres (OH) sur la chaîne moléculaire de cellulose des fibres de papier. En conséquence, il est supposé que la présence d'un grand nombre de liaisons Van der Waals entre groupements chimiques CH_3 et groupements hydroxyle libres (OH) est la raison principale de la cohésion entre la couche de papier et les fils de lin.

Les essais IBS sont exécutés sur les échantillons de renfort fabriqués selon le 1^e DOE. En général, les résultats montrent un coefficient de variation (C_V) assez élevé (entre 18% et 52%). Ceci pourrait être le résultat de l'utilisation d'une trop faible zone de contact (25 mm × 25 mm) entre la couche de papier et les fils de lin dans les échantillons testés. De plus, la liaison de Van der Waals est très faible, ce qui peut rendre la mesure IBS plus variable. Malgré cela, l'analyse d'ANOVA sur les résultants indique que les valeurs moyennes d'IBS augmentent avec la densité surfacique du papier (facteur A) et la température de séchage (facteur D), alors qu'ils diminuent avec l'augmentation de la densité surfacique de la couche de lin (facteur B) et avec la pression de formage (facteur C). D'autre part, aucun facteur n'influence l'écart type des résultats d'IBS, selon la méthode expliqué à l'annexe F.2. Par contre, le graphe des tendances montre clairement que la température de séchage a un effet plus marqué sur le coefficient de variance (C_V). La moyenne de C_V est en effet réduite d'environ 20 % lorsque la température de séchage est à son niveau élevé.

Perméabilité

Toujours selon le 1^{e} DOE, l'analyse ANOVA sur les résultats de mesure de la perméabilité indique que la densité surfacique de la couche de lin (facteur B) est le seul facteur influençant significativement tant la moyenne que l'écart-type de la perméabilité K_1. Cette observation s'explique par la distance entre les fils. En effet, il y a toujours un chemin d'écoulement étroit entre les fils adjacents des échantillons à 16 fils/pouce (facteur B au niveau bas). D'une part, ces chemins d'écoulement laissent la résine s'écouler plus vite et plus facilement entre les fils, comparativement aux échantillons avec 24 fils/pouce (facteur B au niveau haut). D'autre part, en empilant des couches de lin de 16 fils/pouce pour obtenir la préforme, le plus grand espace inter-fils résulte en des empilements où les fils des couches successives soit parfois en vis-à-vis (en phase), parfois en intercalage (déphasés). Dans les couches de 24 fils/pouce, les fils sont beaucoup plus régulièrement disposés d'une couche à l'autre et cet effet de phase ('nesting') est ainsi minimisé.

L'analyse des résultats de la perméabilité K_2 montre que tous les facteurs ont une influence sur la moyenne tandis qu'aucun n'a d'influence sur l'écart-type. Selon le graphe des tendances, les facteurs B et C font augmenter la moyenne de K_2, alors que l'effet des facteurs A et D est inverse.

Pour évaluer le comportement en perméabilité de chaque renfort dans de vraies conditions de moulage, deux empilements de renforts de 24 fils/pouce et 16 fils/pouce sont moulées par injection de résine à une pression de 100 kPa. Dans chaque composite deux zones elliptiques sont distinguées : une région intérieure totalement saturée par la résine (nommée région I),

et une région extérieure partiellement saturée par la résine (nommée région II). En injectant à pression constante le front d'écoulement atteint sa vitesse la plus élevée au point d'injection. Au fur et à mesure qu'il progresse dans le moule sa vitesse diminue. La région I correspond aux vitesses élevées. Les forces visqueuses sont alors dominantes et la résine passe entre les fils (en créant également des micro-vides à l'intérieur des fils). La région II correspond aux vitesses plus faibles. Les forces capillaires sont alors dominantes et la résine passe au travers des fils (en créant également des macro-vides entre les fils). Cette dynamique est confirmée par des micrographies de chaque région où l'on perçoit clairement que la région II contient plus de vides. Les échantillons tirés de chaque région montrent également une densité plus élevée dans la région I. À une certaine distance du point d'injection il existe une vitesse optimale pour laquelle le taux de vide final dans la plaque est théoriquement minimum. Cet aspect n'est pas traité ici et fera l'objet d'études ultérieures.

Tel que mentionné précédemment, la densité surfacique de la couche de lin (facteur B) est le seul facteur qui influence à la fois la moyenne et la variance de la perméabilité K_1. Ceci permet donc de faire une optimisation robuste selon ce facteur. Comme le taux volumique de fibres (facteur E) est depuis longtemps reconnu comme un des paramètres les plus importants pour une étude de perméabilité, ce deuxième facteur a également été inclus dans un deuxième plan d'expérience (appelé 2^e DOE) duquel un modèle de régression pour la prédiction de la moyenne de K_1 est tiré. Deux modèles sont aussi utilisés pour la prédiction de l'écart type de K_1. Le premier est une régression tirée des résultants expérimentaux (appelé modèle R) et le deuxième est plutôt obtenu par la méthode de propagation de l'erreur (appelé modèle P).

Une optimisation bi-objective pour maximiser la moyenne et minimiser l'écart-type est ensuite réalisée sur les deux modèles avec un algorithme génétique. Les deux optimisations (sur le modèle R et sur le modèle P) convergent vers le même point optimal quand le coefficient de pondération pour les deux termes d'optimisation bi-objective est ajusté à 0.5. Il est déduit que le point optimal robuste pour la perméabilité K_1 est :

Paramètre E : $V_f = 0.35$

Paramètre B : Couche de lin UD à 24 fils/pouce

Une étude comparative de la perméabilité du renfort optimal UD lin/papier avec des renforts UD lin sans papier a été effectuée. Il a été démontré que la couche papier permet de réduire l'écart-type de la perméabilité K_1. Ce résultat contribue également à la conception robuste du nouveau renfort.

Densité surfacique

Outre les effets évidents de la densité surfacique des couches de papier et de lin sur la densité surfacique du renfort, une autre analyse ANOVA indique que la température de séchage affecte elle aussi significativement la densité surfacique. Pour l'expliquer, nous partons premièrement du phénomène déjà connu qu'un renfort fibreux humide prend de l'expansion quand il est exposé au flux de chaleur du séchoir. De plus, le séchage s'effectue en pressant le renfort entre un feutre et un rouleau chauffant. Cette combinaison antagoniste chauffage-pression lors du séchage semble à l'origine de l'influence de ce paramètre sur la densité surfacique du renfort résultant.

Ce résultat est d'une grande importance en pratique car densité surfacique du renfort influence le taux volumique de fibre, ce dernier ayant lui-même un impact majeur sur les propriétés mécanique du composite final. Il est donc important de bien contrôler la température de séchage du renfort pendant sa fabrication pour diminuer l'écart type des propriétés finales des pièces composites résultantes.

Propriétés en traction

L'analyse ANOVA sur les propriétés mécaniques en traction des composites obtenus selon le 1er DOE montre qu'aucun des quatre paramètres n'a d'influence statistiquement significative sur l'écart type des résultats. Cela indique que les conditions de fabrication des composites étaient toujours consistantes. Il est aussi rapporté dans quelques articles récents que l'écart-type des propriétés des composites est principalement influencé par la qualité de la fabrication plutôt que la variation inhérente des propriétés mécaniques des fibres naturelles, en raison de l'effet 'averaging' des fibres dans le composite.

Les résultats de l'ANOVA indiquent que les trois paramètres densité surfacique de papier (facteur A) et de lin (facteur B) ainsi que la température de séchage du renfort (facteur D) ont influencé la moyenne de la résistance ultime en traction du composite. Le seul paramètre ayant influencé les deux modules E_1 et E_2 est le facteur B. Le facteur A présente une corrélation inverse sur la moyenne de résistance du composite alors que les facteurs B et D ont une corrélation directe. La relation entre les modules (E_1 et E_2) et le facteur B est aussi une corrélation directe.

Les images microscopiques de la section transversale des composites montrent que la porosité (vides représenté par des lignes minuscules noires autour des fibres) est concentrée autour des fibres de Kraft (couche papier). Il est conclu que lorsque le facteur A augmente et que par conséquent la quantité des fibres de papier augmente, le composite comporte plus de porosités et donc sa résistance diminue.

Il est documenté dans la littérature que le séchage favorise la formation de liaisons fibres-fibres dans les matériaux cellulosiques. Le séchage du renfort à température plus élevée augmente donc la cohésion des fils de lin entre eux. Il en résulte une augmentation de la résistance du composite moulé avec une augmentation de la température de séchage du renfort.

La rigidité spécifique de l'éco-composite final est supérieure à celle d'un composite de fibres de verre pour un même taux de fibres. Ce résultat très important pave la voie à des applications industrielles du renfort étudié. Il pourrait potentiellement être utilisé dans l'industrie automobile, aéronautique, sports et des loisirs ainsi que dans le secteur du bâtiment.

Abstract

Canada is the world's largest producer of flax. However, most of the flax fibers are used either for food production or to weave into clothing and blankets. So, by developing reinforcements of flax fibers to be used in polymeric composites, there is an opportunity to not only produce value-added products, but also be more environmentally friendly. Flax fibers are characterized by a higher specific stiffness (stiffness divided by density) than glass fibers and therefore can be considered as a potential replacement of glass fiber in composite parts. In order to develop flax fiber composites that can be used in load-bearing structures unidirectional reinforcement of flax fibers must be developed.

This thesis aims at developing a new unidirectional flax/paper reinforcement with interesting properties in terms of permeability, tensile mechanical properties and bonding strength between paper and flax fibers in the dry reinforcement. To study and model the important reinforcement parameters on the concerned properties, the classical robust parameter design approach is considered. Moreover, high quality fabrication and characterization methods are developed to yield consistent results. Feasibility of mass scale production of the hybrid unidirectional flax/paper reinforcement on the pilot paper machine of Innofibre is also studied.

To study the reinforcement on a laboratory scale two material parameters, including surface density of the paper sheet and the surface density of the flax layer, as well as two fabrication parameters, including forming pressure and drying temperature, are considered. Effects of these parameters are studied on three properties of the material, comprising the cohesion between the two reinforcement layers (flax and paper), reinforcement permeability

and mechanical properties of the final eco-composite. For the modeling aspect, the design of experiment followed by statistical modeling are used. In addition, effects of different reinforcement architectures as well as the fiber volume fraction are studied through comparative studies.

Effect of temperature on improving the flax- paper cohesion and decreasing its standard deviation in the dry reinforcement was identified. Mean and standard deviation of the permeability along the yarns' direction (K_1) is mainly influenced by surface density of the flax layer. So, this parameter must be adjusted to its maximum value to reduce the standard deviation. It has been shown that the temperature has a statistically significant effect on the reinforcement surface density as well as strength of the eco-composite. Although temperature effect on mean values of surface density and strength could be marginal from an engineering point of view, it is concluded that it should be adequately controlled during manufacturing process of the reinforcement to minimize variance of mechanical properties results. Through comparative studies, it was shown that the paper layer reduces the standard deviation of the K_1 permeability and tensile properties of eco-composite. These results show that the flax/paper reinforcement has a robust architecture compared to sole layer of unidirectional flax. Specific stiffness of the final eco-composite is found to be higher than that of a UD glass fiber composite, at the same fiber volume fraction. This very important finding paves the way for industrial applications of the studied reinforcement. This material could be potentially used in the automotive industry, aerospace, sports as well as the building sector.

The flax yarns are fed into the pilot paper machine of Innofibre and then at the exit of the machine, the paper sheet reinforced by unidirectional flax yarns was rolled up successfully. This result, proves that the mass scale fabrication of reinforcement is feasible and therefore paves the way for attracting industrial interest and also reducing its production costs.

Dedication

To my mother and father.

Acknowledgements

I express my appreciation to my supervisors, Professor Gilbert Lebrun and Professor Luc Laperrière for their guidance and tremendous amount of support during my thesis research efforts.

I express my gratitude to Dany Lemay and Jonathan St-Arnaud, for their tremendous amount of technical support and kind advice given to me through my PhD work at the Laboratory of Mechanics and Eco-Materials of the Université du Québec à Trois-Rivières.

I also acknowledge Jean Paradis of Innofibre from Cégep of Trois-Rivières for his technical advice and preparation and supplying Kraft pulp as well as providing pilot paper machine.

I thank Professor François Brouillette (Lignocellulosic materials research center of the UQTR) and Meriem El Boustani (PhD student) for giving advice on the chemistry aspects of this research.

Funding of the Natural Sciences and Engineering Research Council (NSERC) of Canada is very much appreciated.

My great thanks goes to my family for their unwavering support during the years of my studies.

Table of contents

List of tables

List of figures

List of equations

List of symbols

α	probability of committing type I error / weighting coefficient for bi-objective optimization
$\hat{\beta}, \hat{\gamma}, \hat{\delta}$	regression coefficients
φ	porosity of reinforcement preform
μ	dynamic viscosity of testing liquid (pa.s)
$\bar{\mu}_{y_2}(\boldsymbol{x})$	mean response model
γ	surface tension of test fluid
ρ_A	surface density of paper sheet (g/m^2)
ρ_f	fiber density (g/m^3)
ρ_c	composite density (g/m^3)
ρ_m	matrix density (g/m^3)
$\sigma_{\hat{y}_2}$	standard deviation response model
$\hat{\sigma}^r_{k_1}, \hat{\sigma}_{k_1}$	regression model for standard deviation of K_1 permeability
$\hat{\sigma}^p_{k_1}$	propagation of error model for standard deviation of K_1 permeability
σ^2	residual mean square of regression model
$\hat{\sigma}_u$	regression model for average of composite strength
σ_x	standard deviation of single measurement of a given parameter
$\sigma_{\bar{x}}$	standard deviation of the average of a given parameter
$\sigma^2_{z_i}$	variance of i^{th} noise factor
A	codded setting for paper surface density
A_{fabric}	surface area of forming fabric (m^2)
a	number of levels for each factor
B	codded setting for flax layer surface density
$\hat{b}$	regression coefficient
b	column of regression coefficients
C	pulp consistency (%) / codded setting for forming pressure

$Ca\#$	capillary number
D	codded setting for drying temperature
d_j	distance between the largest and smallest actual setting of factor j
df_r	degree of freedom of each run
df_E	degree of freedom of error
df_A	degree of freedom for factor A
E	codded value for fiber volume fraction
E_1	tensile modulus of NFC before knee point
E_2	tensile modulus of NFC after knee point
$\hat{E}_1$	regression model for average of E_1
$\hat{E}_2$	regression model for average of E_2
f_j	actual setting for input factor j
$\bar{f}_j$	average of all the actual setting for factor j
F_C	critical F value from F-distribution
F_0	F value for ANOVA
$\vec{g}$	gradient vector
h	height of cavity (m)
$\widehat{IBS}$	regression model for average of IBS
[k]	permeability tensor (m^2)
k_e	equivalent permeability
K_1	permeability in the yarns direction (m^2)
$\widehat{K}_1$	regression model for average K_1 permeability
K_2	in-plan permeability perpendicular to the yarns direction (m^2)
$\widehat{K}_2$	regression model for average K_2 permeability
K	number of factors in an experimental design
k_1	conversion factor in Taguchi loss function
k_2	number of controllable factors
L_A	number of levels of factor A

L_i	i^{th} loss function value
$\bar{L}$	average loss function value
L	quality characteristic target
M_f	mass of dry fiber in stock slurry (g)
M_a	mass of non-fibrous additives in stock slurry (g)
M_w	mass of water in stock slurry (g)
m_f	average surface density of flax layer (g/m^2)
m_p	average surface density of paper layer (g/m^2)
m_r	average surface density of hybrid reinforcement (g/m^2)
m_1	slope of R_1-R_2 graph
m_2	slip of F function-time graph
n	sample size / number of reinforcement layers
n_r	number of runs / number of reinforcement samples
n_p	number of paper samples
n_{Aj}	total number of response values for factor A at level j
n_{rep}	number of repeated tests in a DOE
∇p	vector of pressure gradient
R_{1i}	major radius of flow front ellipse at the time t_i
R_{1ie}	equivalent R_{1i}
R_{2i}	minor radius of flow front ellipse at the time t_i
R_0	inlet radius
R_{0e}	equivalent R_0
r	number of noise factors
s	sample standard deviation
s_r^2	variance of run r
S/N	signal to noise ratio
t_i	time at i^{th} time step (sec)
tex	linear density of flax yarn (g/1000m)
$\bar{u}$, v	superficial fluid velocity

V_f	fiber volume fraction (%)
V_m	matrix volume fraction (%)
V_v	void volume fraction (%)
W_f	fiber weight fraction (%)
W_m	matrix weight fraction (%)
x	input factor or codded setting for input factor
x_i	single measurement values for a given parameter
$\bar{x}_i$	average of measured values for a given parameter
X	matrix of DOE
Y	column of response values
y_i	i^{th} response
y_{ri}	i^{th} replicated response value at run r
$\bar{y}$	average of response values
$\bar{y}_r$	average of response values at run r
$\hat{y}$	predictive regression model
$\bar{Y}_{Aj}$	average of response values at level j of factor A
$\bar{\bar{Y}}$	grand average of all the data
z_i	i^{th} noise factor

List of abbreviations

ANOVA	Analysis of variance
ASTM	American society of testing methods
CCD	Central composite design
C_V	Coefficient of variance
CSF	Canadian standard freeness
DOE	Design of experiment
DSF	Dynamic sheet former
DSC	Differential scanning calorimetry
DMA	Dynamic mechanical analysis
EVA	Ethylene-vinyl acetate
Ff	Feather fiber
FACF	Fiber area correction factor
FTIR	Fourier transfer infrared
FP-400	Flax/paper tex 400
FP-200	Flax/paper tex 200
FP-200-40	Flax/paper tex 200 at $V_f = 40$ %
FP-200-45	Flax/paper tex 200 at $V_f = 45$ %
gMA	Glycidyl methacrylate
HDPE	High density polyethylene
IBS	Internal bonding strength
IR	infrared
Kf	Kenaf fiber
LPDE	Low density polyethylene
LCM	Liquid composite molding
LMEM	Laboratory od mechanics and eco-materials
MLR	Multiple linear regression
MSE	Mean square of error

MSB	Mean square between
NF	Natural fiber
NFC	Natural fiber composite
Nf	Newspaper pulp fiber
OM	Optical microscope
PDUDF-200	Pressed, dried UD flax tex 200
PLLA	L-polylactic acide
PLA	polylactic acide
PP	polypropylene
PET	Polyethylene terephthalate
PMC	Polymer matrix composites
PS	Polystyrene
PVC	Polyvinyle chloride
PVOH	Polyvinyl alcohol
PHB	3-hydroxyl butyrate
PBAT	Polybutylene adipate co terephthalate
PBS	Poly butylene succinate.
PFC	Plant fiber composite
Pf	Pulp fiber
RTM	Resin transfer molding
ROM	Rule of mixture
SEM	Scanning electron
SFP-200	Separated Flax/Paper tex 200
TGA	Thermogravimetric analysis
tpm	Turn per meter
TEA index	Tensile energy absorption
UD	unidirectional
UDF-200	UD flax tex 200

Preface

The thesis report consists of 5 chapters. In Chapter 1 a general introduction to the subject is given. Several aspects of natural fibers and their composites have been introduced based on the literature. In chapter 2 it is tried to represent more relevant aspects to the works of this study by reviewing some of the most interesting articles from each category and then the motivation and research objectives of this thesis are described. It is explained that this thesis is part of a long term project aiming at developing natural fiber composite parts having complex geometries. Materials and methods used in this thesis are described in chapter 3. Materials include flax and Kraft pulp fibers as well as epoxy resin and permeability test fluid and the methods comprise laboratory and pilot scale reinforcement fabrication, shear cohesion test, permeability measurement and composites molding and testing. Robust parameter design approach for studying the reinforcement is also described. In chapter 4 experimental results of shear cohesion tests, permeability, composite tensile test as well as pilot scale fabrication of reinforcement with a paper machine, are presented and discussed. At the end, a comprehensive conclusion in chapter 5 gives an overview on the outcomes of this thesis.

CHAPTER 1: INTRODUCTION

1.1. Statement of the problem

In recent times, the exploitation of natural fibers as reinforcing element in polymer composite materials has attracted noticeable attention from scientists and researchers. In fact, after decades of high-tech development of petroleum based plastics and non-biodegradable fibers such as glass, aramid and carbon, the huge increase of material waste has led to disposal problems as well as environmental consequences. Due to this fact, significant scientific research has been directed toward environmentally friendly, sustainable eco-composite materials. These materials are made of natural fibers (NF), mostly cellulose based ones, being impregnated with bio-sourced matrix. In this section the motivations of this global tendency will be discussed.

The application of natural fibers as reinforcement in composite materials dates back to some 3,000 years ago, when the Egyptians used straw reinforced clay to build bricks and walls [1]. Generally speaking, natural fibers are classified into three major groups: cellulose based (plant) fibers as well as animal and mineral ones. As Figure 1-1 illustrates, cellulose based (plant) fibers, as the most important group of natural fibers, are further classified into straw fibers (e.g. corn, wheat and rice straws), bast fibers (e.g. flax, jute, hemp and kenaf), leaf fibers (e.g. sisal, henequen, pineapple leaf fiber), seed/fruit fibers (e.g. coir and cotton),

grass fibers (e.g. bamboo and elephant grass, miscanthus) and wood fibers (e.g. softwood and hardwood) [2]. Flax (Linum usitatissimum) is probably the oldest textile fiber known to mankind. The first well documented application is the use of the linen fabric by the Egyptians to wrap their mummies. This fiber has been used as the basis for fabric not only for clothing but also for sails, tents and war outfits until around 1950, when after that synthetic fibers took over [3].

It is worth mentioning that implementation of plant fibers as reinforcement for polymers has its own advantages and difficulties which need to be considered before their application. On the plus side, employing natural fibers results in positive environmental impacts due to less energy consumption for production, and budget zero CO_2 emissions if recycled.

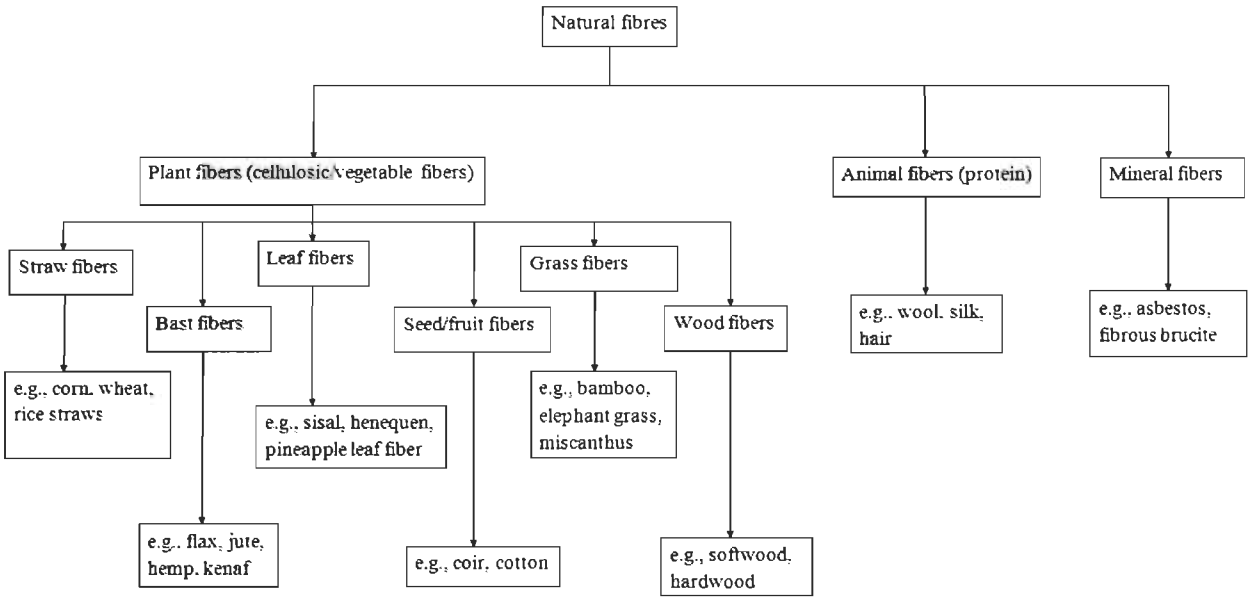

Figure 1-1. Classification of natural fibers

In addition, they are renewable compared to synthetic fibers thus yielding lower cost and less reliance on foreign oil sources. Some other points include low density that brings about high specific properties (particularly specific modulus), health benefits as they are not suspected to cause lung cancer or skin irritation for those involved in production and manipulation, low wear and abrasion on processing tools and good acoustic insulation due to their low density and cellular structure.

On the negative side, hydrophilic nature of fibers results in poor resistance towards moisture absorption and lack of good interfacial adhesion with the matrix which in turn results in inferior mechanical properties. Furthermore, variability of properties due to quality of the harvest and growing conditions as well as extraction techniques and processing operations, could be conflicting with the normal industrial demand of constant product quality. Moreover, lack of heat resistance is another limitation of natural fibers. Table 1-1 briefly summarizes some pros and cons of natural fibers.

Apparently the total balance of properties comes out positive since the major disadvantages like water absorption and low interfacial adhesion can be addressed through chemical or physical treatment of fibers surfaces. In addition their variable quality can be taken into account in the engineering design phase.

Currently most flax fibers around the world are either processed into pulp for special papers (e.g. paper of cigarettes, currency, artwork, etc.) or woven into cloths and blankets. Otherwise they are incinerated in the fields. So there exists an opportunity to not only produce higher value-added products but also to be more responsible towards the environment. As

Table 1-2 indicates, it is documented in the literature that the specific stiffness (stiffness divided by the density) of flax fiber can compete well with some categories of E-glass fibers and it could be considered as a replacement of E-glass fibers for composite parts. On the other hand, unidirectional (UD) glass fiber reinforced composites are often used in load bearing constructions, like wind turbine blades, foot bridges or structural composites for the automotive industry. However, fewer studies have dealt with load bearing composites based on continuous natural fiber reinforcements compared to chopped randomly oriented natural fiber reinforcements (mat) which have already been implemented in industry to produce non-structural parts such as car interior trims [4-10].

Table 1-1. Advantages and disadvantages of natural fibers

Advantages	**Disadvantages**
Lower costs	Poor dimensional stability
Biodegradable	Kink band fractures [11]
No CO2 emission	Low resistance to moisture
Sound damping	Low interfacial adhesion
Low energy requirement for production	Hydrophilic- hydrophobic interaction
No health hazard	Operating condition limited to the temperature
Renewable	Water absorption
Excellent specific module	Variable quality
Reduced abrasion of the tools	Biodegradable

In a nutshell, the objective of this research is characterization of a hybrid unidirectional flax/paper reinforcement in terms of permeability to liquid resin, tensile behaviour of the composites as well as the dry shear strength between flax and paper layers of the reinforcement. Since variability of the properties is an inherent characteristic of natural fibers, it is also aimed at studying the variability reduction of the properties. The feasibility of fabricating this hybrid reinforcement by a pilot-scale paper machine is also studied.

However, throughout this thesis only laboratory-made reinforcements are used for permeability measurements, composites fabrication and dry shear strength measurement.

Table 1-2. Comparing Flax and E-glass fibers' properties

Fiber type	Density (g/cm^3)	Tensile modulus (GPa)	Specific tensile modulus ($GPa/g\ cm^{-3}$)	Tensile strength (MPa)
Flax fiber [12]	1.45-1.55	28-100	19-65	343-1035
Flax fiber[13]	1.4-1.5	27.6-103	45	343-2000
Flax fiber [14]	1.53	58±15	38	1339 ± 486
E-Glass [12]	2.55	78.5	31	1956
E-Glass [14]	2.55	71	28	3400

1.2. **Background**

1.2.1. Cellulose based natural fibers

Figure 1-2 shows the structure and processing of a typical bast fiber from plant stem up to the nanoscale microfibrils. As can be seen the fiber bundles are situated in the periphery of the stem and are continuous throughout the stem length. After harvesting, the stems are exposed to a microbial process named retting. The goal of retting is to break down the chemical bonds which interconnect the fiber bundles. Next, the fibers are extracted and reorganized by some mechanical processes like scutching, defibration, hackling (combing) and drafting, respectively. The scutching process includes two steps namely breaking and swingling. In the breaking step, the core of the stems is broken into small lengths using a pair of profiled rotating rolls. In this step short pieces called shives are detached from fiber bundles which are removed in the swingling step. After scutching the fiber bundles are only partially separated. Therefore a process named defibration is further applied on the fiber bundles to separate even more the technical fibers from fiber bundles. Commonly the collection of fibers that come

out of the defibration process are referred to as filaments. The hackling and drafting steps are used to minimize the variation of properties within the final yarn. The hackling stage aims at aligning the fibers and removing a portion of the shortest fibers. This is accomplished through passing filaments into series of pinned rollers that comb out the short and tangled fibers and align the long fibers. In the drafting process the technical fibers are passed through a series of rollers in order to straighten out the technical fibers [1, 2]. A number of spinning techniques exists to spin discontinuous technical fibers, coming from the drafting process, into yarn. Some of them for instance include ring spinning, rotor spinning, wrap spinning and air-jet spinning.

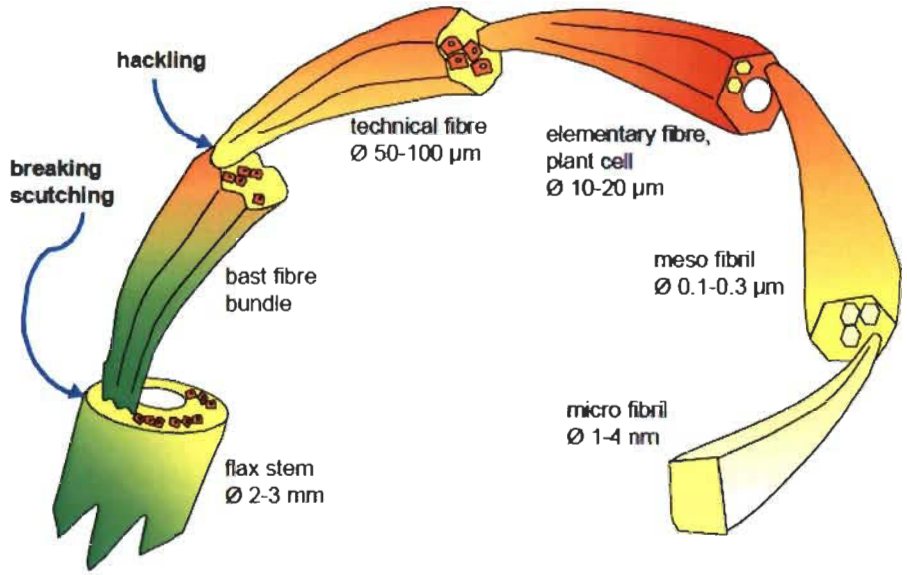

Figure 1-2. Schematic representation of flax fibers processing, from stem to micro fibrils [3].

An elementary plant fiber as a building block of eco-composites is itself an advanced composite material. Figure 1-3 shows a schematic of a unit cell made of crystalline cellulose microfibrils in an amorphous hemicellulose-lignin matrix. Beginning from the outside of the

wall, Figure 1-3 shows that the elementary fiber consists of four layers namely the primary wall, the secondary 1 layer, S_1, the secondary 2 layer, S_2, and the secondary 3 layer, S_3. The hole in the center of the fiber is called the lumen and the region surrounding the fiber is called the cuticle in the case of bast fibers. As S_2 layer is by far the thickest one, it is the most important determinant of the mechanical properties of the fiber. At a higher level, 10 to 40 of these elementary fibers are bundled together with amorphous pectin to form technical fiber with a diameter of about 50 to 100 μm.

As can be seen in Table 1-3, natural fibers have a lower density compared with E-glass fibers, resulting in a higher specific modulus and comparable specific strength. These days, the mostly used natural fiber in composite materials is flax fiber due to its better mechanical properties and availability compared to other natural fibers. Other fibers like hemp, jute, kenaf and sisal are also being used.

Since wood and bast fibers both belong to the cellulose based group of natural fibers, the morphological proportion, characterized by high aspect ratio, and chemical composition of their elementary fibers resemble each other. Tables 1-4 and 1-5 compare the dimensions and chemical characteristics of wood fibers (softwood and hardwood) with other plant fibers, respectively. Hemp and flax fibres have small lumen dimensions [15] while, in wood fibers, the lumen area is between 20 and 70 % of the fiber cross-sectional area [1]. Moreover, micro fibril angle in the S_2 layer of flax fibers is 6-10° while the corresponding value for wood fibers is in the range of 3-50° [1]. Finally, if one travels from the outside of the fiber to the lumen, the lignin concentration decreases while the cellulose concentration increases.

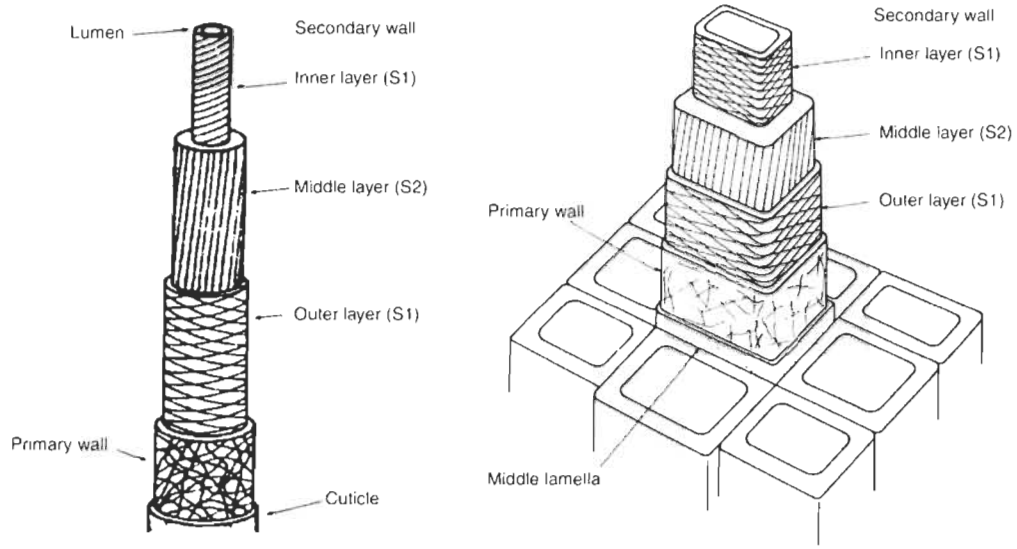

Figure 1-3. Schematic of the morphological structure of elementary plant fibers, (a) bast fiber, (b) spruce wood fiber [2].

Table 1-3. Mechanical properties of natural plant fibers compared with synthetic ones [2].

Fiber	Density (g/cm^3)	Diameter (μm)	Elongation at break (%)	Tensile strength (MPa)	Young's modulus (GPa)	Specific modulus ($GPa \cdot cm^3/g$)	Price (€/Kg)
Flax	1.40-1.50	40-620	2.7-3.2	343-1035	27-80	19-53	2.29-11.47
Jute	1.30-1.50	30-140	1.4-3.1	187-773	3-55	2-37	0.12-0.35
Abaca	1.50	17-21	10-12	980	72	48	0.81-0.92
Sisal	1.30-1.50	100-300	2.0-2.9	507-855	9.0-28.0	7-19	0.70-1.02
Kenaf	1.22-1.40	40-90	3.7-6.9	295-930	22-53	18-38	0.53-0.61
Ramie	1.50	40-60	3.6-3.8	400-938	44-128	29-85	1.44-2.40
Hemp	1.40-1.50	16-50	1.3-4.7	580-1110	3-90	2-60	0.57-1.73
Cotton	1.50-1.60	16-21	2.0-10.0	287-597	5.5-12.6	4-8	1.61-4.59
Coir	1.25-1.50	100-450	15.0-47.0	106-270	3.0-6.0	2-4	0.24-0.48
Banana	1.30-1.35	50-280	3-10	529-914	7.7-32.0	6-24	0.7-0.9
Henequén	1.49	20-500	3.0-5.0	430-580	10.1-16.3	7-11	0.38-0.67
Bagasse	0.55-1.25	200-400	0.9	20-290	2.7-17.0	5-14	0.15
Pineapple	1.52-1.56	200-8800	0.8-3.0	170-1627	6.21-82	4-53	0.36-0.72
E-glass	2.50-2.55	10-20	2.5	2000-3500	73.0	29	1.25
Aramide	1.40-1.45	12	3.3-3.7	3000-3150	63.0-67.0	45-48	7.20
Carbon	1.40-1.75	5.5-6.9	1.4-1.8	4000	230.0-240.0	164-171	12.0

Table 1-4. Mean dimensions of various plant fibers [1].

Plant	Fibre type	Dimensions				Aspect ratio
		Length (mm)		Diameter (μm)		
Hemp	Bast	25	(5-55)	25	(10-51)	1000
Flax		33	(9-70)	19	(5-38)	1750
Jute		2	(2-5)	20	(10-25)	100
Ramie		120	(60-250)	50	(11-80)	2400
Sisal	Leaf	3	(1-8)	20	(8-41)	150
Cotton	Seed	18	(10-40)	20	(12-38)	900
Wheat	Stem	1.4	(0.4-3.2)	15	(8-34)	90
Softwood (e.g. spruce)	Tracheid	3.3		33		100
Hardwood (e.g. beech)		1.0		20		50

Table 1-5. Chemical composition of the cell wall in different plant fibers [1].

Plant	Fibre type	Cell wall chemical composition (w%)		
		Cellulose	Hemicellulose	Lignin
Hemp	Bast	57-77	14-17	9-13
Sisal	Leaf	43-62	21-24	7-9
Cotton	Seed	85-96	1-3	0.7-1.6
Wheat	Stem	29-51	26-32	16-21
Wood	Tracheid	38-49	7-26	23-34

The wood species can be classified into two main groups namely softwood (or conifers), and hardwood (or deciduous trees). Typical softwoods are pines, spruces or firs, while gum, aspen, oak or maple are examples of hardwood. Softwoods and hardwoods differ in their structural characteristics and mechanisms providing structural strength. Softwood fibers have typical lengths of 3-5 mm, while hardwood fibers are 1-2 mm long on average. Hardwoods also have additional elements, compared to softwoods, named vessel elements that conduct fluids.

1.2.2. Natural fiber composites (NFC)

According to Lucintel [16], the automobile industry is the largest industrial sector using bast fiber based composites. Using such fibers in this industry results in fuel consumption economy and other environmental benefits [7]. Application of NFCs in this industry has been evaluated in the literature [3, 9, 17, 18] and some of the challenges to be addressed in this regard are discussed in [13].

The first and foremost problem to be addressed in developing a NFC is establishing a high fiber-matrix interface strength, i.e. the fiber-matrix interface compatibility between polar (hydrophilic) plant fibers on one hand, and non-polar (hydrophobic) thermoplastic or thermosetting matrix [2], on the other hand. This in turn affects the mechanical performance of the resulted composite. Generally, natural fibers are treated chemically or physically to reduce their polarity and subsequently become less hydrophilic. Doing so increases the wettability of fibers to liquid resin and ameliorates the impregnation quality. Another approach is the application of coupling agents which create stronger bonds at the interface of fiber and matrix compared to the former method.

Tensile, bending, fatigue, impact and humidity uptake properties of natural fiber composites are the main properties which have been considerably examined in the literature [19-27]. In addition, fiber/matrix interface properties have been studied by microbond or fragmentation tests [28-32]. Table 1-6 represents some typical tensile properties of plant fiber composites and gives a comparison with glass-fiber reinforced plastics. The results reveal that composites with short plant fibers possess a stiffness of about 9 GPa with biodegradable

PLLA matrix and 5 GPa with thermoplastic PP matrix. The corresponding ultimate strength values are about 100 MPa and 70 MPa, respectively. These values are favorably comparable with those of short glass/PP injection molded composites which account for 8.9 GPa and 50 MPa.

Table 1-6. Some typical tensile properties of NFCs and comparison with glass fiber composites.

Reinforcement	matrix	Vf (%)	Stiffness (GPa)	Ultimate Strength (MPa)	Reference
UD Flax	PP	43-55	27 - 29	251 -321	[33]
UD Flax	Unsaturated polyester	55.2	27.8	234	[11]
UD Hemp	PET	48	28	280	[34]
Short Flax	PLLA	30	9.5	99	[20]
Short Flax	PP-gMA	30	5.7	73.6	[20]
UD Glass	polyester	49	35.2	918	[35]
UD Glass	PP	58	43.6	890	[36]
Short Glass	PP	25	8.9	50	[37]

Unidirectional fiber composites, as expected, produce considerably higher tensile properties compared to short fiber ones. For flax composites either with thermosetting or thermoplastic matrix, stiffness and ultimate strength are about 27 GPa and 230 MPa, respectively. Unidirectional hemp/PET is reported to have stiffness of 28 GPa and strength of 280 Mpa. Table 1-6 demonstrates that the tensile stiffness of unidirectional glass composites is slightly superior to the plant fibers composites. The difference is more pronounced in terms of ultimate strength where it is around 4 times larger for glass reinforced plastics. However, it is usually argued that the lower density of plant fibers with respect to glass fibers could compensate for the slightly higher stiffness of glass fiber composites. Generally speaking, in designs where tensile or bending stiffness is selected as the key parameter, it could be expected

that plant fiber composites provide lower weight for the same values of compliance and fiber volume fraction.

The main objective of research works on plant fibers is the development of green composites made of fully biodegradable constituents. However, their industrial scale application is generaly influenced by cost. Since the price of biodegradable polymers is much higher compared to petrochemical plastics (see Table 1-7) currently the most viable way toward eco-friendly composites is the use of natural fibers as reinforcement in synthetic plastics. Although the current industrial scale natural fiber composites are not totally recyclable, they form a foundation for further investment in research about environmental friendly materials and their future implementation.

Tables 1-8 and 1-9 respectively compare physical and mechanical properties of biopolymers with some synthetic plastics. As can be seen in Table 1-9, two biopolymers, PLA and PLLA can compete with synthetic polymers like PP and Unsaturated polyester, in terms of Young's modulus and ultimate strength.

Table 1-7. Biodegradable vs. traditional plastics – cost comparison [38].

Material		Average cost $/lb.
Biodegradable plastics	PLA (Cargill Dow Polymers)	1.50–3.00
	Starch-based resins (Novon/Novamont)	1.60–2.90
	PHA (BIOTEC/Monsanto)	4.00–6.30
Commodity petrochemical plastics	PP	0.33
	LDPE	0.41
	HDPE	0.37
	PS	0.39
	PVC	0.28
	Polyester	0.52
	PVOH	1.40
	Polycarbonate	1.60

Table 1-8. Melting temperature, T_m, glass transition temperature, T_g and density of some biopolymers [20].

Polymers	T_m (°C)	T_g (°C)	Density (g/cm^3)
Mater-Bi® ZF03U/A	55	−50	1.25
PLLA L9000	169	65	1.25
PHB P226	161	−10	1.25
Ecoflex (PBAT)	115	n.a.	1.27
Bionolle 1020 (PBS)	115	−40	1.26
PLA 4042D	175	56	1.27
PP-g-MA (5%)	170	−10	0.91

Table 1-9. Tensile properties of some bio- and synthetic polymers [20].

Polymer	Young's modulus (MPa)	Ultimate stress (MPa)	Strain to failure (%)
ZF03UA (MaterBi®)	130 ± 6.3	6.8 ± 0.4	32.2 ± 11.3
PLLA	3321 ± 214	60.1 ± 5.0	2.4 ± 0.4
PHB	938 ± 78	21 ± 2,4	6.8 ± 1.6
PBAI (Ecoflex)	62 ± 3.5	11.2 ± 3.9	6.8 ± 1.7
PBS (bionolle)	687 ± 268	17 ± 1	10.4 ± 0.6
PLA	3200 ± 201	66.8 ± 1.8	2.8 ± 0.2
PP-g-MA	1501 ± 99	26.7 ± 0.8	3.9 ± 0.2
Unsaturated polyester	3797 ± 110	46 ± 3	1.2 ± 0.1

1.2.3. Paper processing

The papermaking process starts with wood chips as base raw material and stops with the paper sheet coming off the paper machine. As is schematically outlined in the Figure 1-4, the wood chips pass through the pulp mill, the stock (furnish) preparation facilities and the paper machine, respectively.

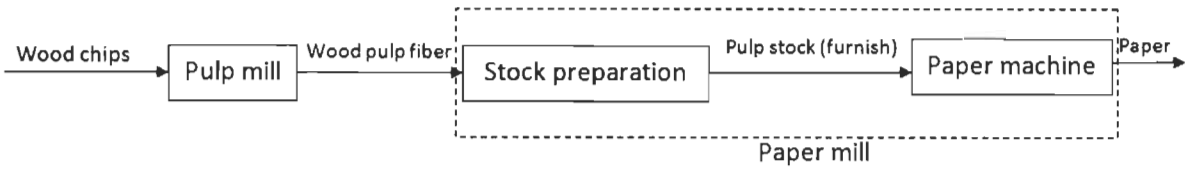

Figure 1-4. Schematic of the paper processing.

The paper machine was invented by the French papermaker Nicholas Louis Robert. It was improved by British Bryan Donkin and John Gamble. As their work was funded by Four-drinier brothers most of the modern papermaking machines nowadays are named after them. Major components of the Fourdrinier paper machine include headbox, forming table, press, dryer, calendar and the reel sections. Figure 1-5 schematically presents different sections of a typical Fourdrinier paper machine. The headbox, forming section and the press section are named the "wet-end", while the dryer, calendar and reel section are referred to as the "dry-end". This grouping is based on the amount of water involved at the two extremities of a paper machine.

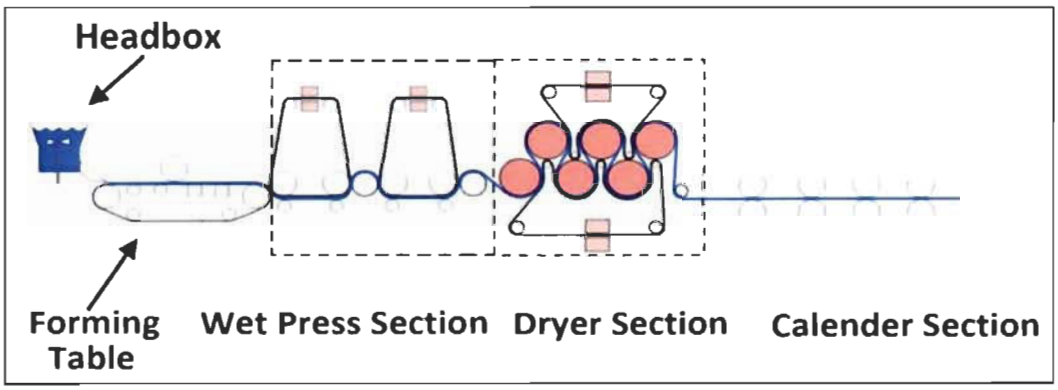

Figure 1-5. Schematic drawing of a Fourdrinier paper machine (www.wikipedia.com, Author: Egmason)

The headbox forms the first part of a paper machine and consists generally of an open box with a narrow opening toward the forming table of the machine. The pulp stock get out the headbox through a tapered outlet manifold where the stock is spread out to the width of the machine. Three basic functions of headbox include spreading furnish out to the width of the paper machine, dispersing fibers and other materials uniformly and matching slurry speed with the fabric speed of forming table.

The section next to the headbox is the forming table. The main objectives of forming table are to form the sheet and dewater it to about 20 % solids (starting from about 1 % in the headbox). The forming table consists of a plastic mesh fabric wound around two principle rollers known as breast roller and the couch roller. As the paper sheet travels down the forming table, it experiences increasing dewatering suction and gravity forces. The approximate solid content at the end of this section allows the paper to withstand the forces exerted on it during transfer from the forming section to the press section.

At the end of the press section, the sheet is dewatered up to 35-45 % solid. The other functions of the press section includes consolidating the paper web and decreasing the surface roughness. The paper strength is considerably influenced by applied pressure which forces the fibers to agglomerate and develop some cohesion.

When the sheet leaves the press section water still remains inside the structure of the pulp fibers as well as the pores of their walls. Evaporative drying is used to remove the remained water and bring the sheet to 94-97 % of solid content. On top of that, heating the sheet web makes it develop fiber-to-fiber bonds, and establish the paper strength. Moreover, since the paper takes the surface characteristics of the drying rollers, the dryer section is also used to improve the surface finish of the sheet.

1.2.4. Design of experiments and empirical modeling

Design of experiments (DOE), also known as experimental design or designed experiments, is a statistical approach toward better understanding a process or a product. It consists

of tabulated rows of tests (runs) in which input factors of the process or material are purposefully changed with the aim of observing corresponding changes in the outputs (responses) and discovering the reasons for these changes. Designed experiments not only play an important role in engineering and design problems like characterization of a new product or a manufacturing process, but also there are many applications in marketing, service operation and general business operations.

Empirical models are used to quantitatively express the results of an experimental design, through fitting a regression equation on the set of sample data. Empirical models are proposed to replace mechanistic models [39]. In situations where scientific phenomena are well understood, useful mechanistic mathematical models could be directly developed. A simple example of a mechanistic model is the Ohm's law, E=IR, which describes the current flow in an electrical circuit. On the other hand, empirical models are experimentally determined models. To this end, one requires observation of the system at work using a designed experiment. Then, based on the analysis of experimental results one can infer an empirical model which describes why and how the system works. These models can be next manipulated by scientists and engineers just the way a mechanistic model can. Throughout this thesis, empirical model approach is considered for analyzing and turning the results of designed experiments into a model for the material under study.

As explained above, in experimental design, one needs to first conduct well controlled tests, and then extract the knowledge of the process or the material from the experimental data, using graphical and statistical strategies. The main inferential statistical approaches

used here to analyze experimental results include analysis of variance (ANOVA) and regression analysis. On the other hand there exist some graphical tools such as cause-and-effect diagram, process flow diagram, Pareto analysis, histogram and marginal average plot. In this work both statistical and graphical approaches are employed. The main objective of ANOVA is for determining the factors changing the average response (location effects), as well as the ones that change the response variability (dispersion effects) and discriminate these two groups from those factors having no effect on the response. Once such a classification is performed on the factors, then in the regression analysis, linear or quadratic polynomial models are built to simulate the average and/or variability responses.

In many cases the purpose of conducting experimental designs is to develop a robust process or material. The robust design principle was originally developed by Taguchi [40] to improve the quality of a product through minimizing variance of performance. Based on the fundamental definition of robust design, a product or process is called robust when it is insensitive to the effects of variability sources, even though the sources themselves have not been eliminated [41]. Generally speaking the variability in the performance of a material could come from four main sources, including experimental uncertainties (e.g uncertainty of fabrication process), material uncertainties (e.g. variation of mechanical and/or physical properties or variation of the parameters of the material) and human factors. In addition, environmental uncertainties which are also called noise factors, such as humidity or ultraviolet radiation, could affect the performance of the material. To be able to draw firm statistical conclusions about the effect of material parameters on result's variation, the experimental uncertainties, noise factors as well as the effect of human factors should be well controlled

during experimentation. In the case of natural fibers, where variability of properties is one of their intrinsic characteristics, it seems relevant to consider robust design approach in designing the products made out of them.

CHAPTER 2: LITERATURE REVIEW AND RESEARCH OBJECTIVES

Natural fiber composites (NFC) provide researchers with diverse areas of research. Some of these for instance include characterization of elementary/technical short fibers, developing and modeling long plant yarn/roving, measuring permeability of fabric/mat reinforcements for different architectures, evaluating the compatibility between thermoplastic/thermosetting resins and the plant fibers, evaluating the mechanical performance of resulting composites, as well as implementing statistical modeling techniques to characterize and optimize natural fiber materials. In this chapter a review of different aspects of NFC research is presented, followed by the research objectives.

2.1. Short natural fibers

Elementary or technical plant fibers, as one of the basic reinforcement constituents, have attracted much attention in the literature because the knowledge of their behavior is necessary to understand how they influence the characteristics of the reinforcements and their composites. Gassan et al. [42] developed two finite element models to evaluate the dependency of elastic modulus of elementary fibers to microfibrils spiral angle, cellulose content and elliptical degree of fiber cross section. Bos et al. [43] showed that the tensile strength of technical flax fiber bundles depends strongly on the clamped length, while tensile and compressive

strength of elementary fiber is affected by the process of isolating flax fibers from stem, as it may induce kink bands on the fiber surface. Baley [44] noticed that the elastic modulus decreases as the fiber diameter increases, and increases with strain during the tensile test. Charlet et al. [45] studied the dependency of elastic modulus, tensile strength and ultimate strain of elementary flax fibers on their location in the stem which subsequently affect morphology (cell diameter and porosity) and chemical composition (hemicelluloses and pectin) of the fibers. It is claimed that fibers taken from middle of flax stem have shown the best mechanical properties. Symington et al. [46] characterized the effect of humidity and alkaline treatment on tensile properties of some bast fibers. It is reported that moisture has a distinct effect on the properties, although trends of change were not entirely clear or conclusive. It is also shown that over alkaline treatment of natural fiber is detrimental to the fibers mechanical properties and treatment time should be less than 10 minutes to obtain optimum properties.

2.2. **Long natural fiber yarns**

Apart from short technical/elementary fibers whose lengths do not exceed a few centimeters, it is also important to consider long yarns/rovings made of twisted elementary fibers, which allow for applying natural fibers in load-bearing applications. In the textile industry context, rovings or pre-yarns are of very low twist levels (e.g. 29 turns/m) and by way of contrast, the level of twist in yarns is considerably higher (e.g. 200 turns/m), which allows their processing in industrial scale reinforcement manufacturing using textile machines. However, the terms roving and yarn are observed to be used interchangeably in the composite materials literature. In 2003, Goutianos and Peijs [47], optimized the level of twist in flax

fiber rovings in order to develop high quality natural fiber composites for structural applications. Tensile tests of dry rovings shows that, as the twist level increases the roving strength increases from zero to reach a maximum at a certain level of twist and thereafter decreases with further increase of twist level. However, for an impregnated roving (composite) the highest strength is obtained for those with low (or no) twist levels and the strength goes down as the twist increases. The 85 turns/m is reported as the optimum level of twist to fulfill the requirements of textile processes for dry rovings, while giving a reasonably high tensile performance of resulted composites. Madsen et al. [48] fabricated textile hemp yarns using the ring spinning method and characterized them in terms of chemical composition, fiber density, yarn structure, moisture absorption properties, and mechanical properties. Using a mathematical model it is shown that for the yarns with surface twisting angle below 40°, the mean twisting angle is approximately related to the surface twisting angle by a factor 0.7. Shah et al. [49] developed an analytical model for tensile strength of aligned plant fiber composites (PFCs) based on the yarn twist level measured in turn per meter (tpm) and on yarn's surface twist angle. It is reported that the model accurately predicts published experimental data.

2.3. **Using wood fibers as reinforcement of plastics**

Among the first works dealing with the use of paper layers as reinforcement in composites, one can refer to Michell et al. [50] in 1975. Commercial bleached bag kraft papers (49 g/m^2) are coated with a low-density thermoplastic polyethylene film (24 g/m^2) and hot-pressed to form laminates up to 6.5 mm thick and 67 wt % of cellulose fibers. The flexural strength and stiffness, tensile strength and elongation at break are reported comparable with those of glass-

filled high density polyethylene and paper-phenolic composites. However, the tensile strength and flexural stiffness are inferior to those of wood. Three years later the same authors evaluated the effect of chemical treatments of paper on the flexural properties of their composites at various humidity levels [51]. Either wood pulp fibers or formed paper sheets were chemically treated and then hot-pressed with low-density polyethylene or ethylene-vinyl acetate copolymer (EVA) to obtain laminates. It is reported that the chemical treatments have markedly maintained the flexural properties of paper/polyolefin laminates upon exposure to water. Moreover, although higher levels of chemical treatment increase the resistance to humidity of the material, it degrades flexural properties due to fiber degradation. In 2006, Bullions et al. [52] fabricated sheets of paper with varying compositions of feather fibers (Ff), recycled kraft pulp fibers (Pf), recycled newspaper pulp fibers (Nf) and retted kenaf bast fibers (Kf) to be used as reinforcements in polypropylene matrix composites. The prepregs were fabricated using a wetlay papermaking equipment and then compression-molded to form multiple plies composites. The contributions to the composite strength of the four different fibers in descending order are: Pf > Nf > Ff > Kf. It is concluded that two factors playing major roles in determining the contributions of each fiber to the composite strength are fiber aspect ratio and fiber strength. Nordin and Varna [53, 54] developed nonlinear viscoelastic and viscoplastic models for phenol–formaldehyde impregnated papers submitted to a compression creep loading followed by strain recovery. The analytical models are validated with experimental test results.

2.4. **Permeability of natural fiber reinforcements**

In liquid composite molding (LCM) processes, the usual practice is to simulate the mold filling process using a flow simulation software to predict the filling time and filling pattern and subsequently optimize the process (e.g. location of resin inlets and outlets) for a good quality impregnation. A prerequisite for such a simulation is the experimentally determined or computationally estimated permeability of the fiber preform to be molded. In fact permeability is a determining parameter in the governing equations (via Darcy's law) of resin flow inside a porous fibrous media. On the other hand, permeability is influenced by several parameters among which the fiber volume fraction (V_f), reinforcement architecture and its intra-ply shearing are the most important ones. Because of these observations, many researchers have extensively studied different methods of permeability measurement and have characterized the permeability of several preforms.

In 1988 Adams et al. [55] proposed a methodology to solve the governing equations of two-dimensional radial flow in an anisotropic porous media based on experimental data of elliptical flow front radii versus time. The original method was further developed by Chan and Hwang [56] and Griffin et al. [57] in 1991 and 1995, respectively. In 1999, Weitzenböck et al. [58, 59] propose a new solving technique for a more general case in which the assumption of symmetric permeability tensor is lifted. In this method, instead of recording the major and minor radii of the elliptical flow front, three points on the flow front along three orientations are recorded with time. Hoes et al. [60] proposed a new permeability measurement set up for radial injection experiment which uses two steel plates as top and bottom mold haves and electrical sensors embedded in the top mold half to detect the flow front. Permeability of

several woven glass fabrics are tested and their statistical distributions are acquired. Endruweit et al. used radial flow injection method to experimentally study the effect of shear angle on the principal permeabilities of various glass fiber fabrics [61]. Effects of stochastic variation of fiber angles and spacing between fibers on permeability uncertainty are also simulated in other works of Endruweit et al. using 2D radial flow injection method [62, 63]. Apart from radial injection technique, linear flow method is also used for permeability measurement [64]. Pan et al. [65] used one-dimensional permeability measurement technique to examine influence of process parameters on permeability variance of knitted and woven glass fabric preforms. It is reported that edge protection, fabric areal weight and complexity of mold shape, have significant influence on the permeability behavior.

As a result of increasing popularity of natural fiber composites, permeability of natural fiber reinforcements has also been studied in recent years. Umer et al. characterized the permeability and compaction response of wood fiber mats [66] and flax fiber mats [67]. For the former mat type the permeability is characterized versus fiber volume fraction while for the latter one, it is characterized versus fiber length and diameter as well as fiber volume fraction. It is claimed that the permeability of natural fiber mats and fabrics is dominated by the characteristics of open channels. Therefore, swelling of fibers impregnated with glucose syrup, which is a polar liquid, is responsible for lower measured permeability compared to the situation where non-polar motor oil is used. For flax fiber mats the permeability of medium yarn diameter (560 μm) mats is reported to be highest in comparison with both small (350 μm) and large (810 μm) yarn diameter mats. Moreover, the permeability of 50 mm chopped yarn length was found to be higher as compared to its 15 mm counterpart. Permeability of medium

yarn diameter and 50 mm yarn length mats is reported about 0.5×10^{-8} m^2, for 20 % fiber volume fraction which is equal to that of glass fiber mats at the same fiber volume fraction. Mekic et al. [68] evaluated the in-plane and out-of-plane permeabilities of preforms made of randomly oriented flax fibers ranging from 12 mm to 50 mm in length and 10 μm to 50 μm in diameter. It is concluded that the in-plane and out-of-plane permeabilities fall in the range of those obtained for randomly oriented fiberglass mats. So, traditional liquid molding techniques can be used for the fabrication of natural fiber composites. In 2010, bidirectional woven jute fabrics are characterized in terms of saturated and unsaturated permeability by Francucci et al. [69]. It is claimed that fluid absorption and fiber swelling are two mechanisms respectively responsible for lower unsaturated and saturated permeability values compared to the permeability of glass fiber fabrics. In unsaturated permeability measurement, hydrophilic nature of plant fibers removes fluid from the main stream and thus decreases flow velocity. On the other hand, saturation of natural fibers causes swelling, thus reducing the porosity and increasing flow resistance. The permeability-porosity relationship is also investigated for bidirectional jute fabrics [69, 70] and random sisal mats [70] based on the empirical Carman–Kozeny model. Recently Lebrun et al. [71] studied the permeability behavior of unidirectional hemp/paper and flax/paper reinforcements, as well as their individual constituents of UD flax layers and absorption papers, using resin infusion molding method and epoxy resin as test liquid. Tensile properties of the resulted composites are as well investigated. These reinforcements have shown lower permeability levels, particularly the hybrid reinforcements, compared to the UD glass reinforcements. It was concluded that the overall

permeability must be improved. More recently, the effect of test fluid on saturated permeability of twill weave flax fabrics was examined by Nguyen et al. [72]. Saturated permeability is reported dependent on the test fluid because of different swelling behaviors of flax fibers to each of the test fluid. The modified Kozeny– Carman model with two model constants is also claimed to well simulate the experimental saturated permeability data. In another work [73], a model for resin flow inside flax fiber preforms which takes into account fiber's mass sink effect and swelling during the mold filling process is proposed.

Despite considerable amount of research on permeability evaluation, an international standard for permeability measurement is still lacking. In response to this, two international permeability benchmarks were conducted [74, 75] and a guideline was published for measuring the unsaturated permeability of preforms using the linear injection method [76].

2.5. **Architecture of natural fiber reinforcements**

To incorporate natural fibers as reinforcing agent of composite laminates one could either develop non-woven mats based on chopped randomly oriented fibers, weave continuous yarns into biaxial fabrics or alternatively develop unidirectional reinforcements [1, 77]. The four common weave architectures include uniaxial and biaxial plain woven fabrics as well as twill and satin weaves [4, 78] as can be seen in Figures 2-1 and 2-2 . These woven fabrics are produced by the interlacing of warp (0°) and weft (90°) fibers in a regular pattern. There are also other textile technologies like knitting, braiding and stitching to develop continuous non-crimp fabric reinforcements [79, 80]. Architecture of the reinforcement plays an important role in its permeability and mechanical properties of the resulting composites as it

affects the flow pattern in the fiber preform and stress distribution in the part. Many researchers have studied different reinforcement architectures and their influence on the responses of the material.

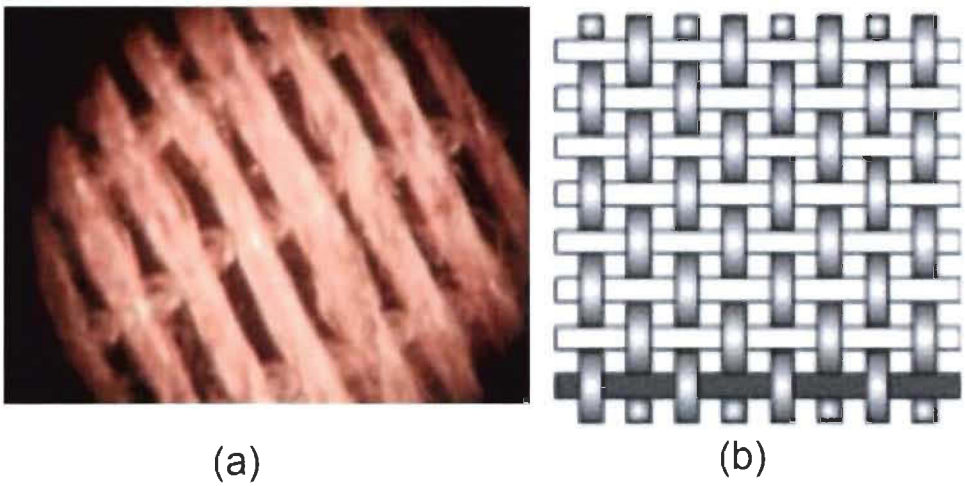

Figure 2-1. Different reinforcement architectures (a) uniaxial reinforcement made of flax fiber yarns [81], (b) schematic of a biaxial plain weave [78].

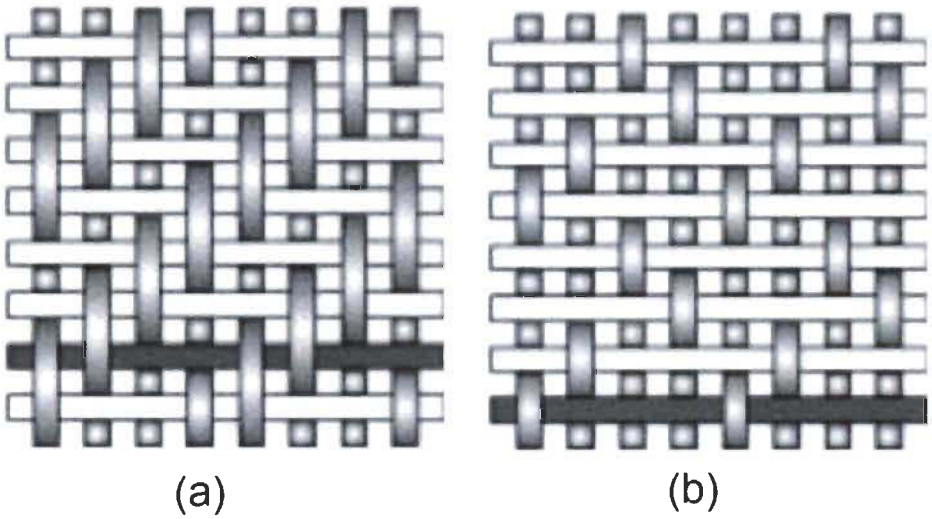

Figure 2-2. Schematic of different reinforcement architectures (a) biaxial twill weave [78], (b) biaxial satin weave [78].

Gassan [82] compared the tension-tension fatigue behavior of unidirectional and woven jute-epoxy composites. Apart from textile architecture, influence of some other material parameters like the type of natural fibers, fiber-matrix adhesion, strength and modulus of the fibers as well as fiber volume fraction on the fatigue behavior is also examined. It is shown that the mechanism of damage development through cyclic loading differs between UD and woven fiber reinforced jute-epoxy systems. For the UD composites the critical maximum applied load is reported around 45 MPa while for the woven based composites it is measured about 20 MPa. Goutianos et al. [81] produced uniaxial and biaxial warp knitted fabrics as well as biaxial plain weaves, out of flax yarns, and evaluated the flexural and tensile stiffness and strength of their thermosetting composites. It is claimed that the responses of the natural fiber composites are close with those of glass fiber composites while in all cases the fiber volume fractions in flax composites was considerably lower than that of glass fiber composites. Moreover, specific flexural and tensile stiffness of the unidirectional flax composites are reported superior to their unidirectional glass fiber counterparts. Pothan et al. [83] analyzed the effects of three weave architectures of sisal yarns including plain, twill and mat weave on the permeability, tensile and flexural behavior of polyester composites. It is concluded that weaving architecture was the crucial factor in determining the response of the composites. The weave architecture with a maximum proportion of fibers oriented in the loading direction (mat weave) is best to improve tensile and flexural properties. Moreover mat weave showed lower macro-flow permeability compared with plain weave, while its capillary pressure and consequently micro-flow within fiber bundles is higher than that of plain weave architecture. Miao and Shan [84] developed highly aligned nonwoven mats of

flax fibers as an alternative to unidirectional woven fabrics for being used in thermoplastic composites. For the reinforcement fabrication a drawing step is added to the conventional nonwoven process to get the fibers aligned. The composites showed similar strength to those made from unidirectional woven flax fabrics while the reinforcement production cost is more affordable. However, the elastic modulus is lower than its unidirectional woven fabric counterpart. Plain weave and weft rib-knitted fabrics made out of flax yarns were manufactured by Muralidhar [85] and several composite plates with different stacking sequences and lay-up angles are hand laid-up using epoxy resin. A maximum specific tensile modulus of 3.0 GPa/gcm^{-3} is obtained for a [0/90] laminate at V_f = 27 %. Xue and Hu [86] introduced a biaxial weft-knitted flax fabric made with a modified flat knitting machine. The reinforcement is characterized in terms of tensile behavior of the flax yarn and fabric as well as the resulting composite. Experimental results showed that sodium hydroxide (NaOH) treatment improves mechanical properties of the composites and tensile strength and stiffness of 176.6 MPa and 8.9 GPa are reported at V_f = 31.6 %. Recently, Khalfallah et al. [87] developed a new unidirectional flax tapes out of long technical flax fibers and used Acrodur^{TM} thermoset resin to impregnate them. Optimum specific tensile modulus and strength of 19.4 GPa/gcm^{-3} and 103 MPa/gcm^{-3} are respectively acquired at V_f = 35 % and based on these values the reinforcement performance is considered adequate for being integrated into automotive applications. In 2013, Shah et al. [77] fabricated a full-scale 3.5 m flax/polyester rotor blade and compared it with its glass/polyester counterpart. It is reported that flax fiber blade satisfies the structural integrity requirements and thus is a suitable replacement to glass fiber

blades in small wind turbine blade applications. However, the flexural rigidity of flax fiber blade was reported around half that of a glass fiber blade.

2.6. **Statistical modeling techniques applied to natural fibers**

Statistics, which is defined as the science of variations, is aimed at understanding variations and what causes them, through collecting, analyzing, interpreting and presenting data. Based on the so-called statistical thinking, all processes are subject to variations so that identifying, characterizing, quantifying and reducing process variations are keys to successful processes [88].

The advantage of composite materials is that their parameters can be tailored to provide the desired performance for a given working condition. To this end, it is well understood that one needs to quantitatively model and then optimize the influences of process and material parameters on the performances of interest. Although mechanistic models are developed to model composite molding processes and the structural behavior of composites, in many situations the complexities and uncertainties involved cannot be well reflected through such models because idealizing assumptions are normally needed to achieve a closed-form solution. For synthetic fiber composites, quite comprehensive studies can be found in the literature on their statistical modeling [65, 89-91]. However, implementation of statistical techniques on natural fiber reinforcements and their composites is an emerging field of research, as variability of natural fibers properties is more pronounced compared to synthetic fibers.

Recently, Summerscales et al. [92] have reviewed the statistical models which have been applied to natural fibers. According to their review, the three main areas for which quantitative models are developed include estimating the true cross-sectional area of fibers, implementation of the Weibull model to simulate the strength of bast fibers and their composites as well as modifying the rule of mixture (ROM) for natural fiber composites to take into account the effects of porosity, fiber diameter distribution, fiber area correction factor (FACF) and yarn twist.

Aly et al. [93] optimized the alkaline treatment of flax fibers using analysis of variance (ANOVA) and response surface methodology according to Box–Behnken designs. The treatment parameters include NaOH concentration, soaking time and treatment temperature, each parameter studied at three levels. The responses were defined as the tensile strength and Young modulus of single fibers. It is concluded that response surface methodology is an accurate technique to optimize the treatment parameters and that the optimum levels of parameters are 5 % NaOH solution concentration at 55°C for 10 min. Peponi et al. employed a new statistical method based on neural network approach to comparatively study the dimensional characteristics and tensile properties of some natural fibers [94] as well as tensile behavior of their random discontinuous PP-matrix composites [95]. The novel statistical model is claimed to show a more accurate prediction of experimental fiber diameter and tensile properties compared to the traditional statistical function estimation approach. However, the predicted values for the composites were much higher than the experimental values which are attributed to the poor fiber/matrix adhesion.

2.7. **Research objectives**

Flax fibers are in direct competition with E-glass fibers in terms of specific tensile stiffness [12, 96]. It was thus considered important to develop a reinforcement which could maximize the effect of this particular characteristic of flax fiber into the final composite. As showed in the earlier sections of this chapter, up to now the vast majority of continuous NF reinforcements use bidirectional fabrics made through weaving and/or knitting methods, while as it is reported in [87, 97] unidirectional (UD) composites perform better than bidirectional ones in terms of mechanical performance. The novel reinforcement proposed in this thesis is a UD hybrid flax/paper reinforcement made of a layer of unidirectional flax yarns laid down on a thin and porous paper layer used as binder for the UD fibers.

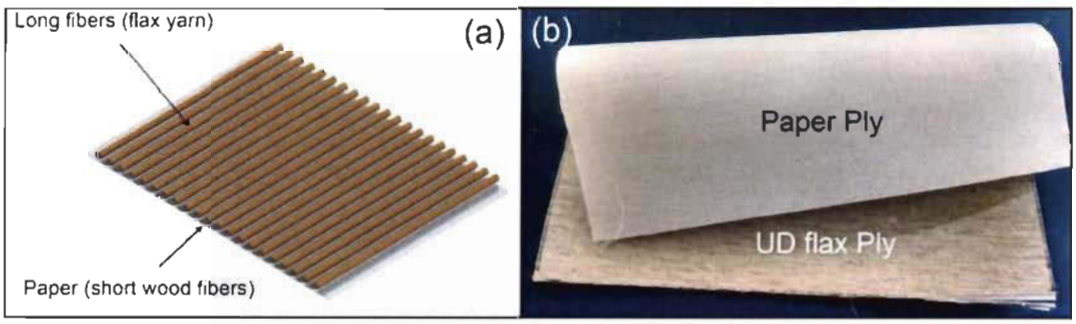

Figure 2-3. Unidirectional flax/paper reinforcement, (a) schematic representation, (b) laboratory-made sample

Figure 2-3a shows a schematic of the reinforcement and Figure 2-3b shows a reinforcement sample developed at the Laboratory of Mechanics and Eco-Materials (LMEM). The benefits of the paper layer could be multifold. Firstly, the paper layer acts as a binder for holding the yarns. This role of the paper can potentially impart consistency into the behavior

and properties of the derived composites through maintaining the yarns' configuration consistent (parallel) during manipulation and molding. Furthermore, it allows using low-twist yarns (which are normally too loose to be handled without a binder) that are proven to result in better composite performances [47, 81]. Moreover, it is already reported in the previous work on this flax/paper reinforcement [71] that the standard deviation of some tensile properties are reduced using a paper layer, and that the samples containing one or two layers of paper show more uniform and confined fracture surface (Figure 2-4). However it was also reported that the specific tensile stiffness of the resulted composites is 52% lower than that of glass fiber composites and permeability of flax/paper reinforcement was very low [71].

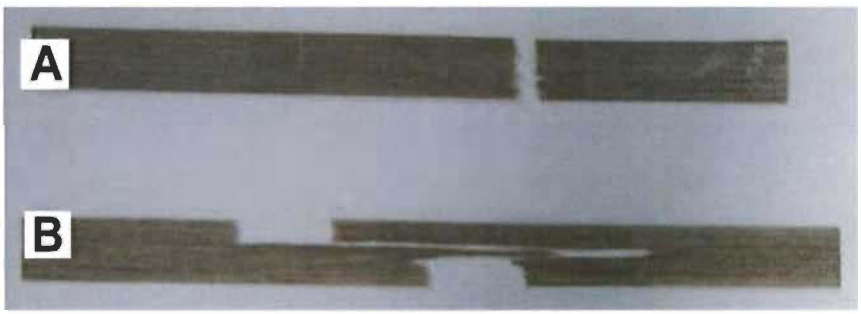

Figure 2-4. Results of tensile test on composite samples made of a layer of flax with (a) and without (b) paper [71]

With the aim of making global characteristics of the unidirectional flax/paper reinforcement compatible with industrial applications, in this thesis three important properties of the reinforcement, namely shear strength between paper and UD flax layers of dry reinforcement, the reinforcement permeability to liquid resin and tensile performance of the derived composite are examined. While the shear strength is an index of quality for the reinforcement ensuring that the yarns remain as much as possible intact during manipulation and molding, the

permeability and tensile performance of the composite (particularly specific stiffness) are the bases for judging if the reinforcement and its resulting composite can compete with glass fiber composites for industrial applications.

To improve the performances of the reinforcement the effects of its parameters on the properties have to be characterized and optimized. In this thesis the effect of four reinforcement parameters, including surface density of paper layer, surface density of flax layer, forming pressure, drying temperature, are studied based on robust parameter design approach. This approach (explained in section 3.9) is considered as a general approach toward studying the variance minimization of the results (due to parameters setting) while maximizing their mean values. Effect of fiber volume fraction (V_f) is also studied with regard to permeability. Feasibility of producing this hybrid reinforcement with a pilot scale paper machine is also examined. Producing the reinforcement in mass scale is necessary to attract industrial interest in mass production of composite parts and also to reduce its production costs.

Because in robust parameter design, variance of results due to parameter setting needs to be identified it is essential to have low results' variance due to measurement or fabrication uncertainties. These aspects are addressed here through developing a standard permeability measurement set-up, reliable permeability measurement procedure and a high quality composite molding technique, to ensure consistency of the results.

A long-term program aiming at manufacturing quality composite parts with arbitrary dimensions and geometries using the new hybrid flax/paper reinforcement is already launched

at the LMEM. This project consists of five phases: choice of constituents, reinforcement design, testing of flat composites, molding and designing more complex composite parts. Figure 2-5 shows the cause-and-effect diagram of this long-term program. As can be seen each phase is a prerequisite to the next phase and each phase itself is influenced by some sub-phases. Within each sub-phase several factors have been extracted based on a comprehensive literature review. These factors which are either parameters (adjustable or fixed) or properties (measurable or computable) are organized in the individual cause-and-effect diagrams shown in appendix A. Since addressing all the phases of the roadmap in a single research project is far from realistic, the research work in this thesis has been narrowed down to a precise topic considered more important in light of the current state of knowledge on this new reinforcement. The phases that are addressed in this thesis are highlighted in Figure 2-5.

With that in mind, a major part of the experimental work is conducted according to design of experiments (DOE) and the results are analyzed using ANOVA and regression. To study the qualitative parameters such as reinforcement architecture, two comparative studies, on permeability and tensile properties, are also conducted.

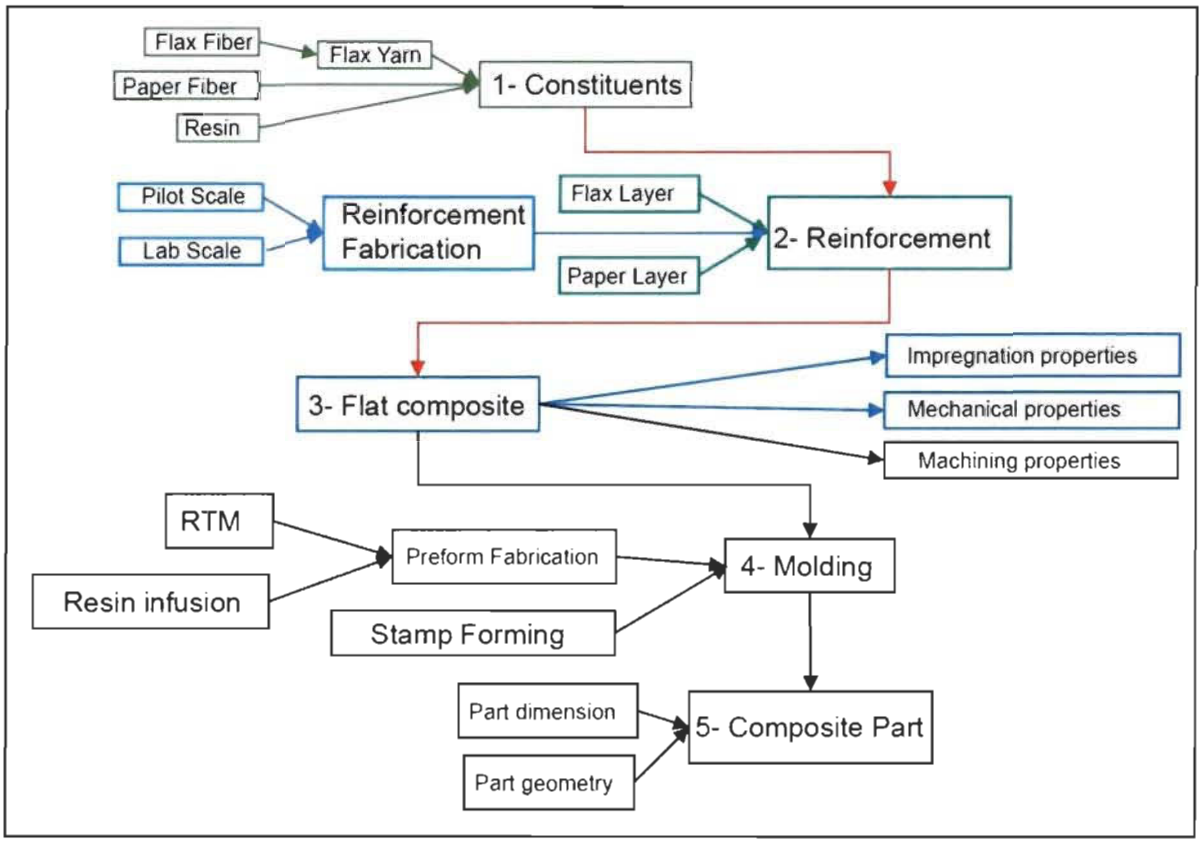

Figure 2-5. The cause-and-effect diagram of the long term project on the reinforcement; topics of this thesis are highlighted; sub-phases are exploded in appendix A.

CHAPTER 3: MATERIALS AND METHODS

Specifications of the raw materials, as well as processing of the hybrid-reinforcement both in laboratory and on a pilot paper machine, are described in this chapter. Furthermore, the methods for characterizing the reinforcement in terms of internal bond strength (IBS), permeability, composite molding and tensile testing are explained. Thereafter, the modeling approach is discussed.

3.1. Materials

3.1.1. Flax yarn

Flax yarns are supplied by Safilin Inc.[1] (France) and are made of 100 % European flax. A common measuring unit for the linear density of yarns in the international systems of units is 'tex', defined as the mass in grams per 1000 meters of the yarn. Apart from linear density, another parameter for a yarn is the twist level measured in number of turns per meter (tpm). Tex 200 and tex 400 low-twist flax yarns used in this study have twist levels of 55 and 30 tpm, respectively. The yarns specifications based on supplier's data are shown in Table 3-1. Data on E-glass and R-glass fibers are also shown for comparison. The values of flax fiber in Table 3-1 are calculated from composite samples molded at $V_f = 48$ %, using a 330 g/m^2

[1] - www.safilin.com

UD fabric and the vacuum molding process with epoxy resin, according to ASTM D303 standard.

3.1.2. Kraft pulp

Softwood Kraft pulp is used in this study to fabricate paper layers. It is provided by Innofibre[1]. Pulp consistency which is defined as the ratio of oven dried fiber mass to the mass of pulp stock is 10 % for the supplied Kraft pulp. The average fiber length and percentage of fines (short fibers up to 0.2 mm in length) are 1.08 mm and 32.77 %, respectively. More detailed specifications of the pulp employed in this study are provided in Appendix B.

Table 3-1. Properties of the low-twist yarns' flax fibers used in this study (source: safilin.com)

Property	Safilin 100 % flax low-twist yarns	Fiberglass E	Fiberglass R
Density (g/cm^3)	1.45	2.6	2.5
Fiber diameter (μm)	20	16	10
Tensile elongation (%)	1.35	3.5	4
Tensile strength (MPa)	742	2500	3200
Tensile modulus (GPa)	72.9	74	86
Specific tensile stiffness (GPa/gcm^{-3})	50.3	28.5	34.4

3.1.3. Epoxy resin

For composite molding, the Adtech Marine 820 epoxy laminating system mixed with 18 % by weight of hardener Marine 824 is used. Based on the supplier's technical sheet, the mix epoxy-hardener has a dynamic viscosity of 0.425 Pa.s (425 cP) and a cured density of ρ_m = 1.09 g/cm^3.

[1] - www.innofibre.ca

3.1.4. Permeability test fluid

SAE 20W-50 synthetic motor oil is used as the test fluid in the permeability measurement experiments. Its average dynamic viscosity is measured 0.458 Pa.s (458 cP) at 21°C and 0.349 Pa.s (349 cP) at 24°C using a DV-E Brookfield viscometer. It is reported that motor oil, as a non-polar liquid, can better mimic the hydrophobic thermoset resins used in LCM processes as opposed to water-based test liquids (e.g. glucose syrup) inducing swelling in natural fibers [66, 68, 72].

3.2. **Laboratory scale fabrication of unidirectional flax/paper reinforcement**

Figure 3-1 schematically illustrates the procedure of reinforcement fabrication in the laboratory. As can be seen it consists of four main steps, namely winding UD flax yarns (Figure 3-1a), fabrication of Kraft paper layer (Figure 3-1b), adding flax layer over the paper sheet and pressing them with a sheet press (Figure 3-1c) and finally drying with a sheet dryer (Figure 3-1d). During the last two steps some chemical and mechanical (anchoring) bonds are developed between flax and paper fibers and so the unidirectional hybrid flax/paper reinforcement is finally assembled. Figure 3-2 shows a typical reinforcement developed in this study. Practical know-how and the details of reinforcement fabrication are described in appendix C.

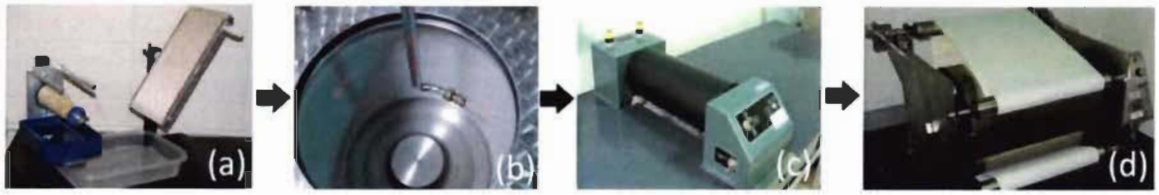

Figure 3-1. Fabrication procedure of hybrid flax/paper reinforcement (a) winding machine (b) Allimand dynamic sheet former (c) Canpa® sheet press (d) Adirondack Machine sheet dryer.

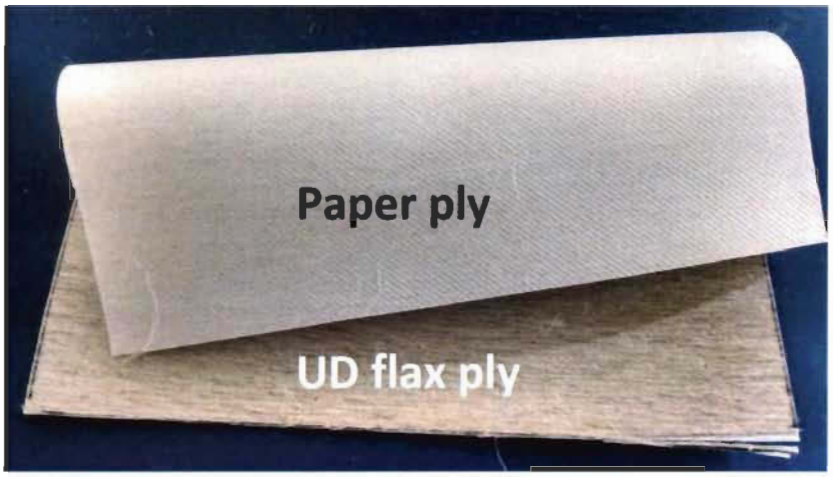

Figure 3-2. A typical laboratory-made unidirectional flax/paper reinforcement.

In the following sections, the use of each apparatus for reinforcement fabrication (Figure 3-1) is explained

3.2.1. Flax yarn winding machine

By turning the handle of winding machine shown in Figure 3-3, one is able to lay down flax yarns adjacent to one another (side by side) to finally end up with a continuous UD flax ply as is shown in Figure 3-4. Distance between yarns is controlled by the number of yarns laid down per inch. To ensure a uniform yarn distribution and consequently repeatable surface density of the UD flax layer, screws with desired number of threads per inch are used at the two ends of winding plate and the threads roots are used to lay down and guide the yarns.

Obviously, the higher the number of yarns per inch and the lower the distance between yarns result in higher surface density reinforcement. Three types of tex 200 UD flax layers used in this study consist of UD flax layers of 16, 20 and 24 yarns per inch, which are fabricated with 1/16″, 1/20″ and 1/24″ pitch screws.

Figure 3-3. Winding machine for aligning the yarn.

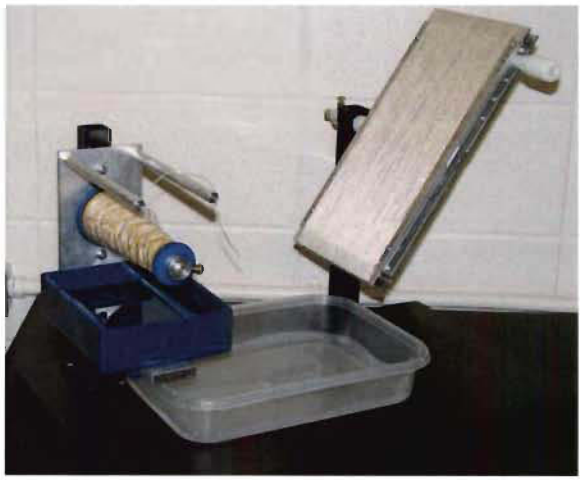

Figure 3-4. Final stage of manual aligning.

Once the UD flax layer is made, it is wetted and left overnight for drying. This allows fragile polar bonds to develop between the fibers, which ease handling of the layer during fabrication of the hybrid flax/paper reinforcement.

Surface density of a UD flax layer is controlled by the yarn linear density (tex) and spacing between the yarns. Equation 3-4 is used to calculate the surface density of a UD flax layer (in g/m^2) knowing yarn tex and spacing between yarns. Considering that width and length of flax layers obtained from the apparatus of Figure 3-4 are 6 inches and 12 inches, respectively, therefore the total length of the yarn used in a ply is:

$$Total\ yarn\ length\ (m) = Spacing\left(\frac{yarn}{in}\right) \times 6\ (in\ ) \times 12(in) \times 0.0254(\frac{m}{in}) \qquad 3\text{-}1$$

so the weight of the total length of yarn calculated in Equation 3-1 would be:

$$Flax\ ply\ weight\ (g) = \big(Total\ length\ used\ (m)\big) \times \frac{tex(g)}{1000\ (m)} \qquad 3\text{-}2$$

dividing the above-calculated weight by the surface area of a ply, that is:

$$Surface\ area\ of\ a\ ply\ (m^2) = 6(in\ ) \times 12(in) \times 0.0254^2(\frac{m2}{in2}) \qquad 3\text{-}3$$

yields the following equation for estimating surface density of a flax ply:

$$Flax\ ply\ Surface\ density\ \left(\frac{g}{m^2}\right) = \frac{Spacing\left(\frac{yarn}{in}\right) \times tex\ (g)}{0.0254\ (\frac{m}{in}) \times 1000\ (m)} \qquad 3\text{-}4$$

From Equation 3-4, it observed that two plies with different values for spacing and tex can have the same surface density as long as the product of spacing × tex are equal. Figure 3-5 shows three types of tex 200 UD flax layers on the flax/paper reinforcement layers.

3.2.2. Dynamic sheet former machine

Figure 3-6 shows the manually controlled dynamic sheet former (DSF) machine of Allimand® Company, utilized in this study to fabricate paper sheets. In the figure, the central cylindrical container is where the sheets are made on a plastic forming fabric installed upon a perforated centrifugal drum (Figure 3-7). In order to develop a paper sheet, first some stock slurry with the desired consistency (usually between 0.1 -1.0 %) is stored in the on-board tank at the right hand side of the central container. Then a wall of water is built on the forming fabric by projecting water on it while it is spinning to provide an even distribution of Kraft fiber. Next, as is shown in Figure 3-7, the prepared stock slurry is evenly distributed across the width of the forming fabric through a spraying nozzle moving upward and downward with a constant speed while the drum is still spinning. There is always a minor loss of pulp in the process of paper fabrication with the dynamic sheet former machine. However, since the machine's parameters have been kept constant at all times (80 rpm for the pump) it is assumed that the portion of pulp loss is constant for all series of paper fabrication. The paper surface densities were measured after fabrication of paper layers and as will be shown in section 3.9, they have small standard deviation signaling consistency of process.

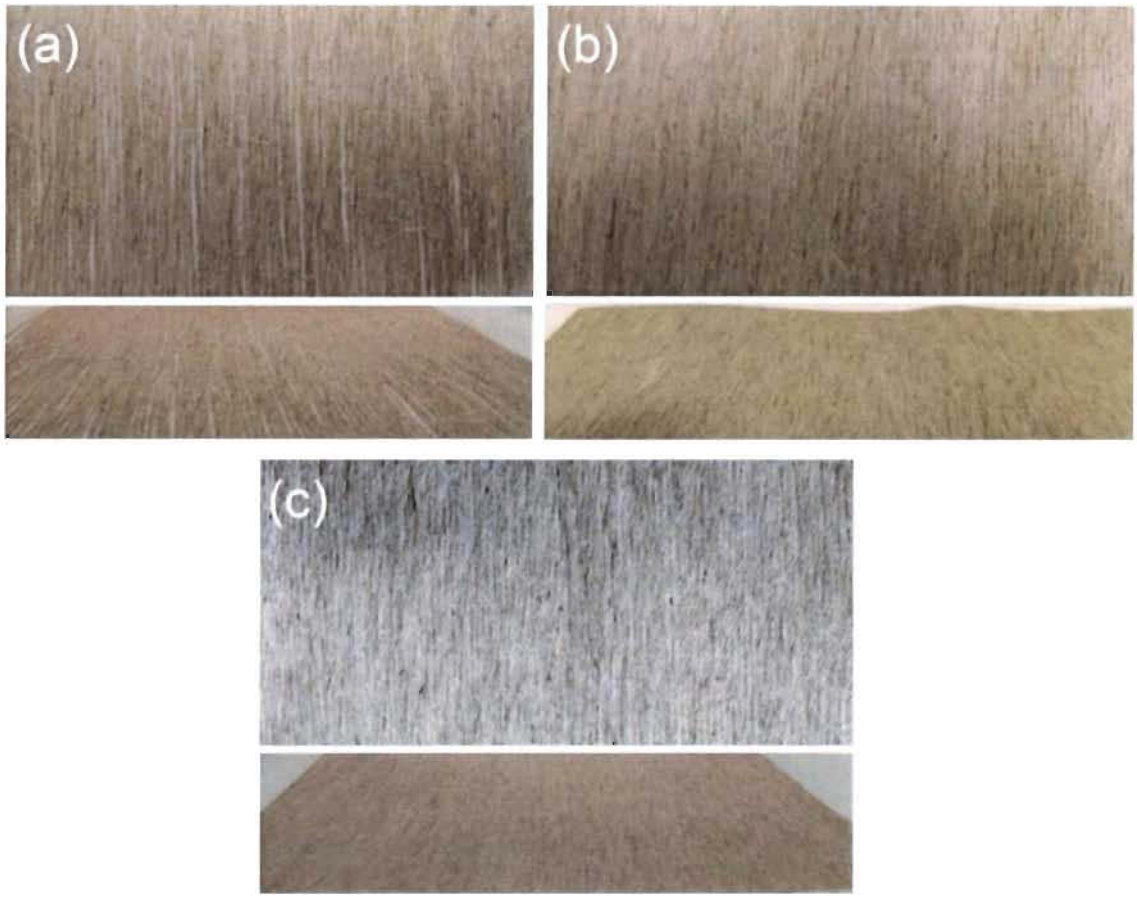

Figure 3-5. Flax/paper reinforcements (flax layer side) with flax layers of (a) 16 yarns per inch, (b) 20 yarns per inch and (c) 24 yarns per inch.

Figure 3-6. Allimand® dynamic sheet former machine.

Actually, the dynamic former is devised to simulate the headbox and forming table of the pilot paper machine (Figure 1-5) using nozzle and forming fabric, respectively. Although the dynamic former is not identical to pilot machine and its parameters differ from those of the pilot machine, an analogy can be made between the two groups of parameters to make them comparable to each other [98]. Moreover, among different laboratory former machines, the dynamic former produces paper sheets having characteristics (such as non-uniformities and anisotropies) comparable to papers made on the pilot paper machines.

Some important parameters of dynamic former which could affect the paper formation quality include the stock volume put in the machine, stock flow rate through the nozzle, water wall thickness, rotational speed of forming fabric, fabric type, dewatering rate, nozzle linear speed as well as nozzle-to-fabric speed ratio which controls the cross direction to machine direction fiber orientation ratio. The specifications of the machine employed in this study are shown in appendix D.

3.2.3. Sheet press

Three main functions of paper pressing include: dewater the paper, consolidate the fiber web and reduce the surface roughness. After formation in the dynamic former, the wet pressing of paper sheet involves pressing the sheet between press rollers while the sheet is sandwiched between the plastic forming fabric kept underneath and a blotter paper placed on top. Figure 3-8 shows the sheet press employed in this study. It is a product of CanPa® Instruments and is specifically designed for pressing the long sheet produced by the dynamic former machine. It features four selectable pressing speed and two selectable pressing loads

(low and high). The specifications of this press are indicated in Table 3-2. It should be mentioned that the standard laboratory pressing method differs significantly from the situation of an industrial paper machine press section. For an industrial machine, the pressing time is substantially shorter (order of milliseconds) and the pressure level is higher. So, the dynamic nature of the pressure pulse of a paper machine nip (squeezing region between two pressing rollers) does not occur in the laboratory press.

Figure 3-7. Spreading pulp furnish upon the plastic forming fabric (modified from [66]).

Figure 3-8. CanPa® four-speed bi-directional sheet press.

Table 3-2. Specifications of the wet sheet press machine

Maximum test sheet size	280 mm wide × 900 mm long (11"× 36")
Roller size	133 mm diameter × 330 mm long (5.25" D × 13" long)
Roller speed	4-speed adjustable, max. 10 cm/sec
Roller nip pressure	200 lbs/inch at 4 bars
Instrument air	100 psi maximum (7 bar)

3.2.4. Sheet dryer

Figure 3-9 shows the sheet dryer consisting of a heated drum over which the sheet of paper, maintained in place by a plastic fabric, rotates during drying. The dryer is a product of Adirondack Machine Corporation, Formax™ model. This standard dryer is specifically designed to evenly dry pulp and paper products and is equipped with a scaled hand-turning switch allowing for drum temperature adjustment. Another hand-turning switch allows adjustment of the drum rotating speed. General specifications of the dryer are indicated in Table 3-3. A digital thermometer from OMEGA Instruments (shown in Figure 3-10) using a type K chromium-Aluminum thermocouple is used to manually measure and adjust the drum surface temperature.

Figure 3-9. Formax™ hand sheet drum dryer of Adirondack Machine Co.

Table 3-3- Specification of the Formax™ drum dryer.

Motor	selectable speed drive motor control, 0-8 rpm
Heat	selectable heat input, 3200 W
Power supply	240 V, 1 Ph, 50 Hz
Drying drum	nickel plated aluminum of 12" diameter with a 16" face
Maximum test sheet size	300 mm × 300 mm

Figure 3-10. Model HH11B digital thermometer with model 98221 type K thermocouple.

3.3. **Pilot-scale manufacturing of the reinforcement with paper machine**

The general specifications of the pilot Fourdrinier paper machine of Innofibre from the Cégep of Trois-Rivières, are shown in Appendix E. In order to develop the hybrid flax/paper reinforcement with the paper machine, flax yarns must be deposited on the forming table of the paper machine (Figure 1-5) while it is running. This is performed using the feeding frame in Figure 3-11, which was designed at LMEM for this purpose. The frame can accommodate up to 16 flax yarn bobbins. The yarn ends pass through the appropriate holes in the eyelet bar and subsequently through the tightener section. The spacing between yarns is next adjusted using calibrated combs. Figures 3-12 and 3-13 show three combs tested in this study. The

comb of Figure 3-12 could be used for feeding 10 yarns with one inch spacing between each. The resulted reinforced paper out of this comb could be potentially employed in packaging applications, where the flax yarn provide higher strength than paper or cardboard alone. The combs of Figure 3-13 are used for producing a one inch wide sample of 16 yarns per inch flax/paper reinforcement. The reinforcement produced with these combs can be used for producing reinforcement samples to be used next to prepare and test composite samples. Technical drawing of the comb of Figure 3-13b is illustrated in Figure 3- 14.

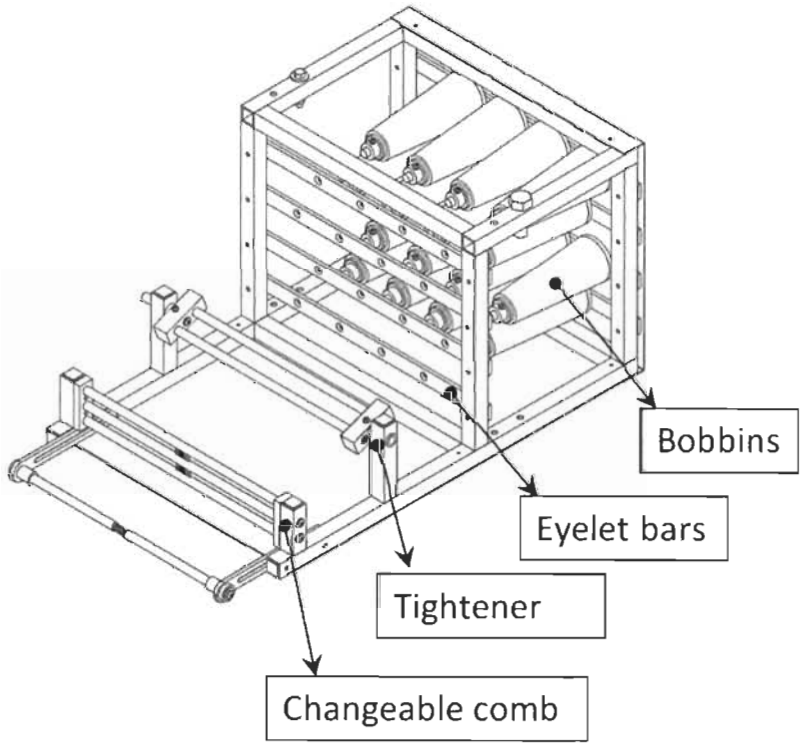

Figure 3-11. The feeding frame to deposit flax yarns into paper machine.

Figure 3-12. The comb with one hole per inch.

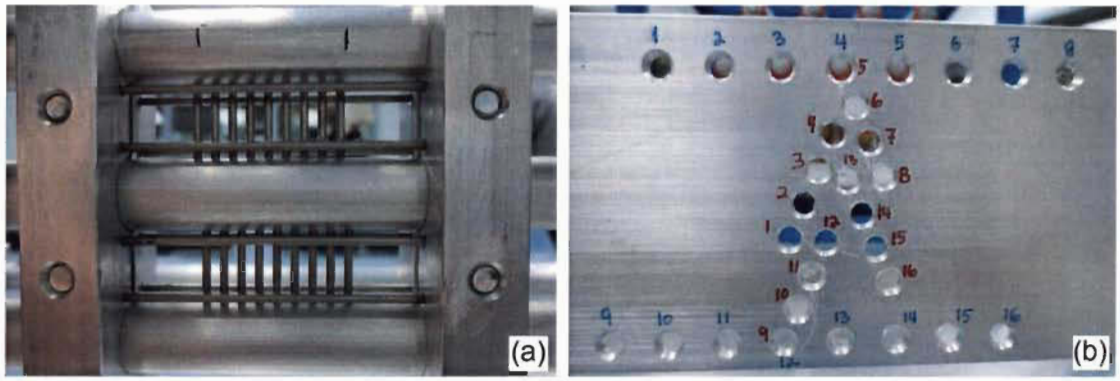

Figure 3-13. Two different comb designs for laying down 16 flax yarns in one inch.

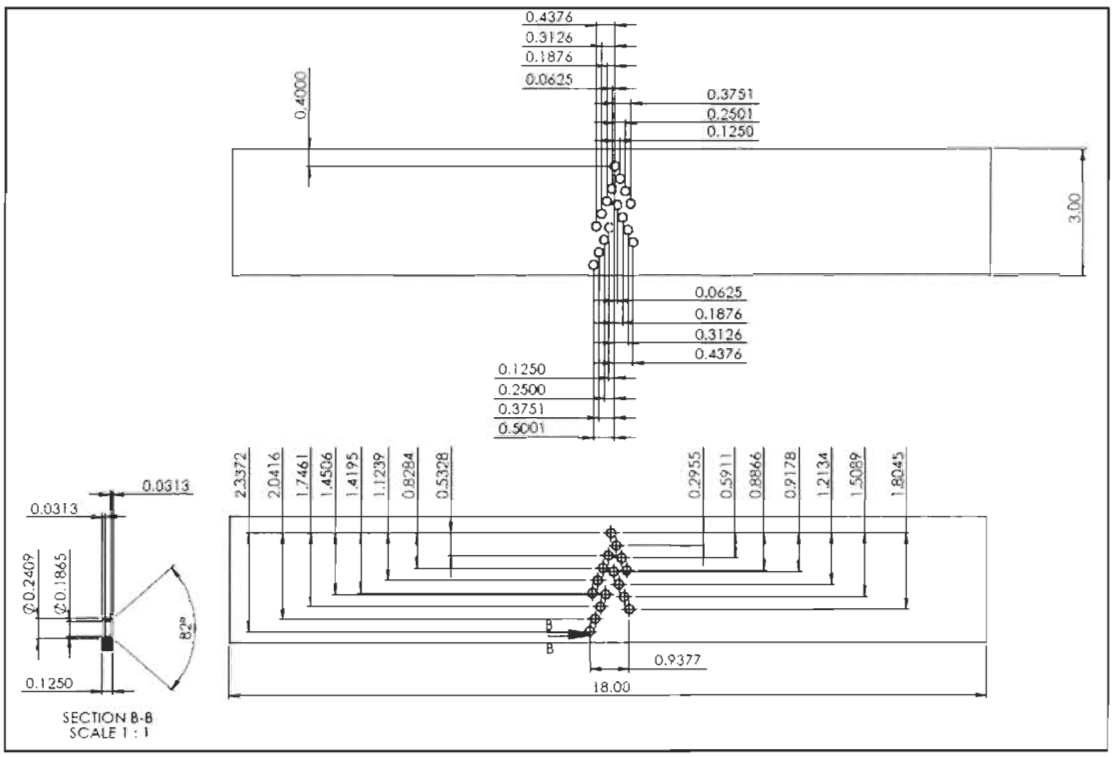

Figure 3-14. Technical drawing for the comb of Figure 3-13b, dimensions are in inches.

After the bobbins are installed on the feeding frame and the low twist yarns ends are passed through the eyelet bars, the tightener and the desired comb, the feeding frame is installed on the paper machine. Figure 3-15 shows the feeding frame installed over the forming table of the paper machine. This frame can be positioned at the desired distance and angle with respect to the top of the table. When the ends of the flax roving contacts the running forming table over which the pulp slurry is spread (using the headbox), the roller in the forming table section (schematically shown in Figure 1-5) causes the flax yarns to be drawn into the paper machine at the end of which the unidirectional hybrid flax/paper reinforcement is rolled up.

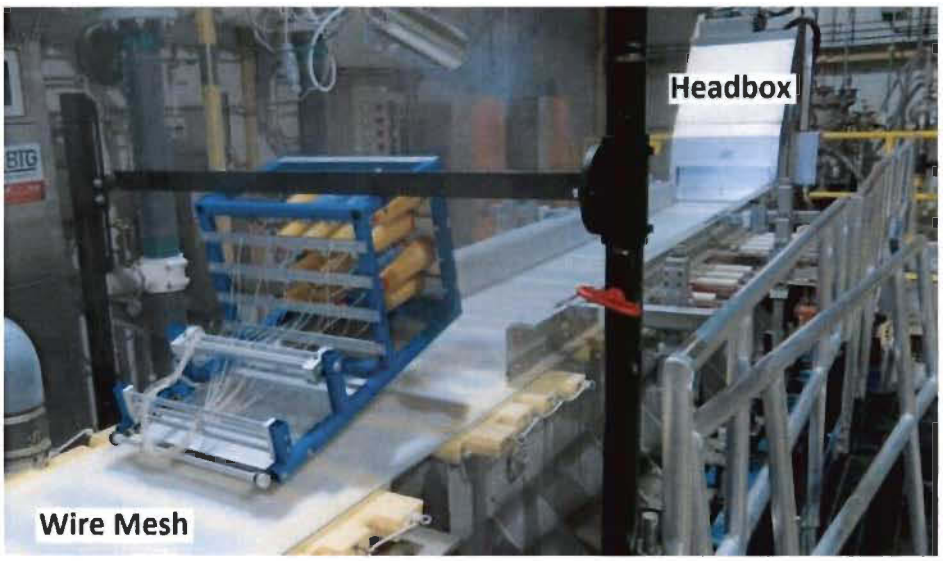

Figure 3-15. Installed feeding frame on the paper machine forming table.

3.4. **Internal bond strength measurement (shear cohesion test)**

Internal bond strength (IBS) is a general term describing the fiber-to-fiber bonding strength of a sheet of paper in a plane located around the mid-thickness of the sheet. As is schematically illustrated in Figure 3-16, a number of different standard methods are available

to measure the IBS of papers and paperboards [99]. In this thesis, to evaluate the shear strength between two adhered layers of flax and paper in the dry reinforcement, the shear cohesion test (Figure 3-16E), was employed and adapted for our particular application.

The modified technique used in this work is depicted in Figure 3-17. Throughout this thesis, shear cohesion tests are always performed on laboratory-made flax/paper reinforcements. Samples of dimension 25 mm × 150 mm (1 in. × 6 in.) are prepared. Next, the test sample is prepared by peeling off each end of a flax/paper reinforcement over a precise length such that an overlap area (jointed area in Figure 3-17) of 25 mm × 25 mm (1 in × 1in) remains in the middle of specimen. Then the samples are exposed to tensile force from both ends, resulting in a shear force (converted to shear stress) in the jointed area. Samples are tested based on D.34 standard of Canadian pulp and paper association, using an Instron tensile machine equipped with a model 2525-816, 0.5 kN load-cell capable to measure a load in the range of 2N (0.2 kgf) to 0.5kN (50 kgf) with a precision of ± 0.25 % of the read value. The cross-head speed was 2.5 mm/min and based on the standard, the test is stopped once 30 % of maximum load is lost. All of the samples are conditioned at relative humidity of 50 % and 23°C for more than 24 hours, and tested under these conditions in the humidity controlled room.

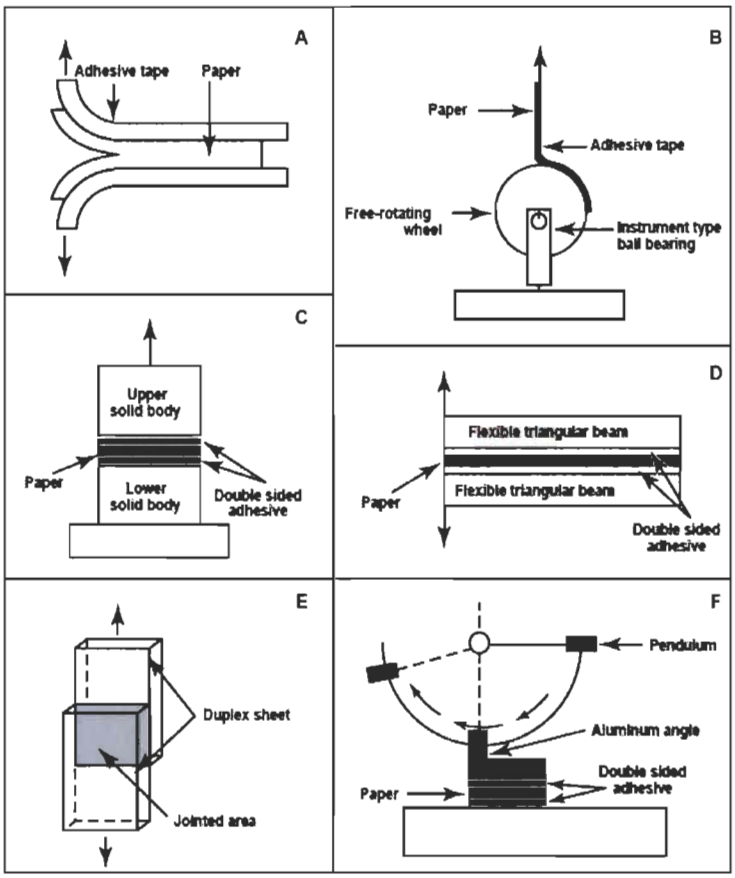

Figure 3-16. Methods of measuring the internal bond strength (IBS): A. Peel cohesion test; B. Delamination test; C. Z-directional tensile test; D. Cantilever beam test; E. Shear cohesion test; F. Scott bond test [99].

3.5. **Thickness measurement of reinforcement layers**

Thickness of reinforcement is measured using Model 549 E micrometer from Testing Machines Inc. shown in Figure 3-18. This device is a standard micrometer in the paper industry to measure thickness of papers and has the accuracy of 1/200 mm. or 1/10000 in, with the measurements made constant and controlled contact pressure.

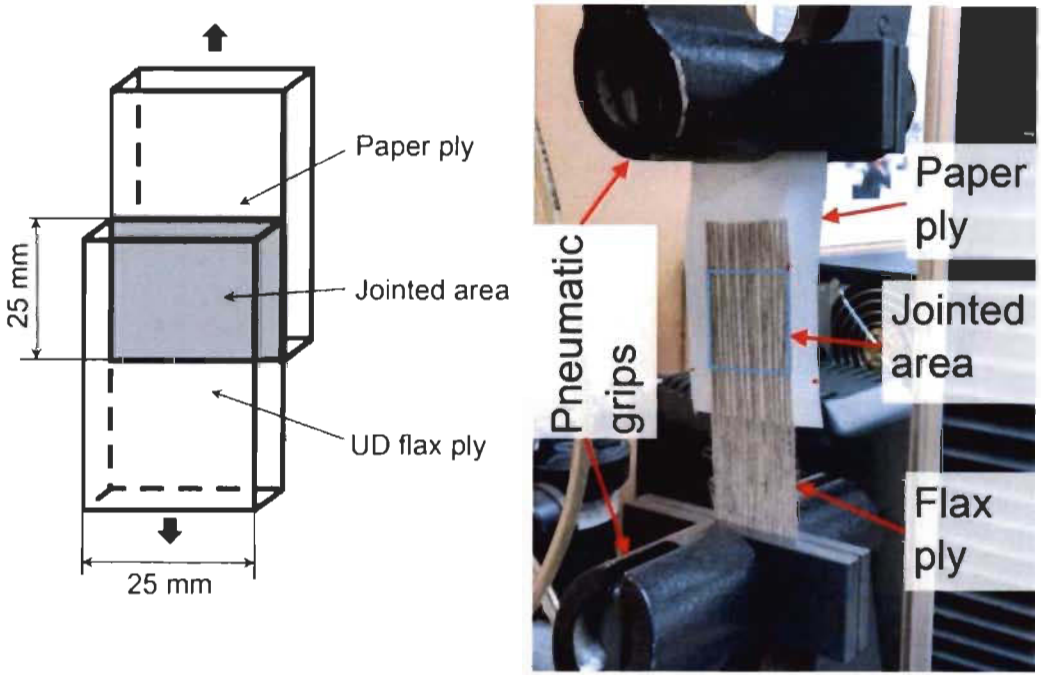

Figure 3-17. Shear cohesion test adapted for this work (a) schematic (modified from [99]) and (b) a typical test specimen installed on the Instron tensile testing machine.

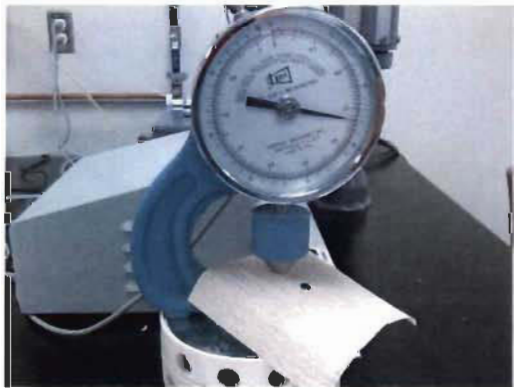

Figure 3-18. Micrometer for measuring reinforcement thickness.

3.6. **Permeability measurement**

3.6.1. Permeability mold

A schematic representation of the permeability mold developed and used in this study is shown in Figure 3-19. The top mold half is made of a 19 mm thick tempered glass plate which allows for visualizing and tracking the flow front progress. The tempered glass

plate has a negligible deflection and so maintains the cavity height as constant as possible throughout the experiment. A metallic fixing frame with a central window of 165 × 127 mm (6.5 × 5 in.) is mounted on the tempered glass and screwed to the bottom steel mold half using six screws of half an inch diameter. This fixing frame minimizes the deflection of tempered glass plate. Precise Starrett shims are used between top and bottom mold halves to adjust the cavity height and consequently the fiber volume fraction. Axes 'x' and 'y' shown on the reinforcement in Figure 3-19 indicate the laboratory coordinate system. The required cavity height (h) to obtain the desired V_f is computed as follow (Equation 4 of [74])

$$h = (n \times m_r)/(\rho_f \times V_f) \qquad 3\text{-}5$$

Where n is the number of stacked reinforcement layers, m_r (g/m^2) is the surface density of each reinforcement layer and ρ_f (g/m^3) is the fiber density. An average fiber density of ρ_f = 1.5 g/cm^3 ([100-102]) is considered for the flax and soft wood Kraft fibers. For each permeability measurement experiment a stack of four (n = 4) hybrid reinforcement layers of 15 × 15 cm (6 × 6 in) is used and each stack has a 12 mm diameter hole in its center. The hole is pierced using a special punch made of a thin razor blade rolled around a 12 mm diameter mandrel (Figure 3-20). Making this hole provides the required circular inlet gate (R_0 parameter in Figure 3-21 described later) while helping improve the precision of permeability results [74]. The test fluid is injected at a constant vacuum of 100 kPa. Vacuum is provided by a vacuum pump connected to the four outlet vents located at the four corners of the mold cavity.

In designing the permeability measurement set-up, the first and foremost criterion is that the cavity thickness should remain constant during the test, with the highest precision possible in order to obtain reliable results with less dispersion. The mold in Figure 3-19 was designed and manufactured to meet this requirement

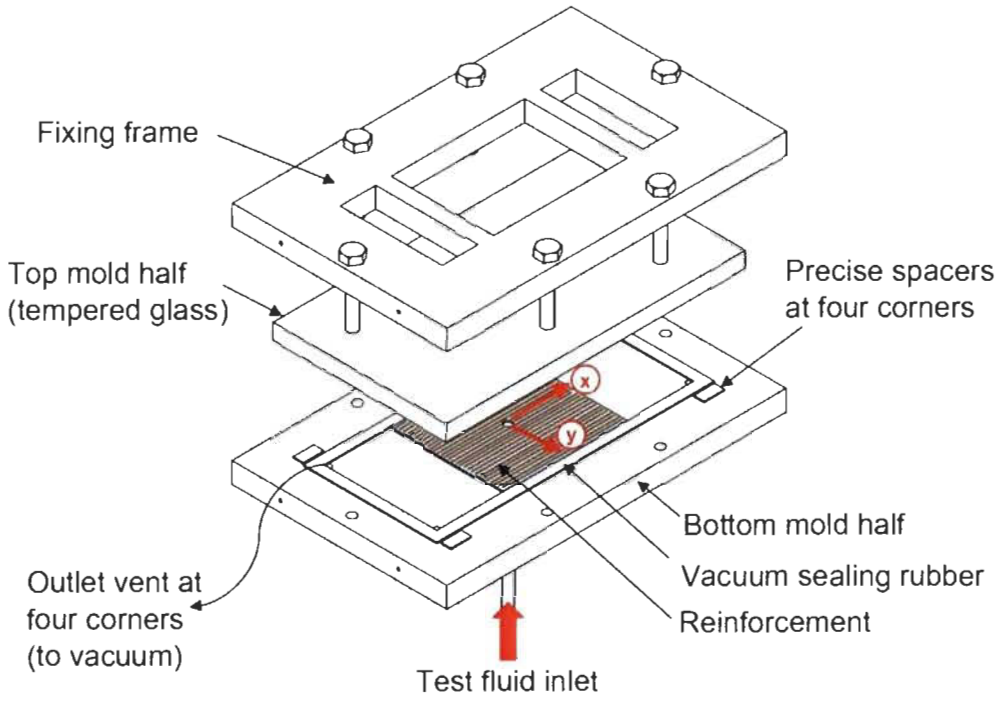

Figure 3-19. Schematic representation of the permeability mold used in this study

Figure 3-20. Custom punch used to cut injection hole in the reinforcements.

According to Alms et al. [76] the deflection of the permeability mold should be evaluated to make sure it is less than 2 % of the nominal cavity height. Accordingly, maximum deflection of the tempered glass was measured using a Mitutoyo model BH305 coordinate measuring machine (CMM). First, the stack of reinforcements was placed inside the mold and vacuum was applied. At $V_f = 35\%$ (same for all tests) and after applying vacuum over the test samples, the glass plate nearly touches the shims (for some of the tests, it was indeed contacting). This means vacuum was almost enough to reach the desired V_f and the fixing frame was mainly required to avoid the upward deflection of the plate during resin injection. The bolts of supporting frame were next tightened to make sure the thickness spacers were in contact and remained in contact with both halves of the mold during injection. Next, the Z coordinates at the surface of the glass plate were measured for a grid of 25 points drawn on top of the plate. Finally, the vacuum pressure was removed and the Z coordinates of the points were measured again. Subtracting Z coordinates of each point before and after vacuum gives the deflection of the given point. Removing vacuum correspond to the extreme situation in terms of deflection variation because during resin injection, vacuum pressure is just partly removed when the flow front progresses. The maximum variation in the Z direction (occurred in the middle of glass plate) was 0.030 mm for the maximum cavity thickness of 1.65 mm (in Table 3-4), and 0.014 mm for the minimum cavity thickness of 1.10 mm (in Table 3-4), which means maximum cavity height variations of 1.8% and 1.3% respectively, that are well below the 2% limit.

Table 3-4. Measured surface density (m_r) of flax/paper reinforcements and nominal cavity height to attain $V_f = 35\%$.

Run	m_r (g/m^2)		Nominal cavity height (mm)
	mean	STD	
1	147	2	1.12
2	144	2	1.10
3	197	9	1.50
4	204	4	1.55
5	152	4	1.16
6	155	5	1.18
7	216	3	1.65
8	204	6	1.55

3.6.2. Measurement procedure

Permeability which is defined as the resistance to fluid flow inside a porous media, is a second order tensor exhibiting point symmetry and thus can be completely characterized by just three principal values, namely two in-plane permeability and a through thickness one. However, as thickness of the part is much smaller than the other dimensions in shell-like structures, studying the in-plane permeability is more relevant for liquid composite molding of thin-walled structures [74]. So in this work and as a first attempt, attention has been given to in-plane permeability measurement, keeping in mind that studying the out-of-plane permeability will be required in future works, especially for molding thick parts.

For an anisotropic 2D medium the permeability tensor is shown as below, where 'x' and 'y' indicate laboratory coordinate system and $k_{xy} = k_{yx}$ due to symmetry.

$$[k] = \begin{pmatrix} k_{xx} & k_{xy} \\ k_{yx} & k_{yy} \end{pmatrix} \qquad 3\text{-}6$$

Permeability is a determining parameter in resin flow inside a porous fibrous media, via empirical Darcy's law given below in the general form,

$$\bar{u} = -\frac{1}{\mu}[k]\nabla p \tag{3-7}$$

where μ is the fluid dynamic viscosity, $\bar{u}$ the fluid velocity vector inside the porous media, and ∇p the vector of pressure gradient inside the porous media.

$$\bar{u} = \begin{bmatrix} u_x \\ u_y \end{bmatrix} \tag{3-8}$$

$$\nabla p = \begin{bmatrix} \partial p/\partial x \\ \partial p/\partial y \end{bmatrix} \tag{3-9}$$

Another equation governing the fluid flow inside a porous media is the continuity equation (mass conservation) written in its general form (supposing a constant fluid density) as.

$$\nabla . \bar{u} = 0 \tag{3-10}$$

Solutions to Equations 3-9 and 3-12 for rectilinear and radial flow in an isotropic media with constant injection pressure or constant flow rate boundary conditions are given in [103].

Two types of permeability to distinguish include saturated and unsaturated permeability. In the unsaturated permeability, the injected test fluid flows through the dry preform by filling macroscopic (between fiber yarns) and microscopic (inside fiber yarns) pores such that a certain region, called unsaturated zone, separates the effective flow front (externally observed flow front) from the fully saturated flow front located behind the effective front. In the saturated case, the fibrous preform is fully impregnated by the test fluid so that any new incoming fluid will just replace the already present one. Both types of permeabilities can be

measured through either constant pressure or constant flow rate injection. A further difference in the types of permeability test set-up includes 1D (or linear flow) experiment and 2D (or radial) injection.

In this study, the unsaturated permeability of the hybrid flax/paper reinforcement is measured using a constant injection pressure and 2D radial flow experiments. The measurement is based on recording several flow front position versus time and then processing them according to the approach proposed in appendix 2 of [57]. Because the reinforcement and consequently resin flow have directionality, during the experiment the liquid flow front is elliptical with R_1 and R_2 representing the length of the major and minor radii of the ellipse, as schematically shown in Figure 3-21, and R_0 is the radius of inlet port where the fluid enters the reinforcement. At the end of experiment we obtain a set of raw data comprising R_1 and R_2 radii with their corresponding absolute injection times, like the data set exemplified in Table 3-5.

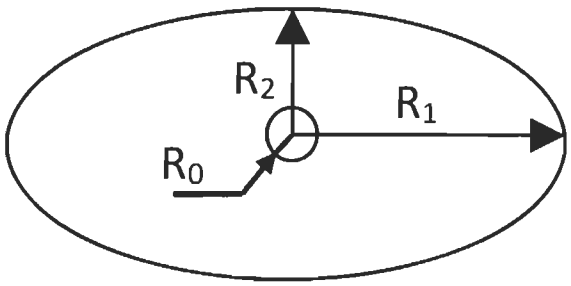

Figure 3-21. Schematic of an elliptical flow front in a two-dimensional permeability measurement.

Table 3-5. A typical set of experimental data acquired from a permeability test.

Absolute injection Time	Major radius	Minor radius
t_1	R_{11}	R_{21}
t_2	R_{12}	R_{22}
t_3	R_{13}	R_{23}
.	.	.
.	.	.
.	.	.
t_n	R_{1n}	R_{2n}

Figure 3-22 shows the permeability measurement set-up used in this study. After the test fluid enters the mold several photos are taken at regular time intervals using a 10 mega pixels A640 Canon photo camera which is adjusted perpendicular to the mold plane. Each photo is time stamped such that impregnation temporal evolution can be monitored. A small video camera recording the very moment of test fluid entry into the mold allows calculating the absolute injection time (starting from test fluid entry) of each taken photo. Using two embedded longitudinal and transverse rulers in the photos (shown in Figure 3-22), a rectangular portion of the captured photos involving the flow front ellipse can be extracted with known physical dimensions. Figure 3-23a shows such an extracted portion. The extracted photo is then treated with a prepared Matlab® image processing code (named code A, hereafter) which fits an ellipse to the flow front and computes the length of major and minor radii in pixel unit. Figure 3-23b depicts a treated digital image. Knowing the precise area covered by the photo enables to convert the pixel units into physical dimensions.

To give an example of the permeability calculation procedure, results of one of the experiments on the natural fiber reinforcements of this study are used. Table 3-6 compares the major and minor radii calculated by code A (Figure 3-23b) with those measured directly from

the photos using the embedded rulers. As can be seen, at small radii (at 5 and 10 sec) the difference is quite noticeable. However, as the time increases the discrepancy becomes negligible.

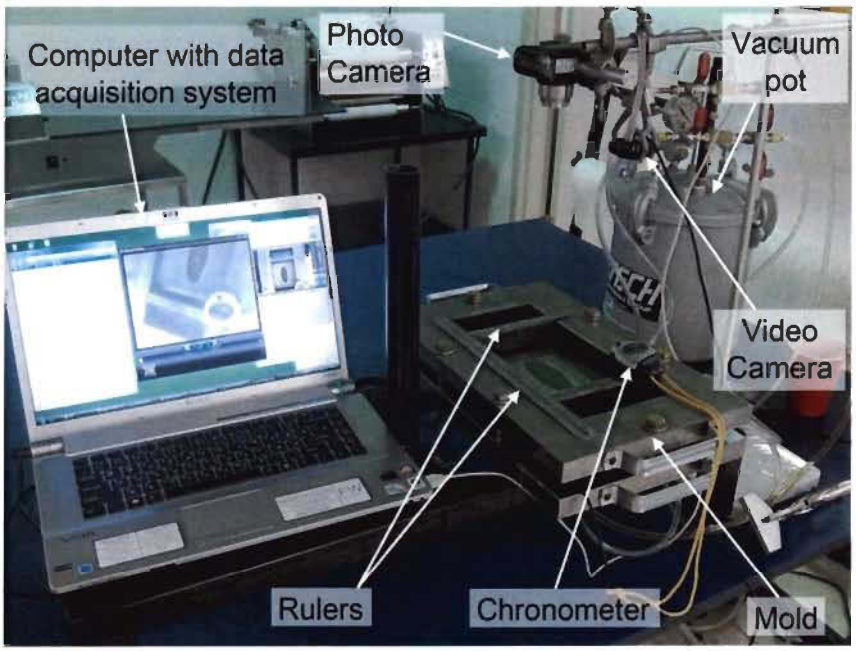

Figure 3-22. Overview of permeability measurement set-up.

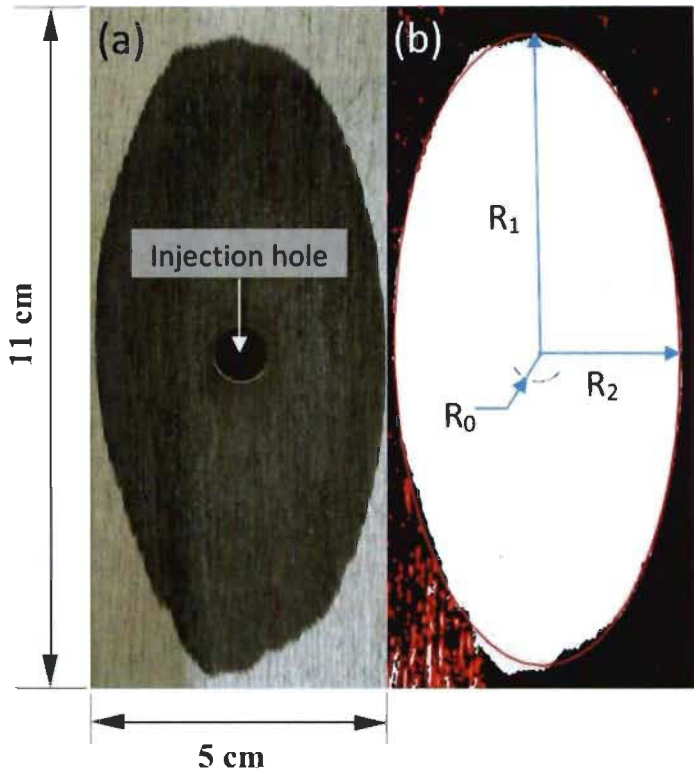

Figure 3-23. Procedure of flow front detection: (a) extracted photo with known physical dimensions (b) treated photo using the Matlab code A.

Table 3-6. Comparison of flow front detection methods.

Time (Sec.)	Code A value		Direct measurement	
	R_1 (cm)	R_2 (cm)	R_1 (cm)	R_2 (cm)
5	1.20	0.84	1.50	0.95
10	1.61	0.95	1.80	1.05
15	1.92	1.05	2.05	1.10
20	2.17	1.11	2.25	1.20
25	2.39	1.18	2.45	1.25
30	2.54	1.24	2.65	1.30
35	2.71	1.29	2.75	1.35
40	2.88	1.34	2.90	1.40
45	3.01	1.38	3.05	1.43
50	3.14	1.42	3.30	1.55

Once the set of raw data (Table 3-5) is obtained, they are treated according to the method described in [57]. The method is summarized below in six steps and a Matlab® code (named code B, hereafter) has been prepared according to these steps in order to routinely calculate permeability values from the sets of raw data. In this study, due to the unidirectional configuration of the flax yarns the reinforcements are considered orthotropic, meaning that directions of principal permeabilities (R_1 and R_2 in Figure 3-23b), respectively coincide with the laboratory coordinate system 'x' and 'y' shown in Figure 3-19. The procedure of calculating K_1 and K_2 permeabilities is as follow [56, 57]:

a) A regression line passing through the origin of graph is drawn through a sequence of experimental points [R_{1i}, R_{2i}] (i=1, 2, 3…, n) and the slope of this line, m_1, is computed (Figure 3-24a).

b) Equivalent values R_{1ie} and R_{0e} are computed for each R_{1i} and for the radius R_0 of the inlet port, as follows:

$$R_{1ie} = (m_1)^{1/2} R_{1i} \ , \ R_{0e} = (m_1)^{1/2} R_0 \qquad 3\text{-}11$$

c) For each R_{1ie} a corresponding parameter, called F_i is computed with:

$$F_i = (R_{1ie}/R_{0e})^2(2ln(R_{1ie}/R_{0e}) - 1) + 1 = 4K_e\Delta P t_i/\varphi\mu {R_{0e}}^2 \qquad 3\text{-}12$$

where K_e is the equivalent permeability, ΔP (Pa) is the difference between the inlet pressure (p_0) and the pressure at the flow front (p_f), μ (Pa.s) is the dynamic viscosity of test fluid and φ is the fiber preform porosity ($\varphi = 1\text{-}V_f$).

d) A regression line is drawn through a sequence of $[F_i, t_i]$ points and the origin and the slope of this line, m_2, is computed (Figure 3-24b).

e) The equivalent permeability, K_e, is calculated as follows:

$$K_e = m_2 \varphi \mu R_{0e}^2 / 4\Delta P \qquad 3\text{-}13$$

f) Principal permeability values K_1 and K_2 are finally computed as:

$$K_1 = \frac{K_e}{m_1}, \; K_2 = m_1 K_e \qquad 3\text{-}14$$

To validate code B based on this procedure, raw data taken from [56] are used to calculate permeability values. Table 3-7 shows that the code B values compare well with those in [56]. Figure 3-24 also shows the experimental data points and the least square regression lines fitted on them.

3.7. **Composites fabrication**

Resin transfer molding (RTM) was used to fabricate composite laminates. Schematic of the RTM mold and the resin injection system employed in this study are shown in Figures 3-25 and 3-26, respectively. The top mold half is a 17 mm thick steel slab. It is mounted with a fixing steel frame screwed to the bottom mold half to firmly hold the top mold half and limit its deflection during resin injection. Four series of precise Starrett shims are used at four corners, between the top and bottom halves of the mold to adjust the cavity height. The required cavity height for obtaining the desired fiber volume fraction (V_f) is calculated based on Equation 3-5. All composites of this study are fabricated using eight layers of reinforcement ($n = 8$).

Table 3-7. Results of code B for permeability calculation.

Parameter	Code B value	Ref. [56]	% error
m_1	0.867	0.863	0.5
m_2	0.182	0.184	1.1
K_1 (m^2) × 10^{-10}	5.34	5.38	0.7
K_2 (m^2) × 10^{-10}	4.01	4.01	0.0

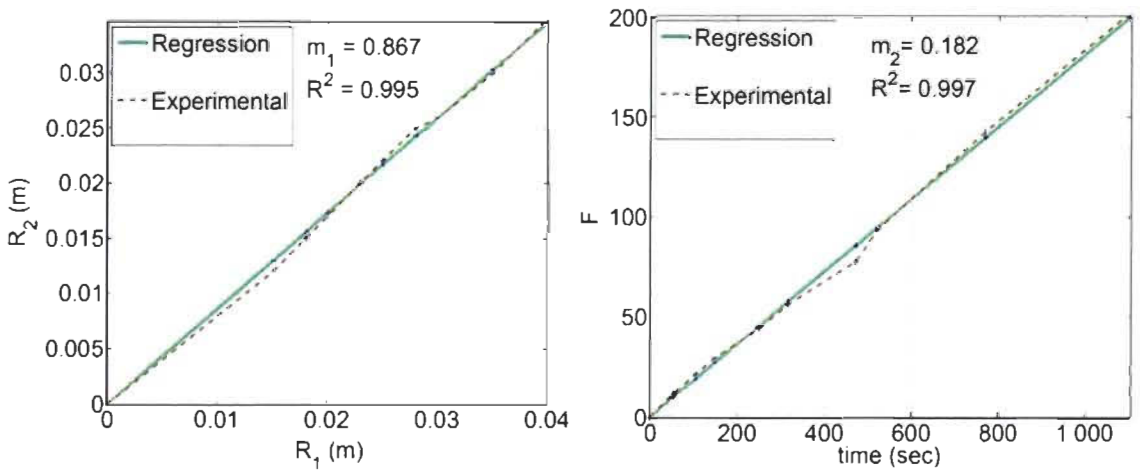

Figure 3-24. Outcomes of code B, (a) principal radii of elliptical flow front, (b) function F versus time, for experimental data of [56].

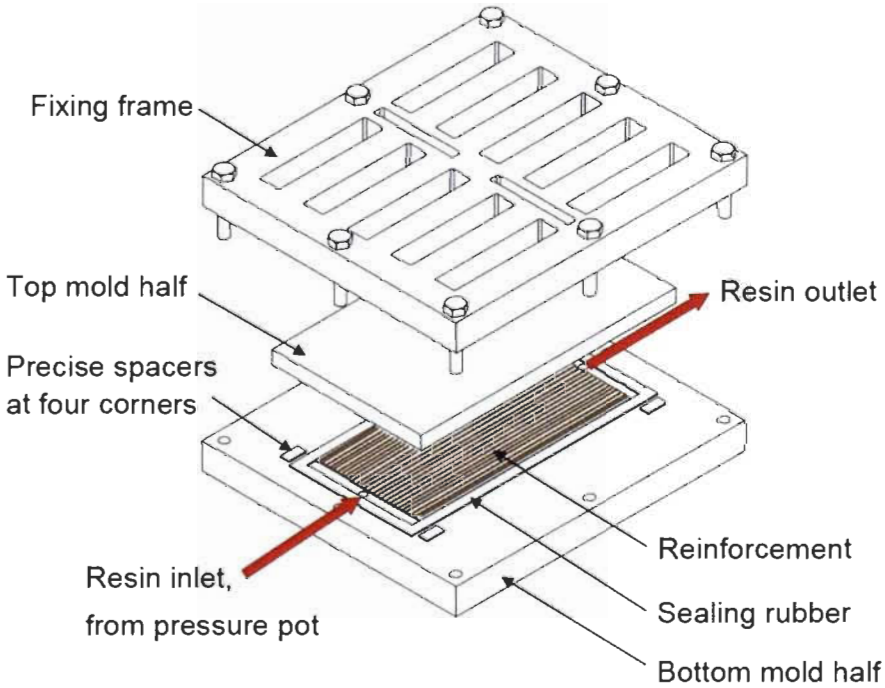

Figure 3-25. Schematic of the RTM mold used in this work.

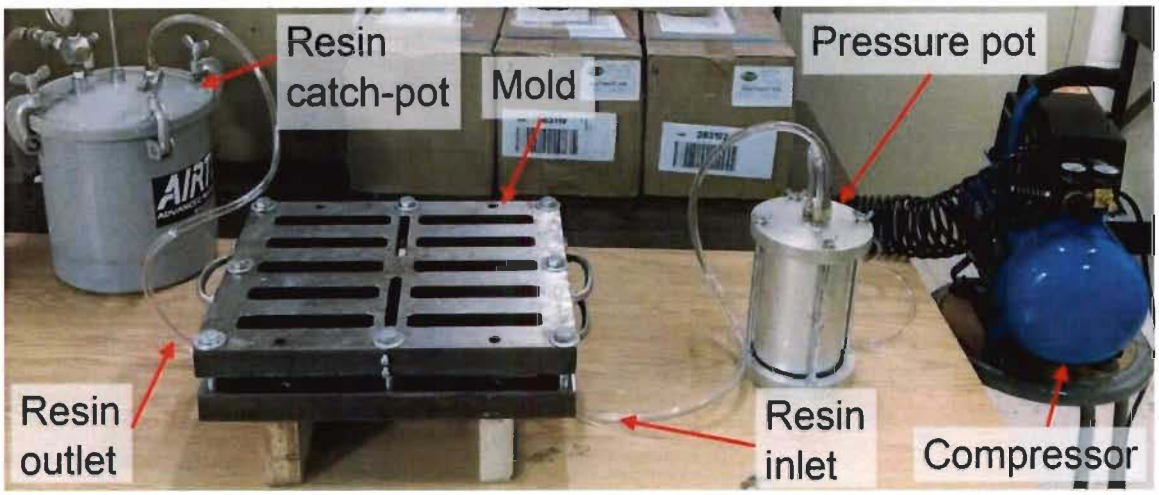

Figure 3-26. RTM composite fabrication setup.

The RTM injection setup (Figure 3-26) includes a compressor and a sealed pressure pot inside which the catalyzed resin cup is placed. Once the pressure (up to 4 bars in this study) is applied inside the pressure pot, resin enters the mold at one end and impregnates the reinforcement through a unidirectional flow along the yarns. Before injection, the catalyzed resin is degassed under vacuum for five minutes. Molded composites are post-cured at 80°C for 4 hours. Reinforcements are firstly impregnated at V_f= 30 % (using the required cavity height), then at the end of injection process when all the epoxy resin is injected, the top mold half is slowly pushed downward (through fastening the screws of the fixing frame in Figure 3-25) to reach the desired V_f, while the excess resin exits from the outlet. This technique ensures a well impregnated laminate and if some dry spots are left in the reinforcement due to permeability issues, they are forced to get impregnated when reducing the cavity thickness to reach the desired V_f. Using this molding technique, it was however not possible to study the relationship between permeability and tensile performance. Numerous molding trials were carried out in order to adjust the manufacturing parameters required for complete impregnation

of the composite plates, and Figure 3-27 shows one of the typical qualified composites used for mechanical testing in this work. 250 mm long by 15 mm wide specimens are cut from the composite plates using a water cooled diamond saw and then dried over-night at 80°C. Figure 3-28 shows some typical tensile test coupons.

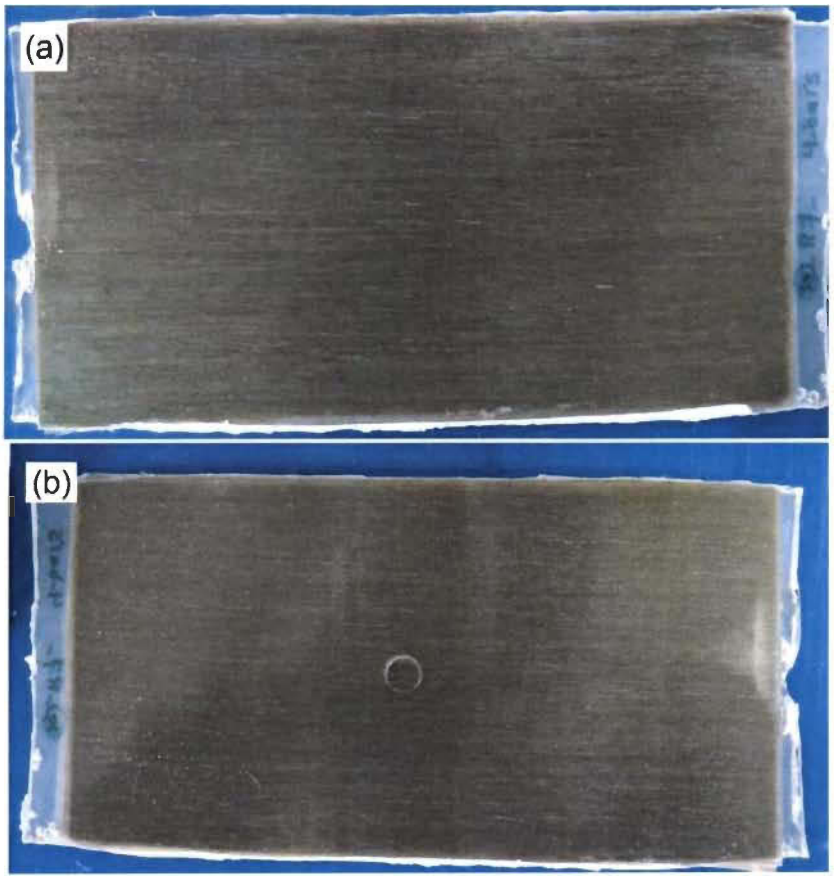

Figure 3-27. An impregnated composite plate (6″×12″) made out of the flax/paper reinforcement, (a) top side, (b) backside.

Figure 3-28. Tensile test coupons of the flax/paper composite (15 mm × 250 mm).

3.8. **Tensile testing of composites**

Figure 3-29a shows the testing setup and the stress-strain curve of a typical tensile test performed on composite samples of this work. The tests are carried out on a LM-U150/I Instron electromechanical machine at a cross-head speed of 2 mm/min according to ASTM D3039 standard. The machine is equipped with a 150 kN load cell and a model 3542 Epsilon Tech extensometer of 50 mm gauge length was used for measuring strain. Samples are gripped between the machine's grips using sandpaper sheets to increase the friction and reduce the need for large gripping forces. At least five composite specimens are tested for each type of composite plate. Because natural fiber composites show a bilinear behavior in their stress-strain curves [11] and a knee point is always noticed at around 0.20 % strain, for the samples of this study (Figure 3-29b) two moduli are evaluated for each sample. E_1 is the modulus before the knee point, calculated for a strain range of 0.025-0.1 % [104] and E_2 is

the modulus after the knee point calculated for a strain range of 0.3-0.4 %. Figure 3-30 shows some typical failed coupons. A Leitz Metallovert optical microscope (OM) and a Jeol JSM-5500 scanning electron microscope (SEM) are used to analyze the microstructure and facture surface of the samples.

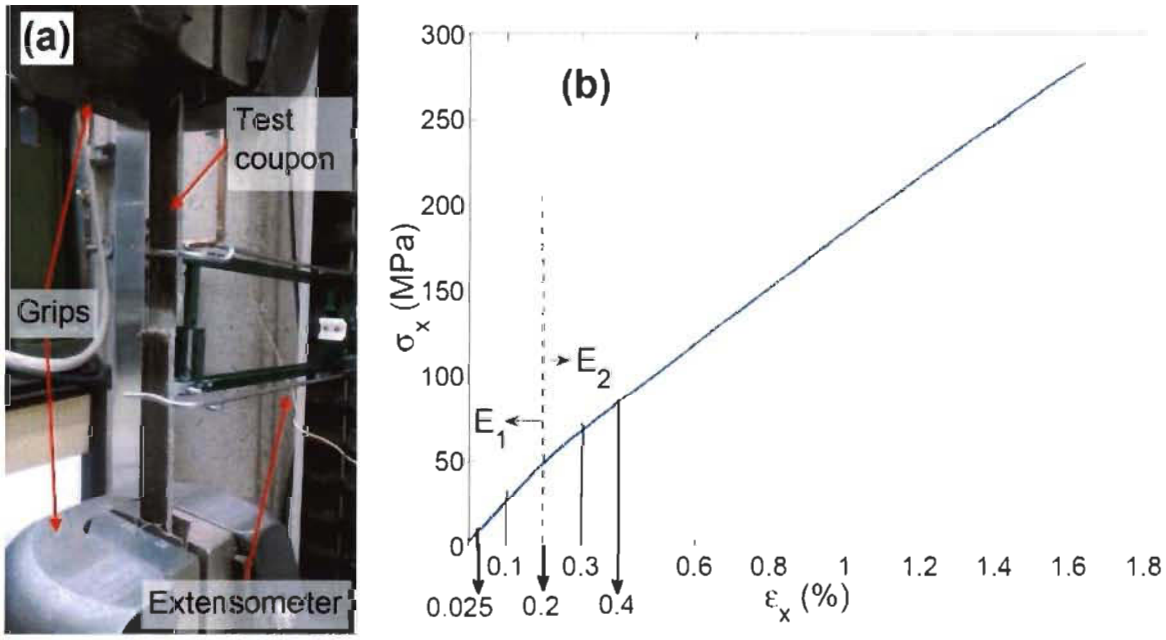

Figure 3-29. A typical tensile test (a) and stress-strain curve (b) of the flax/paper/epoxy

Figure 3-30. Typical tensile-test coupons after test.

3.9. **Robust parameter design approach and statistical modeling**

As explained in the introduction section, the main objective of robust parameter design is to minimize variance of the results while the sources of uncertainty still exist. Main causes that can potentially impart uncertainty into the reinforcement behavior of this study include the fabrication processes, characterization methods and material uncertainties, including inherent natural fiber properties' variation and design parameters setting of the reinforcement. Uncertainties due to fabrication and characterization methods are addressed here through developing consistent reinforcement and composite fabrication methods (explained in appendix C and section 3.7, respectively) as well as using reliable permeability mold and measurement procedures (section 3.6) while composite testing is performed according to ASTM standards. However, as will be explained in the results chapter, the IBS test method (section 3.4) shows a quite large variability in the results. Furthermore, natural fibers of this study have always been supplied from the same companies (Innofibre for Kraft pulp and Safilin for flax yarns) which favor the consistency of constituent material properties and subsequently of results. Principally in this thesis, studying inherent variation in physical/mechanical properties of different natural fiber species was not targeted and such an aspect is already studied in some other research works [102, 105].

For studying the variation of results due to parameters setting, the classical robust parameter design method shown in Figure 3-31 is considered in this thesis, as a general approach. This algorithm is devised based on references [39, 106, 107] and its detailed description is

explained in appendix F (section F.4). Explanations about design of experiment (DOE), analysis of variance (ANOVA) and regression modeling used in this approach are also given in the same appendix.

Taguchi method is reported less efficient than the classical method [106, 107], and with regard to the parameters of this study and their settings, it was hardly possible to implement the notion of outer array design of experiments used in Taguchi's method. Moreover, since the practical domain of each factor was not large and set at the beginning of experiments on the feasible experimental region, the heuristic portion of the algorithm (steps 5 to 10 in Figure 3-31) was not actually applicable and hence was not followed.

Throughout this thesis two DOE trials shown in Table 3-9 (called 1^{st} DOE hereafter) and Table 3-11 (called 2^{nd} DOE hereafter) are used. The 1^{st} DOE is a 2^{4-1} fractional-factorial resolution IV design of experiment considered for step 3 of Figure 3-31 and the 2^{nd} DOE is a full-factorial 3^2 experimental design used for step 11 of Figure 3-31. Because it was difficult to conduct a central composite design (CCD) for the parameter settings of this study (due to axial portion of the CCD), full factorial 2^{nd} DOE is used for step 11 of Table 3-11.

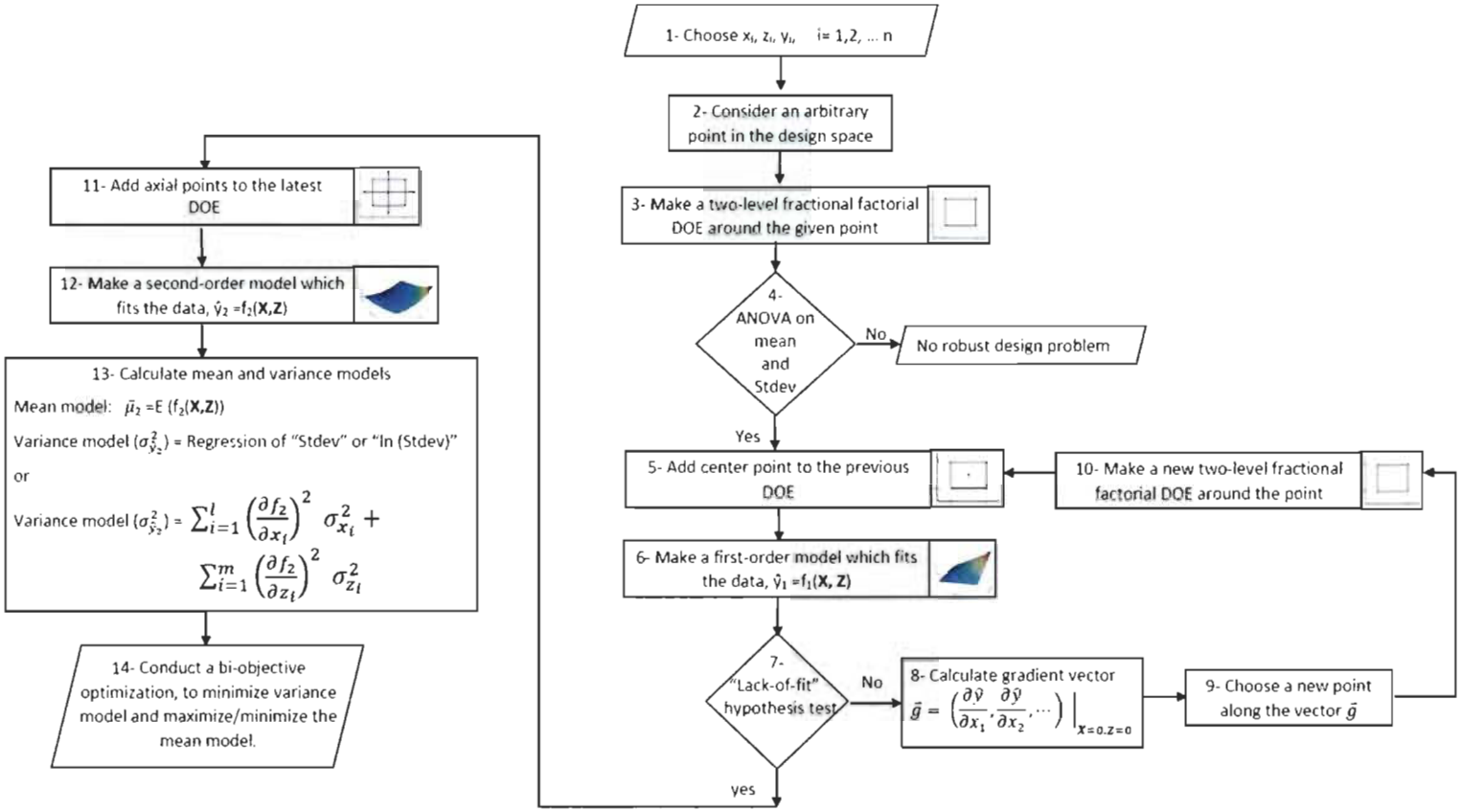

Figure 3-31. Algorithm of classical robust parameter design [39, 106, 107].

Firstly, IBS, permeability and tensile tests are conducted based on the 1st DOE in conformance with step 3 of Figure 3-31 and their results are presented and analyzed in the sections 4.1.2, 4.2.1 and 4.3.2, respectively. As will be explained in these sections, because IBS and tensile test results did not fulfill the criterion of step 4, other steps of Figure 3-31 are no more followed for IBS and tensile behavior evaluation. However, areal density of UD flax layer (factor B in the 1st DOE) is concluded influential on both mean and standard deviation of K_1 permeability (fulfilling robust criterion of step 4), therefore a second series of permeability measurements is conducted based on the 2nd DOE to implement steps 11 to 14 of Figure 3-31 and its results are presented and analyzed in section 4.2.2.

The first two columns of Table 3-8 show the factors used in the 1st DOE and their definitions, and the last two columns indicate their coded and actual settings. In this table, the 116 ± 4.3 and 172 ± 6.9 g/m^2 surface densities correspond to 16 and 24 yarns/in. flax plies (tex 200 yarns) respectively. Likewise, the two studied paper surface densities are 29 ± 0.99 and 38 ± 0.64 g/m2. High and low limits of factors A were chosen low because a low paper surface density is better for the reinforcement permeability. For factor B, it was not possible to put more than 24 yarns/in. and 16 yarns/in. was considered a low limit in tem of yarn spacing. High and low levels for factors C and D are selected based on technical considerations (reasonable drying temperatures and compressing pressures).

Table 3-9 shows the 2^{4-1} fractional-factorial resolution IV design of experiment along with the measured values using this table. In this 1st DOE, the fiber volume fraction was kept constant at 35 % for permeability tests and composite fabrication. Each response indicated in Table 3-9 is measured at least four times. According to appendix M of [107] such a sample

size yields a confidence of 90 % to avoid type II statistical error (β) and 95 % to avoid type I statistical error (α) for standard deviation values. The confidence to avoid both types of error in the case of mean values are higher than this.

Similarly, Table 3-10 shows the factors used in the 2nd DOE with their corresponding actual and coded setting. In this table, the flax ply surface densities of 125 ± 1.8, 153 ± 1.3 and 175 ± 1.8 g/m^2 respectively correspond to using 16, 20 and 24 yarns/inch flax layers. As can be noticed the middle-level surface density of flax ply (153 ± 1.9 g/m^2) is not exactly in the middle of high and low level settings. This is because these values are measured experimentally with inherent variations in the values. Because of this, in the regression modeling of surface density according to Table 3-11, corresponding 'number of yarns per inch' (16, 20 and 24) values are used and once the optimum value of 'number of yarns per inch' is found, it has been converted to flax layer surface density measured in g/m^2.

Table 3-8. Reinforcement factors considered for the 1st DOE.

Factor name	Description	Low and high level setting	
		coded	actual
A	Paper ply surface density (g/m^2)	+1	38 ± 0.60
		−1	29 ± 1.0
B	Flax ply surface density (g/m^2)	+1	172 ± 6.9
		−1	116 ± 4.3
C	Forming pressure (bar)	+1	3 ± 0.1
		−1	1 ± 0.1
D	Drying temperature (°C)	+1	101.5±1.5
		−1	71.5±1.5

Table 3-11 shows the full-factorial 3^2 experimental design (2^{nd} DOE). Other reinforcement factors are set at A = -1 (27±0.67 g/m^2), C = +1 (3 ± 0.1 bar) and D = +1 (101.5±1.5) for the reinforcements fabricated according to this table of experiments. Each run of this table is repeated four times.

Table 3-9. 1st DOE with coded level setting of the factors and the evaluated responses.

Run	Factor				Responses						
	A	B	C	D	Reinforcement				Composite		
					Surface density	IBS	Permeability		E_1	E_2	σ_U
							K1	K2			
1	−1	−1	−1	−1							
2	−1	−1	+1	+1							
3	−1	+1	−1	+1							
4	−1	+1	+1	−1							
5	+1	−1	−1	+1							
6	+1	−1	+1	−1							
7	+1	+1	−1	−1							
8	+1	+1	+1	+1							

Table 3-10. Reinforcement factors considered for the 2^{nd} DOE.

Factor name	Description	level setting	
		coded	actual
B	Flax ply surface density (g/m^2)	+1	175 ± 1.9
		0	153 ± 1.3
		−1	125 ± 1.9
E	Fiber volume fraction (%)	+1	45
		0	40
		-1	35

Table 3-11. 2nd DOE with coded level setting of the factors and the evaluated response.

Run	Factors		Responses	
	B	E	Reinforcement Permeability	
			K1	K2
1	−1	−1		
2	0	−1		
3	+1	−1		
4	−1	0		
5	0	0		
6	+1	0		
7	−1	+1		
8	0	+1		
9	+1	+1		

Tables 3-12 and 3-13 show the surface densities of the flax/paper reinforcements for the 1st and the 2nd DOE, respectively. These values are used in Equation 3-5 to calculate the cavity height. The measured reinforcement surface densities are based on weighting at least 12 reinforcement layers of 140 mm × 140 mm (5.5 in. × 5.5 in.) which are cut using scissors and a precise metallic template of the same dimension (for 1st DOE samples) and using cutter and the metallic template for 2nd DOE samples. Prior to weighting, all samples are dried at 103°C for at least 18 hours and stored in a desiccator to prevent humidity absorption. All other reinforcements used for permeability tests and composites molding are conditioned the same way. This was done to promote consistency in the results as natural fibers are hydro-philic and easily affected by the humidity level. It is reported that drying of fibers before processing is important, because water on the fiber surface can weaken the interface strength and consequently the mechanical properties of composites [100].

Table 3-12. Final surface density (m_r) of flax/paper reinforcements of 1st DOE.

Run	m_r (g/m^2)	
	mean	STD
1	147	2.30
2	144	2.41
3	197	8.54
4	204	3.95
5	152	3.74
6	155	4.82
7	216	3.42
8	204	6.15

Table 3-13. Final surface density (m_r) of flax/paper reinforcements of 2nd DOE.

Run	m_r (g/m^2)	
	mean	STD
1	152	2.73
2	180	1.97
3	202	3.46
4	152	2.73
5	180	1.97
6	202	3.46
7	152	2.73
8	180	1.97
9	202	3.46

CHAPTER 4: RESULTS AND DISCUSSION

4.1. Internal bond strength (IBS)

4.1.1. Chemical analysis

To explore the nature of chemical bonds between paper and flax yarns, Fourier transform infrared (FTIR) spectroscopy is performed on the extracted waxes (substance found at the surface of flax yarns and coming in direct contact with the paper layer) of flax yarns. These waxy compounds were extracted using the Soxhlet extractor shown in Figure 4-1. Flax yarns were inserted into the extractor, mounted with a 250 ml flask containing 150 ml of dichloro-methane as the solvent. The extraction was carried out at 60°C in an oil bath for 24 h. After extraction, the solvent was removed using a rotary evaporator and the extracted compounds were dried in a hot air oven at 104°C to eliminate any residual solvent. At this temperature it was observed that the wax had a high viscosity. Then, the FTIR spectroscopy is performed using a Thermo Scientific Smart iTR spectrophotometer to identify the functional groups of the extracted wax. The samples were exposed to irradiations in reflectance mode in the range of 500 to 4000 cm^{-1} (~15 to 120 THz), with a 1 cm^{-1} (~30 GHz) resolution.

The result of FTIR spectroscopy is shown in Figure 4-2. The peak at 800 cm^{-1} is attributed to Si-alkyl contained in $Si(CH_3)_3$ and $Si(CH_3)_2$ groups, at 1010 cm^{-1} to Si-O stretching in Si-

O-Si, and at around 1250 cm^{-1} to C-H deformation in the Si-CH_3 group [108-112]. The absorptions of C-H bands are also observed at around 1462, 2848 and 2917 cm^{-1} which are assigned to aliphatic methylene groups (-CH_2-) and the small peak at around 2960 cm^{-1} is attributed to methyl groups (CH_3).

Based on these remarks, it is noticed that molecules in the silicon wax contain a large number of CH_3 chemical groups. These chemical groups are capable to create Van der Waals bonds between each other as well as with free hydroxyl (OH) groups (not involved in hydrogen bonds) on the cellulose molecular chain of paper fibers. Accordingly, it is hypothesized that the presence of a larger number of Van der Waals bonds between CH_3 chemical groups on the surface of flax fibers and OH groups on the paper fiber can be the cause of cohesion between paper layer and flax yarns of the dry reinforcement. It could be hypothesized that if the waxy compound had been washed out, OH groups on flax and Kraft fibers would have established hydrogen bond.

The chemical bonds between paper and flax fibers are schematically illustrated in Figure 4-3. It should be mentioned that Van der Waals bond is a fragile type of chemical bond and its bonding strength is generally 10 times less than that of hydrogen bond and 100 times lower than covalent bond.

Figure 4-1. Soxhlet extractor.

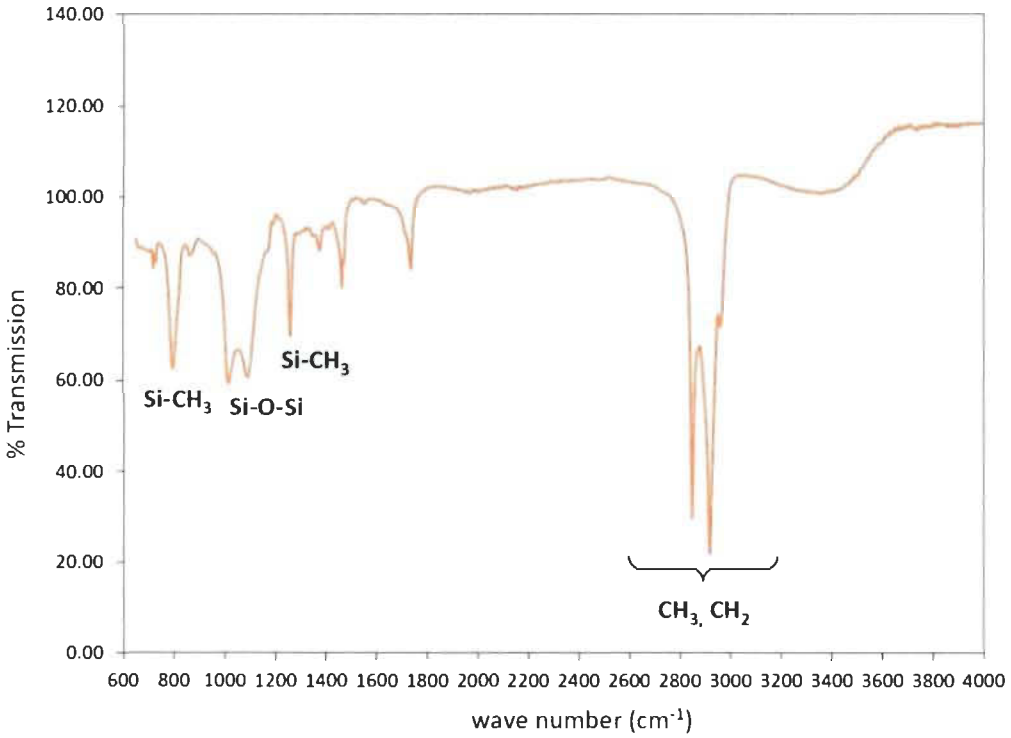

Figure 4-2. Infrared spectra of the wax extracted from flax yarns.

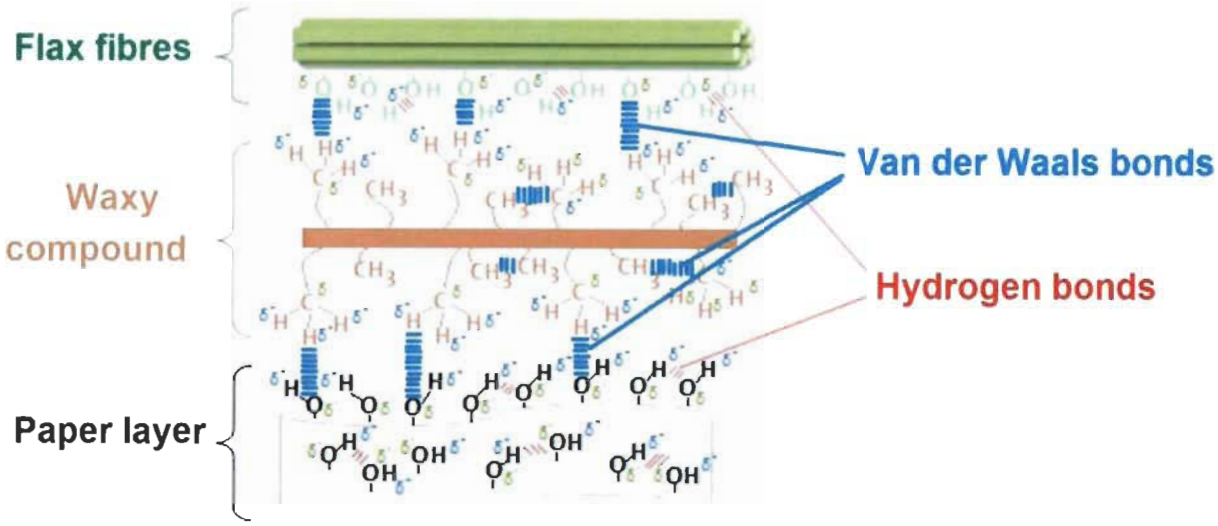

Figure 4-3. Schematic representation of flax-paper chemical bonding.

4.1.2. Analysis of shear cohesion test results

In this subsection, reinforcement samples fabricated according to the 1st DOE (Table 3-9) are tested with the shear cohesion test and their IBS (shear strength) values are studied for evaluating step 4 of the robust parameter design approach in Figure 3-31. Measured shear forces and the calculated IBS are shown in Table 4-1. Typical force-elongation curves are also illustrated in Figure 4-4.

During the tests some samples hardly showed any resistance to the tensile force, meaning that the paper and flax layers were barely bonded to each other. Curves of such samples are pointed out as 'rejected' in Figure 4-4 and their results are not taken into account in the analysis. Moreover as mentioned in section 3.4 based on the specification of the load cell, minimum force that could be measured with precise linearity and repeatability is 2 N. So, shear forces below this threshold are also not taken into account.

Table 4-1. Shear force and shear strength between flax and paper layers of laboratory-made reinforcement samples.

Run	No. of samples		Shear force (N)		IBS (KPa)		
	Total	Rejected	mean	STD	mean	STD	C_V (%)
1	9	0	3.00	1.04	6.09	2.12	34.71
2	10	0	2.94	0.66	5.99	1.34	22.32
3	10	0	5.12	1.15	6.94	1.56	22.43
4	10	1	3.35	1.17	4.55	1.58	34.80
5	18	0	6.81	1.22	13.85	2.48	17.92
6	10	2	4.57	2.38	9.30	4.83	51.96
7	10	1	6.42	3.09	8.71	4.19	48.08
8	10	0	4.91	1.64	6.66	2.22	33.35

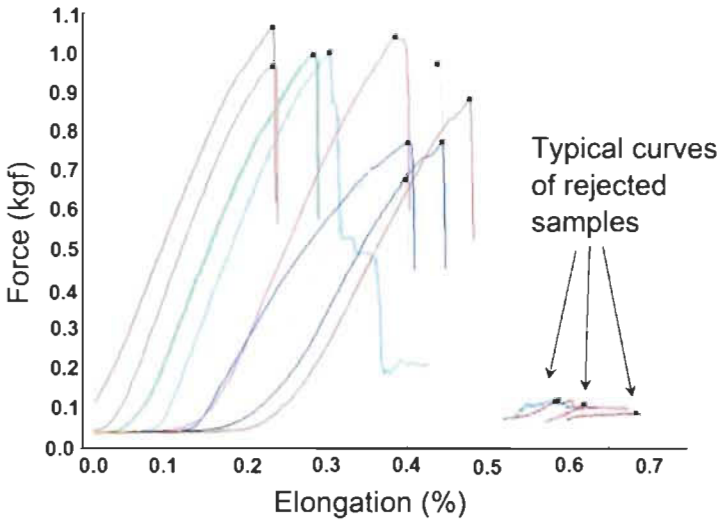

Figure 4-4. Examples of force-elongation curves in shear cohesion test.

To calculate IBS from shear forces in Table 4-1 an estimate of the contact surface area between paper and flax yarns is required. With a detailed look at the shear cohesion samples like the ones shown in Figure 4-5, it is experimentally noticed that after the pressing step of the reinforcement fabrication process (section 3.2.3), the width of the 24 yarns/in. UD flax layer (1″ × 6″) exceeds the initial 1 inch width and on average, only 21 yarns can be placed

side-by-side to fill the 1 inch width (Figure 4-5b). Therefore, The effective width of 24 yarns/in. UD flax layer samples is approximated to 24/21 × 1" = 1.14" and its contact area is approximated to 1.14" × 1" = 1.14 in^2 = 735.5 mm^2. Moreover as Figure 4-5a indicates, in the 16 yarns/in. samples not all the 1 inch width is covered by yarns and therefore the effective width of 16 yarns/in. UD flax layer samples is approximated to 16/21 × 1" = 0.76" and its contact area is approximated to 0.76" × 1" = 0.76 in^2 = 490.3 mm^2

In Table 4-2, the P-values of ANOVA, indicating the probability of making type I error (concluding that a factor is important while in reality it is not), show that all factors have statistical significance on the mean values of IBS. One must keep in mind that having high variability in the results (see C_V in Table 4-1) in spite of a large number of repetitions may result in reducing the mean square of error (MSE) in ANOVA procedure (Equation F-8 in appendix F) which in turn increases the F_0 statistic values for each parameter and consequently the probability of being accepted as an influencing factor for the mean IBS.

None of the factors were found influential on the standard deviation of IBS, based on the method presented in appendix F (section F.2). Equation 4-1 is the regression model for mean values of IBS and its coefficient of determination (R^2) is 0.84. According to this equation and the marginal average plot in Figure 4-6a, average IBS increases with paper surface density (factor A) and drying temperature (factor D), whereas increasing the flax ply surface density (factor B) and forming pressure (factor C) decrease the average IBS.

Having more Kraft fibers in high level surface density paper layers (A = +1) helps establish more Van der Waals bonds with flax fibers and leads to higher IBS. Using 16 yarns/in.

in the flax layer (B = −1) leaves a narrow space between two adjacent yarns (Figure 4-5a) and therefore more surface would be available for each yarn to bond with Kraft fibers.

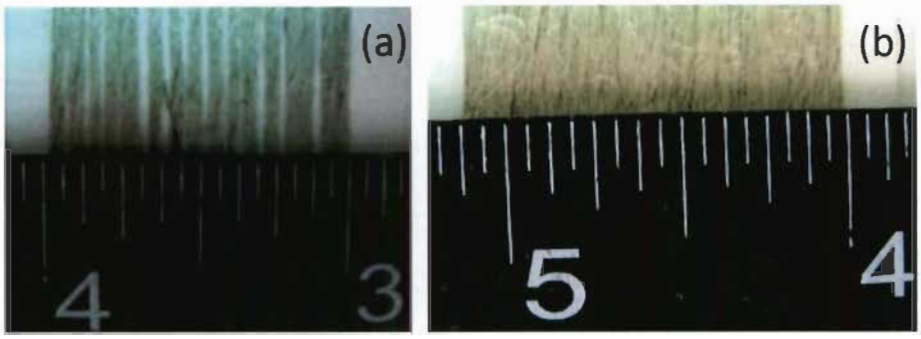

Figure 4-5. Typical width of laboratory-made shear cohesion test samples (a) 16 yarns/in. (b) 24 yarns/in.

A potential hypothesis for decreasing IBS with high level compressing pressure (C = +1) is that Kraft fibers swell during the pulping process and therefore their cell walls are opened, while this is not the case for the flax fibers. Consequently under higher pressure Kraft fibers tend to conform (bond) to each other rather than bond to the flax fibers. Effect of factor D (drying temperature) on increasing average IBS could be explained by the fact that drying promotes formation of fiber-fiber bonds in cellulosic materials [113, 114]. So it is believed that high level of factor D (D = +1) have created more bonding between fibers which in turn increased the average IBS.

Average IBS of run 5 in which each factor setting is at its optimum level (A = +1, B = −1, C = −1, D = +1) has shown a noticeably higher mean IBS compared to the other runs.

Table 4-2.ANOVA results on shear strength of dry reinforcement (significant P values underlined).

Factor	P values for mean IBS	P values for Stdev. of IBS
A	<u>0.00</u>	0.14
B	<u>0.00</u>	0.81
C	<u>0.00</u>	0.94
D	<u>0.03</u>	0.30
	Total DOF=71; Error DOF=67 ; Factor DOF=1;	

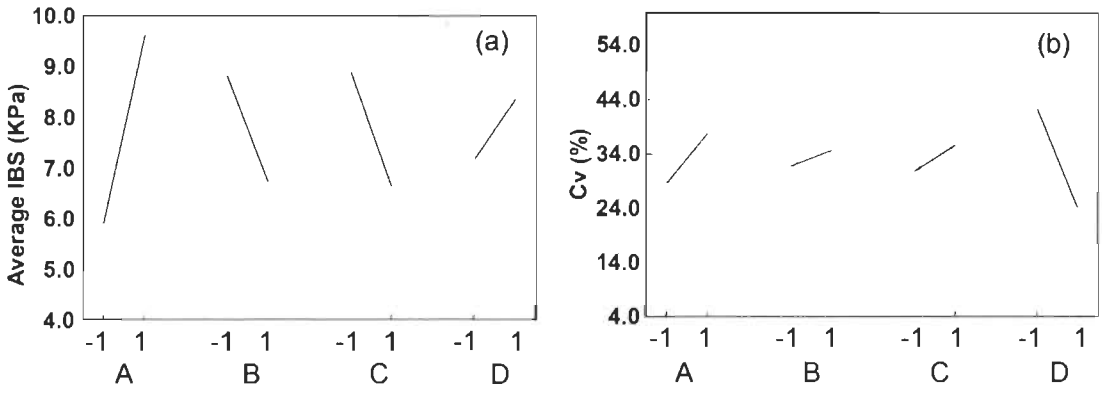

Figure 4-6. Marginal average plot for (a) mean IBS and (b) coefficient of variance.

$$\widehat{IBS} = 7.76 + 1.87A - 1.05B - 1.14C + 0.6D \qquad 4\text{-}1$$

Table 4-1 shows that the coefficient of variance (C_V) is always high. This could be caused by a rather small overlap area (25 mm × 25 mm) between the paper layer and the flax yarns in the test specimens (Figure 3-17) in addition to the fact that Van der Waals forces, considered to be the main cause of flax/paper cohesion, are among the most fragile chemical bond types.

Increasing the overlap area was not an option because it resulted in tearing the thin paper layer before reaching the maximum shear strength of the joint. However, a noticeable trend in the coefficients of variation (C_V) in Table 4-1 is that, they are lower for runs where the drying temperature is at high level (runs 2, 3, 5 and 8) compared to the other runs where drying temperature is at low level (runs 1, 4, 6 and 7). This could also be observed from the marginal average C_V plot in Figure 4-6b showing that average C_V is reduced almost by half when temperature increased to its high setting. In addition, the 'rejected' samples are systematically observed for runs where the drying temperature is at its low level (see Table 4-1, runs 4, 6 and 7). These observations suggest that higher drying temperature brings more consistency to the cohesion of the paper and flax layers, probably by generating more chemical bonds, which in turn increases the average IBS.

4.2. **Permeability**

4.2.1. Two-level design of experiment (screening phase)

4.2.1.1. Analysis of experimental permeability results

In this subsection, unsaturated principal permeabilities of the hybrid UD flax/paper reinforcements fabricated according to the 1st DOE (Table 3-9) are studied for evaluating the robust parameter design approach in Figure 3-31. Table 4-3 shows the experimentally measured K_1 and K_2 permeabilities of the hybrid flax/paper reinforcements according to the 1st DOE (Table 3-9). Permeability results are also depicted in Figure 4-7. All tests are conducted at 21°C.

Typical plots of flow front's radii R_2 versus R_1 and F-function (Equation 3-14) versus time for the flax/paper reinforcements are shown in Figure 4-8. To avoid the local perturbation effect of inlet hole at the beginning of injection [74], only the experimental points acquired

Table 4-3. Principal permeabilities of the flax/paper reinforcement at V_f = 35 %, according to 1st DOE.

Run	K_1 (10^{-12} m^2)			K_2 (10^{-12} m^2)		
	mean	STD	C_V (%)	mean	STD	C_V (%)
1	51.99	12.58	24.2	5.72	0.34	5.91
2	48.33	10.91	22.6	5.59	0.64	11.4
3	20.87	2.71	13.0	5.77	1.16	20.1
4	27.00	1.56	5.77	8.33	0.88	10.6
5	45.91	13.25	28.9	4.68	0.72	15.4
6	53.32	12.70	23.8	6.00	0.40	6.62
7	23.01	2.19	9.51	5.88	0.96	16.3
8	19.41	0.73	3.75	6.21	1.06	17.1

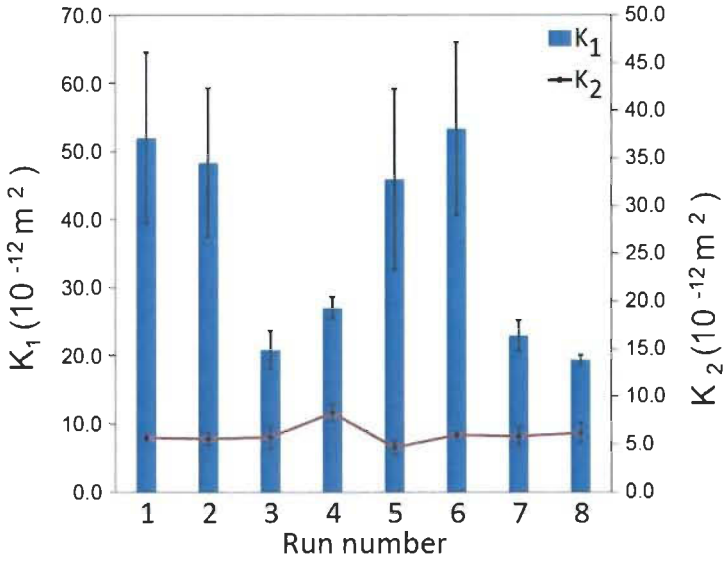

Figure 4-7. Principal permeabilities of flax/paper reinforcement at V_f = 35 %, according to 1st DOE.

after one minute of injection time are taken into account. F-function is obtained from conventional Darcy's law from which no fluid sink effect or swelling phenomena are considered for the fibers, and the relationship between F-function and time (t) is linear. This linearity in Figure 4-8 (with root mean square errors very close to 1) is a sign of very low mass sink effect of flax fibers during impregnation, which could be due to using motor oil for permeability measurement. According to Nguyen et al. [73] where a one-dimensional permeability measurement method is used, a linear relationship between the normalized square of flow front position against time (Analogous to F-function versus time here) corresponds to the absence of mass sink effect of flax fibers in conformance with classical Darcy's law.

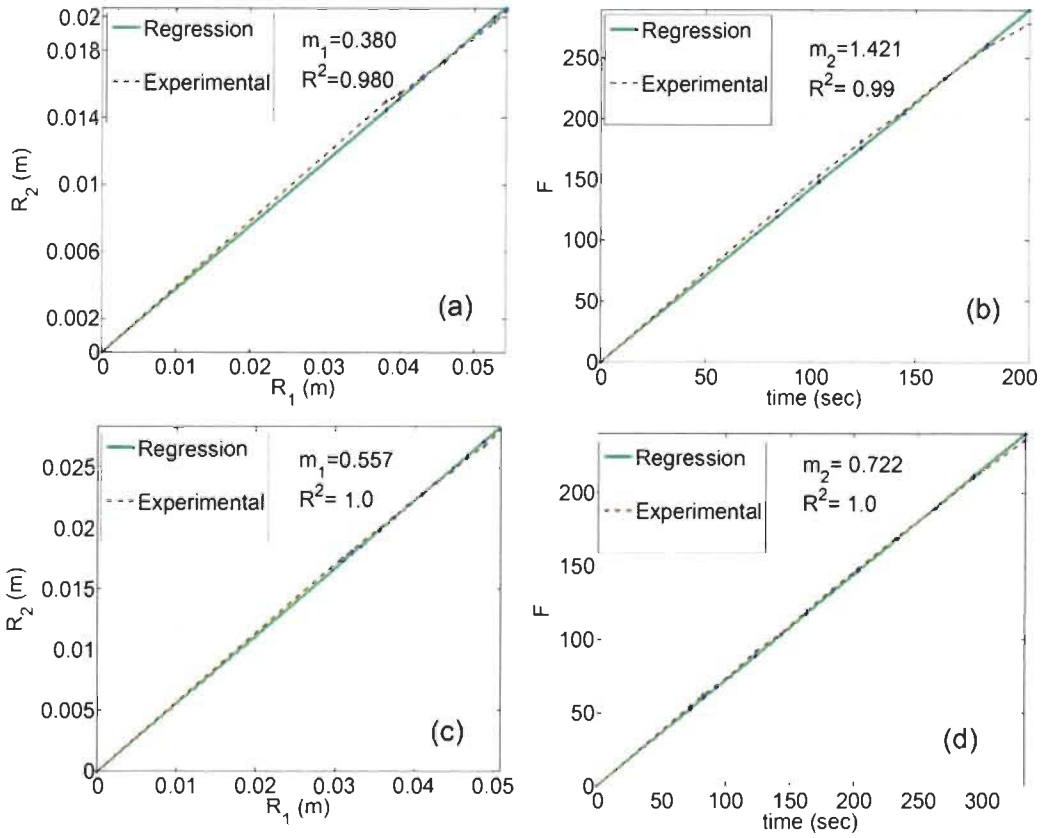

Figure 4-8. Typical principal radii position and function F-time plots for 1st DOE: (a,b) run 1, (c,d) run 8.

In Table 4-3 and Figure 4-7, due to the unidirectional configuration of the yarns, K_1 permeability is one order of magnitude higher than K_2. Furthermore, among average K_1 values those of 24 yarns/in. reinforcements (runs 3, 4, 7 and 8) are much lower than other runs using a flax layer of 16 yarns/in. (runs 1, 2, 5 and 6). However, 24 yarns/in. reinforcements showed more consistent permeability results, considering that K_1 standard deviations are by far lower in runs 3, 4, 7 and 8 compared to runs 1, 2, 5 and 6.

The higher variability in K_1 for 16 yarns/in. reinforcements can be explained by the channeling effect, considering the presence of gaps between yarns as shown in Figures 3-5a and

4-5a. The gaps length and their position being difficult to control, the permeability reproducibility is consequently affected. A more detailed analysis of this phenomenon is presented in the next section.

4.2.1.2. Permeability in the yarns' direction (K_1)

Results of ANOVA on K_1 permeability, shown in Table 4-4, indicate that the flax layer surface density (factor B) is the only parameter with statistically significant influence on both mean and standard deviation of K_1. Figure 4-9 also shows that reducing the surface density of flax layer from 24 yarns/in. to 16 yarns/in. increases the average K_1 by a factor of two, and K_1 standard deviation by a factor of six. This is explained by the distance between flax yarns.

Figure 4-10 compares different optical microscopy images of composites made of four layers stacks of 16 and 24 yarns/in. reinforcements. Based on Figure 4-10a, there is always some narrow flow path between two adjacent yarns in the 16 yarns/in. reinforcements, allowing the test fluid or resin to flow easily between the yarns. On the other hand, in the 24 yarns/in. reinforcements (Figure 4-10c and Figure 4-10d) the yarns are in close contact, which limits the fluid flow between them. It is also reported for a short flax fiber mat that the permeability is governed by the presence and characteristics of open channels [67].

Table 4-4. Result of ANOVA on K_1 permeability (significant P values underlined).

Factor	P value for mean K_1	P value for STD of K_1
A	0.61	0.94
B	<u>0.00</u>	<u>0.00</u>
C	0.62	0.73
D	0.11	0.92
A×B (C×D)	0.73	0.79
A×C (B×D)	0.92	0.95
A×D (B×C)	0.92	0.98
	Total DOF=31; Error DOF=24 ; Factor DOF=1;	

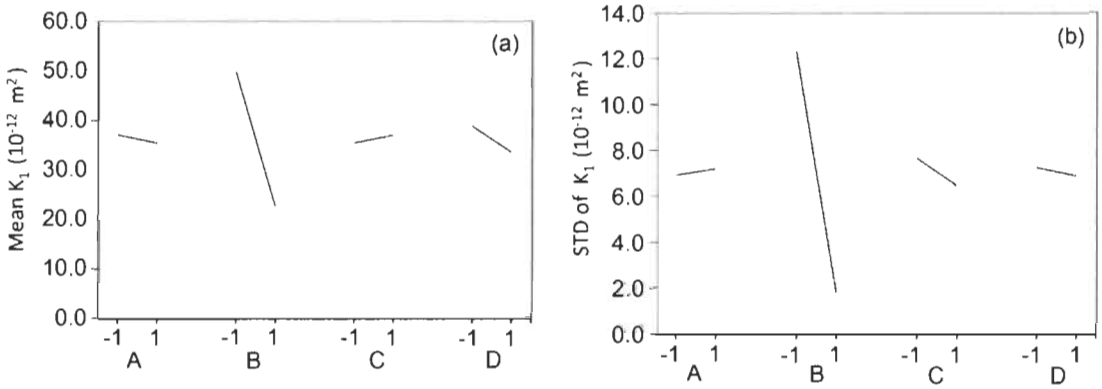

Figure 4-9. Marginal average plot for (a) average and (b) Stdev. of K_1 permeability.

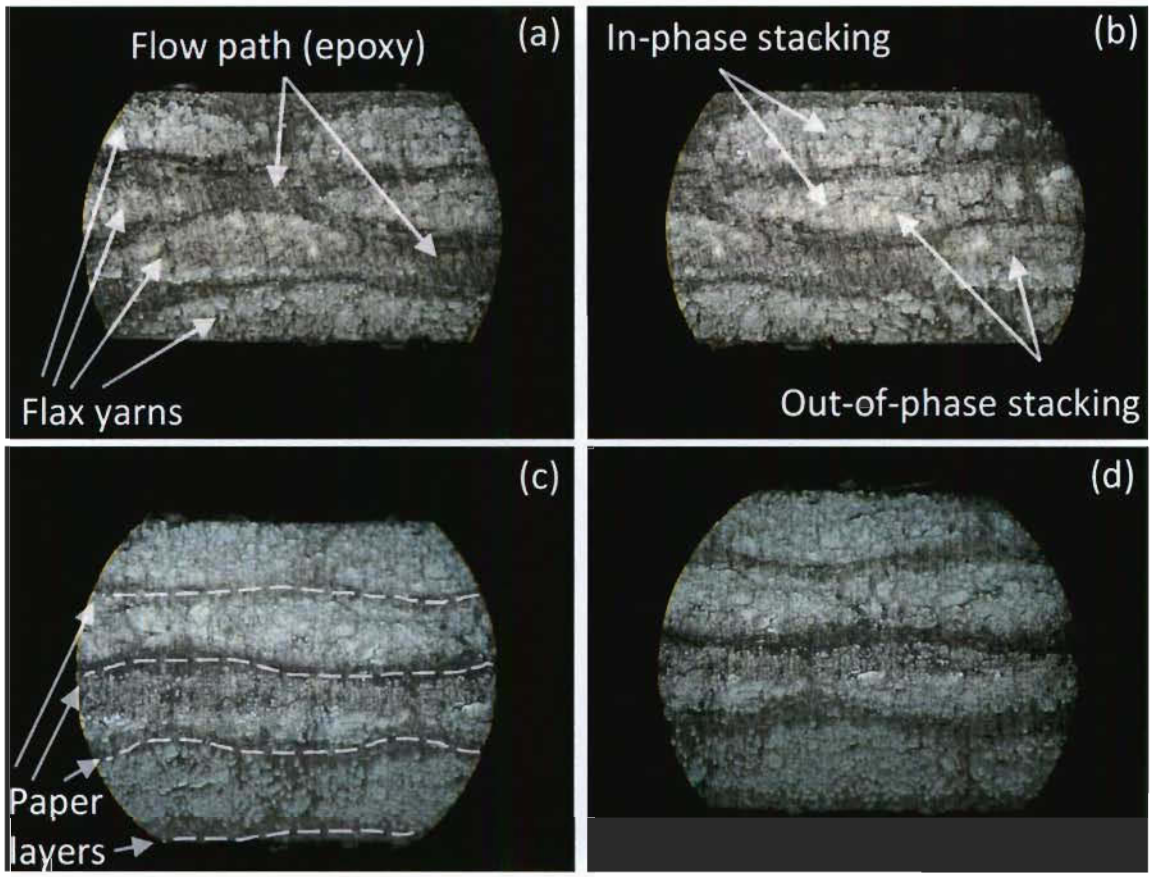

Figure 4-10. Cross-section of UD flax/paper/epoxy composites manufactured from (a,b) 16 yarns/in. reinforcements and (c,d) 24 yarns/in. reinforcements. 100x magnifications.

Figure 4-10b shows that for a stack of 16 yarns/in. reinforcements, the yarns could be positioned randomly one over each other (in-phase) or intercalated (out-of-phase) due to the spacing between the yarns (see Figures 3-5a and 4-5a). The randomness of stacking conducting to 'in-phase' or 'out-of-phase' modes and the possible nesting effect, along with the non-reproducibility of the narrow spacing between yarns, result in high local permeability inhomogeneity leading to global permeability scatter. On the other hand, in 24 yarns/in. reinforcements (Figures 4 10c and 4-10d), the yarns are regularly arranged beside each other, resulting in no nesting effect and a reproducible permeability. This explains why K_1 standard deviation

increases when the flax layer surface density reduces to the low level value. There is no way to control the narrow spacing between yarns and the stacking of reinforcements.

Typical flow front shapes for the two types of reinforcements are compared in Figure 4-11. As can be seen, in the case of 24 yarns/in. reinforcement the flow front is more elliptical than the 16 yarns/in. one, in which local discrepancies from the elliptic shape are observed. This is another sign of higher local permeability inhomogeneity in the 16 yarns/in. reinforcements.

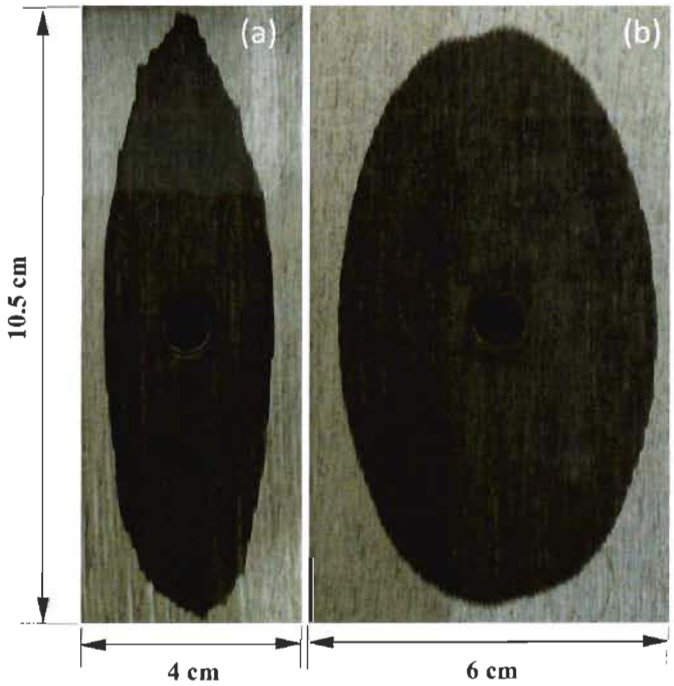

Figure 4-11. Typical flow front shape for (a) 16 yarns/in. and (b) 24 yarns/in. reinforcements.

4.2.1.3. Permeability perpendicular to the yarns' direction (K_2)

Results of ANOVA in Table 4-5 show that all of the four factors have an influence on the mean K_2 permeability, while no parameter has influenced its standard deviation. Moreover, based on the marginal average plot in Figure 4-12, increase of factors B and C (flax layer surface density and forming pressure, respectively) increases the mean K_2, while for factors A and D (paper layer surface density and drying temperature, respectively) the opposite trend is obtained. Result of run 4 in Table 4-3 showed the highest K_2 mean value (8.33×10^{-12} m^2) and run 5 showed the lowest one (4.68×10^{-12} m^2). The reasons for having maximum K_2 at run 4 and minimum K_2 at run 5 is that according to Figure 4-12, the factor levels increasing K_2 (A= −1, B= 1, C= 1, D= −1) are present in run 4 while those making K_2 decrease (A= 1, B= −1, C= −1, D= 1) are set in run 5. However, as can be noticed from Figure 4-12, change of mean K_2 with regard to factors' levels is negligible from an engineering point of view.

Regarding the effect of factor B (flax layer surface density) on increasing mean K_2, it is believed that the tight arrangement of yarns beside each other in 24 yarns/in. reinforcements provides a homogeneous medium for the resin to flow under a continuous capillary force, being dominant in low permeability medium under low fluid velocities conditions. It is even more pronounced when a higher forming pressure is applied on the yarns (high level of factor C), because more connected and homogeneous lateral pores are obtained. As a consequence the capillary effect in lateral direction is favored and an increase in K_2 is observed. The capillary effect in the 16 yarns/in. reinforcement is less consistent for K_2, due to the

spacing between yarns (see Figures 3-5a and 4-5a) provoking a dominant viscous flow in the fibers direction. More details about these effects are given in the next section.

The inverse relationship between mean K_2 and factor D (drying temperature) could be explained by an obstruction of the open channels with increased temperature. As mentioned before, it is a well-known phenomenon that drying promotes formation of fiber-fiber bonds in cellulosic materials [113, 114]. Softening of waxy compound at the surface of flax fibers could also contribute to obstruct the open channels by creating more bonds when spreading into the reinforcement pores. So, it is suspected that more bonds at higher drying temperature could obstruct the connectivity of reinforcement pores, thus reducing K_2. Likewise the high surface density paper (high level of factor A) is less porous and therefore it reduces the overall permeability of the reinforcement.

It is finally observed that K_2 mean values are more sensitive to the reinforcement parameters than the K_1 permeability. This could be due to the much lower values of K_2 compared to K_1 (flax yarns are barrier for K_2 direction fluid flow) and that none of the parameters are dominating in the K_2 direction. However in the longitudinal direction the effects of factors A, C and D may have been hidden by the predominant effect of UD flax yarns (Factor B) and so they have statistically been concluded insignificant (based on ANOVA).

Table 4-5. Result of ANOVA on K_2 permeability (significant P values underlined)

Factor	P value for mean K_2	P- value for STD of K_2
A	<u>0.03</u>	0.93
B	<u>0.00</u>	0.19
C	<u>0.00</u>	0.90
D	<u>0.00</u>	0.51
A×B (C×D)	0.24	0.91
A×C (B×D)	0.51	0.88
A×D (B×C)	0.16	0.92
	Total DOF=31; Error DOF=24 ; Factor DOF=1;	

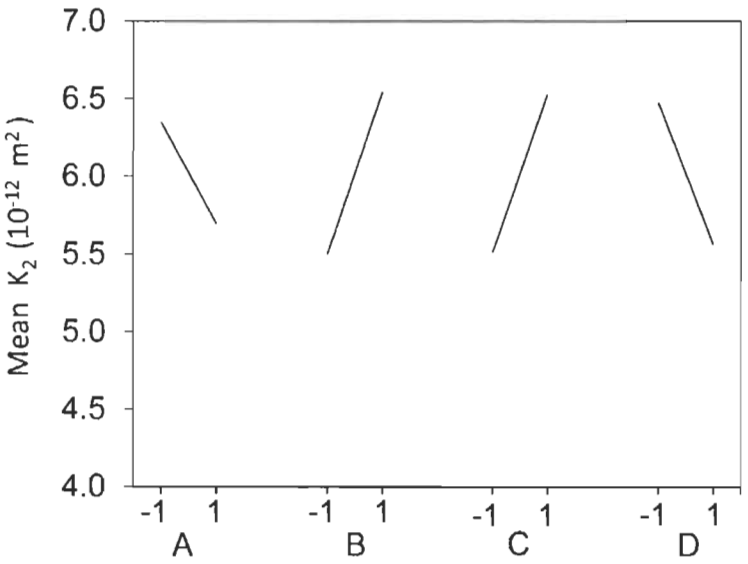

Figure 4-12. Marginal average plot for mean K_2

4.2.1.4. Quality of impregnation

To support the permeability analysis in the previous section, evaluate the behavior of each reinforcement in real molding conditions and assess the influence of permeability on the quality of final composite, two stacks of 24 yarns/in. and 16 yarns/in. reinforcements, each comprising four reinforcements layers, are molded with epoxy resin. The molding parameters

were identical to those used in the permeability measurements, except that the resin is driven into the mold by applying a pressure of 100 kPa instead of using vacuum (providing same pressure gradient as the permeability tests).

Resulting laminates are shown in Figure 4-13. In each laminate two regions are distinguishable. An interior and fully resin saturated region (dark brown region called region I) and an exterior and partly resin saturated region (light brown region called region II). It is well known from literature [115, 116] that the resin flow inside a double-scale reinforcement is driven by two flow inducing forces, namely viscous and capillary forces. At high resin velocities the viscous force is dominant and the flow front is dominated by resin flow between yarns (creating microvoids within the yarns), while at low velocities the capillary forces become dominant and at the flow front the resin flows mainly within the yarns thus inducing macrovoids between yarns.

The dimensionless capillary number given in Equation 4-2, defined as the ratio of viscous to capillary force, is a determining parameter on the micro/macro void formation inside the composite. In this equation μ and V are resin viscosity and velocity, respectively, while γ is resin surface tension.

$$Ca\# = \frac{\mu V}{\gamma} \qquad 4\text{-}2$$

At constant values of μ and γ, an optimum (or critical) flow front velocity (and subsequently an optimum $Ca\#$) is obtained for which the final void content in the laminate is minimum [115]. For flow front velocities higher than the optimum velocity, viscous forces

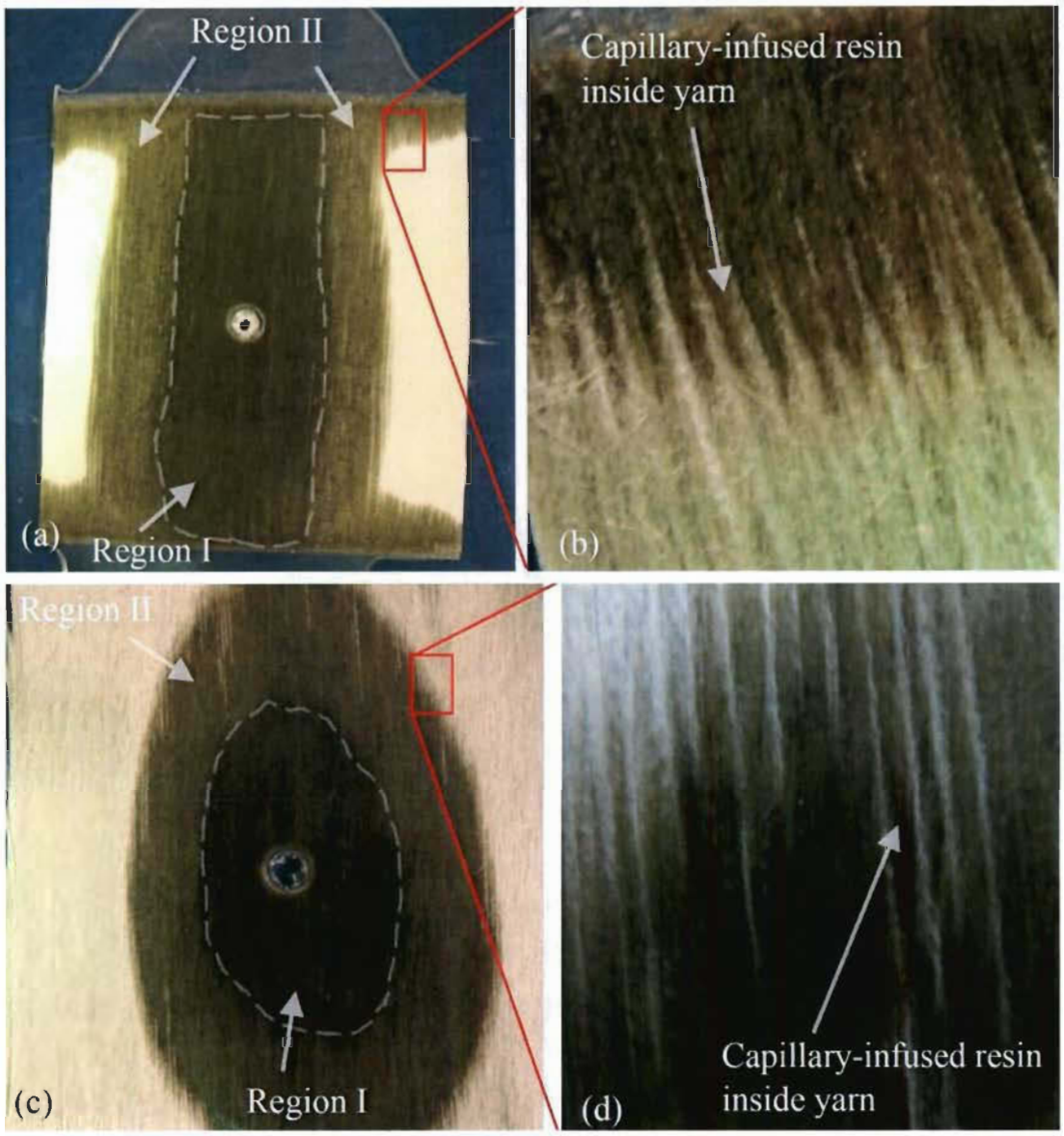

Figure 4-13. Impregnated reinforcements with epoxy resin, (a,b) 16 yarns/in. (c,d) 24 yarns/in

dominate and microvoids are formed within yarns. For flow front velocities below the optimum velocity, capillary forces dominate and macrovoids are obtained between yarns.

At constant injection pressure in the actual experiments, the flow front has its highest velocity at injection port and as the flow front progresses its velocity lowers more and more.

This means that at critical radii in directions 1 and 2 of permeability measurement there exists corresponding critical velocities for which the final void content in the plaque is theoretically at minimum if these velocities are maintained during molding. From these critical radiuses (of an unknown size for now), the resin was probably injected under a very low resin front velocity for which capillary forces were predominant. This is what Figures 4-13b and 4-13d suggest.

The dashed lines in Figures 4-13a and 4-13c are not necessarily related to the critical radiuses because the photos were taken after demolding the plaques, not during resin injection. So resin movements under capillary forces could have occurred after the end of injection and before curing of the resin. Also seen in Figures 4-13a and 4-13c, region I of the 16 yarns/in. reinforcement spreads to a larger extent in the fiber direction than that of 24 yarns/in. reinforcement. This is a direct consequence of higher K_1 permeability of the former reinforcement which allows the resin to flow faster in the K_1 direction and therefore the capillary dominated region (region II) is observed only in the transverse direction in this case.

To better evaluate the quality of impregnation, two specimens were extracted from each region of the laminates for density measurement and optical microscopy evaluation, as is shown in Figure 4-14. Density was measured using a gas pycnometer (nitrogen) model Ultrapyc 1200e (Quantachrome Instruments) with five repetitions. Table 4-6 shows the measured densities as well as estimated volumetric compositions using Equation 4-3 [34, 102], where V,W and ρ respectively represent volume fraction, mass fraction and density, while subscripts c, f, m and v refer to composite, fiber, matrix and void, respectively, fiber and

matrix, correspondingly. Standard deviations of volumetric compositions were also estimated using analysis of uncertainty formulas in [102].

$$V_f = (\rho_c/\rho_f)W_f, V_m = (\rho_c/\rho_m)(1 - W_f),\ V_v = 1 - (V_f + V_m) \qquad 4\text{-}3$$

Composite samples from region II show lower density and higher void fraction (V_v) compared to region I. Because region I is well impregnated, it is believed that capillary forces are not active at small radiuses. However, at the border of the two regions (shown with dashed lines) in Figures 4-13a, and 4-13c, the porosity increases rapidly so capillary forces are acting in region II and resin flows in the intra-yarn space. These results are in line with microscopy images of region II specimens in Figures 4-15b and 4-15d showing noticeable macrovoids compared to their region I counterparts in Figures 4-15a and 4-15c. The higher inter-yarn void content support the above observations that in region II the resin is absorbed by the yarns (intra-yarn impregnation) due to high capillary pressure, leaving inter-yarn voids.

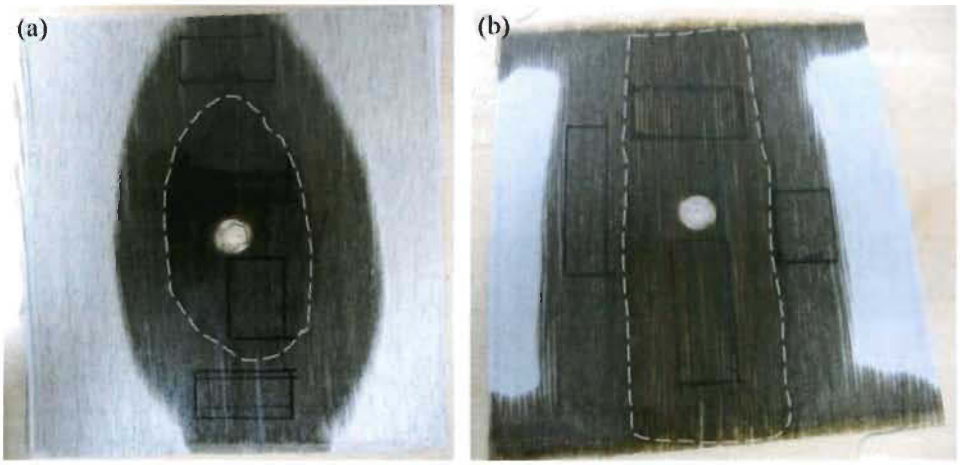

Figure 4-14. Position of samples taken from each region of composites for density and optical microscopy analysis (a) 24 yarns/in. (b) 16 yarns/in., reinforcements.

Table 4-6. Measured density and volumetric composition of the composite specimens.

Composite region		Density, ρ_c (g/cm^3)		Fiber volume fraction, V_f (%)		Void volume fraction, V_v (%)	
		Mean	STD	mean	STD	mean	STD
16 yarns per inch	I	1.270	0.009	37.7	0.24	0.9	0.1
	II	1.239	0.006	37.7	0.23	8.5	0.1
24 yarns per inch	I	1.323	0.006	39.5	0.26	0.4	0.1
	II	1.273	0.008	38.3	0.25	7.4	0.1

Effect of capillary pressure on permeability is studied in the literature [117] and in terms of natural fibers, the magnitude of capillary pressure is reported two or three times higher than in synthetic fabrics [118]. In this study capillary pressure was not considered in the pressure gradient used for permeability measurement (Equation 3-14). However, the above-mentioned explanations and statistical conclusions about permeability remain valid, because the effect of capillary pressure is constant in a given direction of the reinforcement.

4.2.1.5. Regression modeling

Equations 4-4 to 4-6 show the regression models for average and standard deviation of K_1 as well as average K_2 permeability. The R^2 coefficients for these equations are 96 %, 99 % and 92 %, respectively. In these equations, parameters A, B, C and D are in the coded setting domain varying in the interval of [−1, +1]. Because two levels are considered for each parameter, the data was fitted through a linear model. This is in line with the objective of screening the reinforcement parameters and identifying those having an effect on mean and/or standard deviation of principal permeabilities (K_1 and K_2). Equations 4-4 to 4-6 are

therefore approximate and do not necessarily imply linear relationship between the parameters and the permeabilities, as will be shown later.

$$\hat{K}_1 = (36.2 - 13.7B) \times 10^{-12}\,(m^2) \quad 4\text{-}4$$

$$\hat{\sigma}_{K_1} = (7.1 - 5.3B) \times 10^{-12}\,(m^2) \quad 4\text{-}5$$

$$\hat{K}_2 = (6.02 - 0.33A + 0.53B + 0.51C - 0.46D) \times 10^{-12}\,(m^2) \quad 4\text{-}6$$

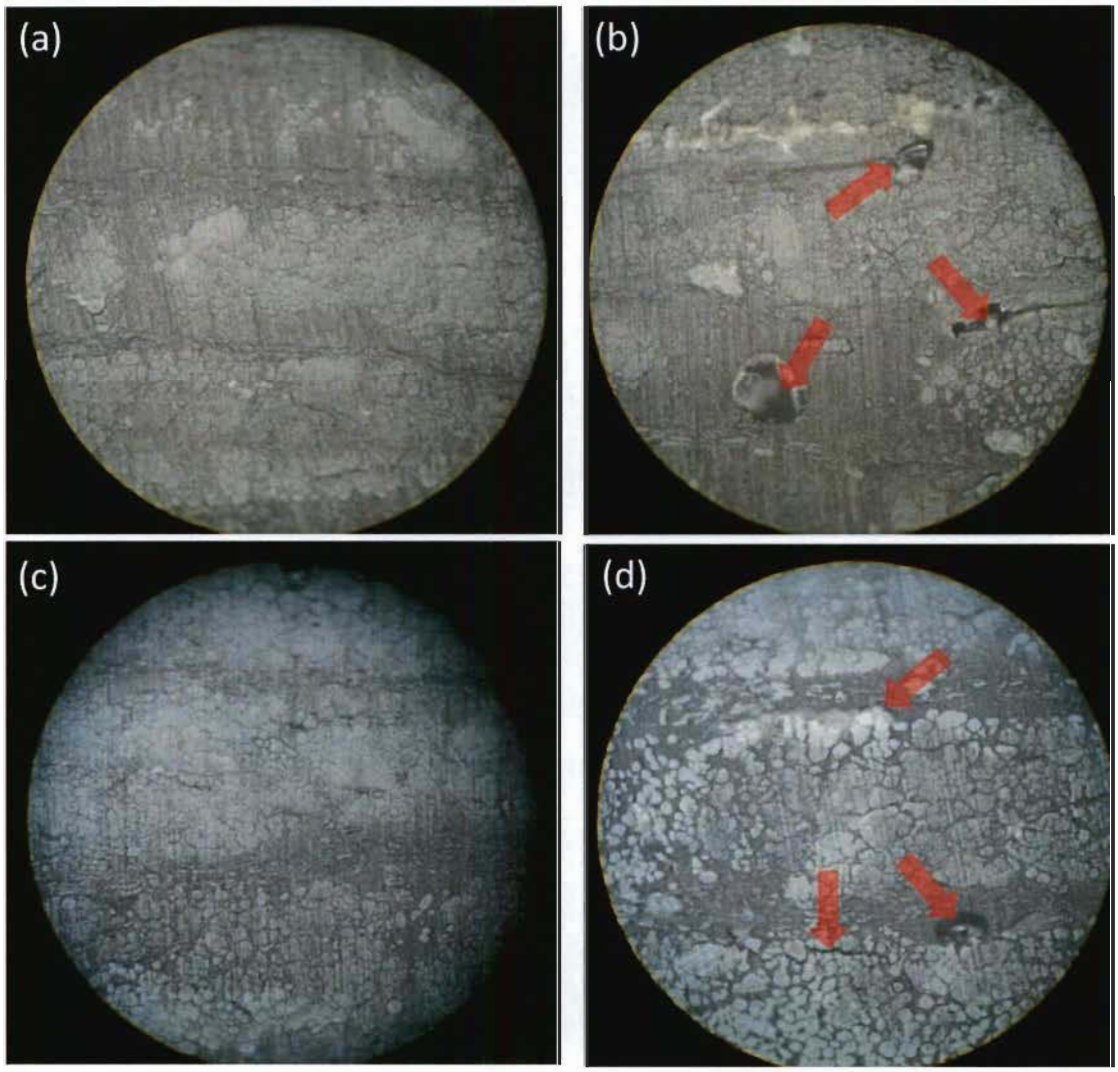

Figure 4-15. Presence of macro-voids in microscopy images of UD flax/paper/epoxy composites (a) 16 yarns/in., region I (b) 16 yarns/in., region II (c) 24 yarns/in. region I, (d) 24 yarns/in. region II. 200X magnifications.

The models are depicted in Figure 4-16. In Equation 4-6 the factors A, C and D are set at optimum levels of −1, +1 and −1, respectively. Therefore all curves are drawn with respect to parameter B (flax ply surface density).

The graphs indicate that $\widehat{K}_1$ and $\hat{\sigma}_{K_1}$ models decline with the increase of B. For now, it thus appears that an optimum design is a compromise between two extend of the design space which in this case is B = 0, and is equivalent to actual setting of 144 g/m^2 (average of high and low level in Table 3-8). Considering a linear relationship between surface density of UD flax layer and the 'number of yarns/inch', the 144 g/m^2 optimum setting corresponds to '20 yarns/inch'. Such an optimum value for factor B results in optimum permeability values of $\widehat{K}_1 = 36.2(7.1) \times 10^{-12}\, m^2$ and $\widehat{K}_2 = 7.3 \times 10^{-12}\, m^2$. Because in this section a two level DOE is employed a linear regression could only be used for modeling the effect of factor B. Quadratic behavior of the K_1 permeability with respect to factor B is studied in the next section, through using a three level DOE.

4.2.2. Three-level design of experiment (modeling phase)

As concluded in the previous section, the flax layer surface density (factor B) influences both average and standard deviation of the K_1 permeability. This allows for (step 4 in Figure 3-31) performing a robustness study on K_1 permeability based on this factor in addition to the fiber volume fraction (V_f) which is reported an important process parameter in determining preform permeability [74]. Therefore in the 2nd DOE (Table 3-11) these two parameters,

each evaluated at three levels, are considered for conducting permeability measurement. Section 4.2.2.1 presents the measured permeabilities and gives a general analysis on them using ANOVA and marginal average plots.

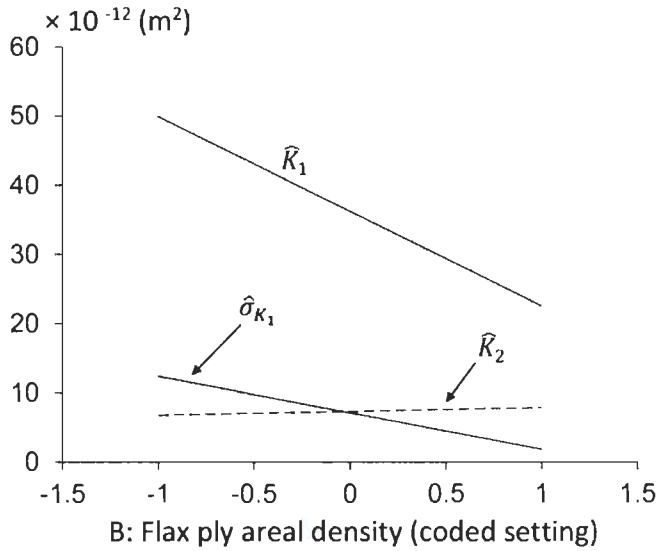

Figure 4-16. Permeability regression graphs with respect to factor B

It is obvious that maximum mean K_1 permeability is attained at low level of flax layer surface density and V_f, and generally it is desired to maximize mean K_1, as much as possible, to reduce the mold filling time. However, apart from maximizing mean value of K_1, the main concern in a robustness study is to minimize standard deviation of K_1, to increase the consistency of mold filling time and part quality. So, to do a robust optimization, mean and standard deviation models are developed in section 4.2.2.2. Mean K_1 model ($\widehat{K_1}$) is approximated with a quadratic regression model. Moreover, two models are estimated for standard deviation of K_1 using error propagation method ($\hat{\sigma}_{k_1}^{p}$) and linear regression modeling ($\hat{\sigma}_{k_1}^{r}$). These two models are used to simulate the standard deviation because in the literature both methods are suggested and it was intended to compare their behavior with each other. Then

in section 4.2.2.3, bi-objective optimization is carried out to simultaneously maximize mean K_1 and minimize its standard deviation. As will be shown, the results of this robust optimization differ from trivial solution of simply choosing minimum values for both V_f and flax surface density.

4.2.2.1. Analysis of experimental permeability results

Table 4-7 and Figure 4-17 show the permeability results according to the 2nd DOE. All of the permeability tests are conducted at 24°C.

Table 4-7. Principal permeability of the hybrid reinforcement according to 2nd DOE.

Run	K_1 (10^{-12} m^2)			K_2 (10^{-12} m^2)		
	mean	STD	C_V (%)	mean	STD	C_V (%)
1	48.6	5.03	10.3	7.18	1.81	25.2
2	20.1	3.65	18.2	6.80	1.20	17.7
3	16.3	3.23	19.8	6.61	1.80	27.2
4	28.9	5.58	19.3	4.57	1.24	27.2
5	14.3	3.77	26.3	3.70	0.50	13.6
6	9.46	1.10	11.6	3.21	0.90	28.2
7	29.1	5.87	20.2	3.67	0.62	16.9
8	9.16	1.21	13.2	2.24	0.37	16.5
9	6.52	0.38	5.89	1.96	0.09	4.37

Similar to the previous section, plots of flow front's radii positions (R_2 vs. R_1) and F-function versus time are also drawn in Figure 4-18. It shows a strong linear relationships between F function against time and therefore conformance to classical Darcy' law (Equation 3-14) for typical results of run 1 and run 9, representing the lowest and the highest fiber content, respectively.

Coefficients of variation (C_V) of 19.7 % and 15.6 % for K_1 and K_2 of glass fabrics are reported reasonable to consider the experimental procedure reproducible [75]. Accordingly

the C_V of Table 4-7 are fairly reasonable. Low standard deviation values acquired here could be due to using a standard permeability mold as well as consistent measurement procedures. However, classical robust parameter design is implemented here to study the behavior of reinforcement permeability.

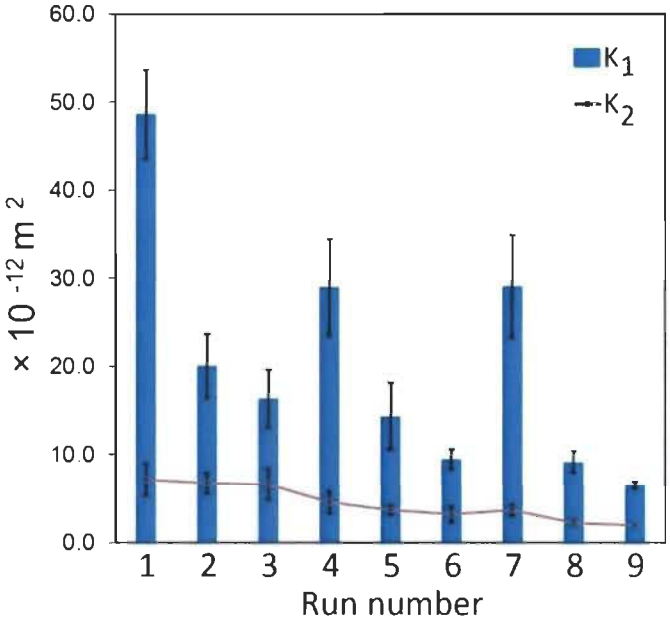

Figure 4-17. Principal permeability of the hybrid reinforcement according to 2nd DOE.

Comparing 2nd DOE (Table 3-11) with the 1st DOE (Table 3-9) one notices that the first run of the 2nd DOE matches with the second run of the 1st DOE in terms of reinforcement parameters and fiber volume faction (A = −1, B = −1, C = 1, D = 1, V_f = 35 %). While equal mean values are interestingly acquired for these two runs (48×10^{-12} m^2), standard deviation of run 1 in 2nd DOE is half of run 2 in 1st DOE. This could be slightly due to different vacuum sealing methods used in the permeability mold (see Figure 3-19), which may have resulted in higher variation of injection pressure in the case of 1st DOE permeability tests. For the

experiments of the 1st DOE, a sealing paste is used and for each test a different strand is installed, while in the 2nd DOE experiment a continuous shore50A rubber frame is consistently employed. Another reason for the higher standard deviation could be due to higher reinforcement surface density variation in the case of 1st DOE.

Results of ANOVA in Table 4-8 indicate that in addition to the main factors B and E (flax layer surface density and fiber volume fraction, respectively) their interaction has also significant effect on mean K_I. Marginal average plots in Figure 4-9a also shows that by increasing values of factors B and E, the mean K_I decreases.

P-values of ANOVA on standard deviation of K_I in Table 4-8 suggests that only factor B has a statistically meaningful effect on standard deviation of K_I. However, interaction plots in Figure 4-20 indicate that, although factor E (fiber volume fraction) hardly shows any effect on standard deviation of 16 yarns/in. reinforcement ($B = -1$), its effect on standard deviation of 20 and 24 yarns/in. reinforcements ($B = 0$ or $B = +1$) is noticeable. So, in spite of being evaluated insignificant by the ANOVA test, factor E will be included in the regression modeling of standard deviation. Figure 4-19b furthermore shows the overall change trend of K_I standard deviation with respect to factors B and E.

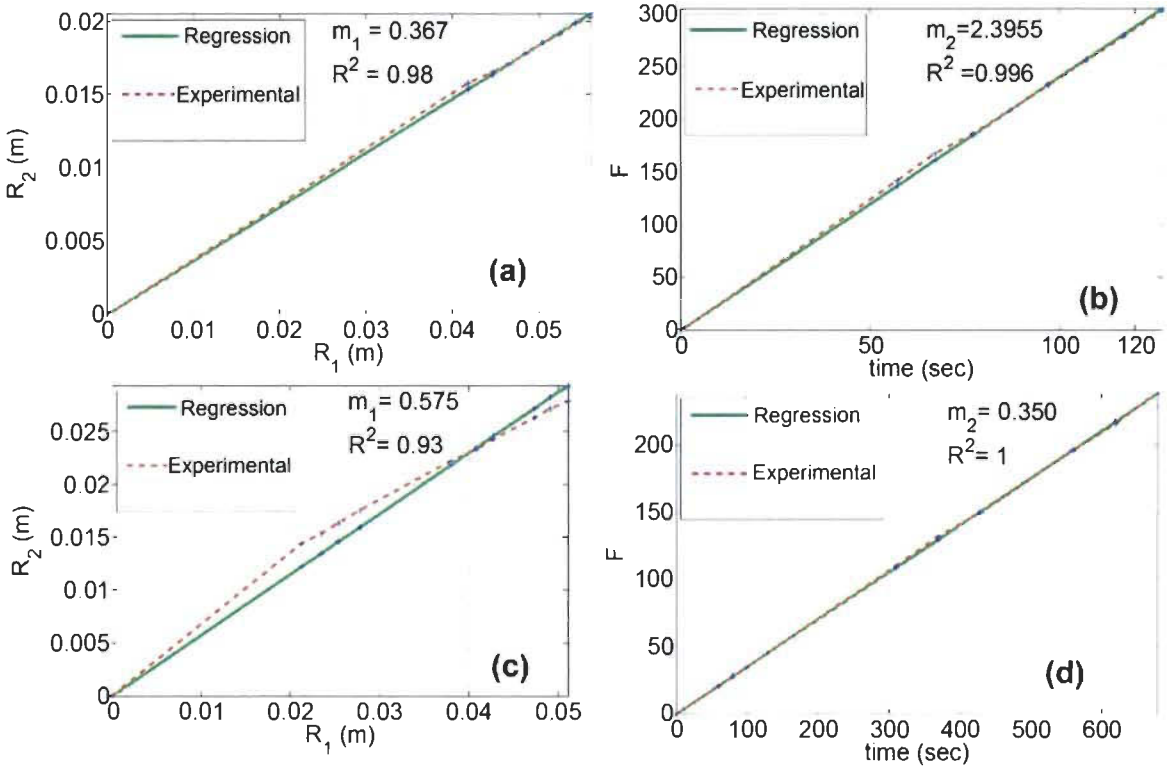

Figure 4-18. Typical principal radii position and function F-time plots for 2nd DOE: (a,b) run 1, (c,d) run 9.

Table 4-8. Result of ANOVA on STD of K_1 (significant P values underlined).

Factor	P- value for average of K_1	P- value for STD of K_1
B	<u>0.00</u>	<u>0.01</u>
E	<u>0.00</u>	0.35
B×E	<u>0.02</u>	0.30
	Total DOF=35; Error DOF=29; Factor DOF=2;	

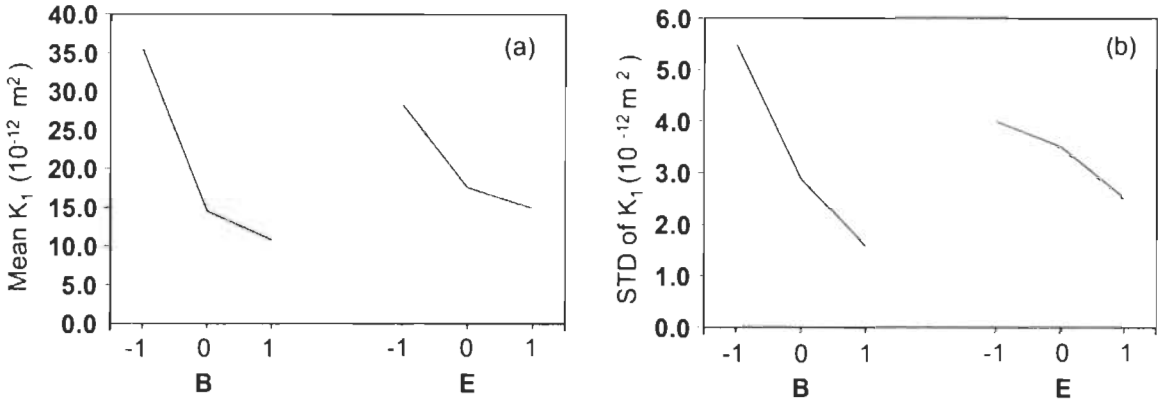

Figure 4-19. Marginal average plots for, (a) mean and (b) standard deviation.

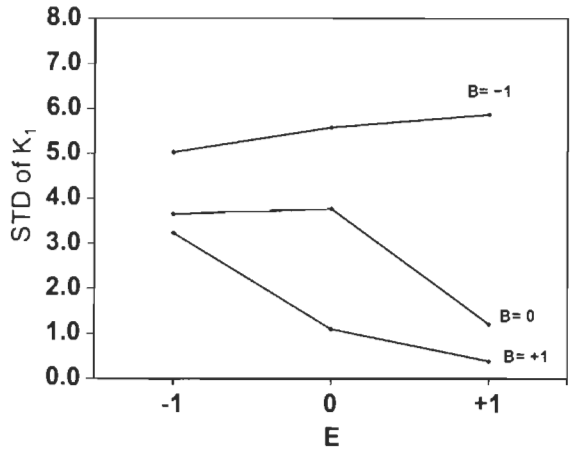

Figure 4-20. Interaction plots for standard deviation values.

4.2.2.2. Statistical modeling of mean and variation of K_1 permeability

Performing a regression modeling on average K_1 yields the response surface model given in Equation 4-7 and shown in Figure 4-21. The R^2 coefficient of determination is 0.90 for this model. The minimum K_1 occurs at [B = 0.63, E = 0.64] with the value of 0.58×10^{-11} m^2 (acquired using a genetic algorithm optimization). Maximum average K_1 permeability at [B = −1 E = −1] has the value of 4.61×10^{-11} m^2.

$$\widehat{K_1} = (11.82 - 12.38B + 8.64B^2 - 6.71E + 4.05E^2 + 2.44BE) \times 10^{-12}\ (m^2) \qquad 4\text{-}7$$

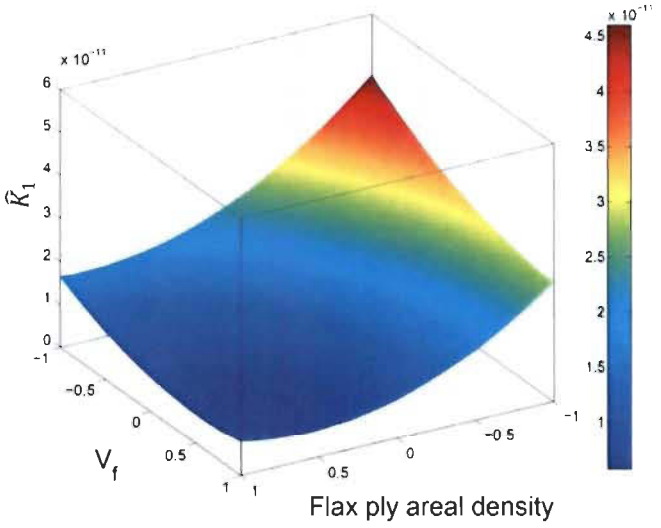

Figure 4-21. Response surface of $\widehat{K}_1$ model.

The regression model fitted on standard deviations of K_I in Table 4-7 is given in Equation 4-8 and plotted in Figure 4-22. The coefficient of determination (R^2) is 0.80 for this model and superscript 'r' indicates that this model is obtained from regression modeling. Maximum and minimum values of this model correspond to $\hat{\sigma}_{k_1}^r = 6\times10^{-12}$ m^2 and $\hat{\sigma}_{k_1}^r = 0.6\times10^{-12}$ m^2, respectively.

$$\hat{\sigma}_{k_1}^r = (3.31 - 1.96B - 0.74E) \times 10^{-12}\ (m^2) \qquad 4\text{-}8$$

Standard deviation model for K_I is also estimated using the propagation of error method. To this end, mean K_I model in Equation 4-7 is used in Equation F-21 of appendix F. The outcome is shown in Equation 4-9 and plotted in Figure 4-23. Superscript 'p' indicates that this model is obtained using the propagation of uncertainty method.

$$\hat{\sigma}_{k_1}^p = \sqrt{\left((-12.38 + 17.28B + 2.44E)\sigma_{\bar{B}}\right)^2 + \left((-6.71 + 8.1E + 2.44B)\sigma_{\bar{E}}\right)^2} \times 10^{-12} \qquad 4\text{-}9$$

The parameters $\sigma_{\bar{B}}$ and $\sigma_{\bar{E}}$ in this equation represent standard deviations of mean flax layer surface density and fiber volume fraction, respectively.

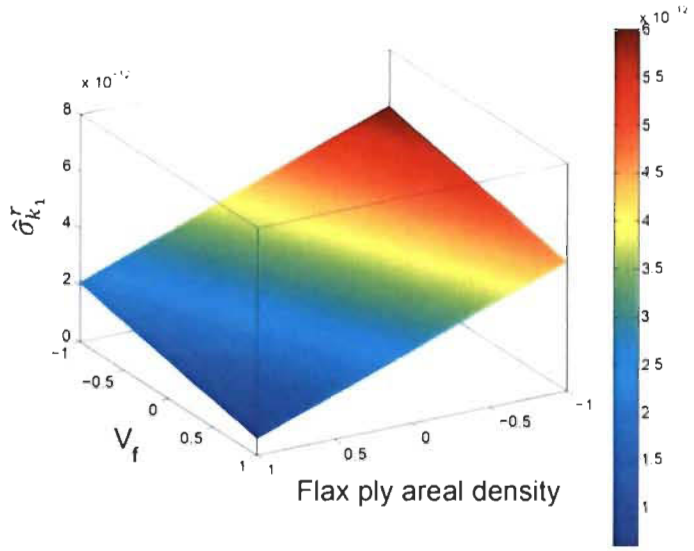

Figure 4-22. Response surface of $\hat{\sigma}^r_{k_1}$ model.

The $\sigma_{\bar{B}}$ is estimated based on experimentally measured surface densities of paper and reinforcement layers, using Equations 4-10 from [102] and Equation 4-11. In Equation 4-10, σ_x is called standard deviation of single measurement (uncertainty of single measurement) and $\sigma_{\bar{x}}$ is the standard deviation of the mean (uncertainty of the mean). Moreover, n, x_i and $\bar{x}$ are respectively the number of samples, the i^{th} measured value, and the average of measured values. In Equation 4-11 standard deviation of single measurement (σ_B) and standard deviation of mean of flax layer surface density ($\sigma_{\bar{B}}$) are calculated based on standard deviations of single measurement of reinforcement (σ_r) and paper layers (σ_p) as well as number of reinforcement samples (n_r) and paper samples (n_p).

Surface densities of reinforcement layers and paper layers are experimentally measured and then their statistics are calculated using Equation 4-10, as is shown in columns 'reinforcement' and 'paper' in Table 4-9. Next, average of flax layer surface density (m_f) is calculated by subtracting average of paper surface density from that of reinforcement ($m_f = m_r - m_p$) and standard deviation of single measurement (σ_B) and standard deviation of mean ($\sigma_{\bar{B}}$) for flax layer surface densities, are calculated using Equation 4-11 and shown in 'Flax layer (factor B)' section of Table 4-9. As can be seen, maximum ($\sigma_{\bar{B}}$) in the last column of Table 4-9 occurred for 24 yarns/in. flax layer and is 1.06. So $\sigma_{\bar{B}}$ = 1.1 g/m^2 is considered in Equation 4-9.

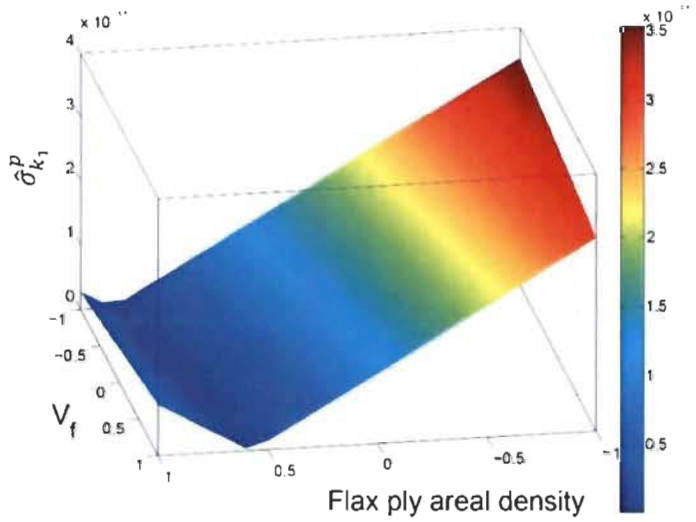

Figure 4-23. Response surface of $\hat{\sigma}^p_{k_1}$ model.

$$\sigma_x = \sqrt{\frac{\sum(x_i - \bar{x})^2}{n-1}} \ , \ \sigma_{\bar{x}} = \frac{\sigma_x}{\sqrt{n}} \qquad 4\text{-}10$$

$$\sigma_B = \sqrt{\sigma_r^2 + \sigma_p^2} \ , \ \sigma_{\bar{B}} = \sqrt{\frac{\sigma_r^2}{n_r} + \frac{\sigma_p^2}{n_p}} \qquad 4\text{-}11$$

Table 4-9. Surface densities and standard deviations of reinforcement, paper and flax layers.

No. yarns / inch	Reinforcement				Paper				Flax layer (factor B)		
	n_r	m_r (g/m^2)	σ_r	$\sigma_{\bar{r}}$	n_p	m_p (g/m^2)	σ_p	$\sigma_{\bar{p}}$	m_f (g/m^2)	σ_B	$\sigma_{\bar{B}}$
16	12	152	2.73	0.79					124	2.97	0.86
20	12	180	1.97	0.57	11	27.11	1.17	0.35	153	2.29	0.67
24	12	202	3.46	1.00					175	3.66	1.06

Standard deviation of mean fiber volume fraction ($\sigma_{\bar{E}}$) is approximated through further applying the method of error propagation (Equation F-21 of appendix F) to Equation 3-5 which yields fiber volume fraction (V_f) as a function of number of reinforcement layers (n), reinforcement surface density (m_r), fiber density (ρ_f) and cavity height (h). This yields Equation 4-12 given below. In this equation $\sigma_{\bar{r}} = 1\ g/m^2$ from Table 4-9, $\sigma_{\overline{\rho_f}} = 0.05\ g/m^2$ from [102], and $\sigma_{\bar{h}} = 0.03 \times 10^{-3}\ m$ just as a conservative approximation of the uncertainty of shims stack used to adjust cavity height.

$$\sigma_{\bar{v}_f} = \sigma_{\bar{E}} = \sqrt{\left(\frac{n}{\rho_f.h}\sigma_{\bar{r}}\right)^2 + \left(\frac{-n.m_r}{\rho_f^2.h}\ \sigma_{\overline{\rho_f}}\right)^2 + \left(\frac{-n.m_r}{\rho_f.h^2}\ \sigma_{\bar{h}}\right)^2} \qquad 4\text{-}12$$

Other parameters in this equation are set as follow: n = 4, $\rho_f = 1.5 \times 10^6\ g/m^2$, h = 0.9×10^{-3} m, m_r = 152 g/m^2. The two latter parameters are from run 1 of the 2nd DOE. Inserting all of these values into Equation 4-12 yields $\sigma_{\bar{E}} = 0.02$. Next, putting estimated $\sigma_{\bar{B}}$ and $\sigma_{\bar{E}}$ into Equation 4-9 results in the propagation model plotted in Figure 4-23. Minimum value of $\hat{\sigma}^p_{k_1} = 0.016 \times 10^{-12} m^2$ occurs at [B = 0.64 E = 0.57] (found using a genetic algorithm optimization) and maximum value of the model at [B = −1, E = −1] has the value of $\hat{\sigma}^p_{k_1} = 35 \times 10^{-12} m^2$.

Both models ($\hat{\sigma}^r_{k_1}$ and $\hat{\sigma}^p_{k_1}$) converge to the same combination of parameters [B = −1, E = −1] for the maximum value. However this maximum value is about six times higher for the $\hat{\sigma}^p_{k_1}$ model compared to the $\hat{\sigma}^r_{k_1}$ model ($\hat{\sigma}^p_{k_1,max} = 35 \times 10^{-12}\, m^2$ and $\hat{\sigma}^r_{k_1,max} = 6 \times 10^{-12}\, m^2$). On the other hand, the minimum value of the $\hat{\sigma}^p_{k_1}$ predicting model at high end combination of [B = 0.64 E = 0.57] is much lower than $\hat{\sigma}^r_{k_1}$ regression model at [B = 1, E = 1] ($\hat{\sigma}^p_{k_1,min} = 0.016 \times 10^{-12}\, m^2$ and $\hat{\sigma}^r_{k_1,min} = 0.6 \times 10^{-12}\, m^2$). The reason for these differences is that, the $\hat{\sigma}^p_{k_1}$ model is obtained from first partial derivation of $\widehat{K}_1$ model and is proportional to the slope of the mean $\widehat{K}_1$ model. At [B = −1, E = −1] where the slope is maximum (see Figure 4-21) $\hat{\sigma}^p_{k_1}$ standard deviation overestimates the practical $\hat{\sigma}^r_{k_1}$ standard deviation and at [B = 0.64 , E = 0.57] where the slope of the plot is close to zero the $\widehat{K}_1$'s extremum happens (see explanation about Figure 4-21) and $\hat{\sigma}^p_{k_1}$ standard deviation underestimates the practical $\hat{\sigma}^r_{k_1}$ standard deviation. High deviation between maximum and minimum values of $\hat{\sigma}^p_{k_1}$ and those of $\hat{\sigma}^r_{k_1}$ model could also be partially due to overestimating of $\sigma_{\bar{B}}$ and $\sigma_{\bar{E}}$ which in turn increases the values of $\hat{\sigma}^p_{k_1}$, in addition to the uncertainty of mean $\widehat{K}_1$ model (considering its $R^2 = 0.9$) from which $\hat{\sigma}^p_{k_1}$ is derived.

4.2.2.3. Robust optimization

To simultaneously maximize average K_1 and minimize its standard deviation, a bi-objective optimization is performed. To this end, the $\widehat{K}_1$ and $\hat{\sigma}^r_{k_1}$ models are mixed up in a single objective function in equation 4-13 such that minimizing it, simultaneously maximizes $\widehat{K}_1$

and minimizes $\hat{\sigma}_{k_1}^{r}$. Parameter α in this equation is a weighing factor that can vary between 0 (single-objective maximization of mean) to 1 (single-objective minimization of standard deviation). Using the two scaling factors of 60×10^{-12} and 0.6×10^{-12} in function Y_1, the terms in parenthesis vary in the range of 1 to 10.

$$Y_1 = (1-\alpha)\left(\frac{60\times10^{-12}}{\hat{K}_1}\right) + \alpha\left(\frac{\hat{\sigma}_{k_1}^{r}}{0.6\times10^{-12}}\right) \qquad 4\text{-}13$$

Similarly, Equation 4-14 shows the objective function mixing the $\hat{K}_1$ and $\hat{\sigma}_{k_1}^{p}$ models. In this case the second parenthesis roughly varies in the range of 0 to 10.

$$Y_2 = (1-\alpha)\left(\frac{60\times10^{-12}}{\hat{K}_1}\right) + \alpha\left(\frac{\hat{\sigma}_{k_1}^{p}}{3.5\times10^{-12}}\right) \qquad 4\text{-}14$$

Tables 4-10 and 4-11 respectively present outcomes of minimizing Y_1 and Y_2 functions using the genetic algorithms (GA) optimization. In these tables Equations 4-15 and 4-16 are used to convert coded settings of factors B and E to their corresponding actual settings of 'No. yarn/inch' and 'V_f'. Furthermore, as mentioned beforehand in the section 3.9, since relationship between 'No. yarn/inch' and 'flax ply surface density' was found nonlinear (due to experimental uncertainties), regression Equation 4-17 is used to relate these two parameters. Coefficient of determination for this equation is $R^2 = 1$.

$$\text{No. yarns/inch} = 20 + 4B \qquad 4\text{-}15$$

$$V_f\,(\%) = 40 + 5E \qquad 4\text{-}16$$

$$\text{Flax ply surface density } \left(\frac{g}{m^2}\right) = -47 + 13.75 \times \left(\text{No.}\frac{\text{yarns}}{\text{in.}}\right) - 0.1875 \times (\text{No.}\frac{\text{yarns}}{\text{in.}})^2 \quad 4\text{-}17$$

Table 4-10. Result of Y_1 function optimization using GA.

α	Coded setting	Actual setting			K_1 ($\times 10^{-12}$ m^2)	
		No. yarn/inch	Flax ply surface density (g/m^2)	V_f (%)	mean	$\hat{\sigma}^r_{k_1}$
0	[B = −1 , E = −1]	16	125	35	46.0	6
0.25	[B = −0.79 , E = −1]	17	132	35	39.7	5.6
0.5	[B = 1, E = −1]	24	175	35	16.4	2.1
0.75	[B = 1, E = 1]	24	175	45	7.86	0.61
1	[B = 1, E = 1]	24	175	45	7.86	0.61

Table 4-11. Result of Y_2 function optimization using GA.

α	Coded setting	Actual setting			K_1 ($\times 10^{-12}$ m^2)	
		No. yarn/inch	Flax ply surface density (g/m^2)	V_f (%)	mean	$\hat{\sigma}^p_{k_1}$
0	[B=−1, E=−1]	16	125	35	46.0	35.3
0.25	[B=0.86, E=−1]	23	170	35	16.2	0.38
0.5	[B=0.86, E=−1]	23	170	35	16.2	0.38
0.75	[B=0.86, E=−1]	23	170	35	16.2	0.38
1	[B=0.63, E=0.64]	23	170	43	5.80	0.07

Comparing the optimum design points in Tables 4-10 and 4-11 (given in codded setting and actual setting) indicates that Y_1 optimization at $\alpha = 0.25$ and $\alpha = 0$ are almost completely similar, and this is also the case for $\alpha = 0.75$ and $\alpha = 1$. However, results of Y_2 optimization at $\alpha = 0.25$ and 0.75 are identical to that of $\alpha = 0.5$. Interestingly, for $\alpha = 0.5$, the results of both Y_1 and Y_2 optimization are quite the same. The observed differences in the converged optimum points at $\alpha = 0.25$ and 0.75 when comparing Y_1 and Y_2, is attributed to the resultant topology of Y_1 or Y_2 at the given α, which provide different absorption region of global optimum.

Considering that at $\alpha = 0.5$ both models have converged to the same point and this α value gives even weight to both mean and variance model, it is believed that this point is the best compromise for permeability robust optimization. This optimum robust point corresponds to run 3 of the 2nd DOE and experimentally measured K_1 permeability at this point, according to Table 4-7, is $16.3 \pm 3.23 \times 10^{-12}$. Figure 4-24 shows the Pareto optimal solutions in the objective function space for Y_1 and Y_2 and at different α values. As can be seen, the design points and corresponding objective functions values for $\alpha = 0.5$ which is chosen here as best trade-off between mean and standard deviation values of K_1 permeability, are quite close to each other for both models.

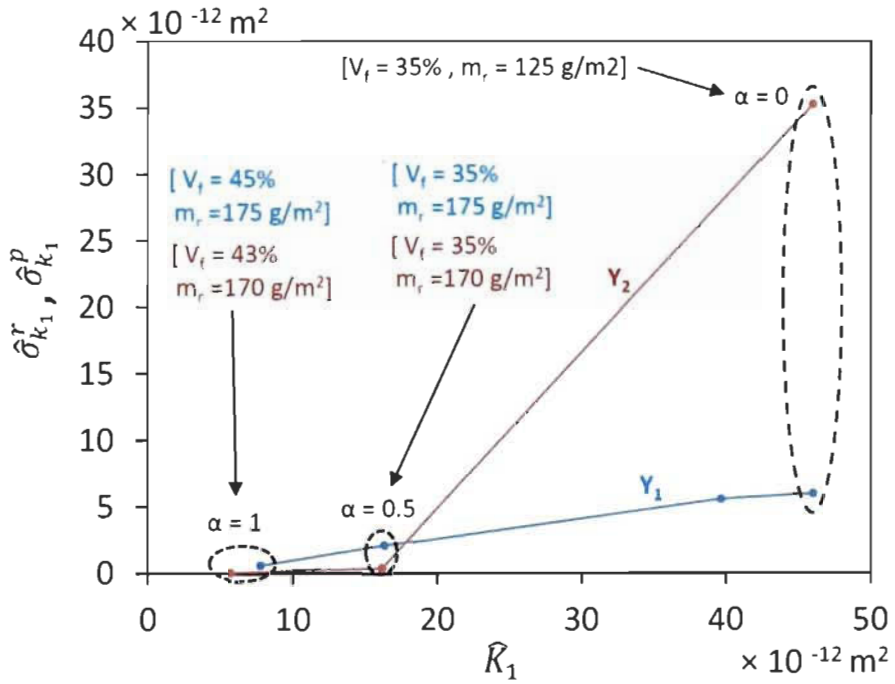

Figure 4-24. Pareto front in objective functions domain. Corresponding optimum design parameter values are shown in the graph with color code for each of Y_1 and Y_2 function. m_r represent surface density of reinforcement.

4.2.3. Comparative study

To complete the permeability study, the effects of different reinforcement architectures on permeability are studied in this section. In section 4.2.3.1, the behavior of tex 200 UD flax/paper reinforcement studied above (through DOE approach) is compared with other laboratory reinforcements made in this thesis, while in section 4.2.3.2 behavior of tex 200 UD flax/paper reinforcement is compared with two commercial reinforcements including Flax-Tape© and a woven glass fabric.

4.2.3.1. Comparison with other laboratory-made flax fiber reinforcements

Figure 4-25 shows the studied reinforcements and the comparison strategy used in this subsection. While fiber volume fraction is kept constant at V_f= 35 % for the experiments of this plan, comparison of results allows for studying the effects of different parameters (mentioned in Figure 4-25) on permeability. These parameters are qualitative ones and cannot be studied through a DOE approach.

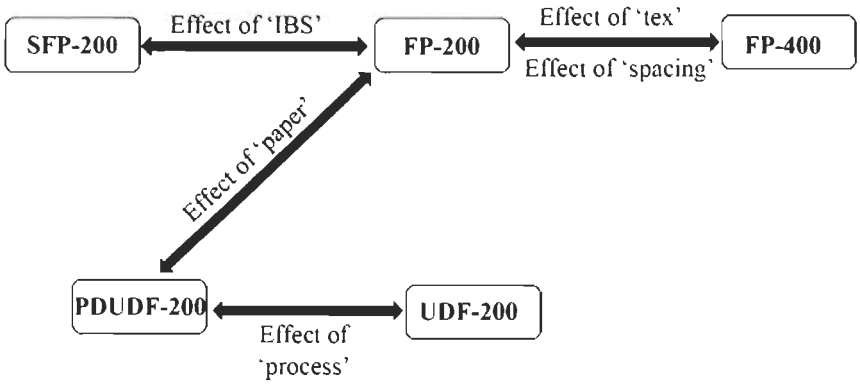

Figure 4-25. Plan of permeability comparative study for laboratory reinforcements.

The first comparison uses two types of flax/paper reinforcements: the Flax/paper tex 200 (FP-200) and Flax/paper tex 400 (FP-400). They differ in linear density (tex) of the yarn and spacing between yarns. They are designed to have equal surface densities, so FP-400 consist of 12 yarns per inch compared to 24 yarns per inch in FP-200 (see Equation 3-4). These two reinforcements are shown in Figure 4-26.

The second comparison concerns the effect of paper/flax cohesion (IBS) on the permeability. To evaluate this, the paper layer of FP-200 is very cautiously peeled off and stacked over flax layer for testing. This reinforcement corresponds to Separated Flax/Paper Tex 200 (SFP-200) preform.

The third comparison is made between two UD flax reinforcements (without paper). The UD flax tex 200 (UDF-200) consists in 24 yarns/in. tex 200 UD flax layer made using the winding machine of Figure 3-4. It is observed that after fabrication of FP-200, its flax layer (Figure 4-26a) becomes more uniform and homogeneous compared to UDF-200 (Figure 4-27) which is directly got from the winding machine. To evaluate this homogenization effect, the paper layer of FP-200, is very cautiously peeled off such that the flax layer remains intact, and therefore the pressed-dried UD Flax Tex 200 (PDUDF-200) layer is acquired following this procedure.

A fourth comparison between FP-200 and PDUDF-200 having identical UD flax layer allows for evaluating the effect of paper layer on the permeability. Table 4-12 shows the surface densities of the studied reinforcements. Surface densities of hybrid reinforcements are acquired through weighting laboratory samples and dividing them by the sample's area.

However, since UDF-200 was fragile and likely to be distorted during weighting, surface density of this reinforcement is calculated using Equation 3-4.

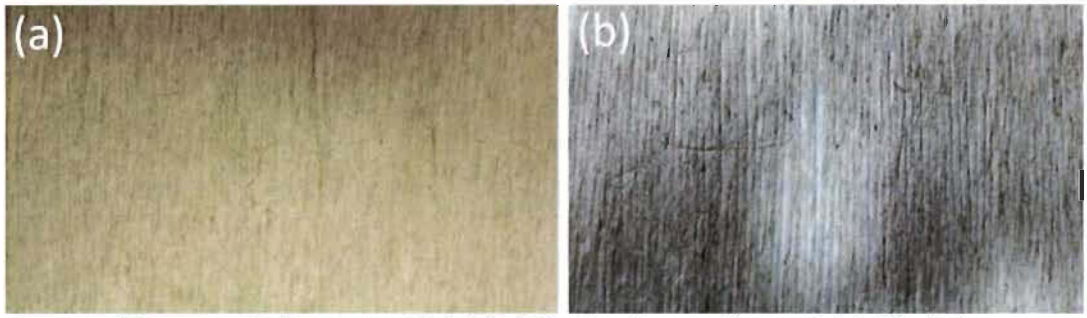

Figure 4-26. Texture of (a) FP-200, flax layer side, and (b) FP-400.

Figure 4-27. Texture of UDF-200.

Table 4-12. Surface densities of reinforcements.

Reinforcement name	Reinforcement type	Surface density (g/m^2)
UDF-200	UD flax tex 200	189
FP-400	Flax/paper tex 400	221 ± 1.5
FP-200	Flax/paper tex 200	216 ± 2.2
PDUDF-200	Pressed, dried UD flax tex 200	175 ± 2.3
SFP-200	Separated Flax/Paper tex 200	213 ± 1.7

Permeability results are summarized in Table 4-13 and depicted in Figure 4-28. Higher average and variance of FP-400 in comparison with FP-200 is attributed to open channels between tex 400 yarns and the consequent nesting effect, as explained for the 16 yarns/in. tex 200 reinforcements in section 4.2.1.2 based on Figure 4-10.

A noticeable observation is that FP-200 and SFP-200 show the lowest average K_1 values and also the most consistent K_1 permeability behavior considering that their standard deviation are much smaller than the other reinforcements. Comparing the results of these two reinforcements also reveals that regardless of the paper bonding to the flax layer (magnitude of IBS = 0), the mean or variance of K_1 permeability is not affected. The slightly smaller mean K_1 in the case of SFP-200 could be simply due to variation of cavity height. During permeability tests for SFP-200, the cavity height was slightly reduced (around 0.05 mm) compared to permeability tests of FP-200 to provide more pressure on the SFP-200 preform and prevent any movement of the separated paper layers during injection, due to the effect of injection pressure.

Table 4-13. Results of permeability comparative study.

Reinforcement type	Nominal V_f (%)	K_1 (10^{-12} m^2)			K_2 (10^{-12} m^2)		
		Ave.	STD	C_V(%)	Ave.	STD	C_V(%)
UDF-200	35	70.7	13.3	18.9	8.12	1.18	14.5
FP-400	35	77.1	22.5	29.2	7.64	1.34	17.6
FP-200	35	23.0	2.19	9.51	5.88	0.96	16.3
PDUDF-200	35	49.0	8.60	17.5	13.6	4.42	32.4
SFP-200	35	14.5	2.00	13.8	4.92	0.97	19.7

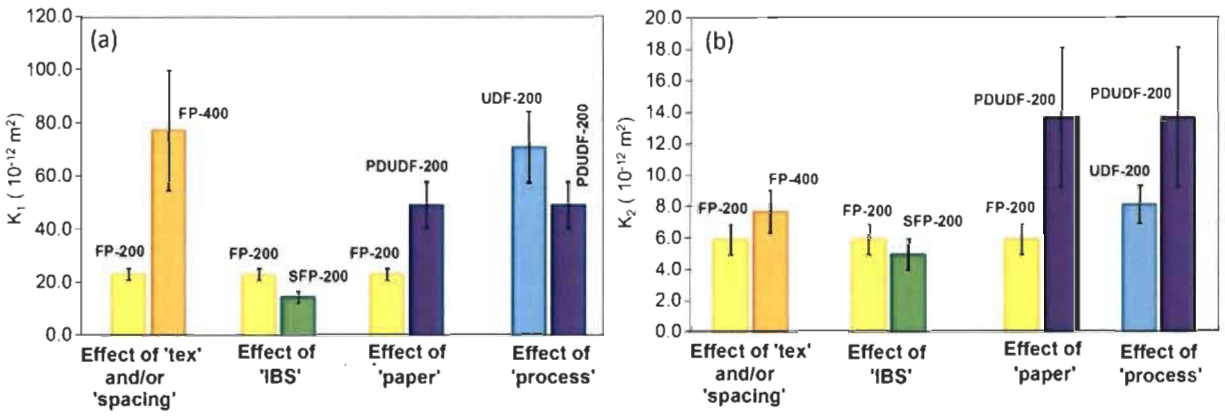

Figure 4-28. Results of permeability comparative study, (a) permeability along yarns (b) permeability perpendicular to yarns.

UDF-200 has shown around 1.5 time higher mean and standard deviation for K_1 than PDUDF-200. As showed in Figure 4-27, the open spacing between yarns in the UDF-200 reinforcement and the consequent nesting effect are probably responsible for higher mean values and standard deviations of K_1 of UDF-200 compared to PDUDF-200.

The PDUDF-200 reinforcement has shown two times higher mean K_1 and four times higher K_1 standard deviation than FP-200. From this results, it appears that paper layer in FP-200 partly obstructs the open channels of flax layer and thus reduces the average K_1. Moreover, the presence of paper reduces the variability of permeability. This is probably a consequence of the homogeneity, uniformity and reduced nesting effect in the FP-200 reinforcement caused by the presence of paper compared to PDUDF-200.

In terms of K_2 permeability, PDUDF-200 have shown higher average values than the other reinforcements. However, PDUDF-200 has also shown highest variability. Other reinforcements are more or less at the same order for both mean and variance of K_2.

Practical experience during preparation and testing of PDUDF-200 indicates that this flax layer becomes very fragile after peeling off the paper ply from FP-200 reinforcement, even more than initial UDF-200 flax layer. Figure 4-29 shows two typical defects in this preform during permeability testing. Uneven flow front in Figure 4-29a is due to distortion of preform during preparation for permeability test and yarn separation in Figure 4-29b could happen at high injection pressure of permeability test, thus increasing variability in the results.

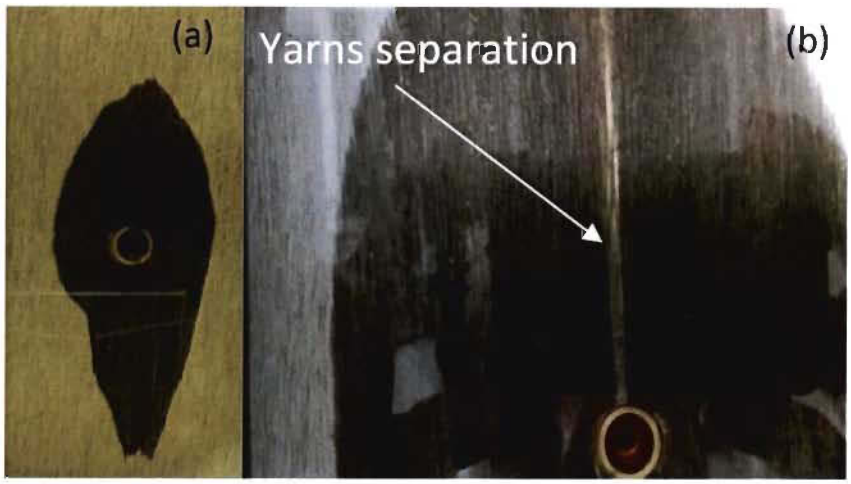

Figure 4-29. Defects in PDUD-200 reinforcement, (a) uneven flow front and (b) yarns separation during permeability test.

From a permeability perspective, the reinforcements developed in this thesis represent a major improvement compared to the first generation of flax/paper reinforcements reported in a previous study [71], where the K_1 and K_2 permeabilities for a tex 1000 UD flax layer (with 820 g/m^2 surface density) were respectively reported 4.98 ± 1.34 × 10^{-12} (m^2) and 1.77 ± 0.318 × 10^{-12} (m^2), much lower than those in Figure 4-28 for FP-200.

4.2.3.2. Comparison with commercial reinforcements

Permeability behavior of hybrid flax/paper reinforcement (FP-200) is compared with two commercial reinforcements: a commercial UD flax reinforcement, FlaxTape© 200 (FT-200) supplied by Lineo Inc. (France) with surface density of 200 g/m^2, and a plain weave glass fiber fabric reported in [60] and called Syncoglas R420 in this reference. FP-200 and FT-200 differ mainly with respect to texture of the fibrous network. Flax fibers on FT-200 have almost no twist and therefore the reinforcement is more hairy than FP-200 as observed by comparing Figures 4-30a and 4-26a. Syncoglas R420 is shown in Figure 4-30b and its surface

density is reported 420 g/m^2. The gaps between warp and fill yarns are also reported G_w = 0.58 mm and G_f = 0.35 mm, respectively. Figure 4-31 also shows the comparison strategy of this subsection.

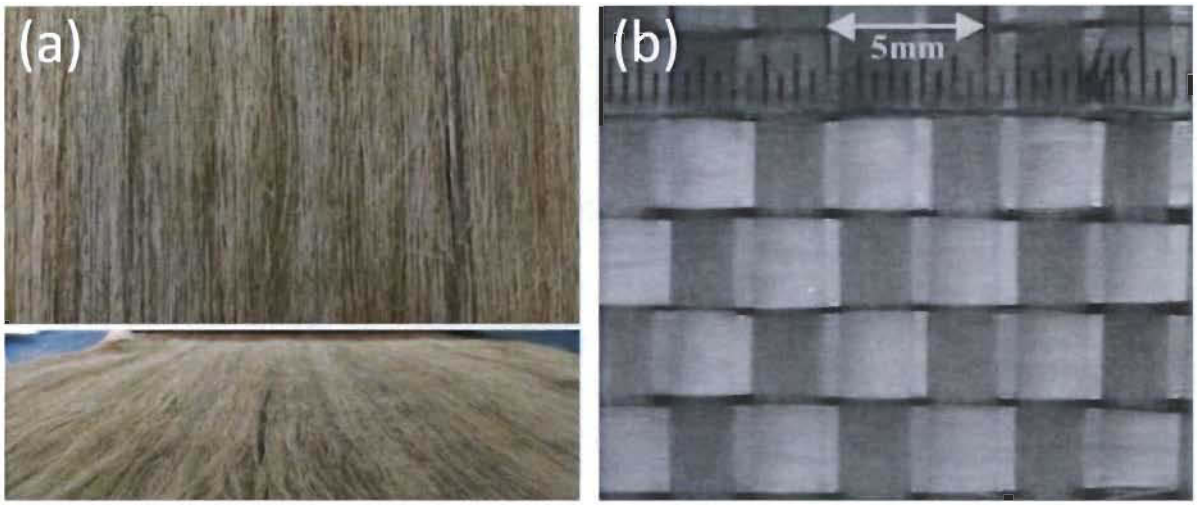

Figure 4-30. Texture of (a) FT-200 and (b) Syncoglas R420.

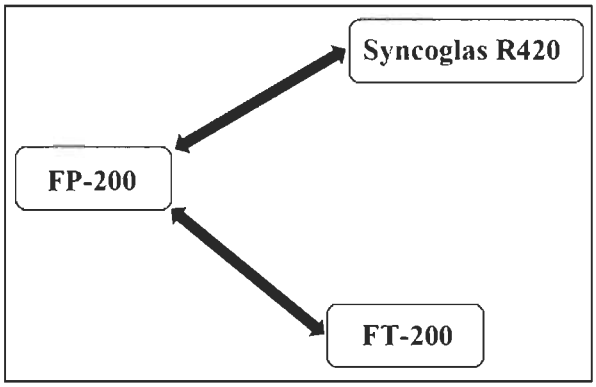

Figure 4-31. Plan of permeability comparative study with commercial reinforcements.

Results of permeability tests are summarized in Table 4-14 and depicted in Figure 4-32. The warp (K_1) and weft (K_2) permeabilities of Syncoglas R420 are reported K_1 = $1.79\pm0.398\times10^{-10}$ and K_2 = $1.43\pm0.301\times10^{-10}$ respectively, at a fiber volume fraction V_f = 41.7 % [60]. These values are respectively one and two orders of magnitude higher than the

FP-200. It is believed that lower average K_1 of FP-200 is mainly due to different architectures of the two reinforcements, with more flow channels in the case of Syncoglas R420, and also due to inherent hairy and rougher surface of natural fibers reinforcements compared to synthetic ones [66, 67].

In the case of average K_2, the much lower performance of FP-200 is mostly related to the unidirectional configuration of the flax yarns in the FP-200. Higher standard deviation of Syncoglas R420 is due to spacing between yarns and nesting effect. Permeability of a twill weave flax fabric at $V_f = 35$ % (measured with engine oil) is reported around 0.4×10^{-10} m^2 [72]. This is in the same order of magnitude than flax fiber reinforcements of this work and close to K_1 permeability of the 16 yarns/in. reinforcements in Table 4-3.

K_1 permeability of FT-200 is higher than FP-200 in terms of both mean and standard deviation and is very similar to that of UDF-200, reported earlier. This similarity between FT-200 and UDF-200 could be due to their quite similar fiber configuration consisting of longitudinal flax fibers which provide tiny longitudinal channels for fluid flow, while not having paper layer in both cases. However, FT-200 is made of long untwisted strand placed side by side while FP-200 is made of low twist yarns placed side by side.

In the following section some mechanical properties will also be investigated to determine whether the new reinforcement's global characteristics show potential industrial applications.

Table 4-14. Permeability comparison with commercial reinforcements.

Reinforcement type	Nominal	K_1 (10^{-12} m^2)			K_2 (10^{-12} m^2)		
	V_f (%)	Ave.	STD	C_V (%)	Ave.	STD	C_V (%)
FP-200	35	23.0	2.19	9.51	5.88	0.96	16.3
FT- 200	35	69.7	16.8	24.1	13.0	1.30	10.0
Syncoglas R420 **[60]**	41.7	179	39.8	22.2	143	30.1	21.05

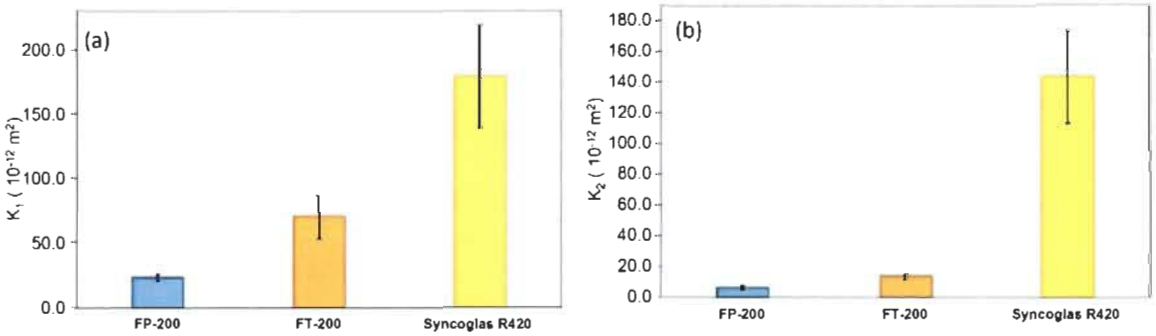

Figure 4-32. Results of permeability comparative study, (a) permeability along yarns/warp direction (b) permeability perpendicular to the yarns/weft direction.

4.3. **Tensile performance of composites**

In this section, tensile performance of composite laminates out of the hybrid UD flax/paper reinforcements fabricated according to the 1st DOE (Table 3-9), are studied for evaluating step 4 of the robust parameter design approach in Figure 3-31. During experimentation it was noticed that the drying temperature of reinforcement had an inverse influence on its surface density (higher drying temperature producing a lower surface density). Considering that fiber volume fraction is influenced by surface density (Equation 3-5) and that composite mechanical properties are strongly influenced by fiber volume fraction, neglecting the influence of drying temperature on surface density can induce variability on V_f, and subsequently on the mechanical properties of the derived composites. Thus the effect of drying temperature is evaluated in the first part of this subsection. A comparative study examining the effect of different reinforcement architectures and fiber volume fractions is also presented.

4.3.1. Analysis of reinforcement surface density

In Table 4-15, P-values of ANOVA on surface densities (m_r) of the reinforcements (Table 3-12) indicate that aside from evident contributions of the paper and flax layers, interestingly the drying temperature of the drum dryer (factor D) also influences the overall surface density of the reinforcement, while the compressing pressure has insignificant effect on it. The marginal plot in Figure 4-33 further indicates that the drying temperature has an inverse correlation with the average reinforcement surface density.

Table 4-15. ANOVA results on the reinforcement's average surface density (significant P values underlined).

Factor	Sum of Sq.	DOF	Mean Sq.	F statistic	P value
A	1812.98	1	1812.98	69.21	0.00
B	72702.86	1	72702.86	2775.49	0.00
C	43.49	1	43.49	1.66	0.20
D	938.70	1	938.70	35.84	0.00
Error	2357.51	90	26.19	-	-
Total	78014.20	94	-	-	-

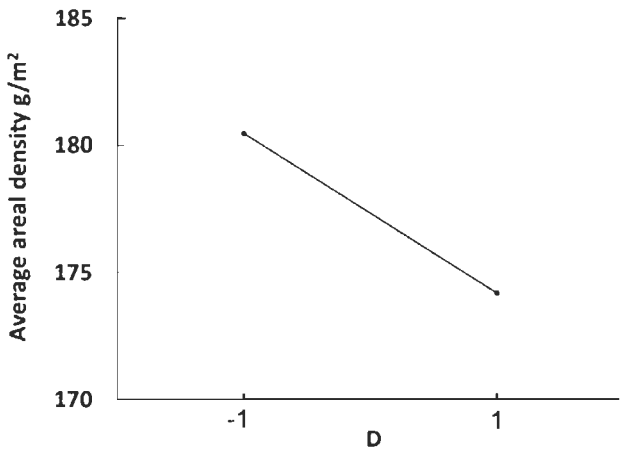

Figure 4-33. Marginal average plot of drying temperature (factor D) on reinforcement surface density.

This result was obtained after conditioning all samples at 103°C for more than 18 hours. Therefore any hypothesis related to mass variations (for example different humidity levels) is rejected. It is believed that this effect could be explained on the grounds that reduction of elastic modulus and increase of elongation as well as formability are reported for cellulose-based materials at an elevated temperature in presence of humidity [119]. So, it is hypothesized that drying at higher temperatures creates more surface expansion on the reinforcement. The reinforcements are squeezed between the drum surface and the fabric and exposed to heat flux from the drum surface (Figure 3-9). Both effects (squeezing and heat flux) will favor a uniform decrease in thickness, which promotes an increase of surface to maintain the overall volume almost constant. It is then believed that the higher the drying temperature the more the reinforcement surface expansion will be.

This hypothesis is supported by the measured reinforcement thicknesses shown in Table 4-16. The values of one-way ANOVA in this table show that the mean thickness is meaningfully less for reinforcements dried at high temperature (runs 2, 3, 5 and 8) compared to their counterparts dried at low temperature (runs 1, 4, 6 and 7, respectively), considering that comparing two consecutive runs (1 vs 2, 3 vs 4...) have identical type of flax and paper layers surface density and only the temperature is changed. This result has the important practical implication that in the manufacturing process of this new reinforcement drying temperature must be carefully controlled in order to reduce the variance of the composite performance. The surface expansion of reinforcement was relied on thickness measurement using a standard and repetitive micrometer used for paper thickness measurement as explained in Section 3.5. Normally, this is made by directly measuring the reinforcement area but because cutting

sharp edges of the reinforcement was not practically possible due to flax yarns, particularly when they are cut in the longitudinal direction of reinforcement, this method was not practical. Secondly there was no accurate device available to reliably detect expansion of the reinforcement (increase in surface area) by comparing the wet and dry area before and after drying.

Table 4-16. Measured reinforcement thicknesses using a micrometer and the results of one-way ANOVA (significant P values underlined), number of sample points N.

Run	Thickness (μm)				P value of one-way ANOVA	
	N	mean	STD	C_V(%)		
1	30	380	20.3	5.35	<u>0.00</u>	Total DOF = 59 Error DOF = 58 Factor DOF = 1
2	30	351	13.2	3.77		
3	30	427	29.2	6.84	<u>0.03</u>	Total DOF = 59 Error DOF = 58 Factor DOF = 1
4	30	449	43.4	9.68		
5	30	382	15.1	3.96	<u>0.00</u>	Total DOF = 59 Error DOF = 58 Factor DOF = 1
6	30	402	16.7	4.15		
7	30	474	28.5	6.02	<u>0.00</u>	Total DOF = 59 Error DOF = 58 Factor DOF = 1
8	30	446	32.5	7.28		

4.3.2. Two-level design of experiment (screening phase)

4.3.2.1. Overview of tensile test results

Tensile performance of composites molded with flax-paper reinforcements is characterized in terms of ultimate tensile strength (σ_u) and tensile modulus before (E_1) and after (E_2) the knee point (see Figure 3-29b). Table 4-17 summarizes the acquired experimental results and Figures 4-34 and 4-35 depict the data of the table.

It is well known that mechanical properties of natural fiber composites, like any composite, are mainly influenced by the fiber volume fraction [12]. So it is not surprising not to have considerable changes in the tensile results as V_f is maintained at 35 % in this study. However, the main objective here is to characterize the flax/paper reinforcement in terms of its material (factors A and B) and process parameters (factors C and D) in order to distinguish factors having an influence on average and/or variance of tensile test results (in conformance with step 4 of Figure 3-31), and if possible conduct a robust optimization of composite properties in the next step (in conformance with steps 12 to 14 of Figure 3-31). Studying the effect of reinforcement factors also allows for better controlling its fabrication process and consequently impart consistency into the behavior of the resulting composite parts. The trends of change in Table 4-17 (Figures 4-34 and 4-35) are small on an engineering point of view but statistically meaningful based on the ANOVA analysis performed in what follows (meaningful by 95% of confidence).

Table 4-17. Results of tensile tests on eco-composites at V_f=35 %, N: sample quantity.

Run	N	σ_u (Mpa)			E_1 (GPa)			E_2 (GPa)			ε_U(%)	
		Mean	STD	C_V (%)	Mean	STD	C_V (%)	Mean	STD	C_V (%)	Mean	STD
1	5	276	6.02	2.18	23.2	0.90	3.90	15.4	0.24	1.53	1.78	0.06
2	5	274	6.27	2.29	23.5	0.36	1.55	15.5	0.11	0.73	1.81	0.06
3	6	285	3.25	1.14	24.0	1.16	4.83	16.9	0.53	3.15	1.68	0.04
4	6	277	12.40	4.47	24.1	0.58	2.42	17.1	0.37	2.17	1.60	0.10
5	5	274	5.04	1.84	22.8	0.59	2.58	15.7	0.53	3.35	1.77	0.02
6	5	269	3.81	1.41	23.0	1.24	5.40	15.4	0.17	1.08	1.78	0.05
7	5	270	6.29	2.33	24.2	0.24	1.01	17.5	0.29	1.69	1.52	0.05
8	6	278	3.37	1.21	24.1	0.53	2.20	17.0	0.38	2.26	1.62	0.04

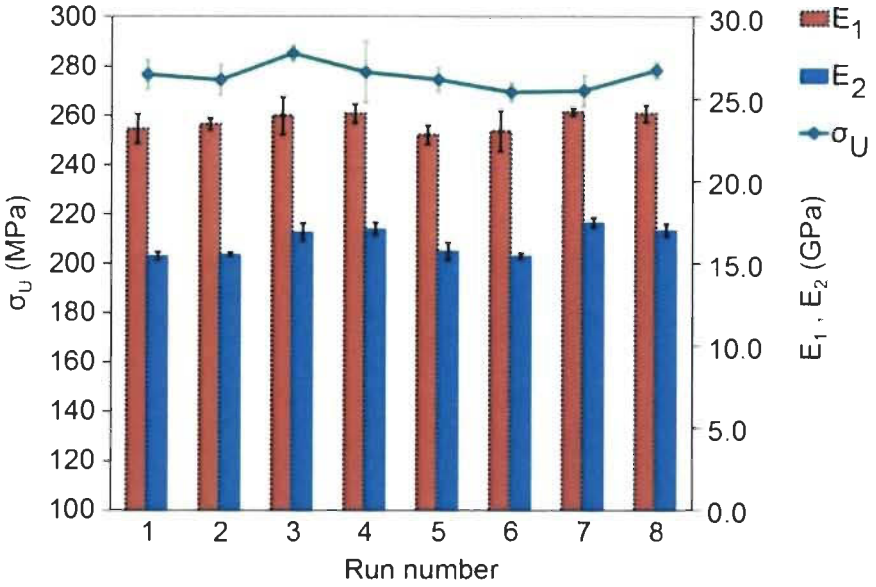

Figure 4-34. Graphs of tensile performance results, at V_f=35 %

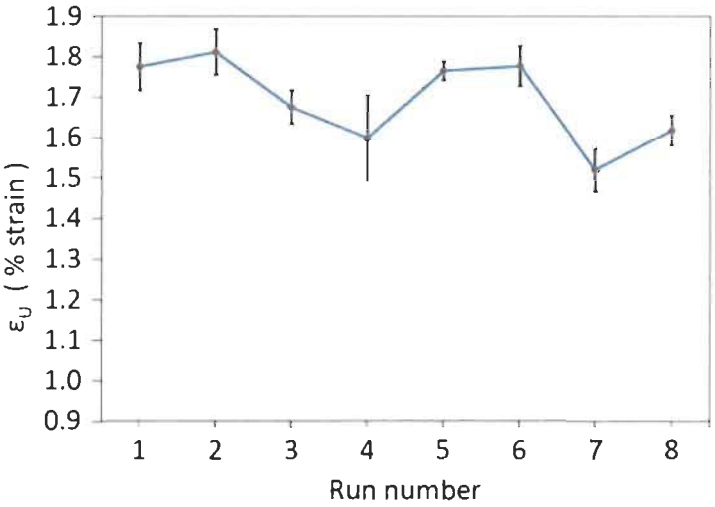

Figure 4-35. Graphs of ultimate strain at break, at V_f=35 %

Results of ANOVA in Table 4-18 indicate that none of the four targeted parameters has statistical significance on the standard deviation of the composites' tensile properties. Even if in Figure 4-34 there are a few cases with a higher standard deviation, they are not statistically meaningful based on the ANOVA analysis. This means that the variability of tensile

properties of composites remains almost the same for whatever combination of high and low values of the chosen material (A and B) and process (C and D) parameters. This is an indication that the manufacturing conditions of the composites have remained under control and consistent. This also goes along the conclusions reported in [120, 121], where it is demonstrated that due to 'averaging' effect of flax yarns, at the laminate scale the variability of flax yarn composite properties is not significantly higher than other composite materials already used for structural applications and that variability of composites is controlled by the quality of fabrication.

On the other hand, the P values in Table 4-19 indicate that average tensile strength (σ_u) is influenced by paper and UD flax layer surface density (factors A and B) as well as drying temperature (factor D). Moreover average modulus E_1 and E_2 are mostly influenced by factor B (flax layer surface density). The interaction effect AC (BD) has also an influence on E_2 modulus.

Table 4-18. P values of ANOVA on standard deviations of tensile results.

Factors	STD of σ_u	STD of E_1	STD of E_2
A	0.21	0.39	0.43
B	0.36	0.34	0.20
C	0.33	0.45	0.19
D	0.18	0.41	0.23
A×B (C×D)	0.41	0.13	0.19
A×C (B×D)	0.12	0.06	0.49
A×D (B×C)	0.26	0.39	0.26

Table 4-19. P values of ANOVA on mean values of tensile results (significant P values underlined).

Factors	mean σ_u	mean E_1	mean E_2
A	<u>0.01</u>	0.57	0.13
B	<u>0.05</u>	<u>0.00</u>	<u>0.00</u>
C	0.41	0.58	0.27
D	<u>0.02</u>	0.86	0.56
A×B (C×D)	0.36	0.30	0.51
A×C (B×D)	0.12	0.76	<u>0.02</u>
A×D (B×C)	0.33	0.63	0.84
Total DOF = 42; Error DOF = 35; Factor DOF = 1			

4.3.2.2. Strength and modulus analysis

Marginal average plot in Figure 4-36 shows that factor A has an inverse correlation with average ultimate strength, while factors B and D show a direct correlation with it. Equation 4-18 is the regression model in coded setting for mean tensile strength. The coefficient of determination is $R^2 = 0.85$ for this model. According to this equation maximizing $\hat{\sigma}_u$ can be achieved by setting factor A to its low level value while B and D should be set high.

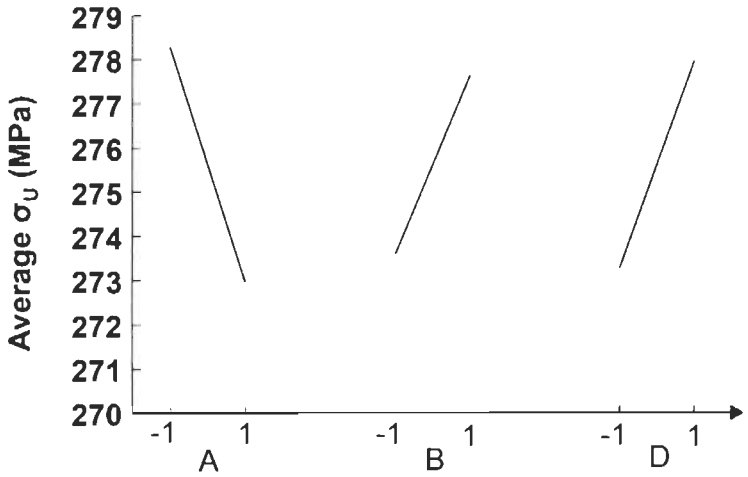

Figure 4-36. Marginal average plot for σ_u

$$\hat{\sigma}_u = 275.682 - 2.686A + 2.086B + 2.432D \qquad 4\text{-}18$$

Moreover, according to marginal average plots of Figure 4-37, the mean modulus E_1 and E_2 have direct correlation with factor B (flax layer surface density) and have, respectively, increased by around 1 and 1.5 GPa at the high level of factor B (24 yarns/in. flax layer). As mentioned previously interaction AC (or BD) is also statistically significant for E_2 modulus. Based on the explanation of appendix F.1, in the 1st DOE which is a resolution IV DOE the two-way interactions are confounded, meaning that the real influencing interaction factor (either AC or BD) can only be distinguished through more analysis or technical considerations. However, looking at the marginal average plot in Figure 4-37b, one notices that the mean value of E_2 is only slightly affected by different levels of this interaction factor.

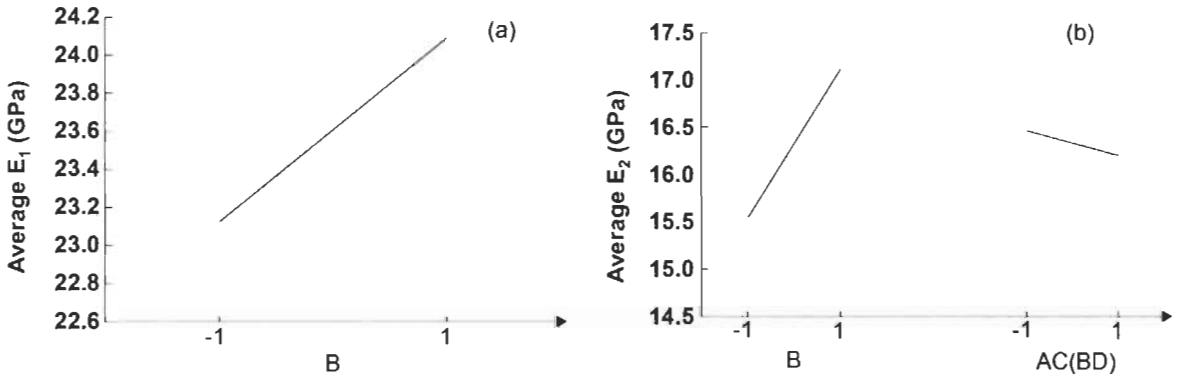

Figure 4-37. Marginal average plot for the modulus (a) before and (b) after the knee point.

Equations 4-19 and 4-20 are the regression models in coded domain for the E_1 and E_2 modulus. The R^2 coefficients for these models are 0.87 and 0.96, respectively. As can be seen, the coefficient of factor AC is much less than that of factor B in Equation 4-20. This is normal considering the modulus is mainly influenced by the unidirectional flax fibers (factor

B) compared to paper surface density (factor A) and forming pressure (factor C). It is however interesting to note that combination AC affects the modulus negatively, suggesting that this interaction parameters must be minimized to reduce their impact on E_2, although its effect is negligible.

$$\hat{E}_1 = 23.606 + 0.481B \tag{4-19}$$

$$\hat{E}_2 = 16.323 + 0.782B - 0.13AC \tag{4-20}$$

Regarding the effect of factor A (paper surface density) and B (flax ply surface density) on the composite strength, optical and scanning electron microscopic (SEM) images of polished cross-sections of virgin composite samples in Figure 4-38 indicate that interfacial porosity (seen as tiny black lines around fibers) is more significant around Kraft paper fibers than flax fibers. Such interface porosity is also reported in [122]. It is suspected that increasing the paper surface density and subsequently the paper mass content in the composite could impart more porosity into the composite and consequently weaken its strength. However, comparing the images in Figure 4-38 with that of the previous work [71] in Figure 4-39 suggests that porosities are highly reduced in the present study. According to [12] this could be due to RTM method used in this study for composite processing which yields lower void content than the vacuum bagging method used previously [71].

In Figure 4-40, the pulled out fibers and imprints of removed fibers on the matrix (some of them pointed out with arrows) are visible. It is also observed that there is almost no residual

matrix material on the pulled out fibers, which is also another sign of weak fiber/matrix adhesion. These observations lead us to conclude that fiber pullout is one of the fracture mechanisms of the flax/paper composites developed in this work, and that fiber/matrix interface is currently a weakness of the composite.

The effect of drying temperature (factor D) on the IBS and reinforcement surface density (m_r) was already identified and explained in sections 4.1.2 and 4.3.1, respectively. Not surprisingly the effect of drying temperature also comes out statistically significant on the mean composite tensile strength, although average strength has just slightly increased from 273 at low level temperature to 278 at the high level one. Morphological changes of reinforcement due to thickness reduction, and larger number of chemical bonds between flax fibers of yarns (as drying promotes formation of fiber-fiber bonds in cellulosic materials [113, 114]), could result in higher strength of yarns, and subsequently have helped promote higher composite tensile strength.

Two typical stress-strain curves from runs 1 and 8 (having flax layer surface density at low and high levels, respectively) in Figure 4-41 indicate that the intersection of two tangent lines drawn through the linear portions of the curves, occurs at a higher strain for samples of run 8. This phenomenon was also repeatedly observed when the stress-strain curves of other runs were compared. This implies that increasing the surface density of UD flax layer postpones the knee point to a higher strain. However, composite samples with flax layer at its high level have generally shown lower ultimate strain at break (runs 3, 4, 7 and 8 in Figure 4-35). Furthermore, it is also systematically observed, based on all the results of Table 4-17,

that composites with higher flax layer surface density lost 29 % of their initial stiffness after the knee point, while corresponding value for composites with low level flax ply surface density was 33 %.

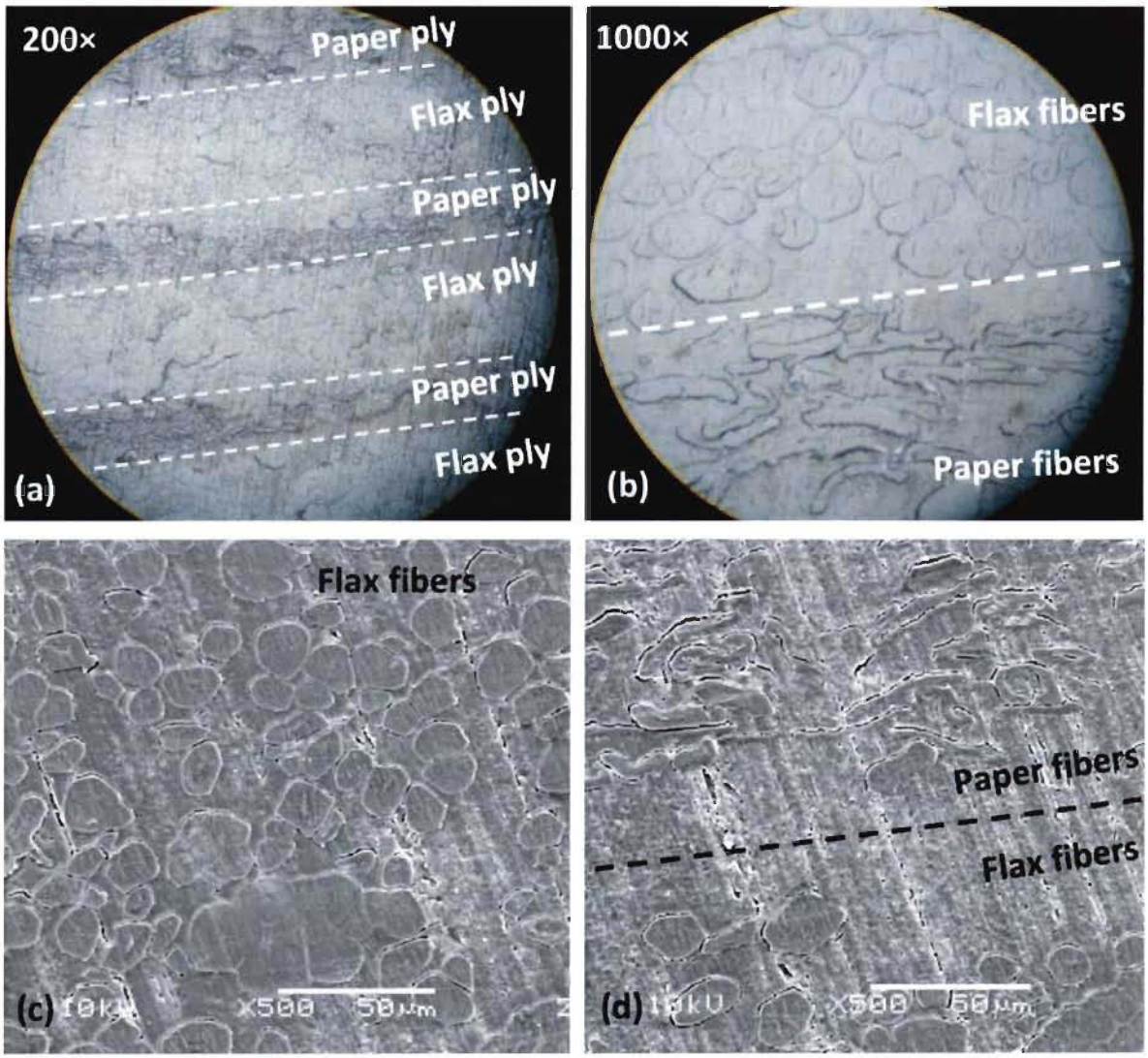

Figure 4-38. Images of virgin samples cross-section, (a and b) optical microscope, (c and d) SEM.

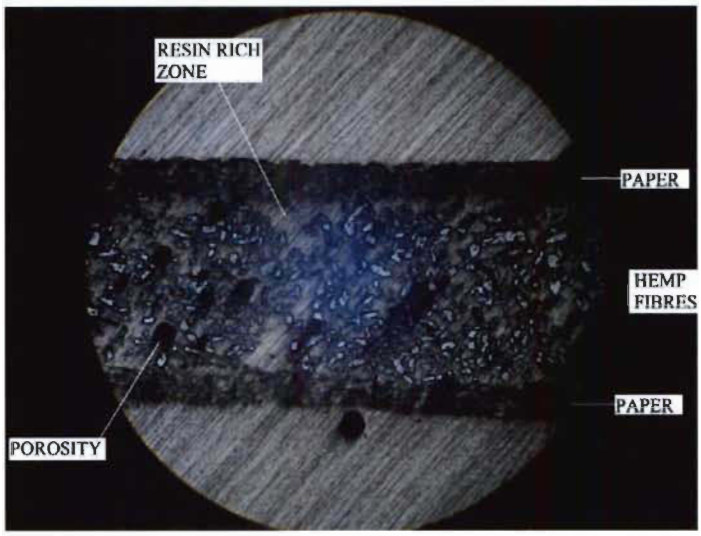

Figure 4-39. Microscopy image of the cross-section of hemp/paper/epoxy [71].

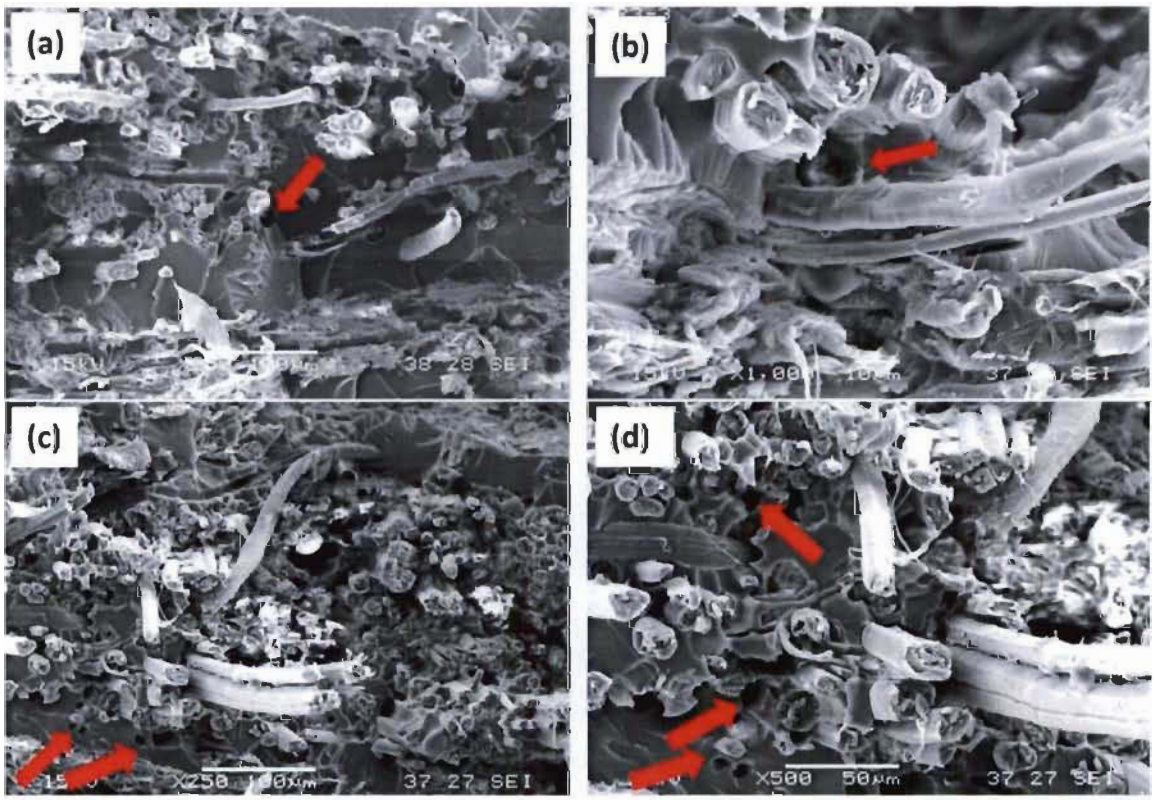

Figure 4-40. SEM images of tensile coupon fracture surfaces, run 3 (a and b), run 6 (c and d).

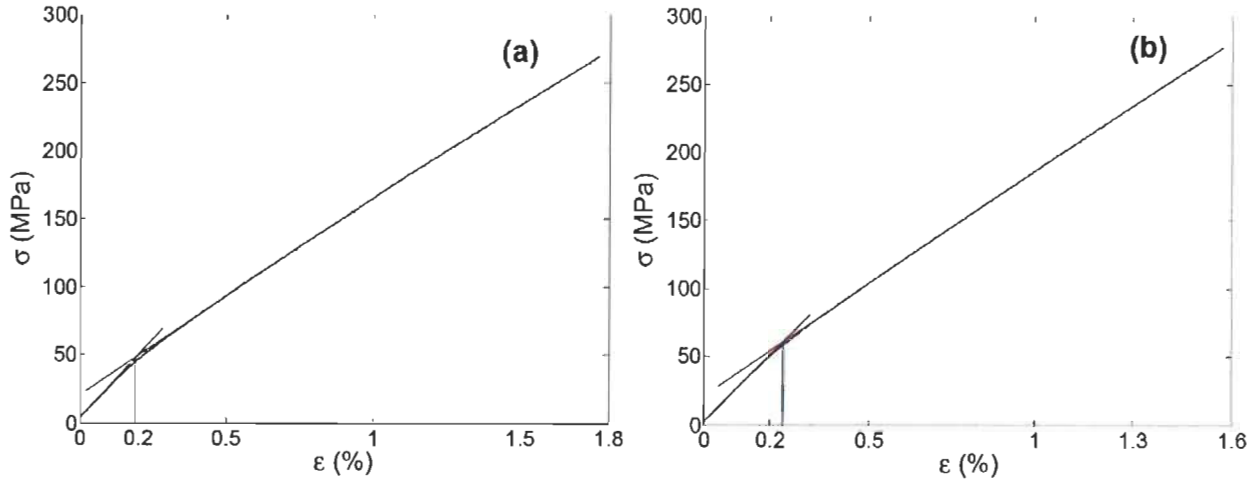

Figure 4-41. A typical stress-strain curves for samples of (a) run 1 and (b) run 8.

4.3.3. Comparative study

As concluded in the previous section none of the four studied reinforcement parameters have statistically meaningful effect on standard deviation of the mechanical properties. Therefore, based on step 4 of the robust parameter design algorithm in Figure 3-31, classical robustness study could not be performed in terms of composite tensile properties. However, it is worth mentioning that the standard deviation of composite mechanical properties in Table 4-17 are reasonably low, which is believed to be mainly due to employing a high quality RTM technique that is reported to provide low void content [12], in addition to consistent fabrication of reinforcement and composite samples (eliminating the effect of human factor on variance of results).

Similar to the comparative study of permeability, in this section the effect of different reinforcement fiber configurations on the tensile behavior of composites are evaluated and compared with the aim of studying the effect of reinforcement architecture on variance of the

results (robustness study). In section 4.3.3.1 the behavior of a tex 200 UD flax/paper/epoxy composite studied above (through DOE approach) is compared with other composites made from laboratory reinforcements. On the other hand in section 4.3.3.2, the tex 200 UD flax/paper/epoxy composite is compared with two commercial composites including the FlaxTape© and a UD glass.

4.3.3.1. Comparison with other laboratory-made flax fiber reinforcements

Figure 4-42 shows the studied reinforcements and the comparison strategy through which the effects of different parameters (mentioned in the figure) on the tensile behavior are assessed. This comparison strategy is similar to that of permeability comparative study (in section 4.2.3.1) except that SFP-200 is replaced with FP-200-40 (Flax/Paper Tex 200 with V_f = 40 %) and FP-200-45 (Flax/Paper Tex 200 with V_f = 45 %). These two latter reinforcements are identical to FP-200 (explained in permeability comparative study) except that they have been molded at 40 and 45 % of fiber content, respectively (instead of 35 % for FP-200). For explanations about the reinforcements of the plan shown in Figure 4-42, one can refer to section 4.2.3.1. For each reinforcement configuration at least five tensile tests are performed.

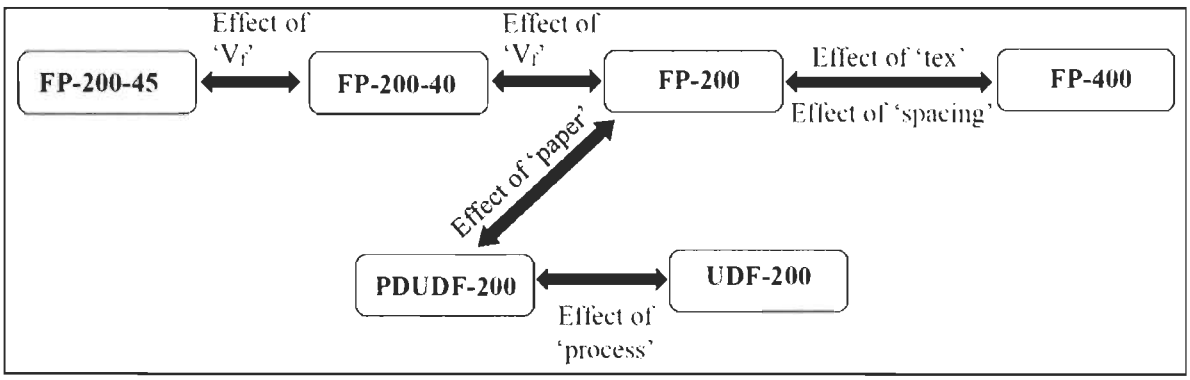

Figure 4-42. Plan of tensile performance comparative study.

The results of tensile performance comparative study are shown in Table 4-20 and in visual form in Figure 4-43. According to Table 4-20 standard deviations of E_1, E_2 and σ_u for FP-200 are respectively about six, three and two times lower than both UDF-200 and PDUDF-200, in which the paper layer is absent, while the average modulus of all three composites are almost equal. As is also mentioned in the previous works [71], this observation signals the positive effect of the paper layer in reducing the standard deviation of tensile modulus. Based on this remark, it appears that the paper layer probably enables a more uniform distribution of tensile stress inside the composite and therefore imparts consistency into the behavior of composite material.

Table 4-20. Results of tensile performance comparative study.

Reinforcement type	Nominal V_f (%)	E_1 (GPa)		E_2 (GPa)		σ_U (MPa)	
		Ave.	STD	Ave.	STD	Ave.	STD
UDF-200	35 %	25.4	3.2	18.6	1.0	303	7.3
FP-400	35 %	24.2	0.7	16.9	0.36	259	5.2
FP-200	35 %	24.1	0.5	17.0	0.38	278	3.4
PDUDF-200	35 %	25.1	3.9	17.8	1.3	334	7.5
FP-200-40	40 %	25.5	0.7	17.3	0.33	297	3.4
FP-200-45	45 %	27.5	0.8	18.6	0.41	325	4.8

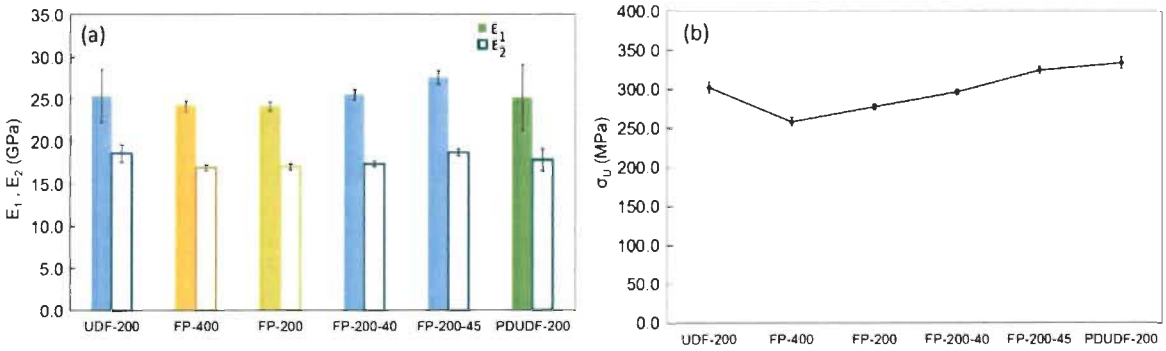

Figure 4-43. Results of tensile performance comparative study, (a) modules before, E_1, and after, E_2, knee point, (b) ultimate strength.

Effect of paper layer on tensile behavior of composites can also be seen in Figure 4-44. Longitudinal cracks propagating from the fracture sections of UDF-200 and PDUDF-200 have been repeatedly observed, while this is not the case for FP-200. It is believed that in the absence of paper layer the composite material is more sensitive to small irregularities of the flax yarns (e.g. kink-bands [11]), and such regions become points of stress concentration with severe cracks propagating along the fibers in samples without paper. A similar observation has already been reported for UD hemp/epoxy samples made using the vacuum bagging process [71] and UD jute/polyester and flax/polyester composites in [104]. On the other hand, FP-200 showed brittle fracture behavior with fracture section always perpendicular to the tensile direction, while cracks in the UDF-200 and PDUDF-200 are inclined to the stress direction mimicking the 45° maximum shear stress fracture mode of ductile materials.

UDF-200 and PDUDF-200 have respectively shown 9 % and 20 % higher ultimate strength (σ_u) than FP-200. This is due to higher flax volume fraction in the UDF-200 and PDUDF-200 compared to FP-200 where the paper layer was taken into account in the calculation of V_f. In the FP-200 all fibers (paper and flax) are considered at $V_f = 35\%$, while in UDF-200 and PDUDF-200, $V_f = 35\%$ just corresponds to flax fibers. However, by comparing microscopy images of FP-200, PDUDF-200 and UDF-200 in Figure 4-45, it is suggested that more porosity is present at the interface of hydrophilic Kraft fibers and hydrophobic epoxy resin in FP-200. This effect could also contribute to lower the strength of FP-200.

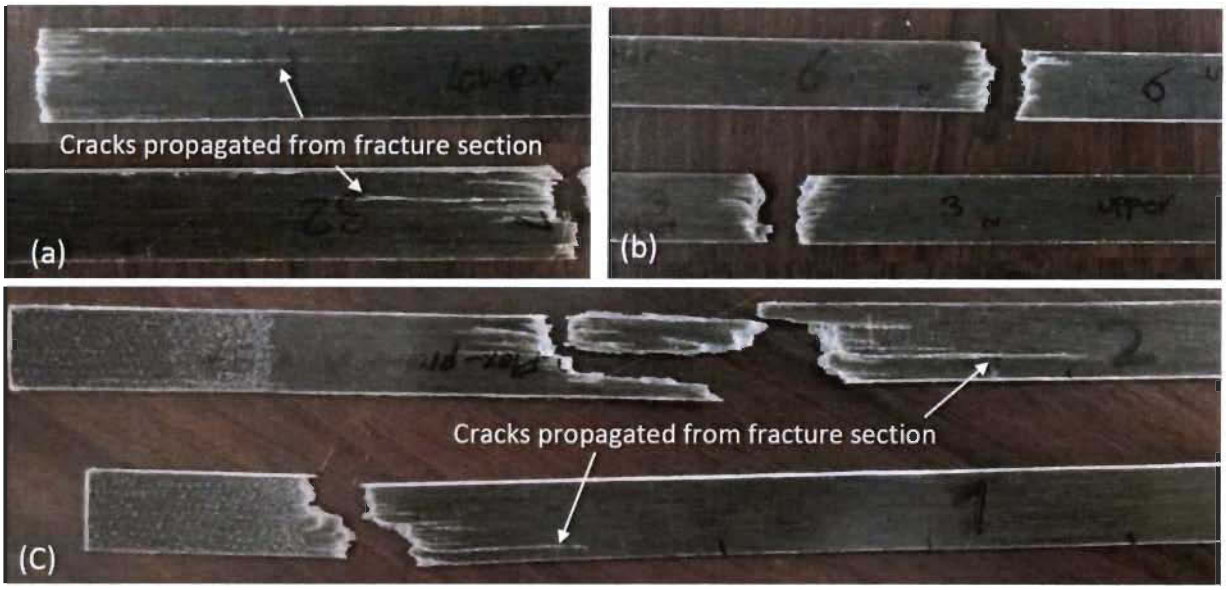

Figure 4-44. Comparing failure section of composite samples made of, (a) UDF-200, (b) FP-200, (c) PDUDF-200.

While having almost equal average tensile modulus and modulus standard deviation, the higher tensile strength of PDUDF-200 compared to UDF-200 could be due to more organized arrangement of yarns in the former reinforcements as can be noticed by comparing Figure 4-46a and Figure 4- 46b. This means that pressing and drying bring uniformity in the fiber distribution inside the composites.

FP-400 and FP-200 have shown almost equal mean and standard deviation tensile modulus. However lowest strength (σ_u) in Table 4-20 belongs to FP-400. Spacing between yarns in FP-400 (see Figure 4-26b) can create resin rich zones (pointed out in Figure 4-47), and so during the tensile tests the cracks initiate from such regions. This is supported when comparing the strength of FP-400, having fewer numbers of yarns in the cross-section of tensile samples (12 yarns/in.), with the strength of FP-200 (having 24 yarns/in.) and with the 16

yarns/in. tex 200 flax/paper composites reported in Table 4-17 (strength 273 MPa, average of runs 1, 2, 5, 6).

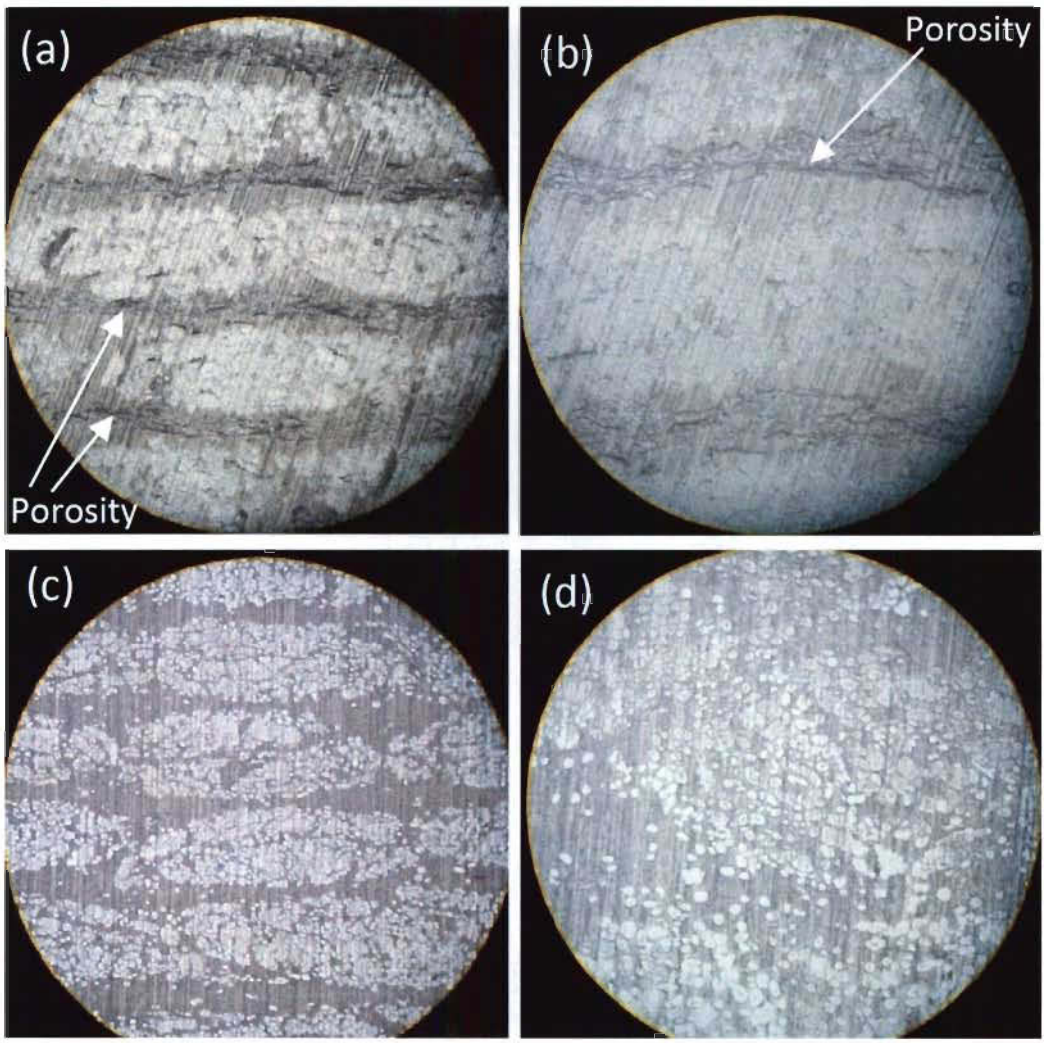

Figure 4-45. Comparing optical microscopy images of (a, b) FP-200 with 100X and 200X magnification respectively (c) PDUDF-200, 100X magnification (d) UDF-200, 200X magnification.

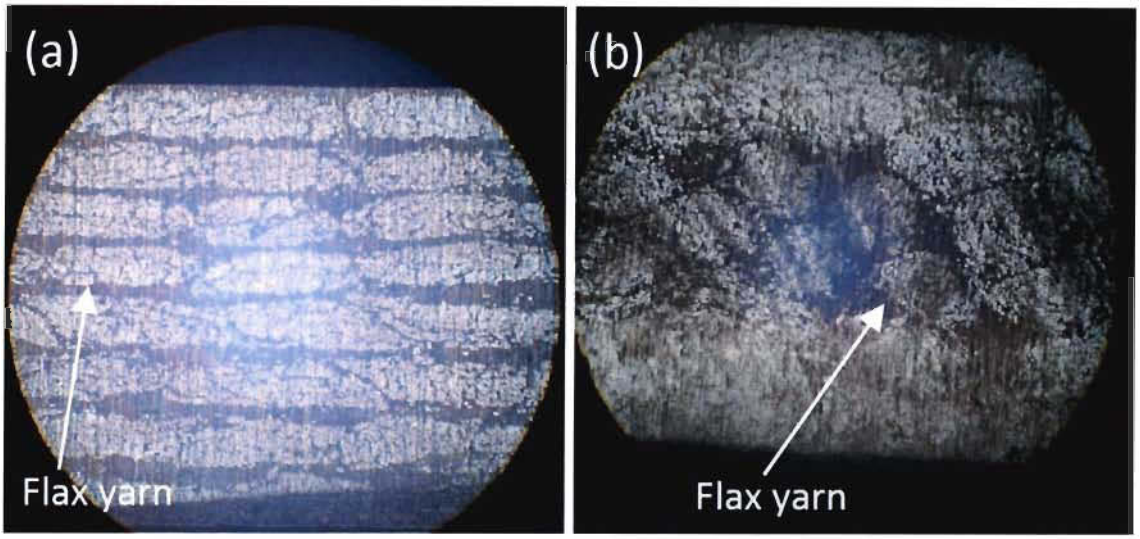

Figure 4-46. Comparing optical microscopy images of (a) PDUDF-200, 50X magnification, (b) UDF-200, 50X magnification.

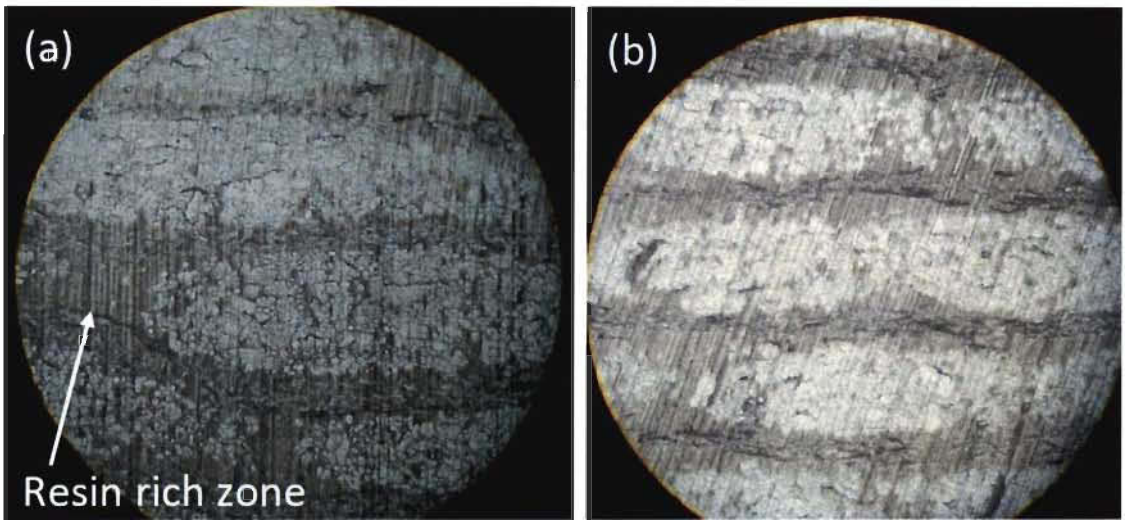

Figure 4-47. Comparing optical microscopy images of (a) FP-400, 100X magnification, (b) FP-200, 100X magnification.

Results of FP-200, FP-200-40 and FP-200-45, are shown in Table 4-21 and Figure 4-48. The rule of mixture is applicable to UD flax layer as mentioned in [104]. It is also assumed applicable in the actual case even if the paper layer is present. This means that compaction behavior of flax/paper reinforcement is mainly influenced by the UD flax yarns, assuming

the thickness of paper layer doesn't change much and its influence remains almost constant. This assumption relies on the fact that the paper layers are thin and made of very short Kraft fibers, so under consolidation pressure they are more difficult to compress than the flax layers. Nonetheless, the author is aware that in future works, the real individual thicknesses will be required to study the influence of each individual layer.

First, the experimental data points at V_f = 35 % has been corrected to zero porosity (to calculate the first point of the ROM in Figure 4-48) by dividing by the factor $(1-V_p)^2$ [34], where V_p denotes porosity content in the composites. For a composite sample of FP-200, the density (ρ_c) is measured at 1.31 g/cm^3 (using a gas pycnometer model Ultrapyc 1200e from Quantachrome Instruments) and the porosity content is estimated at 1 ± 0.1 % using Equation 4-3. Next, the corrected zero porosity values (referred to as ROM) at V_f = 40 % and V_f = 45 % are estimated by linear proportion. It can be observed that experimental tensile properties deviate more and more from theoretical (ROM) values as V_f increases. Such a deviation is also reported in [34] and claimed to be due to void content of composites. The presence of macroscopic voids in FP-200-40 can be observed in Figure 4-49. Such macroscopic voids are not observed in the case of FP-200 composites made at 35 % fiber content in Figures 4-45a and 4-45b as well as 4-38.

Table 4-21. Tensile properties of FP-200 with respect to fiber volume fraction.

V_f(%)	σ_U (MPa)			E_1 (GPa)			E_2 (GPa)		
	Experiment	ROM	Deviation (%)	Experiment	ROM	Deviation (%)	Experiment	ROM	Deviation (%)
35	278	284	2.1	24.1	24.6	2	17.0	17.3	1.7
40	297	318	6.6	25.5	27.5	7	17.3	19.4	11
45	325	358	9.2	27.5	31.0	11	18.7	21.9	15

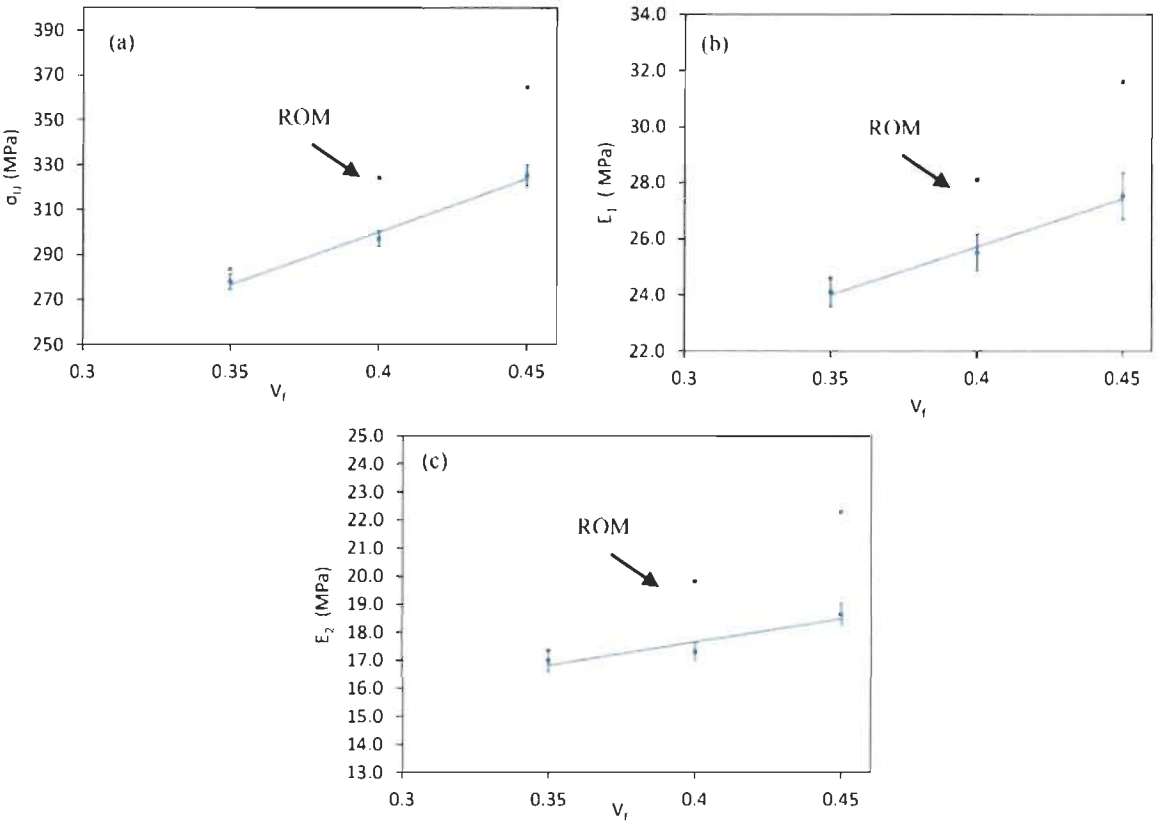

Figure 4-48. Tensile properties of FP-200 for different fiber volume fractions: (a) strength, (b) modulus before knee point, (c) modulus after knee point.

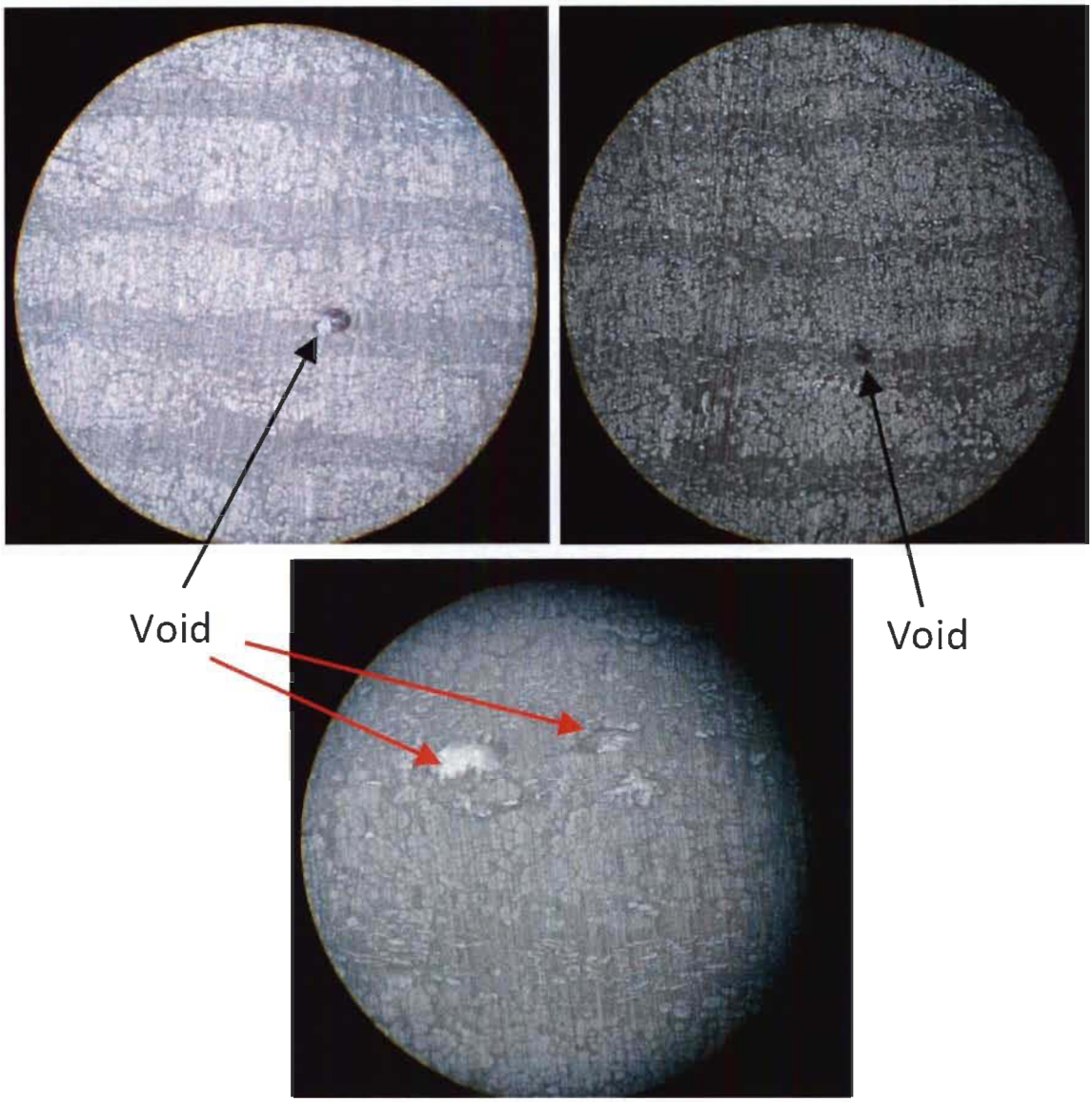

Figure 4-49. Presence of macro-voids in microscopy images of FP-200-40, (a, b) 100X magnification (c) 200X magnification.

4.3.3.2. Comparison with commercial reinforcements

Tensile behavior of FP-200 and FP-200-45, are respectively compared with commercial FT-200 and a UD glass/epoxy reported in the literature. This bilateral comparison allows for comparing at almost similar V_f. Figure 4-50 shows the comparative study plan and the composites results are shown in Table 4-22 and Figure 4-51.

The specific tensile stiffness of the UD E-glass/epoxy has been reported 18 GPa/(gcm^{-3}) at V_f = 48 % [123]. Corresponding values for FP-200-45 is 21 GPa/(gcm^{-3}) before the knee point and 14.3 GPa/(gcm^{-3}) after knee point (considering the experimentally measured density of 1.31 g/cm^3 using gas pycnometer). This represents a 17 % increase in specific stiffness before knee point but a 20 % decrease after the knee point. Such a result is in general promising and indicates that the FP-200-45 has well exploited the advantage of flax fibers over glass fibers in terms of higher specific tensile stiffness. Strength of glass/epoxy is evidently much higher than FP-200-45, due to the higher tensile strength of glass fibers.

FT-200 has shown slightly higher mean modulus than FP-200. However it has demonstrated lower value of ultimate strength (σ_u) than FP-200. Figure 4-52 indicates that porosities, shown as black lines in the micrographs, are more prevalent in FT-200 compared to Figures 4-45a and 4-45b for FP-200, which could be the cause of lower strength for FT-200.

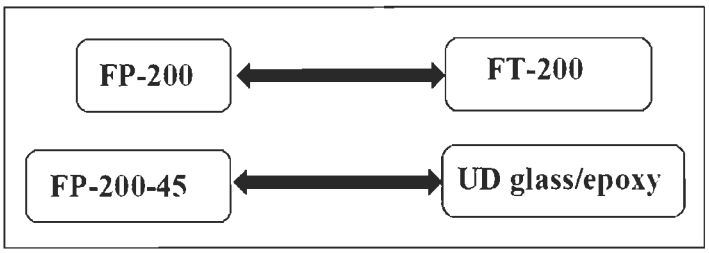

Figure 4-50. Comparison of flax/paper tex 200 composite with composites of commercial reinforcements.

Table 4-22. Comparative study with commercial reinforcement composites.

Reinforcement type	Nominal	E_1 (GPa)		E_2(GPa)		σ_U(MPa)	
	V_f (%)	Ave.	STD	Ave.	STD	Ave.	STD
FP-200	35 %	24.1	0.5	17.0	0.38	278	3.4
FT-200	35 %	27.7	0.9	20.8	0.40	265	3.7
FP-200-45	45 %	27.5	0.8	18.6	0.41	325	4.8
UD glass/epoxy [123]	48 %	31.0	1.0	N/A	N/A	817	35.0

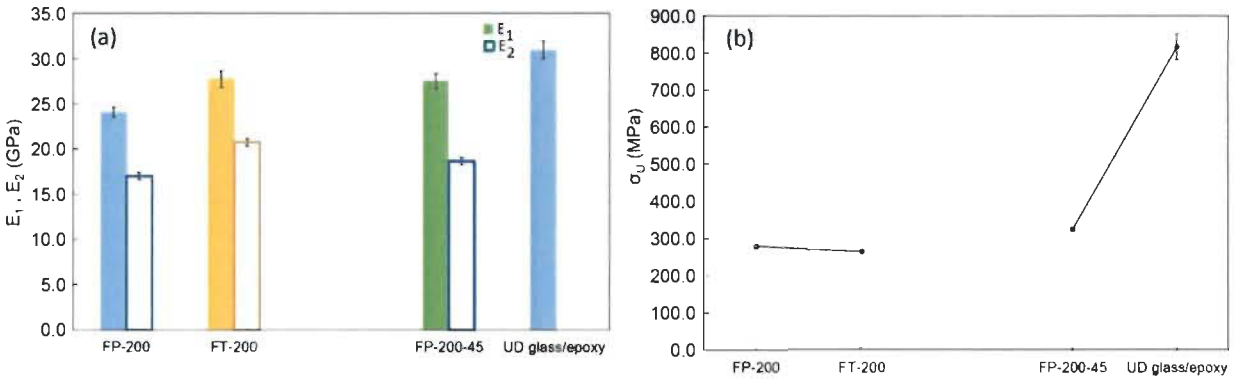

Figure 4-51. Comparative study with commercial reinforcement composites (a) modules before (E_1) and after (E_2) the knee point and (b) ultimate strength.

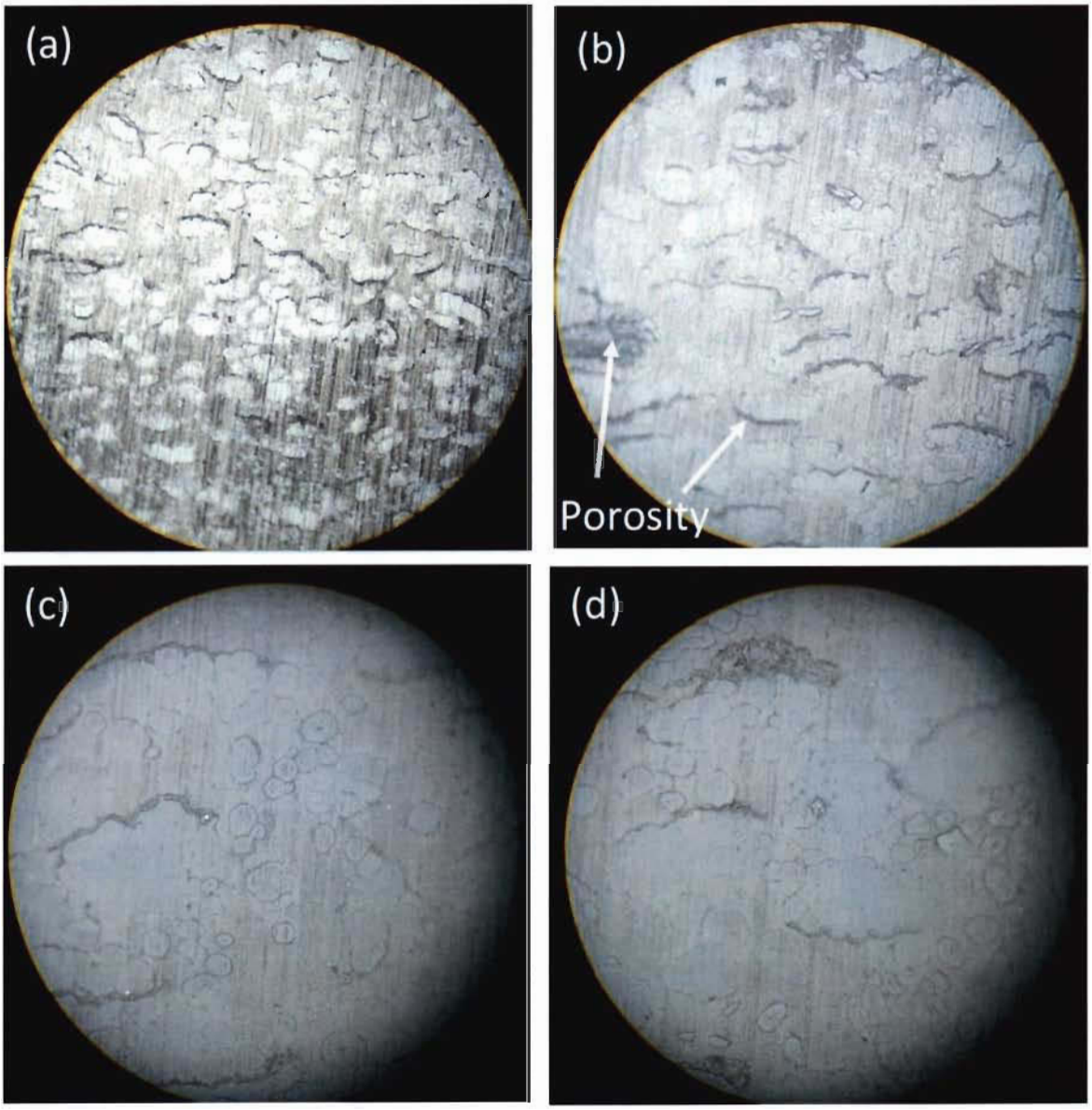

Figure 4-52. Microscopy images of FT-200 (a) 100X, (b) 200X, (c) 500X, (d) 500X

4.4. **High volume reinforcement manufacturing using a pilot paper machine**

In this section, outcomes of some trials for fabricating the flax/paper reinforcement on a pilot-scale paper machine of Innofibre are described. For all of these trials speed of paper machine is set at its minimum which is 200 m/min.

Figure 4-53 shows the result of first experiments for fabricating 16 yarns/in. reinforcement on a 100 g/m^2 paper sheet. As can be seen in the figure the yarns are well attached to the paper surface and the initial one inch width is more or less maintained. However, as Figure 4-53b shows flax fibers are drawn by the comb during feeding process due to high friction between yarns and the teeth of the comb. Due to this problem, this comb is modified to the comb shown in Figure 3-13a and next trial is performed using this modified comb.

Figure 4-54 shows the results of second experiment in which the comb of Figure 3-13a is mounted on the feeding frame. Before passing the yarns through the comb they are passed through a mesh plate to bring the yarns closer to each other and to make them ready to pass through the 16 yarns/in. comb. In this experiment, the paper surface density of 50 g/m^2 is used, because having lower surface density favors the impregnation to liquid resin (higher permeability to resin) and composite quality. Figure 4-54 shows that the yarns are not attached on the paper surface and they are loose and wavy. In addition the initial one inch feed was spread into three inches width at the end. It appears that having more pulp in the former test (100 g/m^2 vs. 50 g/m^2 in this trial), restricts the movement of fibers throughout the paper machine.

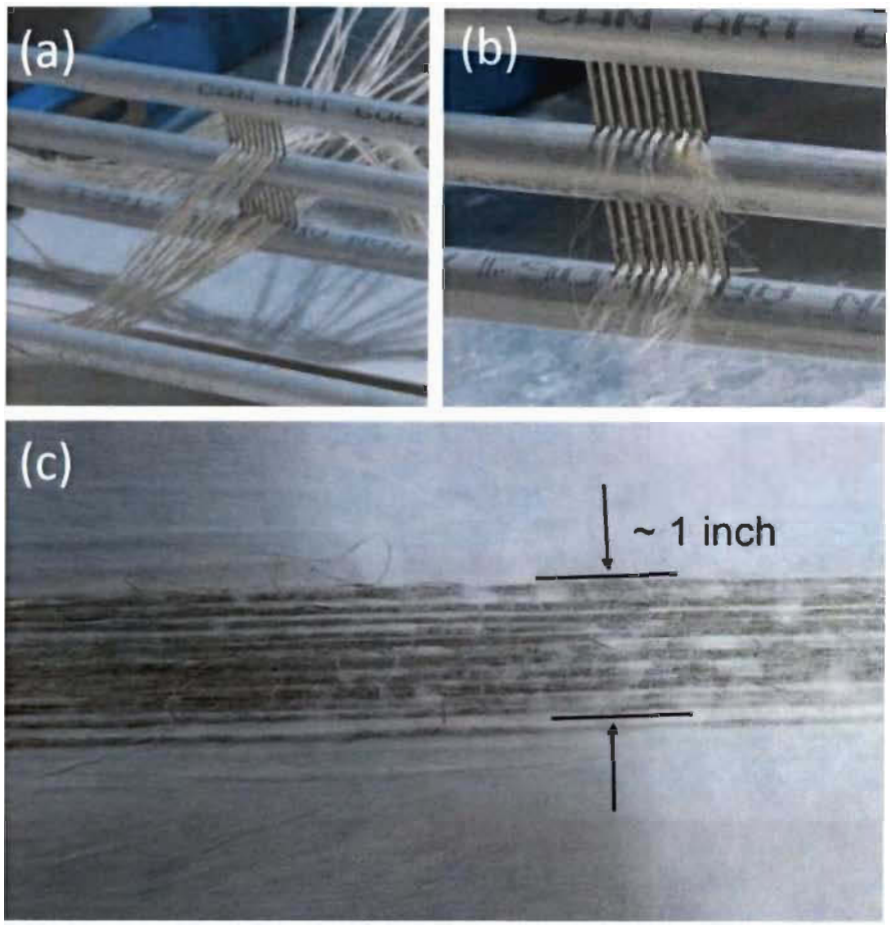

Figure 4-53. Outcome of first trial with 100 g/m^2 paper layer (a) feeding setup, (b) feeding comb after experiment, (c) acquired reinforcement.

Outcomes of third trial using the comb of Figure 3-13b are shown in Figure 4-55c. After passing the yarns through the comb they are passed between a tightener shown in Figure 4-55a to bring the yarns to the same level before laying them down on the machine table. Figure 4-55c indicates that the initial one inch width is spread to some 2.5 inch width in the final sample and also the flax yarns are not well attached on the paper surface.

In the fourth experiment a layer of pulp slurry is sprayed on top of the flax yarns (as is shown in Figure 4-55b) while they were traveling along the wet-end machine table. The purpose of spraying fibers was to increase cohesion between yarns (by having Kraft fibers on

both surfaces of the flax yarns) to restrict them to get separated from each other. Result of this experiment is shown in Figure 4-55d. Compared to the result of third experiment the yarns are attached to the paper and are more straight and parallel to each other. However, a 50 g/m^2 paper layer was used in both cases but once again the distance between yarns was increased to about three inches.

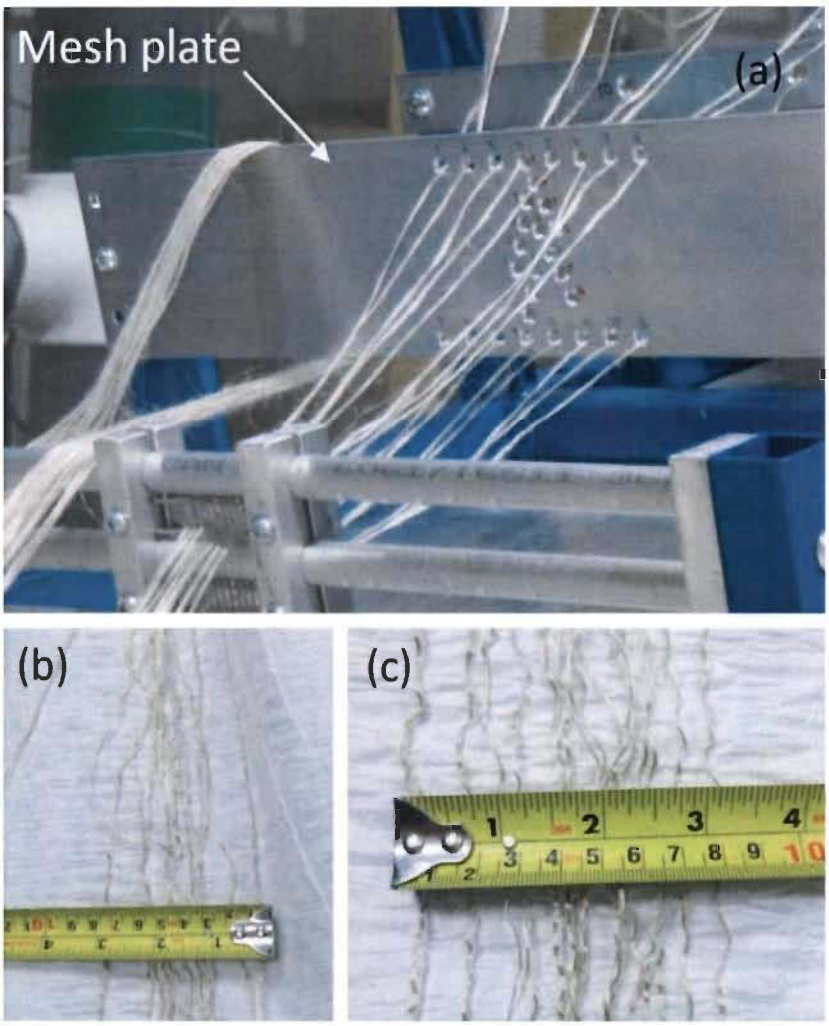

Figure 4-54. Outcome of second trial using the comb of Figure 3-13a with 50 g/m^2 paper layer, (a) feeding setup, (b and c) resulting sample.

In a fifth and final test, the comb of Figure 3-12 is used to feed the yarns into the paper machine and produce a reinforced paper. In this case the yarns are passed directly from the bobbins to the comb and then directly to the machine table and neither a mesh plate nor the tightener are used. Surface density of paper layer is 100 g/m^2 and extra pulp is added over the yarns using the setup shown in Figure 4-55b. Results of this experiment in Figure 4-56 suggest that the yarns are aligned, straight and quite well attached to the surface of paper. Moreover, they have more or less kept the one inch initial spacing between each of them

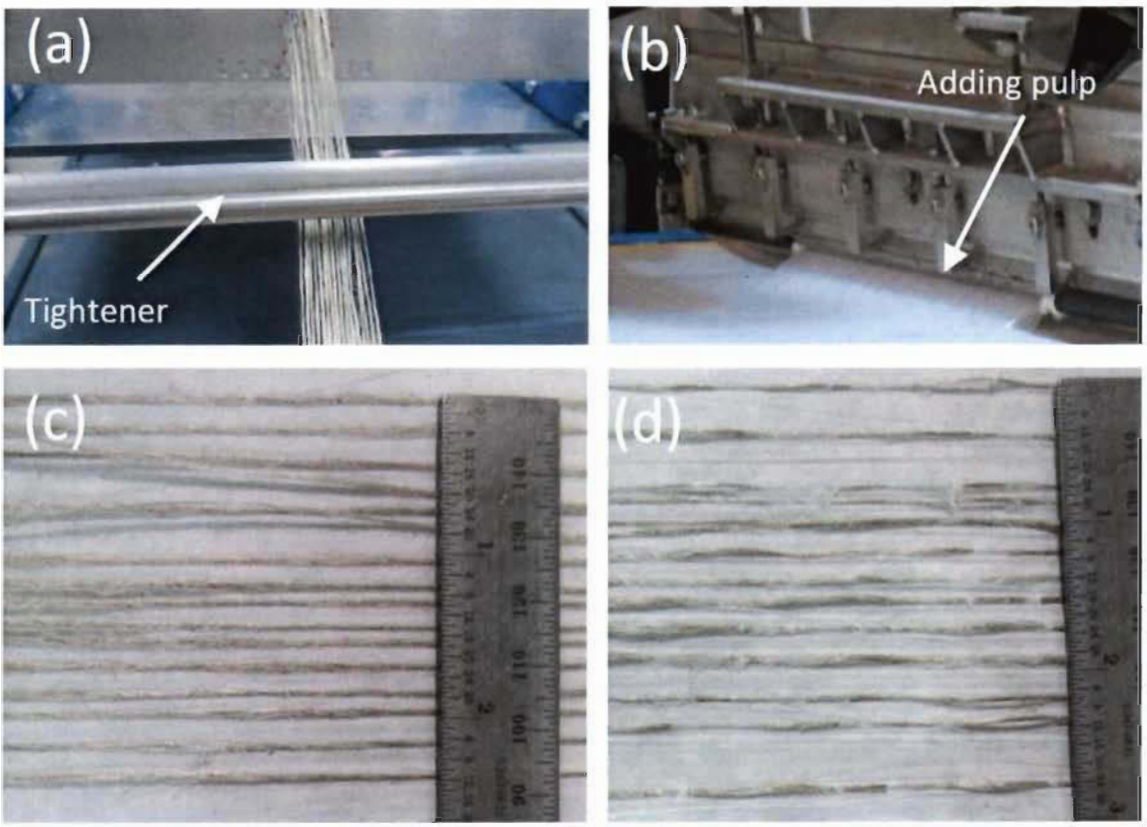

Figure 4-55. Outcome of third and fourth trial with 50 g/m^2 paper, (a) Passing the yarns through tightener after being passed through the comb, (b) adding pulp over yarns for fourth test, (c) result of third test, (d) result of fourth test.

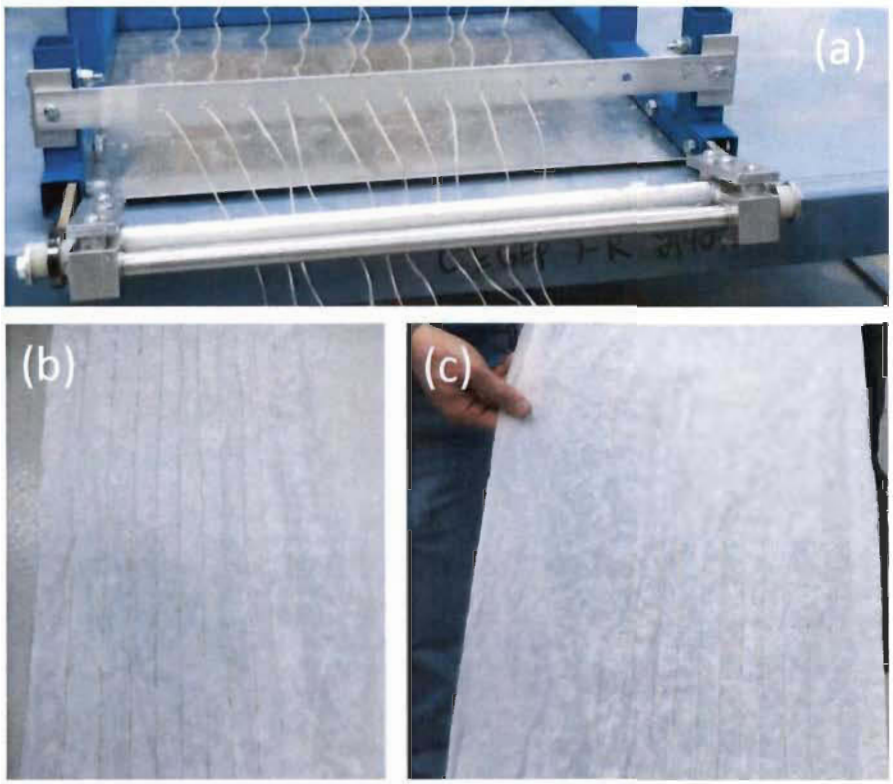

Figure 4-56. Result of fifth test, (a) comb for feeding 10 yarns each with one inch distance, (b and c) resulted reinforcement.

Based on the results of this section, particularly the ones in Figures 4-53c, 4-55d and 4-56, it is concluded that continuous production of the reinforcement using a pilot paper machine is feasible. However, an in-depth study on the paper machine is still required to adjust its parameters and develop the desired reinforcement type. For example, the location of the frame on the machine table (with respect to the headbox), the effect of yarn size (tex), the influence of paper machine parameters (speed, pressure, temperature…), are all questions that need to be addressed in future works. If the parameter limits of the paper machine such as minimum speed or minimum paper surface density do not allow for acquiring favorable reinforcement, like the ones acquired in laboratory, then developing a specific production line for this reinforcement is suggested.

CHAPTER 5: CONCLUSIONS

In this thesis, a new natural fiber reinforcement for liquid composite molding processes has been characterized and optimized. It consists of a unidirectional layer of long flax yarns deposited on a layer of short Kraft fibers which mainly acts as the binder for the UD flax yarns.

Classical robust parameter design approach was the general road map according to which the experiments were conducted. Executing the experimental tests based on design of experiment tables as well as comparative study strategies, allowed for evaluating the effect of different reinforcement parameters. These include UD flax and paper layers surface densities (factors A and B, respectively), reinforcement's forming pressure and drying temperature (factors C and D, respectively), fiber volume fraction (factor E), yarn linear density (tex), as well as different reinforcement architectures. The characterization tests include, the shear cohesion test (IBS) measuring shear strength between reinforcement's paper and UD flax yarns, unsaturated permeability test, as well as tensile test of the resulted composites. Micrographs of samples cross sections and fracture surfaces were also used to support the analysis.

5.1. **Important achievements**

Classical robust parameter design is the matter of adjusting parameters settings of a material or a process such that standard deviations of the results are minimized while the sources of uncertainty still exist. Sources of deviation of the measured values could be classified in three categories: experimental uncertainty consisting of fabrication and measurement uncertainties, material uncertainty including inherent material properties variation as well as uncertainty due to material design parameters, and last but not least, human factors. One of the objectives of this work was to evaluate the effect of material design parameters on the standard deviation of the results. So, much care was taken to control other sources of uncertainties. In this regard, the following procedures were developed in this thesis.

5.1.1. Good control of the experiments

5.1.1.1. Laboratory scale fabrication of hybrid flax/paper reinforcement

Know-how of high quality fabrication of the reinforcement sample in the laboratory is developed and it has been always followed for fabrication of reinforcements to keep the consistency. This procedure is documented and explained in detail in appendix C, which allows to fabricate consistent reinforcements in any probable future work on this reinforcement.

5.1.1.2. New permeability measurement setup

A standard permeability mold and a reliable permeability measurement procedure were developed. This method can simplify the process of flow front measurement and improve the

reliability and repeatability of permeability results of radial injection method which are reported the main drawbacks of this method compared to the linear flow method [74, 75, 117].

5.1.1.3. Composite processing

An existing RTM mold was modified for enabling injection up to 4 bars. When combined with the molding technique described in section 3.7, good impregnation of the reinforcement and therefore consistent, quality composite plates could be obtained. As a result, favorably low standard deviation values were acquired in this work for the results of composite tensile tests

5.1.1.4. Conditioning of the samples

Since natural fibers are hydrophilic the atmosphere humidity could be considered as a noise factor for the reinforcement of this study. It is also reported in [100] that drying of fibers before processing is important for mechanical properties of composites. So, prior to permeability tests and composite molding, all of the reinforcements are dried at 103°C for at least 18 hours and stored in a desiccator to prevent absorbing humidity. IBS samples are all conditioned at relative humidity of 50 % and 23°C for more than 24 hours, according to the Canadian pulp and paper association D.34 standard

5.1.2. Modeling results

Table 5-1 summarizes the effect of each parameter on the measured properties. Explanation of these effects are given in the following subsections.

5.1.2.1. IBS

ANOVA analysis on IBS results based on 1st DOE showed that increase of paper layer surface density (A) and drying temperature (D) increase mean IBS, while increase of flax layer surface density (B) and forming pressure (C) make average IBS decrease. Although results of ANOVA on standard deviation of IBS were not conclusive, marginal average plot of coefficient of variance accompanied with experimental observation signal the effect of higher temperature in imparting consistency into the cohesion of paper and flax fibers

Table 5-1. Effect of material factors on the measured properties. ⇗ Indicates increase of propertiy with increase of factor level, ⇘ indicates decrease of property with increase of factor level, × indicates no statistical significance was found, N/A is for not applicable.

Factors	Response											
	Reinforcement								Composite			
	IBS(KPa)		K_1(×10^{-12} m^2)		K_2(×10^{-12} m^2)		σ_U (MPa)		E_1(GPa)		E_2(GPa)	
	Ave.	Std.	Ave.	Std.	Ave.	Std.	Ave.	Std.	Ave.	Std.	Ave.	Std.
A (g/m^3)	⇗	×	×	×	⇘	×	⇘	×	×	×	×	×
B (g/m^3)	⇘	×	⇘	⇘	⇗	×	⇗	×	⇗	×	⇗	×
C (bar)	⇘	×	×	×	⇗	×	×	×	×	×	×	×
D (°C)	⇗	⇘	×	×	⇘	×	⇗	×	×	×	×	×
E (%)	N/A	N/A	⇘	⇘	⇘	×	⇗	×	⇗	×	⇗	×

5.1.2.2. Permeability

Results of permeability measurement based on 1st DOE show that flax layer surface density (factor B), which is controlled by the average distance between UD yarns, is by far the most important factor on both mean and standard deviation of K_1 permeability, while all four parameters are found influential on the average K_2 permeability. The dominant effect of UD flax yarns in the K_1 direction is such that the K_1 permeability is one order of magnitude higher

than K_2. Factor B may have also concealed the influence of factors A, C and D on the K_1 permeability and so they have statistically been concluded insignificant (based on ANOVA).

On the other hand, the phenomena induced by varying other parameters than B have more impact on K_2 permeability and become statistically significant, due to having no predominant factor in K_2 direction. Permeability optimization based on 2nd DOE indicates that the design point of B= '24 yarns per inch' (flax layer surface density) and E = 35 % (fiber volume fraction) is the robust optimum point for K_1 permeability while the factors A, C and D were respectively set at −1, +1 and +1 level settings. The results also raise the effect of fiber volume fraction (factor E) on reducing standard deviation of K_1, for 20 and 24 yarns per inch reinforcements

5.1.2.3. Tensile properties

Results of tensile tests according to 1st DOE reveal that low paper areal density, high flax layer areal density and, again, high temperature levels help optimize the tensile strength. To a lesser extent tensile modulus E_1 and E_2 (before and after the knee point, respectively) are also optimized when using high flax layer areal density. While the reinforcement drying temperature is precisely controlled for the reinforcement fabrication of the 1st DOE, it has been found statistically influential on the surface expansion and consequently the areal density of the reinforcement, in addition to the strength of the composite. So, in the manufacturing process of this new reinforcement the drying temperature should be carefully controlled to avoid variations in composite mechanical properties which could occur through two mechanisms. First, through the areal density (m_r) which affects V_f, which in turn is the most influencing

parameter on the mechanical properties, and second, through the direct effect of temperature on composite ultimate strength (σ_U) found based on the results of 1st DOE

5.1.2.4. Effect of paper layer

The comparative studies of permeability and tensile performance of different reinforcements significantly highlight the effect of paper layer in reducing the standard deviation of K_1 permeability as well as composite tensile properties as compared to sole layer of UD flax. It is hypothesized base on these observations that paper layer introduces uniformity and homogeneity into the reinforcement and subsequently into permeability and composite behavior.

5.1.3. Robust parameter design results

To be able to implement the classical robust parameter design, the behavior of the parameters of material should fulfill some prerequisites. As is described in the algorithm of Figure 3-30, there should be at least one parameter affecting standard deviation of the result and another (or the same one) affecting the mean values of the response (dispersion and location factors). Moreover, the given parameter should have a quadratic relationship with the response mean value (step 12 of Figure 3-30). In addition the experimental methods should be consistent and of low noise.

For the K_1 permeability these prerequisites are fulfilled in terms of flax layer surface density (factor B) and fiber volume faction (factor E), so a robustness study is conducted for K_1

permeability in section 4.2.2. However, for tensile performance of composites the four studied parameters (factors A to D) did not show any statistical significance on standard deviation and their effect on varying the mean values were marginal from an engineering point of view. Although this later observation implies the importance of controlling the studied factor to impart consistency into the behavior of composites, the classical robust parameter design could not be conducted for tensile performance behavior of the eco-composites. It is also mentioned in [120, 121] that at the laminate scale the variability of flax fiber properties is covered by the 'averaging' effect in the composite laminate and that, scattering in composite results is more attributable to the uncertainties of manufacturing process.

IBS standard deviation results also did not show sensitivity to the parameters settings. It is probable that standard deviation of IBS results due to material parameter setting have been concealed by the high variability of measurement method. However from marginal average plots, the effect of drying temperature (factor D) on reducing coefficient of variance and increasing mean value was obvious. It was shown by the comparative study that IBS does not affect permeability values. Moreover, from microscopy images of composites cross-sections (for instance in Figure 4-38) one can notice that there is no direct bonding between paper and flax fibers in the final composite and paper-to-flax bonding in the dry reinforcement is replaced by paper-matrix and flax-matrix interfaces in the derived composites. So, it is also believed that IBS does not directly affect composite tensile performance results and so the paper layer is mainly the matter of keeping yarns' configuration stable and intact during manipulation and molding and consequently promotes results consistency.

5.1.4. Comparative study

Firstly, the results in this study represent a major improvement when compared to those published earlier on the same type of reinforcement. Strength of σ_u =173 MPa and modulus E_1= 12.7 GPa and E_2= 9.55 GPa were reported at V_f = 33.5 % for the flax paper reinforcement in the earlier work on this reinforcement [71]. Corresponding optimal values in this study represent 65 %, 89 % and 77 % improvements, respectively, at V_f=35 %.

Ultimate tensile strength σ_u = 318 MPa and tensile modulus E_1= 22.8GPa are reported for a UD flax/epoxy composites at V_f= 43 % [121]. Corresponding values from our own experiments at V_f= 45 %, are: σ_u = 325 MPa and E_1 = 27.5 GPa.

Specific modulus and strength of a UD E-glass/epoxy at V_f = 48 % are claimed 18 GPa/gcm^{-3} and 478 MPa/gcm^{-3} respectively [123]. Considering the experimentally measured composite density of 1.31 g/cm^3 using gas pycnometer, the corresponding values for the new flax/paper composite at V_f = 45 % are 21.2 GPa/gcm^{-3} and 250 MPa/gcm^{-3}, respectively. These results represent a 17 % improvement in specific stiffness accompanied with a 48 % decrease in specific strength.

Finally the obtained properties represent a 5 % decrease in specific stiffness and a 113 % increase in specific strength when compared to the commercial flax tape reported in [87], at same V_f of 35 %. Table 5-2 summarizes the above-mentioned comparisons between properties of flax/paper composites gained in this thesis with the other reported values.

With that in mind, the results of this thesis on the flax/paper reinforcement can be interpreted as follows. General principles of making a new flax/paper reinforcement (both in laboratory and pilot scale) are established. Internal bond strength and permeability of reinforcement as well as tensile behavior of its derived composite are well measured and characterized. Based on the results the reinforcement can be easily manipulated and fulfill the qualifications in terms of permeability and tensile mechanical properties, for industrial applications.

Table 5-2. Comparison of composite tensile properties of this work with literature.

Composite type	V_f (%)	σ_{xU} (MPa)	E_1 (GPa)	E_2 (GPa)	Specific strength (MPa/gcm^{-3})	Specific modulus of E_1 (GPa/gcm^{-3})
UD flax/ paper/epoxy	35	285±3.25	24.0±1.16	16.9±0.53	218	18.3
UD flax/ paper/epoxy	40	297±3.4	25.5±0.7	17.3±0.33	232	19.9
UD flax/ paper/epoxy	45	325±4.8	27.5±0.8	18.7±0.41	250	21.2
UD flax/ paper/epoxy [71]	33.5	173 ±8.3	12.7±0.8	9.55±0.4	140[a]	10.3[a]
UD flax/epoxy [121]	43	318±12	22.8±1.0	-	248[a]	17.8[a]
UD E-glass/epoxy [123]	48	817±35	31±1.0	-	478	18
UD flax tape/ Acrodur [87]	35	96.0±11	18±1	-	103	19.4

a- This value is not given in the reference but is approximated here using the composite density and the ROM.

5.1.5. Other achievements

5.1.5.1. New method for measuring IBS

A method for measuring IBS is developed for this work and the results are presented in terms of shear strength. The method is adapted from the shear cohesion test which is one of

the methods used in the paper industry to measure bonding ability of duplex paper and paperboards through applying shear stress. Tests are conducted on a precise Instron machine calibrated based on requirements of D.34 standard of Canadian pulp and paper association, which is originally used to measure the tensile strength of paper products.

Coefficients of variance (C_V) of the results are rather high, probably due to fragile Van der Waals bonds between paper and flax fibers and/or small overlap area (25 mm × 25 mm) considered for the shearing region. However, high variability is also reported for the results of paper products [99] .

5.1.5.2. High volume production using a pilot paper machine

For the first time, in this thesis, flax yarns are fed to a pilot scale paper machine and at the end of the machine reinforced paper with unidirectional flax yarns are acquired. This proves the feasibility of continuous production of the reinforcement with a paper machine. However, results presented here are preliminary ones and still more in-depth study is required to characterize and optimize production of reinforcement on a paper machine in order to produce qualified reinforcements.

5.2. **Future work**

On the grounds of the results and observations of this work, a number of subjects are proposed for future works:

- Considering that composites of this study are molded with epoxy resin which is petroleum based resin, it is suggested to use a bio-based resin to develop 'green'

composites. Considering that the present composite molded with epoxy has shown interesting properties, the bio-based resin should also possess similar mechanical properties to epoxy.

- Once such a biodegradable composite is developed it should be characterized and optimized from different point of view. Some of these could be TGA, DSC and DMA for behavior of material with temperature as well as analysis of flammability, fatigue analysis both in tension and bending modes with the characterization of the different fracture mechanisms involved, impact strength, and static mechanical analysis like tensile, compression, bending and shear testing.

- Considering that paper layer interface with epoxy resin was concluded a weak point in the flax/paper composites, performing chemical treatment on Kraft paper fibers (and also probably in flax yarns) to improve the quality of the interface with the employed resin could have significant effect on performance of the composites.

- Considering that in the 'impregnation quality' section, large area of capillary dominated area was found for 24 yarns/in. reinforcements. It would be of interest to characterize the molding of this reinforcement for finding optimum flow velocity for having minimum void content. In this regard measuring and characterizing capillary pressure of reinforcement for different directions and stacking sequences could be also useful for deciding on injection pressure as well as evaluating its effect on the calculated permeabilities.

- Studying and optimizing parameters of paper machine for producing consistent flax/paper reinforcement in mass scale, and if the limitation of paper machine does not allow to reach such a goal, then developing a production line for this purpose. Such a development paves the way for industrial implementation of the reinforcement.

- Considering that a Matlab® code is prepared in this thesis to ease calculating dimensions of elliptical flow fronts, while many preliminary manipulation should be done on the captured photos to make them ready to be introduced to the code. A software could be developed based on code A to automate the overall permeability calculation process. Which allows for introducing the captured photos to the software and then having the K_1 and K_2 permeabilities as output. The feasibility of this project however should be discussed with a software engineer.

- Characterizing engineering constants of this composite material (E_1, E_2, E_3, G_{12}, G_{23}, G_{13}, v_{12}, v_{23}, v_{13}) and then developing a finite element model to simulate these characteristics. This model could be used in designing and simulating industrial structures out of this material.

- Studying, characterizing and optimizing the reinforcement for molding into complex geometrical shapes is necessary for industrial implementation of this reinforcement. The molding could be either through preparing a preform and impregnating with a thermoset resin or using hot stamping with a thermoplastic resin.

Reference

[1] Madsen B. Properties of Plant Fibre Yarn Polymer Composites, Technical University of Denmark, PhD Thesis, 2004.

[2] Biagiotti J, Puglia D, Kenny JM. A Review on Natural Fibre-Based Composites-Part I. Journal of Natural Fibers. 2004;1:37-68.

[3] Bos HL. The Potential of Flax Fibres as Reinforcement for Composite Materials, Eindhoven University of Technology, PhD Thesis, 2004.

[4] Gianluca Cicala GC, Giuseppe Recca, and Alberta Latteri (2010). Composites Based on Natural Fibre Fabrics, Woven Fabric Engineering, Polona Dobnik Dubrovski (Ed.), ISBN: 978-953-307-194-7, InTech.

[5] Mike, Brady P. Automotive composites – the search for efficiency, value and performance. Reinforced Plastics. 2007;51:26-9.

[6] Stewart R. Automotive composites offer lighter solutions. Reinforced Plastics. 2010;54:22-8.

[7] Birat KC, Panthapulakkal S, Kronka A, Agnelli JAM, Tjong J, Sain M. Hybrid biocomposites with enhanced thermal and mechanical properties for structural applications. Journal of Applied Polymer Science. 2015;132:n/a-n/a.

[8] Stewart R. Lightweighting the automotive market. Reinforced Plastics. 2009;53:14-21.

[9] Holbery J, Houston D. Natural-fiber-reinforced polymer composites in automotive applications. JOM.58:80-6.

[10] Mike, Brady P. Technology developments in automotive composites. Reinforced Plastics. 2010;54:25-9.

[11] Hughes M, Carpenter J, Hill C. Deformation and fracture behaviour of flax fibre reinforced thermosetting polymer matrix composites. Journal of Materials Science. 2007;42:2499-511.

[12] Shah D. Developing plant fibre composites for structural applications by optimising composite parameters: a critical review. Journal of Materials Science. 2013;48:6083-107.

[13] Dittenber DB, GangaRao HVS. Critical review of recent publications on use of natural composites in infrastructure. Composites Part A: Applied Science and Manufacturing. 2012;43:1419-29.

[14] Summerscales J, Dissanayake NPJ, Virk AS, Hall W. A review of bast fibres and their composites. Part 1 - Fibres as reinforcements. Composites Part A: Applied Science and Manufacturing. 2010;41:1329-35.

[15] Madsen B, Gamstedt EK. Wood versus Plant Fibers: Similarities and Differences in Composite Applications. Advances in Materials Science and Engineering. 2013;2013:14.

[16] Opportunities in Natural Fiber Composites. Available at : http://www.lucintel.com/lucintelbrief/potentialofnaturalfibercomposites-final.pdf, Lucintel Brief (March 2011).

[17] Koronis G, Silva A, Fontul M. Green composites: A review of adequate materials for automotive applications. Composites Part B: Engineering. 2013;44:120-7.

[18] Ashori A. Wood–plastic composites as promising green-composites for automotive industries! Bioresource Technology. 2008;99:4661-7.

[19] Stamboulis A, Baillie CA, Peijs T. Effects of environmental conditions on mechanical and physical properties of flax fibers. Composites - Part A: Applied Science and Manufacturing. 2001;32:1105-15.

[20] Bodros E, Pillin I, Montrelay N, Baley C. Could biopolymers reinforced by randomly scattered flax fibre be used in structural applications? Composites Science and Technology. 2007;67:462-70.

[21] Low IM, McGrath M, Lawrence D, Schmidt P, Lane J, Latella BA, et al. Mechanical and fracture properties of cellulose-fibre-reinforced epoxy laminates. Composites Part A: Applied Science and Manufacturing. 2007;38:963-74.

[22] Ku H, Wang H, Pattarachaiyakoop N, Trada M. A review on the tensile properties of natural fiber reinforced polymer composites. Composites Part B: Engineering. 2011;42:856-73.

[23] Alamri H, Low IM. Mechanical properties and water absorption behaviour of recycled cellulose fibre reinforced epoxy composites. Polymer Testing. 2012;31:620-8.

[24] Bensadoun F, Vallons KAM, Lessard LB, Verpoest I, Van Vuure AW. Fatigue behaviour assessment of flax–epoxy composites. Composites Part A: Applied Science and Manufacturing. 2016;82:253-66.

[25] Le Duigou A, Bourmaud A, Gourier C, Baley C. Multi-scale shear properties of flax fibre reinforced polyamide 11 biocomposites. Composites Part A: Applied Science and Manufacturing. 2016;85:123-9.

[26] Muthuraj R, Misra M, Defersha F, Mohanty AK. Influence of processing parameters on the impact strength of biocomposites: A statistical approach. Composites Part A: Applied Science and Manufacturing. 2016;83:120-9.

[27] Shah DU. Damage in biocomposites: Stiffness evolution of aligned plant fibre composites during monotonic and cyclic fatigue loading. Composites Part A: Applied Science and Manufacturing. 2016;83:160-8.

[28] Le Duigou A, Davies P, Baley C. Interfacial bonding of Flax fibre/Poly(l-lactide) bio-composites. Composites Science and Technology. 2010;70:231-9.

[29] Le Duigou A, Davies P, Baley C. Macroscopic analysis of interfacial properties of flax/PLLA biocomposites. Composites Science and Technology. 2010;70:1612-20.

[30] Le Duigou A, Baley C, Grohens Y, Davies P, Cognard J-Y, Créach'cadec R, et al. A multi-scale study of the interface between natural fibres and a biopolymer. Composites Part A: Applied Science and Manufacturing. 2014;65:161-8.

[31] Le Duigou A, Kervoelen A, Le Grand A, Nardin M, Baley C. Interfacial properties of flax fibre–epoxy resin systems: Existence of a complex interphase. Composites Science and Technology. 2014;100:152-7.

[32] Marrot L, Bourmaud A, Bono P, Baley C. Multi-scale study of the adhesion between flax fibers and biobased thermoset matrices. Materials & Design. 2014;62:47-56.

[33] Madsen B, Lilholt H. Physical and mechanical properties of unidirectional plant fibre composites-an evaluation of the influence of porosity. Composites Science and Technology. 2003;63:1265-72.

[34] Madsen B, Hoffmeyer P, Lilholt H. Hemp yarn reinforced composites - II. Tensile properties. Composites Part A: Applied Science and Manufacturing. 2007;38:2204-15.

[35] Reyes-Araiza JL, Manzano-Ramírez A, Rubio-Avalos JC, González-Sosa E, Pérez-Robles JF, Arroyo-Contreras M, et al. Comparative study on tensile behavior of inorganic fibers embedded in unsaturated polyester bisphenol "A"-styrene copolymer. Inorganic Materials. 2008;44:549-54.

[36] Rijsdijk HA, Contant M, Peijs AAJM. Continuous-glass-fibre-reinforced polypropylene composites: I. Influence of maleic-anhydride-modified polypropylene on mechanical properties. Composites Science and Technology. 1993;48:161-72.

[37] Fu SY, Lauke B, Mäder E, Yue CY, Hu X. Tensile properties of short-glass-fiber- and short-carbon-fiber-reinforced polypropylene composites. Composites Part A: Applied Science and Manufacturing. 2000;31:1117-25.

[38] Mohanty AK, Misra M, Hinrichsen G. Biofibres, biodegradable polymers and biocomposites: An overview. Macromolecular Materials and Engineering. 2000;276-277:1-24.

[39] Montgomery DC. Design and analysis of experiments. Seventh ed: Wiley, 2009.

[40] Taguchi G, Phadke MS. Quantity engineering through design optimization. pt 1 ed1986. p. 32-9.

[41] Zang C, Friswell MI, Mottershead JE. A review of robust optimal design and its application in dynamics. Computers and Structures. 2005;83:315-26.

[42] Gassan J, Chate A, Bledzki AK. Calculation of elastic properties of natural fibers. Journal of Materials Science. 2001;36:3715-20.

[43] Bos HL, Van Den Oever MJA, Peters OCJJ. Tensile and compressive properties of flax fibres for natural fibre reinforced composites. Journal of Materials Science. 2002;37:1683-92.

[44] Baley C. Analysis of the flax fibres tensile behaviour and analysis of the tensile stiffness increase. Composites - Part A: Applied Science and Manufacturing. 2002;33:939-48.

[45] Charlet K, Jernot JP, Gomina M, Bréard J, Morvan C, Baley C. Influence of an Agatha flax fibre location in a stem on its mechanical, chemical and morphological properties. Composites Science and Technology. 2009;69:1399-403.

[46] Symington MC, Banks WM, West OD, Pethrick RA. Tensile Testing of Cellulose Based Natural Fibers for Structural Composite Applications. Journal of Composite Materials. 2009;43:1083-108.

[47] Goutianos S, Peijs T. The optimisation of flax fibre yarns for the development of high-performance natural fibre composites. Advanced Composites Letters. 2003;12:237-41.

[48] Madsen B, Hoffmeyer P, Thomsen AB, Lilholt H. Hemp yarn reinforced composites - I. Yarn characteristics. Composites Part A: Applied Science and Manufacturing. 2007;38:2194-203.

[49] Shah DU, Schubel PJ, Clifford MJ. Modelling the effect of yarn twist on the tensile strength of unidirectional plant fibre yarn composites. Journal of Composite Materials. 2013;47:425-36.

[50] Michell AJ, Vaughan JE, Willis D. Wood fiber-synthetic polymer composites - 1. laminates of paper and polyethylene. J Polym Sci Polym Symp. 1975:143-54.

[51] Michell AJ, Vaughan JE, Willis D. Wood fiber–synthetic polymer composites. II. Laminates of treated fibers and polyolefins. Journal of Applied Polymer Science. 1978;22:2047-61.

[52] Bullions TA, Hoffman D, Gillespie RA, Price-O'Brien J, Loos AC. Contributions of feather fibers and various cellulose fibers to the mechanical properties of polypropylene matrix composites. Composites Science and Technology. 2006;66:102-14.

[53] Nordin LO, Varna J. Nonlinear viscoelastic behavior of paper fiber composites. Composites Science and Technology. 2005;65:1609-25.

[54] Nordin LO, Varna J. Nonlinear viscoplastic and nonlinear viscoelastic material model for paper fiber composites in compression. Composites Part A: Applied Science and Manufacturing. 2006;37:344-55.

[55] Adams KL, Russel WB, Rebenfeld L. Radial penetration of a viscous liquid into a planar anisotropic porous medium. International Journal of Multiphase Flow. 1988;14:203-15.

[56] Chan AW, Hwang S-T. Anisotropic in-plane permeability of fabric media. Polymer Engineering & Science. 1991;31:1233-9.

[57] Griffin PR, Grove SM, Russell P, Short D, Summerscales J, Guild FJ, et al. The effect of reinforcement architecture on the long-range flow in fibrous reinforcements. Composites Manufacturing. 1995;6:221-35.

[58] Weitzenböck JR, Shenoi RA, Wilson PA. Radial flow permeability measurement. Part A: Theory. Composites Part A: Applied Science and Manufacturing. 1999;30:781-96.

[59] Weitzenböck JR, Shenoi RA, Wilson PA. Radial flow permeability measurement. Part B: Application. Composites Part A: Applied Science and Manufacturing. 1999;30:797-813.

[60] Hoes K, Dinescu D, Sol H, Vanheule M, Parnas RS, Luo Y, et al. New set-up for measurement of permeability properties of fibrous reinforcements for RTM. Composites - Part A: Applied Science and Manufacturing. 2002;33:959-69.

[61] Endruweit A, Ermanni P. The in-plane permeability of sheared textiles. Experimental observations and a predictive conversion model. Composites Part A: Applied Science and Manufacturing. 2004;35:439-51.

[62] Endruweit A, Long AC, Robitaille F, Rudd CD. Influence of stochastic fibre angle variations on the permeability of bi-directional textile fabrics. Composites Part A: Applied Science and Manufacturing. 2006;37:122-32.

[63] Endruweit A, Long AC. Influence of stochastic variations in the fibre spacing on the permeability of bi-directional textile fabrics. Composites Part A: Applied Science and Manufacturing. 2006;37:679-94.

[64] Sharma S, Siginer DA. Permeability Measurement Methods in Porous Media of Fiber Reinforced Composites. Applied Mechanics Reviews. 2010;63:020802-.

[65] Pan R, Liang Z, Zhang C, Wang B. Statistical characterization of fiber permeability for composite manufacturing. Polymer Composites. 2000;21:996-1006.

[66] Umer R, Bickerton S, Fernyhough A. Characterising wood fibre mats as reinforcements for liquid composite moulding processes. Composites Part A: Applied Science and Manufacturing. 2007;38:434-48.

[67] Umer R, Bickerton S, Fernyhough A. The effect of yarn length and diameter on permeability and compaction response of flax fibre mats. Composites Part A: Applied Science and Manufacturing. 2011;42:723-32.

[68] Mekic S, Ulven CA, Akhatov IS, Jerke E, Kerr-Anderson E. Evalutation of in-plane and transverse permeability of flax fiber preforms for biocomposite materials. Journal of Biobased Materials and Bioenergy. 2009;3:156-64.

[69] Francucci G, Rodríguez ES, Vázquez A. Study of saturated and unsaturated permeability in natural fiber fabrics. Composites Part A: Applied Science and Manufacturing. 2010;41:16-21.

[70] Rodríguez E, Giacomelli F, Vazquez A. Permeability-porosity relationship in RTM for different fiberglass and natural reinforcements. Journal of Composite Materials. 2004;38:259-68.

[71] Lebrun G, Couture A, Laperrière L. Tensile and impregnation behavior of unidirectional hemp/paper/epoxy and flax/paper/epoxy composites. Composite Structures. 2013;103:151-60.

[72] Nguyen V, Lagardère M, Park C, Panier S. Permeability of natural fiber reinforcement for liquid composite molding processes. Journal of Materials Science. 2014;49:6449-58.

[73] Nguyen VH, Deléglise-Lagardère M, Park CH. Modeling of resin flow in natural fiber reinforcement for liquid composite molding processes. Composites Science and Technology. 2015;113:38-45.

[74] Arbter R, Beraud JM, Binetruy C, Bizet L, Bréard J, Comas-Cardona S, et al. Experimental determination of the permeability of textiles: A benchmark exercise. Composites Part A: Applied Science and Manufacturing. 2011;42:1157-68.

[75] Vernet N, Ruiz E, Advani S, Alms JB, Aubert M, Barburski M, et al. Experimental determination of the permeability of engineering textiles: Benchmark II. Composites Part A: Applied Science and Manufacturing. 2014;61:172-84.

[76] Alms J, Correia N, Advani S, Ruiz E. Experimental procedures to run longitudinal injections to measure unsaturated permeability of LCM reinforcements. Available at: http://cchp.meca.polymtl.ca/fichiers/permeabilityBenchmarkII/PermBenchmark_letter.pdf, FPCM Collaboration (2010).

[77] Shah DU, Schubel PJ, Clifford MJ. Can flax replace E-glass in structural composites? A small wind turbine blade case study. Composites Part B: Engineering. 2013;52:172-81.

[78] Fuqua MA, Huo S, Ulven CA. Natural fiber reinforced composites. Polymer Reviews. 2012;52:259-320.

[79] John MJ, Thomas S. Biofibres and biocomposites. Carbohydrate Polymers. 2008;71:343-64.

[80] Slade J, Pillai KM, Advani SG. Investigation of unsaturated flow in woven, braided and stitched fiber mats during mold-filling in resin transfer molding. Polymer Composites. 2001;22:491-505.

[81] Goutianos S, Peijs T, Nystrom B, Skrifvars M. Development of Flax Fibre based Textile Reinforcements for Composite Applications. Applied Composite Materials. 2006;13:199-215.

[82] Gassan J. A study of fibre and interface parameters affecting the fatigue behaviour of natural fibre composites. Composites Part A: Applied Science and Manufacturing. 2002;33:369-74.

[83] Pothan LA, Mai YW, Thomas S, Li RKY. Tensile and flexural behavior of sisal fabric/polyester textile composites prepared by resin transfer molding technique. Journal of Reinforced Plastics and Composites. 2008;27:1847-66.

[84] Miao M, Shan M. Highly aligned flax/polypropylene nonwoven preforms for thermoplastic composites. Composites Science and Technology. 2011;71:1713-8.

[85] Muralidhar BA. Study of flax hybrid preforms reinforced epoxy composites. Materials & Design. 2013;52:835-40.

[86] Xue D, Hu H. Mechanical properties of biaxial weft-knitted flax composites. Materials and Design. 2013;46:264-9.

[87] Khalfallah M, Abbès B, Abbès F, Guo YQ, Marcel V, Duval A, et al. Innovative flax tapes reinforced Acrodur biocomposites: A new alternative for automotive applications. Materials & Design. 2014;64:116-26.

[88] Stuart M. An Introduction to Statistical Analysis for Business and Industry: A Problem Solving Approach: Wiley, 2003.

[89] Wakeman MD, Cain TA, Rudd CD, Brooks R, Long AC. Compression moulding of glass and polypropylene composites for optimised macro- and micro- mechanical properties - 1 commingled glass and polypropylene. Composites Science and Technology. 1998;58:1879-98.

[90] Milani AS, Wang H, Frey DD, Abeyaratne RC. Evaluating three DOE methodologies: Optimization of a composite laminate under fabrication error. Quality Engineering. 2009;21:96-110.

[91] Yoon SY, Park CK, Kim HS, Kim S. Optimization of fusing process conditions using the Taguchi method. Textile Research Journal. 2010;80:1016-26.

[92] Summerscales J, Virk A, Hall W. A review of bast fibres and their composites: Part 3 - Modelling. Composites Part A: Applied Science and Manufacturing. 2013;44:132-9.

[93] Aly M, Hashmi MSJ, Olabi AG, Benyounis KY, Messeiry M, Hussain AI, et al. Optimization of Alkaline Treatment Conditions of Flax Fiber Using Box-Behnken Method. Journal of Natural Fibers. 2012;9:256-76.

[94] Peponi L, Biagiotti J, Torre L, Kenny JM, Mondragòn I. Statistical analysis of the mechanical properties of natural fibers and their composite materials. I. Natural fibers. Polymer Composites. 2008;29:313-20.

[95] Peponi L, Biagiotti J, Kenny JM, Mondragòn I. Statistical analysis of the mechanical properties of natural fibers and their composite materials. II. Composite materials. Polymer Composites. 2008;29:321-5.

[96] Wambua P, Ivens J, Verpoest I. Natural fibres: can they replace glass in fibre reinforced plastics? Composites Science and Technology. 2003;63:1259-64.

[97] CELC. Flax and hemp fibers. A natural solution for the composite industry: JEC Composites, 2012.

[98] Trepanier RJ. Dynamic forming : Parameters for making oriented sheets in the laboratory. Pulp & Paper Canada. 1989;90:45-8.

[99] Koubaa A, Koran Z. Measure of the internal bond strength of paper/board. Tappi Journal. 1995;78:103-11.

[100] Bledzki AK, Gassan J. Composites reinforced with cellulose based fibres. Progress in Polymer Science (Oxford). 1999;24:221-74.

[101] Brahim SB, Cheikh RB. Influence of fibre orientation and volume fraction on the tensile properties of unidirectional Alfa-polyester composite. Composites Science and Technology. 2007;67:140-7.

[102] Oksman K, Mathew AP, Bismarck A, Rojas O, Sain M. Handbook of green materials, Vol.4 Biobased composite materials, their processing properties and industrial applications. : World Scientific, 2014.

[103] Hoa S. Principles of the Manufacturing of Composite Materials Destech Publications, 2009.

[104] Shah DU, Schubel PJ, Licence P, Clifford MJ. Determining the minimum, critical and maximum fibre content for twisted yarn reinforced plant fibre composites. Composites Science and Technology. 2012;72:1909-17.

[105] Kellogg R, Wangaard F. Variation in The Cell-Wall Density of Wood. Wood and Fiber Science. 1969;1:180-204.

[106] Chen W, Allen JK, Tsui KL, Mistree F. A procedure for robust design: Minimizing variations caused by noise factors and control factors. Journal of Mechanical Design, Transactions of the ASME. 1996;118:478-85.

[107] Schmidt SR, Launsby RG. Understanding Industrial Designed Experiments: Air Academy Press, 1989.

[108] Zhai Q, Zhao S, Zhou C, Li W, Peng C. Determination of the Si□H content of hydrogen silicone oil by a combination of the fourier transform near infrared, attenuated total reflectance–fourier transform infrared, and partial least squares regression models. Journal of Applied Polymer Science. 2014;131:n/a-n/a.

[109] Front Matter. In: Noll W, editor. Chemistry and Technology of Silicones: Academic Press; 1968. p. iii.

[110] Kim CH, Joo C-K, Chun HJ, Yoo BR, Noh DI, Shim YB. Instrumental studies on silicone oil adsorption to the surface of intraocular lenses. Applied Surface Science. 2012;262:146-52.

[111] Kim SH, Cherney EA, Hackam R. Suppression mechanism of leakage current on RTV coated porcelain and silicone rubber insulators. Power Delivery, IEEE Transactions on. 1991;6:1549-56.

[112] El Boustani M, Brouillette F, Lebrun G, Belfkira A. Solvent-free acetylation of lignocellulosic fibers at room temperature: Effect on fiber structure and surface properties. Journal of Applied Polymer Science. 2015:n/a-n/a.

[113] Peel JD. Paper Science and Paper Manufacture: Angus Wilde Publications Inc., 1994.

[114] Scott WE, Abbott JC, Trosset S. Properties of paper: an introduction: TAPPI Press, 1995.

[115] Leclerc JS, Ruiz E. Porosity reduction using optimized flow velocity in Resin Transfer Molding. Composites Part A: Applied Science and Manufacturing. 2008;39:1859-68.

[116] Rohatgi V, Patel N, James Lee L. Experimental investigation of flow-induced microvoids during impregnation of unidirectional stitched fiberglass mat. Polymer Composites. 1996;17:161-70.

[117] Amico S, Lekakou C. An experimental study of the permeability and capillary pressure in resin-transfer moulding. Composites Science and Technology. 2001;61:1945-59.

[118] Francucci G, Vázquez A, Ruiz E, Rodríguez ES. Capillary effects in vacuum-assisted resin transfer molding with natural fibers. Polymer Composites. 2012;33:1593-602.

[119] Vishtal A, Hauptmann M, Zelm R, Majschak J-P, Retulainen E. 3D Forming of Paperboard: The Influence of Paperboard Properties on Formability. Packaging Technology and Science. 2014;27:677-91.

[120] Blanchard JMFA, Sobey AJ, Blake JIR. Multi-scale investigation into the mechanical behaviour of flax in yarn, cloth and laminate form. Composites Part B: Engineering. 2016;84:228-35.

[121] Liang S, Gning PB, Guillaumat L. Quasi-static behaviour and damage assessment of flax/epoxy composites. Materials and Design. 2015;67:344-53.

[122] Aslan M, Mehmood S, Madsen B. Effect of consolidation pressure on volumetric composition and stiffness of unidirectional flax fibre composites. Journal of Materials Science. 2013;48:3812-24.

[123] Oksman K. High Quality Flax Fibre Composites Manufactured by the Resin Transfer Moulding Process. Journal of Reinforced Plastics and Composites. 2001;20:621-7.

APPENDIX A. Cause-and-effect diagrams for global development of the new hybrid flax/paper reinforcement

A.1 *Constituents sub-phase*

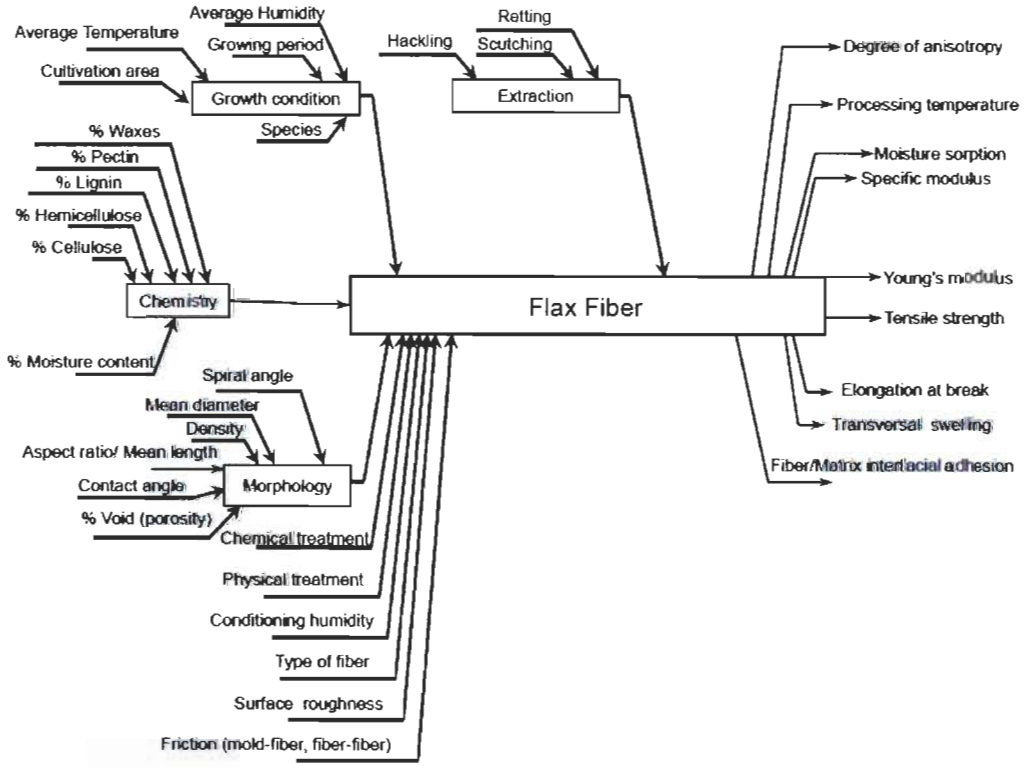

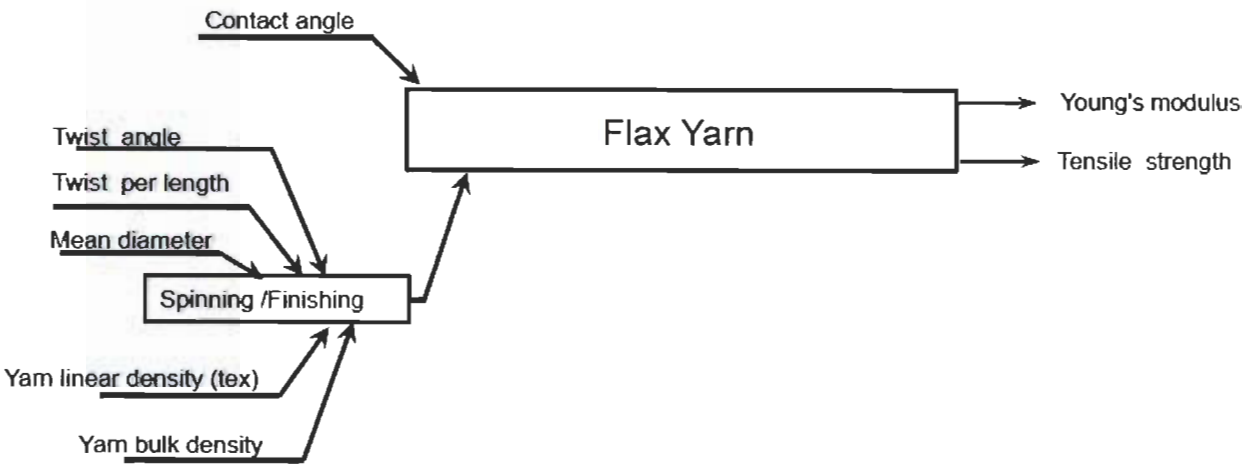

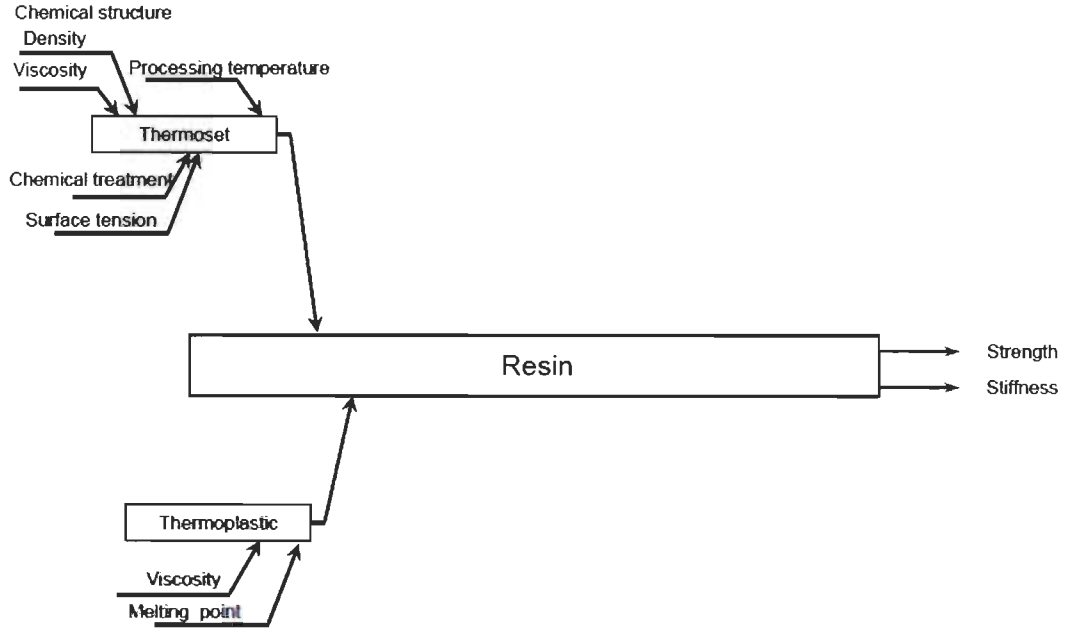
Chemical structure
Density
Viscosity
Processing temperature
Thermoset
Chemical treatment
Surface tension
Resin
Strength
Stiffness
Thermoplastic
Viscosity
Melting point

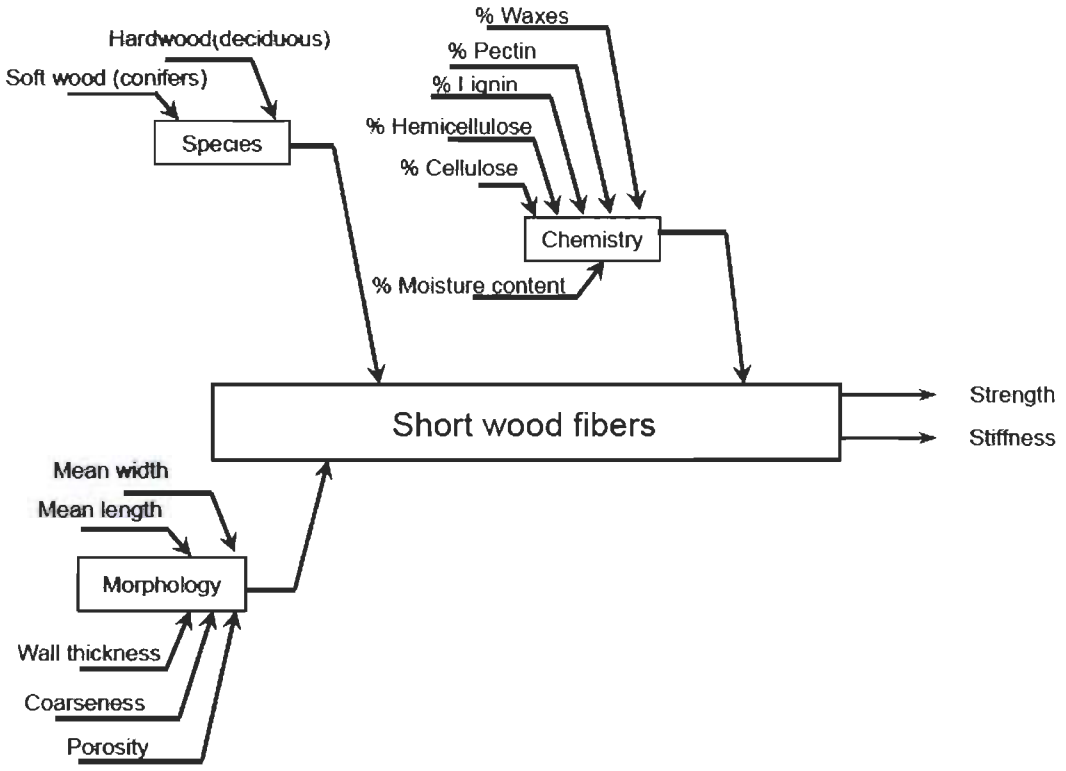
Hardwood(deciduous)
Soft wood (conifers)
Species
% Waxes
% Pectin
% Lignin
% Hemicellulose
% Cellulose
Chemistry
% Moisture content
Short wood fibers
Strength
Stiffness
Mean width
Mean length
Morphology
Wall thickness
Coarseness
Porosity

A.2 *Reinforcement sub-phase*

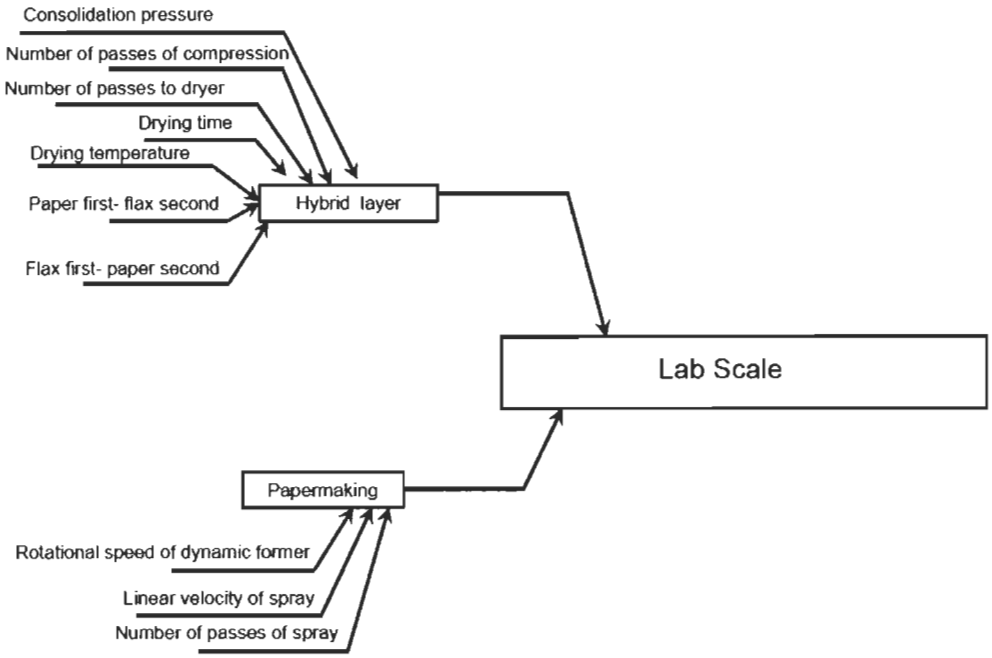

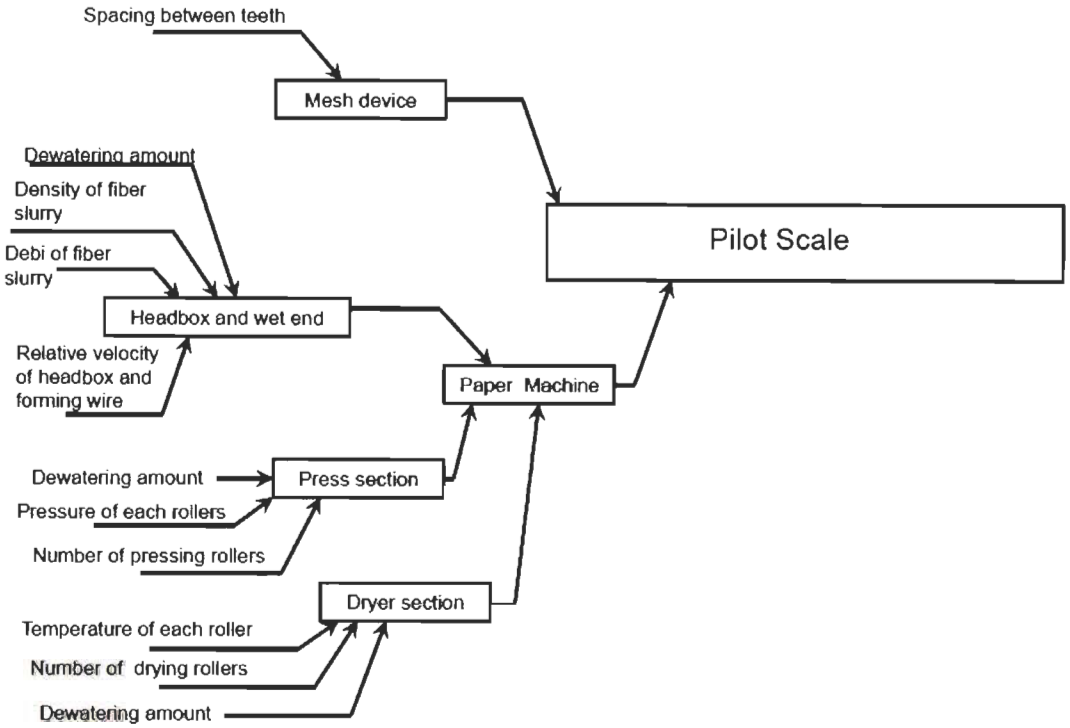
Spacing between teeth
Mesh device
Pilot Scale
Dewatering amount
Density of fiber slurry
Debi of fiber slurry
Headbox and wet end
Relative velocity of headbox and forming wire
Paper Machine
Dewatering amount
Press section
Pressure of each rollers
Number of pressing rollers
Dryer section
Temperature of each roller
Number of drying rollers
Dewatering amount

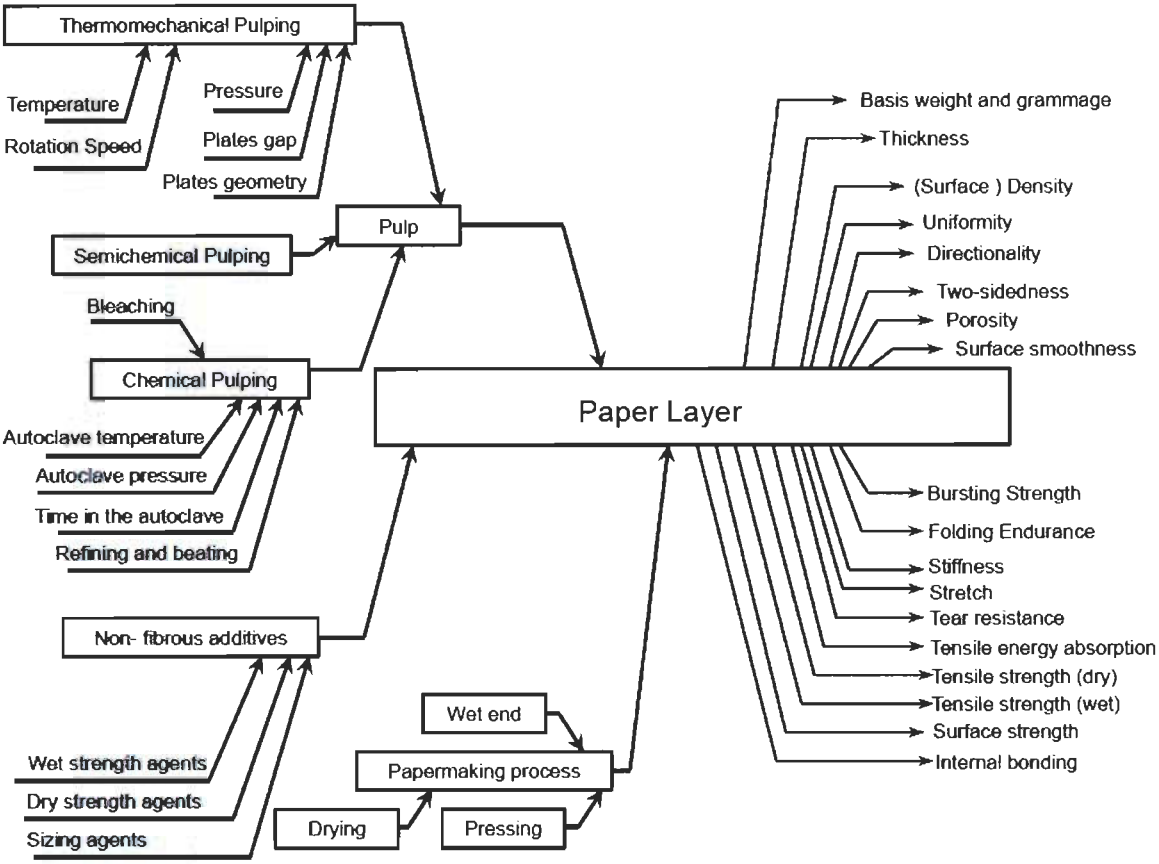
Thermomechanical Pulping
Temperature
Rotation Speed
Pressure
Plates gap
Plates geometry
Pulp
Semichemical Pulping
Bleaching
Chemical Pulping
Autoclave temperature
Autoclave pressure
Time in the autoclave
Refining and beating
Non- fibrous additives
Wet strength agents
Dry strength agents
Sizing agents
Wet end
Papermaking process
Drying
Pressing
Paper Layer
Basis weight and grammage
Thickness
(Surface) Density
Uniformity
Directionality
Two-sidedness
Porosity
Surface smoothness
Bursting Strength
Folding Endurance
Stiffness
Stretch
Tear resistance
Tensile energy absorption
Tensile strength (dry)
Tensile strength (wet)
Surface strength
Internal bonding

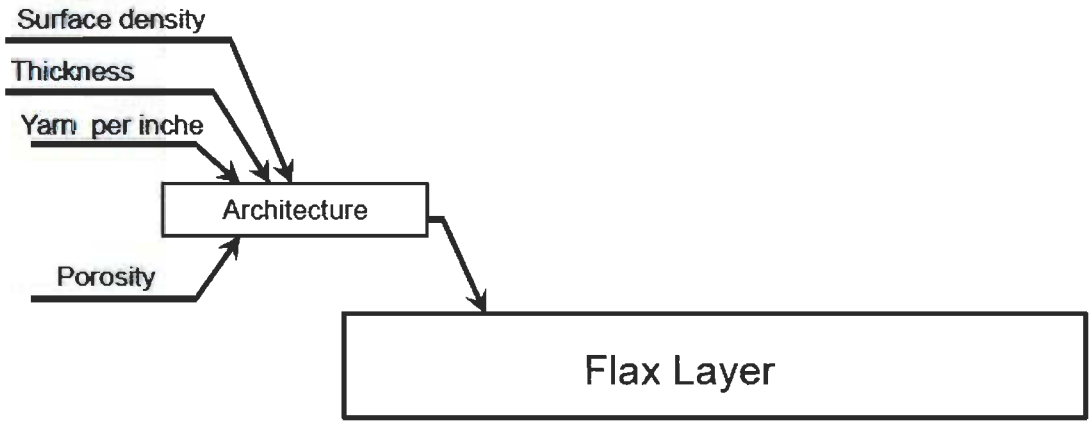
Surface density
Thickness
Yarn per inche
Architecture
Porosity
Flax Layer

A.3 *Flat composite sub-phase*

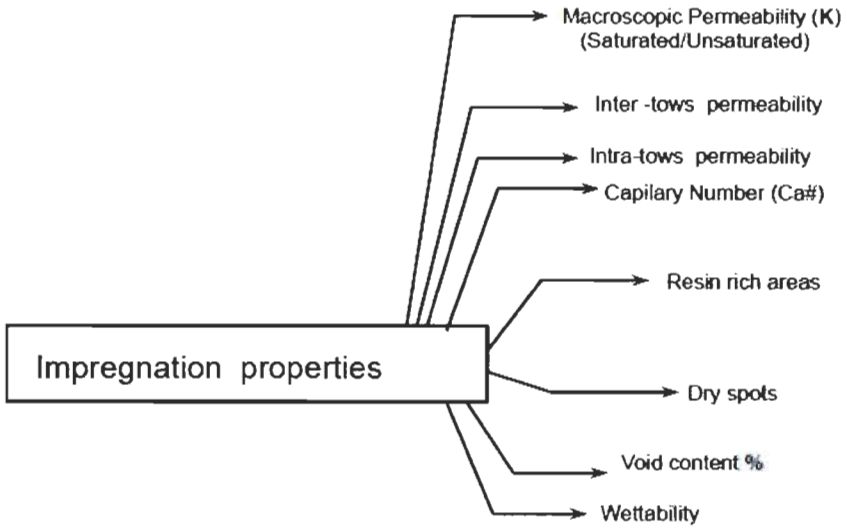

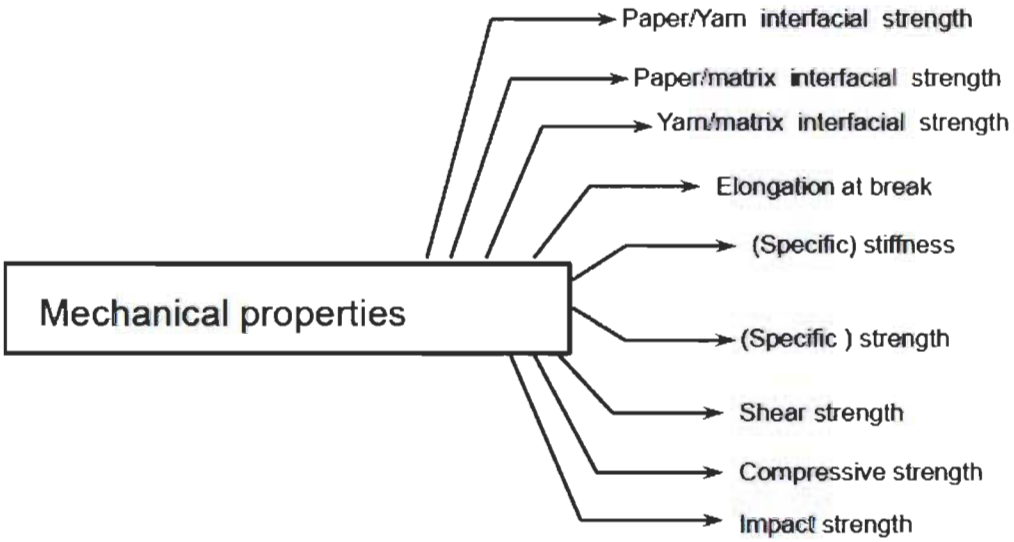

A.4 *Molding sub-phase*

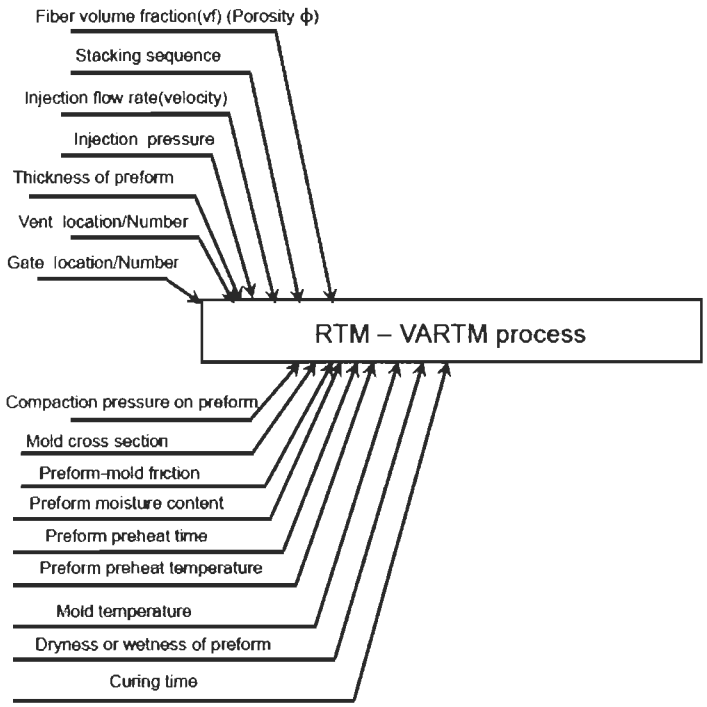

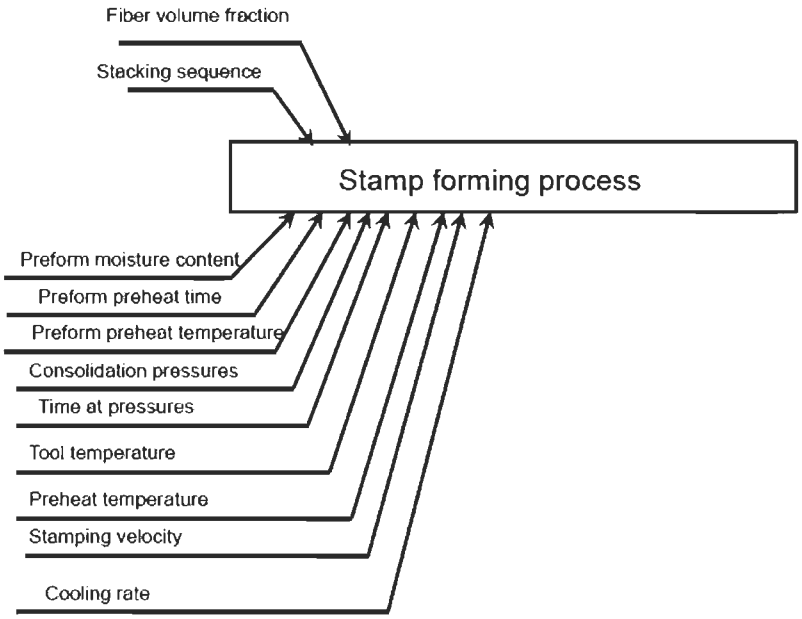

APPENDIX B. Specifications of the softwood kraft pulp

Table B 1. Properties of 100 % softwood kraft pulp used in this study.

	Beating time (min.)		**0**	**15**	**45**	**60**	**75**	**90**
Pulp Properties	Freeness, CSF (mL)		702	607	454	354	251	157
	Fibers length, (mm) (using Fiber Quality Analyzer)	Arithmetic mean	1.19	1.19	1.21	1.13	1.08	1.08
		Weighted mean	2.34	2.39	2.42	2.38	2.28	2.28
	Fines (using Fiber Quality Analyzer) (0,00..0,20 mm) (%)	Arithmetic	33.12	33.06	30.68	32.68	33.94	32.77
		Weighted	3.17	3.15	2.92	3.36	3.65	3.49
	Grammage (g/m^2)		62.1	59.7	59.8	59.0	59.5	61.1
	Dryness (%)		92.3	92.3	92.1	92.1	92.1	92.4
	Bulk (cm^3/g)		1.99	1.70	1.55	1.53	1.50	1.46
Handsheet properties	Thickness(µm)		123.7	101.4	93.0	90.3	89.3	89.3
	Tear index ($mN*m^2/g$)		19.25	17.79	11.64	11.55	11.16	10.83
	Burst index($kPa*m^2/g$)		1.70	5.99	8.81	9.28	9.64	9.90
	Rupture length(km)		2.55	7.19	9.24	11.68	10.44	10.67
	Elongation (%)		1.26	2.60	2.68	3.30	2.55	2.66
	TEA (J/m^2)		13.0	71.9	92.3	142.7	99.4	108.6
	Elastic modulus(MPa)		1274	2251	2581	2863	2968	3065
	Bendtsen porosity(mL/min)		> 5000	2982	614	260	97	28
	Roughness PPS S-10	Plastic fabric	7.38	6.35	5.92	5.91	6.07	7.04
		Wool fabric	8.88	9.28	9.64	9.69	9.69	10.08

APPENDIX C. Know-how of laboratory scale reinforcement fabrication

C.1. *Pulp preparation*

Among different properties of pulp, pulp consistency is the most important one in the pulp preparation step for the dynamic sheet former machine. Pulp consistency is defined as the percentage of total weight of oven dry fibrous material and non-fibrous additives (i.e. ash) dropped in a water solution. It is calculated by the following formula.

$$C\,\% = \left[\frac{M_f + M_a}{M_f + M_a + M_w}\right] \times 100 \qquad \text{C - 1}$$

Where:

C = consistency of pulp or stock slurry expressed in %

M_f = mass of dry fibrous material in stock slurry

M_a = mass of non-fibrous additives in stock slurry

M_w = mass of water in stock slurry

Preparation of the pulp is as follows:

1. If the pulp is ready to be diluted, add some water to get approximately 0.8 % of consistency.
2. If the pulp is dry and thick, disintegrate the pulp using an appropriate method, before dilution.

3. The required weight of the dry pulp (excluding the quantity of pulp lost through the forming fabric) would be multiplication of forming fabric area and surface density of interest. This is shown in the formula below:

$$M_f(g) = \rho_A\,(g/m^2) \times A_{felt}(m^2) \qquad \text{C - 2}$$

Where:

ρ_A (g./m^2) = paper surface density

A_{fabric} (m^2) = area of fabric

It is supposed that no additives are added to the slurry (M_a=0).

4. Put the pulp slurry in the reservoir of the machine and add water to reach to maximum of 2 % consistency, otherwise it may block the nozzle which projects the slurry on the canvas
5. Run the agitator.

C.1. *Preparation of dynamic sheet former machine and fabrication of paper sheet*

1. Install the press-section fabric of 22.5×88cm (probably soaked) in the former machine.
2. Start rotating the drum and adjust the speed to 1250 RPM and then stop. This allows the fabric to properly stick to the wall of the drum.
3. Install the forming-section fabric over the press-section fabric and start rotating the vessel until the speed of 1250 rpm and then stop it.

4. Position the feeding pipe at the bottom of centrifugal drum.
5. Position the dewatering handle on the position ZERO
6. Start the centrifugal drum.
7. Once the drum reaches its highest speed (1250 RPM) spread the water on the installed fabric, with the hose. When the color of the fabric changes to purple it shows that they are saturated and a water wall is built on them.
8. Put the speed controller of the pump at the 100 RPM.
9. Put the first handle on the right-hand side of the machine at the "vere buse" position, to let the pulp slurry pass through the injection nozzle.
10. Put the plexiglas cover on top of the drum. Start the pump and when the pulp jet at the outlet of the nozzle is uniform, start sweeping the nozzle by pressing the "balayeuse" button.
11. Verify the feeding pressure of pulp slurry. It should remain constant. If the pressure increases spontaneously it shows that the nozzle is getting blocked. A decrease of pressure indicates that an accumulation of pulp has just gone out of the nozzle, so there will be a pile of pulp on the sheet. A pressure of 16 psi shows that the nozzle is completely blocked.
12. If the nozzle is blocked stop the pomp and the sweeping nozzle, disassemble the nozzle to unblock it and start from step 4.
13. When it rests around 3/8" of pulp in the reservoir add about 1/2" of water, repeat it two other times or until there is no more pulp in the reservoir.

14. Once all the content of the reservoir is rinsed stop the sweeping nozzle and then the pomp. Always stop the nozzle when it is at the lowest point of its course.
15. Gradually extract the water of the sheet using the dewatering handle. Take at least 5 minutes to gently move the arm to its maximum position to not affect the sheet formation. Keep the handle in its maximum position to let the sheet dewater completely. When it rests only a small stream of water following through drain of machine stop the spinning of drum.
16. Bring the feeding pipe to its maximum position.
17. Handsheet should be removed from machine with the forming fabric. Break the joint of the fabric (where the ends of the fabric overlap) from the highest point of fabric, then press a ruler on the joint of the fabric and gently pull it down to the other side of the fabric, in order to detach two ends of the handsheet. Form a very small roll of the fabric and take it out.

C.2. *Pressing flax layer on top of the paper sheet*

1. Put the forming fabric on the table of press machine, while the sheet side is upward.
2. Peel off gently the sheet from fabric and once again spread it evenly over it. This prevents the tight attachment of the sheet to the fabric once it is totally dry.
3. Spray some water over the handsheet. This not only allows the paper to conform well over the forming fabric, but also during the press step causes flax plies to better attach to the paper layer. Due to this fact that, the blotter paper is used

during pressing, it absorbs completely the water squeezing out the paper and gets it quite dry. So adding some water help the two layers develop some bond while getting dry from a wet condition.

4. Gently deposit the already prepared flax plies on the sheet.
5. Place one layer of blotter paper over the flax plies.
6. Detach some paper at the two front corners of the forming fabric and instead of removed paper stick some yellow sealing tape on the forming fabric.
7. Put another forming fabric on top of the blotter papers, such a way that its front corners stick to the yellow tapes which are already stuck on the lower forming fabric. By sticking the two forming fabrics, they are prevented from having relative movement while passing between pressing rollers.
8. Make a pressing of 1.0 bar for the first pass and then press the reinforcement three other times with the advised value in the design table.

C.3. *Drying hybrid reinforcement*

1. Detach the upper fabric, by taking off the yellow sealing tape.
2. Gently remove the blotter papers, since the cohesion between two layers of paper and flax are still fragile.
3. Spray some water over the flax layer and paper. This help the two layers develop more chemical bounds while getting dry in the drum dryer.
4. Put another forming fabric on the hybrid-reinforcement which is already formed in the press section.

5. While the reinforcement is made sandwich between two upper and lower forming fabric, introduce it to the drum dryer at the preselected temperature and rotating speed.
6. Once the reinforcement is got out of dryer, leave it overnight in room temperature and then extract test samples out of them according to sampling standards and tests requirements.
7. Condition the samples at standard humidity and temperature before conducting tests.

APPENDIX D. Specifications of dynamic sheet former machine

Table D 1. Specification of the dynamic sheet machine fabricated by Allimand.

Surface density of resulted sheets	Maximum (g/m^2)	300
	Minimum (g/m^2)	10
Surface density accuracy in the sheet	Upper level	+2 %
	Lower level	-2 %
Useful sheet dimension	Length (mm)	800
	Width (mm)	200
Stock consistency	Maximum (g/lit.)	15
	Minimum (g/lit.)	0.5
Wet handsheet dryness	Maximum (%)	15
	Minimum (%)	10
fabric speed during sheet making	Maximum (m/min)	1700
	Minimum (m/min)	600
Stock speed	Maximum (m/min)	1450
	Minimum (m/min)	400
Stock flow rate	Maximum (lit. /min)	3.3
	Minimum (lit.min)	0.6
$\frac{CD}{MD}$ **fibre orientation ratio**	Maximum	0.55
	Minimum	0.2
Time of making one wet sheet	Maximum (min)	8
	Minimum (min)	6
Precision of reproducing characteristics of commercial papers	Maximum (%)	10
	Minimum (%)	5

APPENDIX E. Specifications of pilot paper machine

Table E 1. General characteristics of the paper machine.

Speed	Maximum (m/min)	1000
	Minimum (m/min)	200
Sheet Width	Maximum (cm)	45
Surface density	Maximum (g/m^2)	300
	Minimum (g/m^2)	30
Headbox	Number of dilution zones	5
Formation table	Table length(m)	21
	Number of top formers	2
Presses	Bi-nip press (pond per linear inch)	0-500
	Jumbo press (pond per linear inch)	0-2000
	Extended nip press (pond per linear inch)	0-6000
dryers	Number of sections	3
	Total number of cylinders	28
Calender	Type of calender	Soft nip
	Configuration	tandem
	Maximum temperature (°C)	150
	Maximum load (pond per linear inch)	0-3000
Reel	Bobbin maximum diameter (m)	2
	Number of bobbins	6
Winder	Maximum speed (m/min)	1000
	Maximum core diameter (m)	1

APPENDIX F. Design and analysis of experiments

F.1. Design of experiments

A design of experiments is a matrix, usually indicated by letter X , whose rows are named "run" and show combination of factors levels for conducting experimentation, and its columns, which are referred to as "vector" are equal to the number of factors and show level settings for each factor. Therefore, a design with n runs and K factors is a matrix with the dimension of n x K.

Factors levels in a design table could be either in actual or coded settings. Actual settings are to conduct experimentation in laboratory while for the purpose of analysis, factor units are required to be scaled and standardized into coded settings. To convert from actual setting to coded one and vice versa the following formulas are used.

$$x_j = 2\frac{f_j - \bar{f}_j}{d_j} \qquad \text{F - 1}$$

and

$$f_j = \bar{f}_j + \frac{d_j}{2}x_j \qquad \text{F - 2}$$

where:

x_j = coded setting for factor j

f_j = actual setting for factor j

$\bar{f}_j$ = average of all the actual settings for factor j

d_j = distance between the largest and smallest actual settings of factor j.

When all factors of a design are measured at two levels the design is referred to 2-level design while for 3-level designs a center point (or 0 coded setting) is added to the levels of each factor to allow for curvature modeling of the factors. By way of contrast, 2-level designs are useful for factor screening and estimating linear models with or without interactions. A 2-level or 3- level design is named orthogonal when their coded values fulfill the following two conditions.

$$\sum_{i=1}^{n_r} x_{ij} = 0, \text{for each factor j} \qquad \text{F - 3}$$

$$\sum_{i=1}^{n_r} x_{ij}\, x_{ik} = 0, \text{for all combinations of columns j and k, where j} \neq \text{k} \qquad \text{F - 4}$$

Two vectors of a design table are called independent as long as they satisfy the relation F-4. However, if they are totally identical or negative of each other the summation F-4 would not be equal to zero and the two columns are called identical, aliased or perfectly confounded. On the other hand when two vectors are neither independent nor identical they are called partially correlated (confounded) design columns.

The reason why having independent vectors is important is that it allows the desired vectors to be evaluated independently. While if for example two factors B and C are aliased or partially confounded and factor B is truly important, factor C may appear important during analysis due to its dependency with B. So, non-orthogonality must be avoided whenever possible since it will confound effects and complicate analysis.

Given that there exist 'K' factors each of which at 'a' levels, the design consisting all possible combinations or runs is named full factorial design, and the number of runs (n_r) for such a design is given by

$$n_r = a^K \qquad \text{F - 5}$$

With a full factorial design the experimenter is capable to not only evaluate all the factors (main effects) but also all possible interactions between factors (interaction effects). For such a design the number of vectors representing all possible effects will be n_r-1. For instance, if there exist K=3 factors (A, B and C) each of which at two levels (a=2) the number of runs in a full factorial design accounts for 2^3=8 and this design could consist a total of 7 columns corresponding to main effects (A, B C), 2-way interactions (AB, AC and BC) as well as a 3-way interaction (ABC). So, we end up with an 8 x 7 matrix. Coded setting levels for 2-way and 3-way interactions are acquired by multiplying coded setting of the corresponding main effects. However, the interaction columns are just used in the analysis phase of the experiments.

Although with full factorial designs an experimenter would be capable to evaluate all main effects and their interactions, full factorial designs are resource demanding especially when number of factors is large. Due to this fact many researchers have focused their work on devising new designs which require less runs compared with full factorial designs. Some of these for example include fractional factorials, Plackett-Burman, Box-Behnken, Box-Wilson (Central-Composite) and Taguchi designs. However, reducing the number of runs is always at the expense of not being able to evaluate independently all possible interactions. In other

words, some effects could be perfectly or partially confounded with each other. For such designs, a term commonly used by experimenters to express the degree of aliasing among effects of a design matrix is resolution (R). Specific meaning of resolution degree is as follow:

- R_{III}: A design in which main effects are not aliased with each other, but main effects are aliased with 2-way interactions.
- R_{IV}: A design which does not alias main effects with 2-way interactions. However, does alias 2-way interactions with other 2-way interactions.
- R_V: A design which contains 2-way interactions aliased neither with main effects nor with other 2-way interactions. However, 2-way interactions are aliased with 3-way interactions, although 3-way interactions are typically insignificant.

There is a general consensus among experts, that when large numbers of factors (greater than 5) are involved in the problem, experimentation process is divided into two parts namely screening and modeling. Screening means to separate large number of trivial factors from a subset of few important ones for more in-depth testing. R_{III} designs are typically used for screening phase, while R_{IV} and R_V are usually used for building prediction equation in the modeling phase.

As mentioned beforehand, fractional factorial designs are an important family of designs allowing for evaluating main effects and desired interactions through a wide range of R_{III}, R_{IV} and R_V designs, while Plackett-Burman and Taguchi design are typically orthogonal R_{III} types screening designs. On the other hand, Box-Behnken, Box-Wilson (central composite) and optimality designs (A-, D-, G-, and V-optimality) are of either R_{IV} or R_V type and employed to model nonlinearities and interactions of the factors. To build a fractional factorial

design, one needs to write the full factorial design for K-q factors (q is an integer and 0<q<K), then coded setting for the extra q factors are generated by multiplying coded setting vectors of a few original K-q factors.

F.2. Analysis of variance (ANOVA)

In ANOVA input factors are analyzed to distinguish the factors which influence mean value of response (location factors) and those having an effect on the response's standard deviation (dispersion factors).

In the case of location factors, ANOVA actually infers if variance of the mean response values is statistically significant while an input factor level is changing. To show the procedure of data analysis using ANOVA, Table F-1 simulates experimental data resulted according to a design of experiments with eight runs like that is shown in Table F-2.

In the Table F-1 , two last columns show average and variance of response values of each run, respectively, and are calculated based on the following formulas, where, n_{rep} is number of replicated tests in each row.

$$\bar{y}_r = \frac{\sum_{i=1}^{n_{rep}} y_{ri}}{n} \qquad \text{F - 6}$$

and

$$S_r^2 = \frac{\sum_{i=1}^{n_{rep}} (y_{ri} - \bar{y}_r)}{n_{rep} - 1} \qquad \text{F - 7}$$

Table F 1. A typical sample data resulted from experimentation.

Run	Replicated tests values				$(\bar{y}_r)$	S_r^2
	1	2	3	4		
1	y_{11}	y_{12}	y_{13}	y_{14}	$\bar{y}_1$	S_1^2
2	y_{21}	y_{22}	y_{23}	y_{24}	$\bar{y}_2$	S_2^2
3	y_{31}	y_{32}	y_{33}	y_{34}	$\bar{y}_3$	S_3^2
4	y_{41}	y_{42}	y_{43}	y_{44}	$\bar{y}_4$	S_4^2
5	y_{51}	y_{52}	y_{53}	y_{54}	$\bar{y}_5$	S_5^2
6	y_{61}	y_{62}	y_{63}	y_{64}	$\bar{y}_6$	S_6^2
7	y_{71}	y_{72}	y_{73}	y_{74}	$\bar{y}_7$	S_7^2
8	y_{81}	y_{82}	y_{83}	y_{84}	$\bar{y}_8$	S_8^2

Table F 2. A design of experiments with eight runs and four main factors.

Run	A	B	C	D
1	-1	-1	-1	-1
2	-1	-1	+1	+1
3	-1	+1	-1	+1
4	-1	+1	+1	-1
5	+1	-1	-1	+1
6	+1	-1	+1	-1
7	+1	+1	-1	-1
8	+1	+1	+1	+1

One estimate of the overall population variability (σ^2) of the response could be approximated by pooled estimate of run variances which is referred to as the mean square error (MSE) or within runs mean square and is calculated in Equation F- 8, where, df_r is run's degree of freedom and df_E is degree of freedom of MSE.

$$MSE = \frac{\sum_{r=1}^{n_r}[(df_r)\times S_r^2]}{df_E=\sum_{r=1}^{n_r}(df_r)} = \frac{\sum_{r=1}^{n_r}[(n_{rep}-1)\times S_r^2]}{\sum_{r=1}^{n_r}(n_{rep}-1)} \qquad \text{F - 8}$$

On the other hand, another estimates of σ^2 can also be calculated from each of the effects. This type of variance is called mean square between (MSB) or between runs mean square and is given by Equation F-9, where it is presumed that factor A is intended to be evaluated.

$$(MSB)_A = \frac{\sum_{j=1}^{L_A} n_{Aj}(\bar{Y}_{Aj}-\bar{\bar{Y}})^2}{df_A} = \frac{\sum_{j=1}^{L_A} n_{Aj}(\bar{Y}_{Aj}-\bar{\bar{Y}})^2}{L_A-1} \qquad \text{F - 9}$$

where:

$L_A = Number\ of\ levels\ of\ factor\ A$

$\bar{Y}_{Aj} = Average\ of\ response\ values\ \ for\ them\ factor\ A\ is\ at\ level\ j$

$n_{Aj} = Total\ number\ of\ test\ values\ used\ to\ determine\ \bar{Y}_{Aj}$

$\bar{\bar{Y}} = Grand\ average\ of\ all\ the\ data$

The ratio of F_0 = MSB/MSE is then calculated and compared with F_C critical value which comes from F-distribution, using 1-α, df_A and df_E, as three required input parameters for this distribution. That is to say:

$$F_C = F(1-\alpha, df_A, df_E) \qquad \text{F - 10}$$

In the above equation, α is an attributed probability which represents the risk of judging the factor A as an important factor while in true state of nature (entire population) it is an unimportant one (type I error). α is usually set at 0.05 or 0.01 for industrial experiments.

Based on the comparison of F_0 and F_C, if $F_0 > F_C$ one can conclude, with (1- α)100 % confidence, that factor A (or any other intended factor) is an important factor and changing its level setting has a statistically significant influence on the mean value of the response. On the other hand, the state of $F_0 \leq F_C$, indicates that there is no enough evidence to conclude the importance of factor A, so it can be excluded from prediction equation.

ANOVA could be also used to identify the factors which shift the response variability (dispersion effects). To this end, the method advised in the references [39, 107] is used. Based on this method for each factor absolute value of natural logarithm of average response variance at high (+1) over low levels (-1) (That is to say : $\left|\ln\left(\bar{s}^2_{(+1)}/\bar{s}^2_{(-1)}\right)\right|$) is computed. Next, this statistics value is compared with normal distribution value which gives (1-α/2) cumulative probability (That is to say: Z(1-α/2)). For a probability of α = 0.05 the Z score accounts for Z(0.975)=1.96. If value of the statistic for a given factor is higher than the Z score then the factor is concluded influencing on the standard deviation of the response.

F.3. Regression modeling

To quantitatively represent the results of the experiment one can build an empirical model, through fitting a multiple linear regression (MLR) model to the sample data set. General form of such a predictive model is as follow:

$$\hat{y} = \hat{b}_0 + \sum_{i=1}^{K} \hat{b}_i x_i + \sum_{i=1}^{K} \hat{b}_{ii} x_i^2 + \sum \sum_{i<j} \hat{b}_{ij} x_i x_j \qquad \text{F - 11}$$

Where, x's represent main factors and b's are regression coefficients to be estimated. By saying linear regression model it means that the model is linear in terms of the parameters (the b's) regardless of the shape of the response surface that it generates.

The method of least squares is typically used to estimate the regression coefficients in a multiple linear regression model. According to this method, the sum of the squares of the errors between practical response values and predicted ones is minimized. Using this method one can attain formula F-12 to calculate the regression coefficients. First column of the matrix X in equation F-12 is all 1's (to predict b_0) and other columns are coded levels of effects (main and/or interactions) in the order of their appearance in the regression model.

$$\hat{\boldsymbol{b}} = [\hat{b}_0 \quad \hat{b}_1 \quad \cdots]^T = (X'X)^{-1}X'Y \qquad \text{F - 12}$$

Sometimes, when regression is conducted by statistical software the P values are used to indicate the significance of each regression coefficients as well as the whole regression model itself. The symbol P refers to the minimum value of probability that can be considered in order to still conclude that the given coefficient of the model or the model itself is important. It is also needed to measure the model effectiveness. In this regard, the parameter R^2 is used which indicates how well the regression equation can fit the experimental data. R^2 can vary between zero and one. While $R^2= 1$ means that all experimental observations are simulated by the model, $R^2=0$ is an indication of no relationship between dependent and independent variables.

F.4. Robust parameter design

In a product or process development three phases can be differentiated, namely robust system design, robust parameter design and tolerance design. In the robust system design step preliminary lay-out is modified to reduce sensitivity of the product or process to the uncertainties. This step of product development can be seen by comparing Figures F.1a and F.1b. Robust parameter design step is where robust optimization is implemented to the system to optimize control factors levels such that variance of the response in minimized. This phase can be noticed by comparing Figures F.1b and F.1c. Tolerance design occurs in the final detailed stage of design when manufacturing tolerances are specified. Regarding robust parameter design phase, three categories of parameters are recognized. These include control factors (x_i), noise factors (z_i) and responses (y_i). Control factors which are also known as design variables, are the parameters that a designer adjusts to reach a desired product or process performance. Noise factors are external parameters that affect the performance of a product or process but are not under the control of designer. Responses are the performance metrics of the process or material to be optimized.

The sources that impart uncertainty into the performance (response) of a process or material can be classified into two types. Accordingly, robust parameter design problems are also classified into two types based on the source of uncertainty to be addressed. Type1 uncertainty source of response is originated from environmental or noise factors and type 2 uncertainty source of response is due to variance of control factors. Correspondingly, type 1 and type 2 robust parameter design problem address type 1 and type 2 sources of variability. It is also possible to have both types of uncertainty source at the same time.

First step toward realizing a robust parameter design problem is to identify the control, noise and response factors of the process or material and subsequently range of each factor. Then deciding on the types of robust parameter design problem (type I and/or type II). In the following sections two approaches toward exploring a robust point in the experimental region (design space) will be explained. The approaches include Taguchi method and classical method.

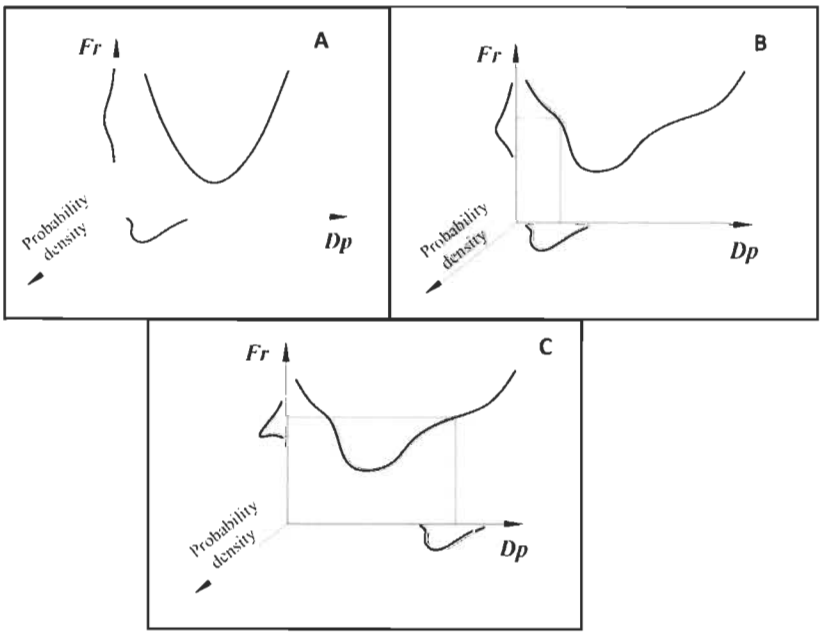

Figure F 1. Process of robust product development, (a) preliminary design, (b) robust system design, (c) robust parameter design.

F.4.1 Taguchi method

The Taguchi approach toward robust parameter design is based on crossed-array designs. It means that there would be two tables of designed experiments, one for controllable factors (inner array) and one for noise factors or control factors having variance (outer array). Then

each run of inner array will be repeated for all runs of the outer array. Table F-3 exemplifies inner and outer arrays, where the controllable factors in the inner array are x_1, x_2 and x_3, and the noise factors or the controllable factors with variance in the outer array are z_1 and z_2.

Table F 3. An example of crossed-array designs for Taguchi method.

				Outer Array			
			z_1	-1	-1	1	1
Inner Array			z_2	-1	1	-1	1
Run	x_1	x_2	x_3				
1	-1	-1	-1	-25.50	-5.11	5.09	24.96
2	-1	0	0	-23.29	-3.00	-1.45	19.23
3	-1	1	1	-32.49	-12.56	-19.10	0.89
4	0	-1	0	5.11	0.66	3.16	-0.68
5	0	0	1	13.07	8.71	2.84	-0.13
6	0	1	-1	-23.73	-4.58	6.51	25.87
7	1	-1	1	22.90	-4.80	-11.28	-39.39
8	1	0	-1	-5.46	-8.99	0.84	-3.16
9	1	1	0	6.20	2.39	4.07	-0.73

Taguchi's main contribution in robust parameter design is the application of the quadratic loss function to the measurement of quality. Using this function, the loss associated with each product deviation from its target value would be computes as follows:

$$L_i = k_1(y_i - L)^2 \qquad \text{F - 13}$$

Where, y_i is the i^{th} response of the quality of interest, L is the quality characteristic target and k_1 is a constant that converts the deviation to a monetary value. For n_{rep} repetition of response values the average loss $\bar{L}$ is

$$\bar{L} = k_1\left[\sigma_y^2 + (\bar{y} - T)^2\right] \qquad \text{F - 14}$$

In practice, this loss function is translated to signal-to-noise ratio function. This function is devised such that maximizing it simultaneously minimizes the response variability and brings the mean value on target. Depending on whether one would like to maximize or minimize the mean response value or either makes it as close as possible to a specified target value three different formulas given below are defined for signal-to-noise ratio function.

$$(S/N)_L = -10\,\mathrm{Log}_{10}\left\{\frac{1}{n_{rep}}\sum_{j=1}^{n_{rep}}\frac{1}{y_{rj}^2}\right\} \quad \text{For an infinite target (larger is better)} \qquad \text{F - 15}$$

$$(S/N)_S = -10\,\mathrm{Log}_{10}\left\{\frac{1}{n_{rep}}\sum_{j=1}^{n_{rep}} y_{rj}^2\right\} \quad \text{For a zero target (smaller is better)} \qquad \text{F - 16}$$

$$(S/N)_N = 10\,\mathrm{Log}_{10}\frac{\bar{y}_r^2}{{s_r}^2} \quad \text{For a specified target (nominal is better)} \qquad \text{F - 17}$$

Taguchi proposed that one can make a regression model of signal-to-noise ratio and determines which controllable factors' settings maximize it. However, this method is reported inaccurate [39] as it can result in confounding of location and dispersion effects. So, it is proposed that more appropriate method is to individually model mean and signal-to-noise ratio or mean and natural logarithm of response standard deviation and then perform a bi-objective optimization.

F.4.2 Classical method

In this section the algorithm of classical robust parameter design approach shown in Figure 3-31 is described in more details. In contrast to crossed array designs of Taguchi method explained above, in the classical method combined array design are employed. That is to say,

controllable (with or without variance, x_i) and noise factors (z_i) are expressed in a single design table. Therefore, the developed response model includes both controllable (with or without variance) and noise factors and their interactions. In case of having noise factor, interaction between controllable and noise factors is the key to robust parameter design problems and unless at least one interaction exists, there will be no robust parameter design problem [39]. Two important steps in the classical robust parameter design approach are firstly finding factors of the material or system having an influence on mean and standard deviation of the response (step 4) and secondly a heuristic for locating the experimental region over which a curved response surface and hence a robust parameter design problem can be defined (steps 5 to 10). Figure F-2 schematically illustrates the notion of heuristic approach of the response surface methodology (steps 5 to 10). This is a sequential approach which gradually shifts parameters setting toward optimum condition. When the point of maximum response is desired, the response surface methodology can be thought of as "climbing a hill". On the contrary, if the true optimum is a point of minimum response then the response surface methodology can be considered as "descending into a valley".

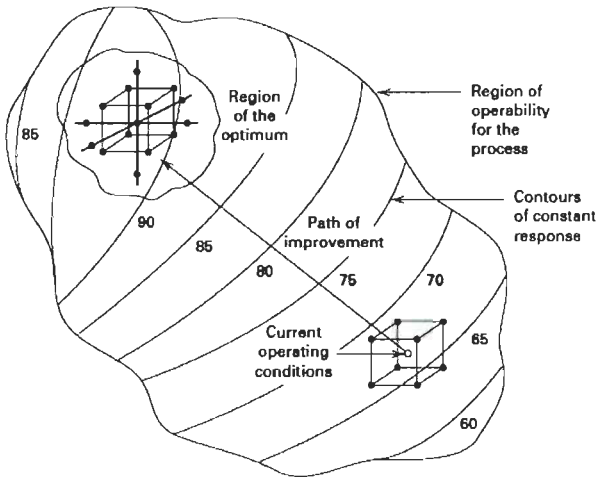

Figure F 2. Notion of heuristic approach of the response surface methodology [39]

Classical robust parameter design algorithm in Figure 3-31 could be described as below:

1. Choose the controllable (with or without variance, x_i) and nose factors (z_i) and their corresponding ranges as well as responses (y_i) of the material or system.
2. Select an arbitrary start point in the design space considered in the step 1.
3. Plan a two-level DOE for the control and noise factors around the start point selected in step 2.
4. Acquire experimental results and conduct ANOVA on mean and standard deviation to find location and dispersion factors. If there is no factor affecting mean and standard deviation of the response, robust parameter design is not applicable to the problem. Otherwise, go to the step 5.
5. Acquire experimental results at the center of the two level DOE previously planned (This result is used for the "lack-of-fit" hypothesis test in step 7)

6. Build a first order model including the main effects and linear interactions, using multiple linear regression method.

7. Test the developed model for the lack of fit of quadratic terms. If quadratic terms are concluded insignificant, this indicates that the optimum lies outside of the initial experimental region. So, go to the step 8. Otherwise, go to the step 11.

8. Take the derivatives of the already developed first order model with respect to each of the factors. This gives a vector pointing out the next experimental region. This gradient vector ($\vec{g}$) is calculated as below. To experiment along the gradient vector in reasonable increment, divide the components of $\vec{g}$ by the smallest absolute value among them.

$$\vec{g} = \left(\frac{\partial \hat{y}}{\partial x_1}, \frac{\partial \hat{y}}{\partial x_2}, \cdots, \frac{\partial \hat{y}}{\partial z_1}, \frac{\partial \hat{y}}{\partial z_2}, \cdots\right)\Big|_{X=0,\ Z=0} \qquad \text{F - 18}$$

9. Some subsequent experiments should be performed at the normalized gradient vector ($\vec{g}$) and some of its multiples until the factor limits are reached. The vector which yields the best response value should be considered the center of new experimental design.

10. Build a new two-level DOE around this point. To calculate the updated coded settings of new experimental design one can add the components of the vector $\vec{g}$ to the corresponding coded setting of the old DOE. Then, using Equation F-2 convert the new coded settings back to the new actual setting and conduct experimentation based on these new actual settings.

11. Add axial points to the latest DOE to finally build a central composite design (CCD).

12. Fit a quadratic regression model on the experimental data of the CCD table. The most general form of a response surface model including l controllable factors (with or without variance) and m noise factors can be expressed as below:

$$\hat{y}_2(\boldsymbol{x},\boldsymbol{z}) = \hat{\beta}_0 + \sum_{i=1}^{l}\hat{\beta}_i x_i + \sum_{i=1}^{l}\hat{\beta}_{ii} x_i^2 + \sum\sum_{i<j}\hat{\beta}_{ij} x_i x_j + \sum_{i=1}^{m}\hat{\gamma}_i z_i + \sum_{i=1}^{l}\sum_{j=1}^{m}\hat{\delta}_{ij} x_i z_j \qquad \text{F - 19}$$

Where, $\hat{\beta}_0$, $\hat{\beta}_i$, $\hat{\beta}_{ii}$, $\hat{\beta}_{ij}$, $\hat{\gamma}_i$ and $\hat{\delta}_{ij}$ are least square estimates of regression coefficient to be calculated using Equation F-12.

13. Calculate the mean and standard deviation models from the quadratic regression model of step 12. The mean model is acquired through replacing the noise expected mean values in the Equation F-19. So, the expected mean response model just includes the controllable factors. Such a model could be expressed in a general form as:

$$\bar{\mu}_{y_2}(\boldsymbol{x}) = E[\hat{y}_2(\boldsymbol{x},\mu_{\boldsymbol{z}})] \qquad \text{F - 20}$$

A standard deviation model of the response could be acquired through regression modeling of the standard deviation (s) or natural logarithm of standard deviation (ln(s)) of the results. These two parameters are more preferable than direct modeling of variance (s^2) because they are less sensitive to occasional extreme values and therefore their distributions are less skewed [107].

Alternatively, standard deviation model could be estimated through transmission of error approach [106]. Using this approach, the variance model would be as below:

$$\sigma_{\hat{y}_2} = \sqrt{\sum_{i=1}^{l}\left(\left[\frac{\partial \hat{y}_2(x,z)}{\partial x_i}\right]\sigma_{x_i}\right)^2 + \sum_{i=1}^{m}\left(\left[\frac{\partial \hat{y}_2(x,z)}{\partial z_i}\right]\sigma_{z_i}\right)^2} \qquad \text{F - 21}$$

Where, σ_{z_i} is standard deviation of noise factor and σ_{x_i} is standard deviation of controllable factors.

14. Having built mean and standard deviation models of the response, a global search techniques such as Genetic Algorithms could be used to conduct a bi-objective optimization in order to minimize standard deviation and bring the mean to target. This could be done through a weighted-sum function of the mean and standard deviation models, like the one exemplified below:

$$Y = (1-\alpha)\left(\frac{1}{\bar{\mu}_{y_2}(x)}\right) + \alpha\,\sigma_{\hat{y}_2} \quad , \quad 0 \le \alpha \le 1 \qquad \text{F - 22}$$

Here α is a weighting parameter varying in the range of 0 (single objective maximization of mean) to 1 (single objective minimization of standard deviation), and any value of α within this range results in simultaneously minimization of standard deviation and maximization of mean, depending on the importance allocated to each of them through parameter α.

APPENDIX G. List of publications

- Journal papers

Ameri E., Laperrière L. and Lebrun G., "Mechanical characterization and optimization of a new unidirectional flax/paper/epoxy composite", Composites Part B: Engineering. 2016; 97: 282-291.

Ameri E., Lebrun G. and Laperrière L., "In-plane permeability characterization of a unidirectional flax/paper reinforcement for liquid composite molding processes", Composites Part A: Applied Science and Manufacturing. 2016; 85: 52-64.

- Conference papers

Ameri E., Lebrun G. and Laperrière L. "A study of permeability and mechanical properties of unidirectional flax fiber reinforced composites", Canadian international conference on composite materials, 17-20 August 2015, Edmonton, Alberta, Canada.

Ameri E., Lebrun G. and Laperrière L. "A novel process for the production of unidirectional hybrid flax/paper reinforcement for eco-composite material ", The 47th CIRP conference on manufacturing systems, 28-30 April 2014, Windsor, Ontario, Canada.